CONFLATION OF COMPUTATIONAL FLUID DYNAMICS AND BUILDING THERMAL SIMULATION

Cezar O. R. Negrão

A thesis submitted for the
Degree of Doctor of Philosophy

Department of Mechanical Engineering
Energy Systems Research Unit
Energy Systems Division
University of Strathclyde, Glasgow, UK.

September 1995

To

Satiko and Natália

TABLE OF CONTENTS

ACKNOWLEDGEMENTS

ABSTRACT

The present work is a contribution towards the integration of building simulation tools in order to better represent the complexity of the real world. It attempts to overcome certain shortfalls of contemporary simulation applications with respect to indoor air flows. As a result, the evaluation of building energy consumption and indoor air quality is expected to be improved.

Advanced fluid flow models (as employed within Building Thermal Simulation - BTS - and Computational Fluid Dynamics - CFD) with different degrees of detail were investigated and their modelling deficiencies identified. The CFD technique which defines the fluid flow on a micro scale was integrated into BTS in which fluid flow is described in a larger scale. The resulting combined approach strengthens the modelling potential of each methodology by overcoming their specific deficiencies. BTS's inability to predict air flow property gradients within a single space was surmounted and the difficult of estimating CFD boundary conditions are now supplied by BTS. The conflation approach is expected to be employed where gradients of indoor air flow properties can be considered crucial to the evaluation of thermal comfort and energy consumption. The BTS environment, ESP-r, was elected to perform the current work and a new CFD program, *dfs*, was specifically developed for the analysis of three-dimensional, turbulent, transient air flow. Finally, the two approaches were integrated.

The integration work focuses on the CFD boundary conditions where the interactions of BTS and CFD take place; these occur at the inside zone surfaces and at the zone openings. Three conflation approaches were devised addressing different degrees of complexity and sophistication. The first one, involving the two types of zone boundaries, corresponds to a simple approach where the BTS and CFD systems exchange information without any direct interaction. The second approach consists of three other schemes to handle the thermal coupling at the internal zone surfaces. The third approach comprises coupling between the nodal network approach as employed by the BTS environment, and the continuity and momentum equations in the CFD technique.

A validation methodology consisting of analytical validation, intermodel comparison and empirical validation is described and applied. The technique is shown to be adequate for modelling indoor air flows when compared to existing models. Three situations, covering the different types of air flows encountered within buildings are discussed to demonstrate the combined method's applicability when compared with the nodal network approach. Finally, general conclusions are presented and some possible future work is identified showing that the developed methodology is very promising.

LIST OF SYMBOLS

A	- area (m^2).
$\boldsymbol{A}$	- future coefficient matrix of equations (3.12) and (4.23).
a	- coefficients of the discretised finite volume equations (3.11) and (4.10) (kg/s).
$\boldsymbol{B}$	- source term matrix of equations (3.12) and (4.23)
b	- source term of equations (3.11) and (4.10) (kg/s multiplied by the unit of ϕ).
C	- concentration (-).
c	- power law coefficient of equation (4.11) (-).
C_D	- coefficient of the source term of the turbulent energy equation (=1.0).
C_μ	- coefficient of equation (4.2) (=0.09).
C_1	- coefficient of the source term of the dissipation energy equation (=1.44).
C_2	- coefficient of the source term of the dissipation energy equation (=1.92).
C_3	- coefficient of the source term of the dissipation energy equation (=1.44).
c_p	- specific heat (J/kgK).
D	- duct diameter (m).
d	- coefficients of the matrix of Figures 5.9 and 5.10.
e	- coefficients of equation (6.17) and (7.2).
e_1, e_2	- coefficients of equations (6.14).
E	- logarithmic constant (=9.793).
f	- function.
G	- generation of turbulent energy (W/m^3).
G_b	- generation/destruction of turbulent energy due to buoyancy (W/m^3).
g	- gravitational acceleration (m/s^2).
H	- height (m).
h	- convection coefficient (W/m^2K) and opening height (m).
I	- inlet turbulence intensity (=0.03).
J	- flux of the transport property ϕ (kg/m^2s multiplied by the unit of ϕ).
K	- conductance coefficient (kg/s).
k	- kinetic turbulent energy (J/kg).
L	- length (m).
M	- wall function coefficient of equation (4.16) (kg/s).
$\dot{m}$	- mass flow rate (kg/s).
N	- wall function coefficient of equation (4.17) (kg/s).

n - number of finite region in contact with the finite region P (-).

nf - number of inter-volume interactions with the surface f (-).

na - number of inter-volume interactions with the air volume (-).

ns - number of surfaces in contact with the air volume (-).

Nu - Nusselt number (-).

P - mean pressure (Pa).

p - pressure (Pa).

Pr - Prandtl number (-).

Q - heat transfer (W).

$q^{''}$ - heat transfer per unit of area (W/m^2).

R - Residuals of conservation equations.

Ra - Rayleigh number (-).

Re - Reynolds number (-).

S - mean source term per unit of volume ($kg/m^3 s$ multiplied by the unit of ϕ).

s - source term per unit of volume ($kg/m^3 s$ multiplied by the unit of ϕ).

Sc - Schimdt number (-).

T - temperature matrix of equation (3.12).

T - temperature ($^o C$).

t - time (s) and opening height (m).

U - mean velocity component in x direction (m/s) and overall heat transfer coefficient ($W/m^2 K$).

U_i, U_j - index notation of mean velocity components (m/s).

u - velocity component in x direction (m/s).

u_i, u_j - index notation of velocity components (m/s).

V - mean velocity component in y direction (m/s).

v - velocity component in y direction (m/s).

W - mean velocity component in z direction (m/s) and construction thickness (m).

w - velocity component in z direction (m/s).

X - duct entrance length (m).

x_i, x_j - index notation of Cartesian coordinates (m).

x, *y*, *z* - Cartesian coordinates (m).

y^* - dimensionless y position ($2y/D$).

Greek symbols

α - linear under-relaxation factor (-) or thermal diffusivity (m^2/s).

β_T - thermal expansion coefficient ($1/K$).

$\Delta(\ )$ - difference of properties.

δ - finite interval and boundary layer thickness (m).

δ_{ji} - Kronecker delta.

δt_f - fictitious time-step.

ε - kinetic turbulent energy dissipation (W/kg).

Γ - diffusion coefficient ($kg/m\ s$).

γ - weighting factor between explicit and implicit formulation (-).

κ - von Karman's constant (=0.4187).

λ - conductivity ($W/m\ K$) and length scale factor of the equation (4.21).

μ - molecular viscosity ($Pa\ s$).

ν - kinematic viscosity (m^2/s).

ϕ - mean conservation variable (U, V, W, T, C, k, ε).

ψ - maximum admissible value for the residuals (-).

ρ - density (kg/m^3).

σ - turbulent Pr or Sc number.

σ_k - turbulent energy diffusion coefficient (=1.0).

σ_ε - turbulent energy dissipation diffusion coefficient (=1.3).

τ - shear stress (N/m^2).

θ - represents any variable within the integrating time interval.

υ - volume (m^3).

Z   - mean scalar variable.

ζ - instantaneous scalar variable.

Subscripts

a   - air.

C   - concentration of pollutant.

c   - constant, core.

CS   - control surface.

CV   - control volume.

D   - duct diameter.

E   - east cell.

e   - interface between cells *P* and *E*.

ef   - effective.

f   - surface.

H   - high cell.

h   - interface between cells *P* and *H*.

in   - inlet condition.

k   - turbulent energy.

L   - low cell.

l   - interface between cells *P* and *L*.

m   - bulk flow.

N   - north cell.

n   - interface between cells *P* and *N*.

o   - wall, outside.

P   - finite region.

S   - south cell.

s   - interface between cells *P* and *S*.

T   - temperature.

t   - turbulent.

tot   - total.

U_i - index notation of mean velocity components.

u_i - index notation of velocity component.

W   - west cell.

w   - interface between cells *P* and *W*.

ε - energy dissipation.

ϕ - mean conservation variable.

Z   - mean scalar variable.

ζ - instantaneous scalar variable.

Superscrips

o   - previous iteration.

x   - coefficients of the matrices of Chapter 3 and 5 which are modified once.

xx   - coefficients of the matrices of Chapter 3 and 5 which are modified twice.

′   - fluctuating component of an instantaneous value.

‴   - flux per unit of volume.

−   - present time-row.

−1   - time-row immediately before the present time-row.

+   - dimensionless.

ξ - value between present and future time-row.

Introduction

1.1 BUILDINGS, CLIMATE AND ENERGY

As a result of mechanisation and industrialisation, the possibility to create, artificially, an indoor climate was offered. With such available technology virtually any indoor environmental condition can be produced to satisfy the occupants. Usually, the final aim is to provide an indoor climate where the occupants are in thermal comfort: a condition (as described by Fanger (1970)) of mind which expresses satisfaction with the thermal environment. To accomplish this, a collection of physical properties must be kept within an acceptable range which satisfies the human requirements. Over the years, not only have the levels of comfort been enhanced with improved building insulation, advanced HVAC systems, automatic control, etc, but also man's demands for a comfortable environment have reached higher standards.

However, the benefits of such an industrialised world has its price; a certain amount of energy must be consumed to make such demands of the society possible. After the fuel shortage in the 1970s, several measures towards energy efficient buildings were enacted. For instance, the reduction of air volumes supplied and sealed window frames led to smaller quantities of outdoor air intake resulting in an air tight environment. At the same time, many sources of contaminants have been introduced to the working and living environments. Contaminant sources, allied to inadequate ventilation, contribute to the impoverishment of the indoor air quality (IAQ), contributing to the so called "sick building syndrome" and thus compromising human health. Contaminants found within the built environment come from a variety of indoor and outdoor sources, such as industrial pollutants, vehicle exhaust, dust, tobacco smoke, cooking, cleaning products, etc. Poor IAQ may have acute or chronic effects on health, although the indoor environment is rarely so poor that people become seriously ill after a short period spent indoors. However, allergic reaction and biological infections are examples of acute effects. As reported by Appleby (1990), some office building occupants show a range of acute symptoms, such as headache, fatigue, nausea, dryness of the mucous membranes, running and itchy eyes, stuffy or running noses, etc. Allergy, which may also appear after a long period of exposure to allergens, and lung cancer caused by continuous inhalation of asbestos are examples of long-term effects (Clausen 1990).

The building industry, one of the largest in the world, is the second industrial sector in Europe accounting for 12% of gross domestic product (Kennington and Monaghan 1993). In Western Europe,

for example, 52% of energy is delivered to maintain acceptable climate conditions within buildings (Clarke and Maver 1991). Unfortunately perhaps, the western-type developments seem attractive to most of the world's population (from 15% in 1971, the developing countries now account for about one-quarter of the world's energy consumption (IEA 1994a)). The worldwide escalating figures suggests that ensuring a thermally efficient building can reduce the profligate use of fossil fuels. Studies in the United States revealed that energy-saving actions regarding design and retrofits could prevent a loss of $100 billion US a year until the year 2010 (Mathews and Richards 1993). According to the U.K. Department of Energy, 50% of the energy consumption could be reduced if new building design standards were enhanced and also, if appropriate interventions on existing buildings were undertaken, 25% of the current figures could be saved (Clarke and Maver 1991).

On the other hand, the expenditure of non-renewable sources of energy has direct impact on the environment with potentially devastating results. The new technology that brings such high productivity and comfort also destroys man's biological capital - the air, water and other parts of the ecosystem. The combustion of fossil fuels produces millions of tonnes of gases such as sulphur dioxide (SO_2) and carbon dioxide (CO_2) which are released into the atmosphere. The high emission of SO_2 produces acid rain as a direct consequence which can destroy woods, forests and historic buildings in our cities. CO_2 accumulates in the upper atmosphere and traps the sun's heat causing the so-called "greenhouse" effect. This may lead to major climatic and ecological changes in the long term, compromising the wellbeing of future generations. CO_2 emissions have fluctuated over the last 20 years; sharp falls after the oil shocks in 1973 and 1979 were followed by prolonged periods of increase - emissions in 1992 were around 5% higher than in 1973 (IEA 1994b). The continuing depletion of the ozone layer by chlorofluorocarbons (CFCs) is another example of environmental damage which can have disastrous effects on humankind. The air-conditioning industry alone is responsible for spending approximately 25% of the worldwide consumption of CFCs (Rousseau *et al* 1993).

1.2 APPROACHES TO ENERGY/ENVIRONMENTALLY CONSCIOUS BUILDINGS

Such figures have raised a global awareness to reduce energy consumption and environmental impact in order to attain sustainability. The building industry, governments and the research community have been examining different approaches to the problem. Several initiatives to accomplish a more energy efficient and environmentally "friendly" buildings have come into practice. Examples of these are codes of practices, design advice, good practice and computer modelling. In order to understand the premise of current work, a brief explanation of these practices are given.

Code of practices

Holm (1993) states that "... architects and building owners are not exposed to the realities of life-cycle energy costs nor to the environmental and societal costs", and he goes further, "... the present money value of energy is perceived to be a minor consideration in the eyes of decision-makers who grew up with the expectation that this would remain so". This fact urges on governments to take appropriate interventions. Actions such as high prices and taxation, seeking the equilibrium between supply and demand, are not necessarily effective in this situation. In this case, the final consumers may struggle to minimise the wastes but they cannot improve the system performance. Although publicity campaigns towards a more energy/environmentally conscious society have some repercussion, other actions of direct results must be taken. An appropriate legislation for energy conservation usage seems the most attractive way to enforce good practice in the design of new buildings. Governments have been responding with suitable codes of practice which must always be updated with the advent of new technologies. The International Energy Agency (IEA) reports that most of the IEA member countries have adopted minimum energy efficiency standards for the building sectors and members who have not adopted such practices are in the process of doing so (IEA 1994b). Some authorities have devoted greater attention to revise existing codes and standards to be in agreement with the new technologies. In Germany, for example, the thermal insulation ordinance was amended in October 1993 to reduce the heating requirements for new buildings by about 30%. Canada, on the other hand, has developed revised codes for new residential and commercial buildings and is working to implement them (IEA 1994b).

Good practice

A building is a system in constant interaction with its surrounding environment and which is affected by climatic changes and by the temporal requirements of occupants. The design practice in the twentieth century seeks to avoid the interactions controlling them with expensive heating, cooling and lighting equipment. Usually, the designers only start to think of cooling, heating and lighting requirements after the building is conceived and almost completed. Although the approach is pragmatic and convenient, the opportunity to design a building which reacts to the environmental changes is reduced and consequently the possibility to minimise the use of machinery is diminished. Controversially, the seasonal and daily climatic changes can be employed to lessen their own effects on buildings for the well-being and comfort of the occupants. Knowledge of climate, available technology and comfort conditions and how these are affected by climatic changes constitutes the requisites to accomplish this. Goulding *et al* (1992) suggests alternative solutions to achieve the design of buildings in harmony with their environment.

Design advice

As designers, architects and building owners look for solutions to fulfill the requirements of good practice, alternatives to meet their short-term needs should be provided. Governments, design and research communities should find means to bridge the gap between design professionals and technology developers. One solution is the establishment of programmes which can support designers with technical advice, acting as vehicles of technology transfer. An example of this is the technical consultancy provided by the Energy Design Advice Scheme (EDAS) (McElroy 1993). The Scheme aims to ensure that refurbishment and new build projects are undertaken with the full awareness of the latest energy saving technology available. It has been proven that significant savings can be achieved with little or no extra capital costs, providing an increased environmental quality and reduced running costs. EDAS offers an initial consultation free of charge, which can last up to one working day. If further consultations are needed, which can be 50% subsidised, an in-depth analysis on specific subjects, such as architectural design, building services engineering, building science, quality surveying and computer modelling, is carried out.

Computer modelling

Significant research has been carried out to provide methods for building designers to examine the energy implications of their design decisions. The development of digital computers encouraged rapid advances in calculation procedures to predict the thermal performance and energy demands of buildings. Initially, computers were used only to speed up calculations which were performed manually. Due to computational restrictions, calculations of energy requirements were based on very simplified algorithms. As the computer technology developed and computer prices decreased, the ability to accurately assess building energy performance evolved. Progressively, energy analysis tools moved from simplified methods towards more comprehensive simulation[#] models. In computer simulation, all existing energy flow-paths within the real system are modelled without any simplifying assumptions. Ayres and Stamper (1995) present a review work of how building energy calculations evolved from the early days of computer modelling to sophisticated dynamic analysis of the present day.

1.2.1 Application of Computer Simulation

As computer technology evolved, the real world could be more realistically represented by means of simulation. A more precise estimation of building energy consumption and indoor air quality could be accomplished. Such advances are encouraging the use of computer simulation in a variety of areas. For example, computer simulation can help with the establishment of codes of practice, aid professionals working on technology transfer and assist building practitioners to understand physical

_____

[#] Simulation can be defined as the emulation of the reality by means of a model.

phenomena in order to achieve good practice.

Computer simulation can be employed to check the application of new technologies (for example, new materials, advanced control systems, etc.). Consequently, energy efficient standards can be enhanced since building energy requirements can be more accurately determined. Legislations can thus be constantly revised based on the simulation analysis enforcing better practice at the design stage.

Advisers can make use of simulations to endorse their physical intuition and also to provide estimations of energy consumption reductions resulting from their proposed measures. EDAS is already employing simulation to aid its counselling work; for example the advantages and disadvantages of different types of glass and the effect of increasing wall and roof insulation levels on summer overheating and winter energy requirements are typically and routinely evaluated. Simulation is also one of the products which can be transferred to the design practice.

The intrinsic knowledge available within computer simulation programs can aid designers to understand the interactions between the built environment and the climate. The best building orientation, window positions and shading are parameters which can be analysed in order to achieve good practice. Energy efficiency and air cleanness can be accomplished with the minimum use of machinery.

1.2.2 Integration of Design Tools and Detailed Design

On the other hand, even the simplest simulation method is difficult to effectively deploy in practice. If, for example, any simulation is employed, this is carried out after the design is substantially completed, to evaluate the heating and/or cooling requirements of the plant system. Generally, the architect starts with the basic concept proceeding towards the detail design. Generic decisions regarding the design are taken during the initial stages and these decisions determine the major thermal characteristic of the design (see Figure 1.1). By the time thermal simulations are applied, as described by Holm (1993), "... the building owner and/or architect may have fallen in love with the design or be even married to it, in which case the cost of divorce would exceed the cost of hanging on".

By contrast, a simulation process evolves by accretion of detail, leading towards the complete design (see Figure 1.2). This approach moves from the constituent parts towards the whole, and therefore, opposes the direction of the architectural design. In principle, they cannot meet halfway since the second cannot start before the first has been finished.

Additionally, the building industry involves professionals of different areas, including architects, structural, electrical and mechanical engineers, developers and interior designers. Each discipline represents a specialisation that is often not well understood by the others. Variations in background, education and experience lead to discrepancies in terminology, attitude, style and

organisation; each professional has their own perspective of the design. As a result, there is a lack of proper exchange of information among the professionals since they are unable to "speak the same language". On the other hand, isolated computer applications have been developed to fulfill the requirements of each specialist taking part in the design process. For example, CAD systems are used by architects to produce drawings, structural engineers employ finite element programs to analyse walls, framing and slabs of the building and mechanical engineers use building thermal simulation to investigate the implications of the design on the energy consumption. However, any decision taken for one of the design participants may have a direct affect on other areas.
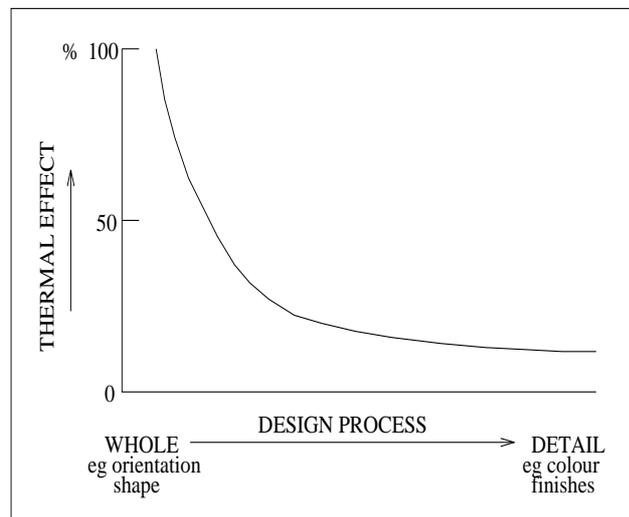
Figure 1.1 Design process (Holm 1993).
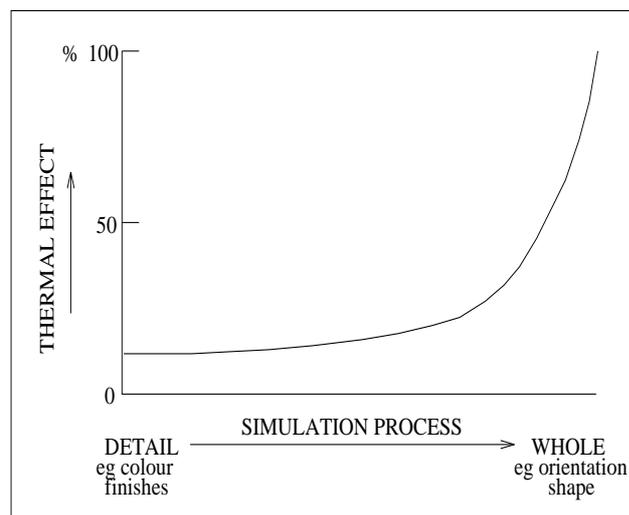
Figure 1.2 Simulation process (Holm 1993).

As increasing segments of the design-construction process become computer-based, the need for appropriate forms of electronic communication and integration becomes increasingly apparent (Fenves *et al* 1994). The alternative solution is a computational system which merges a whole range of building evaluation tools into an integrated environment. Such an environment should make available all information required by various design participants in a format they understand and at a level of detail with which they feel comfortable. Users from different backgrounds are allowed to access and exchange information through the integrated system. Any participant can thus intervene in the design at any stage looking for the different implications of a decision. For example, thermal simulation could take part in the early stages of the design process when the building is being conceived.

At the same time, the physical phenomena must be represented as close as possible to reality in order to provide confidence to building practitioners. Engineers should be able to analyse the problem in a degree of detail which can minutely affect their final decision; for instance, concerning occupancy (human comfort and indoor air quality) and energy consumption. Within the integrated environment, the high degree of detail should be invoked only where required. In this sense, overall cruder models should be conflated to specific refined models. In other words, an overall analysis could be performed with some refinements applied to specific parts of the system where it is judged necessary. This also adds flexibility to the computational environment and therefore specialists and general practitioners can make use of the same tool. The integrity of the real world, however, must be conserved within the computational medium because if disregarded will compromise simulation predictions and therefore the related design decisions. Thus, the interactions among the sub-systems comprising the building should be reproduced in the electronic form.

In terms of simulation, air flow within buildings is one of the areas which requires refinements to attain the demands of engineers regarding detail. An appropriate representation of air flow phenomena is essential to the evaluation of energy consumption, comfort conditions and indoor air quality. Therefore, advanced fluid flow techniques, with different degrees of detail, must be made available within building simulation environments in order to better describe the air flow phenomena.

1.3 OBJECTIVES OF THE WORK

Considering the refinements required in building air flow models, this thesis aims to enhance the potential of analysis of building simulation applications and concurrently improve their integrity. To accomplish this, the complexity of the interrelation and interdependence of energy/mass flows within the building system is investigated. Two advanced air/energy flow models with different degrees of detail are examined and their deficiencies are identified. In order to overcome such deficiencies, the cruder air/energy flow models of building thermal simulation - (BTS), is combined with the more refined CFD (Computational Fluid Dynamics) model. In the former, a distributed capacity domain is discretised and in the latter a fluid domain is discretised.

In the BTS simulations, air is usually considered mixed within single spaces and gradients of air flow properties are not accounted for. However, gradients of such properties can not always be neglected in which case the evaluation of local thermal comfort and air quality can be compromised. Although CFD can predict air property gradients, the dynamic behaviour of the boundary conditions is not well represented. This deficiency may reduce the flow modelling accuracy.

When the techniques are conflated, the deficiencies of each approach can be thus expected to reduce. Therefore, an increasing potential of analysis of ventilation, infiltration, comfort conditions, dispersion of pollutants, etc. is contemplated. Such an approach is intended for application only where gradients of air flow properties may be crucial to the evaluation of the performance of the system. For example, the CFD technique may be invoked to model a large hall within the building, while the rest of the system is modelled by the usual BTS approach.

The resulting computational tool should help designers and developers to better understand the physical phenomena and therefore to find means to reduce energy consumption, to protect the environment and at the same time to satisfy the human requirements. Confidence on simulation tools are expected to be increased since the representation of the real world is improved.

Chapter 2 describes how thermal simulation has evolved over the years leading to the functionality of contemporary systems. The deficiencies of contemporary systems, some ongoing developments and an explanation of how the present work is placed within this context are also discussed in this chapter. Chapter 3 and 4 are concerned with the theoretical basis necessary to understand the combined technique. Conflation mechanisms of the investigated fluid flow models are proposed in Chapter 5. Chapter 6 and 7 address, respectively, the validation and application of the conflated system. Finally, Chapter 8 presents the conclusions of the work and identifies the trends for the future.

REFERENCES

Appleby, P., 1990, Assuring Indoor Air Quality, *Heating and Air Conditioning Journal*, Vol. 60, No. 694, pp. 27-29, April.

Ayres, J. M. and Stamper, E., 1995, Historical Development of Building Energy Calculations, *ASHRAE Journal*, Vol 37, No. 2, Feb.

Clarke, J. A. and Maver, T. W., 1991, Advanced Design Tools for Energy Conscious Building Design: Development and Dissemination, *Building and Environment*, Vol. 26, No. 1, pp. 25-34.

Clausen, G., 1990, Indoor Pollution Control, *Heating and Air Conditioning Journal*, Vol. 60, No. 694, pp. 42-44, April.

Fanger, P. O., 1970, *Thermal Comfort, Analysis and Applications in Environmental Engineering*, MacGraw-Hill Book Company.

Fenves, S., Flemming, U., Hendrickson, C., Maher, M. L., Quadrel, R., Terk, M. and Woodbury, R.,

1994, *Concurrent Computer Integrated Building Design*, PTR Prentice Hall.

Goulding, J. R., Lewis, J. O. and Steemers, T. C. (ed.), 1992, *Energy Conscious Design, A Primer for Architects*, B. T. Batsford Ltd, London.

Holm, D., 1993, Building Thermal Analyses: What the Industry Needs: The Architect's Perspective, *Building and Environment*, Vol. 28, No. 4, pp. 405-407.

IEA, 1994a, *Energy Policies of IEA Countries, 1993 Review*, OECD, Paris.

IEA, 1994b, *Energy in Developing Countries, a Sectorial Analysis*, OECD, Paris.

Kennington, J. and Monaghan, P. F., 1993, COMBINE: The HVAC-Design Prototype, *Building and Environment*, Vol 28, No. 4, pp. 453-463.

Mathews, E. H. and Richards, P. G., 1993, An Efficient Tool for Future Building Design, *Building and Environment*, Vol. 28, No. 4, pp. 409-417.

McElroy, L., 1993, The Energy Design Advisory Service as an Aid Towards a New Working Frame, *Proc. 3rd European Conference on Architecture*, Florence, Italy

Rousseau, P.G., Mathews, E. H. and Grobler, L. J., 1993, Integrated Thermal Simulation of Buildings and Regenerative Evaporative Coolers, *Building and Environment*, Vol. 29, No. 1, pp. 33-42.

2.1 INTRODUCTION

Computer simulation has consistently increased its application in a variety of engineering disciplines and has become an indispensable tool in design and operational managements contexts. Computer technology has encouraged rapid advances in calculation procedures to predict the thermal performance and energy demands of buildings. A considerable effort by the research community has been focussed on the development of building design tools which are able to examine the energy implications of design decisions.

The present chapter is concerned with building thermal simulation in general. Section 2.2 explains how building thermal calculations have evolved from the early days to the present day. The necessity for more integrated design tools is emphasised in Section 2.3. Section 2.4 describes how the present work is placed within this context of integration and finally Section 2.5 introduces the simulation tools chosen to perform the work.

2.2 EVOLUTION OF BUILDING SIMULATION

The built environment can be classified as a complex system with several sub-systems interacting each with the other. Continuous energy transfer processes take place among the building's inter-connected regions such as rooms, walls, windows, duct linings, etc. This complexity is further magnified by the dynamic behaviour of the system responding to the climate changes. Highly non-linear equations are thus necessary to represent inter-related energy exchanges among the regions. Therefore, accurate system modelling becomes a complicated task if the spatial and temporal integrity of the systems is to be preserved.

As described by Clarke and Maver (1991), building energy modelling has rapidly evolved over the years from the early traditional methods to the contemporary simulation design tools (see Table 2.1). Traditionally, building modelling methods were employed to evaluate the energy requirements and construction budgets at the detailed design stages. Such approaches are based on manual and handbook oriented methods. The calculations are analytical and many assumptions are necessary to make the formulation possible. For instance, the system is only partially modelled and the dynamic system behaviour is assumed steady. The methods are fragmented and no apparent interactions

between the individual calculations take place. Consequently, system integrity is not maintained since the real energy flow-paths cannot be fully represented and therefore, only a qualitative assessment of the building performance is possible. The modelling methods require from the user a refined knowledge to evaluate the results applicability as the lack of sophistication of such methods cannot provide realism.

Table 2.1 Evolution of building simulation tools (Clarke and Maver 1991).

1st generation	Handbook oriented Analytical Simplified Piecemeal	Indicative Application limited Difficult to use
2nd generation	Dynamics important Still analytical Still piecemeal Less simplified	Increasing integrity vis-a-vis the real world
	Feedback loop	
3rd generation	Field problem aproach Move to numerical methods Heat and mass transfer considered Better user interface Partial CABD integration	Leading to
4th generation	Full CADB integration More advanced numerical methods Intelligent knowledge-based Advanced software architecture	Predictive Generalized Easy to use

The 2nd generation methods are more computer oriented and can include some dynamic aspects of the system such as the temporal response of constructional elements. Nevertheless, they are still analytic in nature and can only be applied if the system for simulation is linear and described by time invariant parameters. The modelling remains piecemeal with a low level of integrity since sub-systems are treated separately with no evident linking between them. Although some of the traditional method's deficiencies were overcome, and more confidence in design tools was acquired, some problems concerned with technology transfer came to light. The absence of user interfaces and the abundant amount of required input information made the end-user even more skeptical about such design tools. A high degree of knowledge was still necessary to analyse the results and consequently few contributions were made to the design decision process.

The 3rd generation design tools arose to surmount the above mentioned problems. In such systems, all parameters and quantities are interrelated and treated with the same degree of importance and the only independent variables are space and time. All processes are considered interdependent and therefore simultaneous processing methods must be invoked. Considering the non-linearity and

complexity of the system of equations involved, advanced numerical solution methods are required to accomplish efficient and accurate time and space integrations. More user friendly interfaces started to be developed with inbuilt I/O graphical facilities. As modelling integrity improved and appropriate user interfaces were developed, the reality can be better predicted and the design tool is becoming easier to use and more widely applicable.

2.3 IMPROVING MODELLING INTEGRITY

Although thermal modelling is a complicated task, this is only one aspect to be considered in the design process. Building design is a complex process in which many elements are combined into a unified structure. Economy, functionality, aesthetics and security aspects are all interrelated subjects to be taken into account during building design. For convenience, complexity and/or economic reasons, there is a lack of information among the professionals involved in these areas. They usually operate on an island of isolation and communication only takes place in the late design stages when this is inevitable. Consequently, the design becomes the attainment of a simple solution to satisfy the minimum requirements of aesthetic, comfort, security and functionality.

Nevertheless, any decision taken by any design participant may have significant effects in other areas during the whole design process. Many decisions made at the early design stages have substantial influence on the building energy requirements. Building form, orientation or glazing design are decided without much consideration of cooling and heating loads. For instance, increasing the window size will increase conduction losses/gains (increasing heating/cooling loads), increase solar gains (reducing heat loads and increasing cooling loads) and increase daylight (reducing lighting loads and therefore cooling loads and possibly increasing heating loads). If energy efficient solutions are intended, the balance of such considerations must be found. Few designers can really perceive all the energy implications of this single aspect, and when they do only a qualitative evaluation is possible. Simulation tools would appear to offer an alternative for these intricate matters. The required knowledge if assimilated into such design tools which must guide the designer to safe solutions.

Undoubtedly, the 3rd generation tools with progressive refinement and validation will achieve a degree of confidence and will start to form the core of CABD (Computer Aided Building Design) systems. However, building designers are still not convinced about simulation tools and are constrained to traditional methods. The reasons for this have been discussed in the literature (Andre and Nicolas 1994, Clarke 1993 and Morel and Faist 1993) and include the following:

• More powerful, comprehensive design tools are required to adequately represent the complexity of reality.

- The existing simulation tools involve complex theories and the user must be quite knowledgeable in the subject. There is a need for simpler and more straightforward tools to make their use easier.

- Huge amount of input parameters required. A voluminous amount of data is required at a high level of sophistication which are not available at early design stages. Also, the task of supplying input data is a time consuming process.

- Fragmentation of design tools. Separate tools do not allow a global view of the building and consequently optimisation of building quality, accounting for all domains is not directly possible. In addition, stand-alone tools force the user to enter the same data more than once. This is usually performed in different interfaces, which make the process even more inconvenient and more liable to mistakes.

- End-users are not sufficiently educated. Designers are not familiar with the concepts and terminology of technically oriented programs. Furthermore, the education process involves training and time.

- Not enough time available. The building energy analysis is usually considered a secondary matter in the eyes of the decision-makers, when deadlines are too tight.

- There is a mismatch in terminology among the various professionals involved in the design process.

Improving integrity of design tools is suggested by many (including the authors) as the solution for most of the above shortcomings. They envisage a design tool which incorporates aspects of the different disciplines involved in the building design process, such as thermal analysis, structure, lighting, economics, etc. The environment should embody highly focused models together with generalised ones, first principle approaches linked with empirical or simpler approaches in order to deal with contradictory issues such as power and simplicity. Advanced interfaces, together with a degree of expert knowledge, must be available to support users unfamiliar with the models and computers in general. This universal environment would erode professional barriers, encouraging interdisciplinary collaboration and improve the quality of the design. Therefore, simulations would become part of the design process, rather than a separate constraint added to the many competing for the designer's attention.

The research and industry community have recognised the need and are moving the 3rd generation tools towards more intelligent integrated design environments. With the advent of low price, powerful personal computers with good graphical capabilities, it is now possible to contemplate the provision of the 4th generation design tools. In order to emphasise the importance of integration, some ongoing developments are discussed. These examples seek to approach the problem from

different perspectives:

COMBINE project

This project aims to develop a conceptual basis for future Intelligent Integrated Building Design Systems (IIBDSs) (Clarke *et al* 1995). It is mainly concerned with providing an integrated environment for IIBDSs rather than developing a specific IIBDS. COMBINE (Computer Models for the Building Industry in Europe) seeks to identify the data requirements of a representative set of design tool prototypes (DTPs) (for CAD, for lighting design, for thermal design, for HVAC design, for layout planning, etc). The DTPs are thus united within an integrated data model (IDM) in a way that they can exchange information. The IDM interface intermediates the exchange mechanism by storing and supplying data to DTPs in a format that can be understood by the design tools involved. The tasks, however, is not a trivial one and the evolution of design tools and the possibility to incorporate others in the future must always be considered.

The AEDOT project

The AEDOT (Advanced Energy Design and Operation Technologies) is the US initiative, led by Pacific North-West Laboratory, towards the establishment of an IIBDS (Wright *et al* 1992). The project aims to develop advanced computer-based tools to aid in the design, proper operation and management of energy-efficient buildings. It envisages an enhanced transfer of information from designers to contractor, commissioner, building owner and operator, and also a feedback from the actual building performance to the design team.

Neutral Model Format

The available simulation programs differ much in nature - some are restricted to steady-state methods involving algebraic equations and some are dynamic involving differential and algebraic equation. They also differ in their applicability - some aim at building energy calculation and others at the simulation of HVAC systems. Consequently, a system component is specifically written for a particular solver. If users wish to implement a model developed for a different solver, usually they have to rewrite one or several routines, compile and debug the code. The Neutral Model Format (NMF), first proposed at the Building Simulation '89 conference aims to overcome such difficulties (Sahlin *et al* 1992). The main objective of NMF is to create a common format of model expression for emerging and existing simulation environments. The source standard format is defined and from that the models are automatically translated into the specific format of any simulation program. A second objective is to provide a natural form of model representation in a way that the expression of new models for any environment becomes an easy and fast task. Sahlin also pointed out three possible benefits of such a format:

- The potential of analysis of the simulation environments is enhanced by the creation of common model libraries.

- The model quality and usage is expected to be enhanced since the communication between users of different environments becomes more frequent.

- As the users are free to "navigate" through the environments, repeated environmental comparisons will be carried out, resulting in more accurate information about relative performances.

Energy Kernel System

Considering the stiffness and inflexibility of the current simulation programs, a more flexible and general environment for building energy simulation has been conceived. As a result, some systems, denominated energy kernel systems, have emerged in recent years, such as the US SPARK (Simulation Problem Analysis Kernel), the Swedish MODSIM (Wright *et al* 1992) and the UK EKS (Energy Kernel System) (Clarke and MacRandal 1993). The EKS, for example, has as its main objective the creation of a software environment which facilitate the development, validation and maintenance of thermal simulation programs. The EKS is based on the object-oriented paradigm and is comprised of a taxonomy of classes which allows models of different functionality to be built. The classes represent physical elements of the building - walls, rooms, occupants, light, etc - and abstract elements - heat transfer theories, numerical methods, etc. Simulation programs of different capability and sophistication can thus be automatically constructed by simply selecting and combining the required classes. This means that the user or model developer does not need to handle source code. Additionally, the program integrity is improved since programs of different structures can be constituted from a basic set of classes.

ESP-r

ESP-r (Environment System Performance; r signifying the system's research orientation) (Clarke 1985) is a transient simulation program which enables energy and fluid flow analysis within combined building, plant and control systems. ESP-r allows building modelling with a high degree of integrity by applying a first principle approach. All aspects of energy/fluid flow interactions among the subsystems are treated simultaneously using numerical techniques. The user can invoke the system to assess fabric design, comfort conditions and risks of condensation, and also to evaluate the performance of control and plant systems. Its use is intended not only at the late design stages where detailed information is available but also at the beginning of the design when a simple appraisal of the system is required.

The system has also continuously evolved in order to reproduce the integrity of the real world, incorporating aspects of different disciplines. These are some current developments in this direction:

- MacQueen (1995) incorporated into the system advanced control capabilities such as algorithms of artificial intelligence, features of building energy management systems allowing multi-sensors and hierarchical control, etc.

- Nakhi (1995) is conducting work to account for intra-construction moisture transfer, two and three-dimensional heat conduction in the fabric and construction materials with varying thermo-physical properties.

- Kelly (1995) is attempting to bring power simulation into the ESP-r environment and combining the two forms of energy, electrical and thermal.

- Lighting is being simulated by RADIANCE[#] while controlled by ESP-r at the time-step level (Janak 1995).

- The user interface has constantly been maturing as the system capabilities are enhanced with some integration with CAD (Computer Aided Design) tools already available.

The examples above demonstrate how simulation and design tools are moving towards integration. Within this context, the present work seeks to give its own contribution to this inter-disciplinary integration.

2.4 THE PRESENT WORK

Many elements within the building system, such as air volumes, fabric, plant components and control systems, are in constant heat/fluid flow interactions. Nowadays, building practitioners can rely on powerful simulation modelling tools to predict the complexity involved in such phenomena. As mathematical, discretisation and numerical methods improve, and application knowledge increases, the software systems are becoming more and more sophisticated. Two concurrent development areas, have received much attention in recent years - Building Thermal Simulation (BTS) and Computational Fluid Dynamics (CFD). The methodologies consider the problem in two different ways: a distributed capacity domain is discretised in the first approach, and a fluid domain is (typically) discretised in the second one.

In the BTS context, the building system is composed of a number of interrelated finite regions holding uniform properties with different capacities. These regions, representing fabric, air volumes

---

[#] RADIANCE (Ward 1992) is a research tool developed to predict the distribution of visible radiation in illuminated spaces.

and plant components, are interconnected by means of time varying thermal/flow resistances. Conservation equations of mass and energy are written for each finite region to prescribe convective, conductive, radiative, fluid flow and storage processes at region interfaces while subjecting the system to appropriate climatic conditions, these equations are solved simultaneously and the state of the whole system in time and space is established. In this approach, the finite volumes are usually relatively large and a moderately sized building might be represented by 2000 - 7000 conservation equations (Clarke 1985).

Conceptually, the CFD technique is much the same, differing only in that momentum equations are added to the set of governing equations. This confers to CFD the capability of appling conservation principles at a smaller scale. Because of the possibly higher resolution involved, complex fluid flow phenomena are better described. However, as the size and complexity of the domain is raised, complicated grid structures and prohibitive computing demands are encountered. For example, a coarse grid of 10x10x10 cells would require 7000 conservation equations to represent one single office (if turbulent model equations are included). Therefore, its application is usually restricted to single spaces and a set of boundary and initial conditions must be well-posed (Patankar 1980).

Despite their common characteristics, the techniques focus on different parts of the problem. The BTS focus is on the overall system in the sense that several building aspects are embraced such as plant systems, inter-space air flow, intra-constructional heat flux, occupancy and control systems. On the other hand, a higher system resolution can be obtained with CFD, but generality is usually lost; fluid flow analysis might be restricted to specific components because of the high computational burden involved. Obviously, the situation brings some limitations to the approaches, such as:

- BTS usually do not account for air flow property gradients within a single space and also internal surface convection cannot properly be computed. Surface heat fluxes, local thermal comfort and air quality may not be well represented, compromising the evaluation of the whole system performance.

- CFD representation of dynamic boundary conditions (such as ventilation, infiltration rates, surface temperatures) is deficient. This lack of proper information at the boundary may lead to the reduction of flow modelling accuracy.

As can be observed, the approaches can cover each others deficiencies and a combination of the two seems appropriate to overcome such problems. BTS can provide CFD with boundary conditions to enhance local flow calculation, and the flow property gradients evaluated by CFD can be utilised by BTS to improve the whole building performance prediction. The resulting conflated tool would

strengthen the modelling potential of each method by combining their functionality. The application of such an approach might be convenient in cases where only part of the system needs a more detailed analysis. For example, the whole building system comprising fabric, plant, control, etc can be modelled employing BTS, while CFD is invoked to model a small part of the building. For instance:

- a local source of pollutant spreading to the rest of the building;
- buildings embodying large horizontal (eg open-plan offices) or vertical (eg atria, staircases) enclosures;
- spaces with thermal stratification (eg displacement ventilation, large openings).
- complex fluid flow phenomena taking place in specific plant components (eg evaporators, condensers)

In the context of the ongoing developments, the proposed approach aims to increase the power and robustness of simulation tools by improving their integrity. The intention is to bring the two techniques within one single simulation environment. Since different degrees of complexity and sophistication are involved in the integration, the hope is that both designers and developers will benefit from this work.

The need to integrate such techniques has also been recognised by others, and some initiatives have already been taken:

- Schaelin *et al* (1993) have linked the multizone air flow program COMIS to the commercial CFD package PHOENICS. Pressure, velocity and contaminants are the variables interchanged at the interface of the domains but the multizone model does not handle energy transport and the temperature profile must be known in advance. One program is executed after the other in sequence to account for reciprocal effects. A source of contaminant within a zone was modelled either by CFD or COMIS and its effect throughout the building was accounted for by COMIS. They concluded that an average contaminant value is not representative for the zone where the source is located and that this average value may compromise the evaluation in the whole building.

- Chen (1988) pointed out the importance of temperature gradients on the determination of air conditioning loads. He suggests that this problem could be overcome by combining the cooling load program ACCURACY and a CFD model. In his work, he assumes that temperature gradients do not influence the air flow pattern and that buoyancy can be determined for typical situations. His technique consists of computing previously the air flow distributions for different kinds of boundary conditions, such as various inlet mass flow rates and different heat gains from

windows and then, when an annual simulation is performed by the cooling load program (ACCURACY), the program searches for one of the air flow patterns pre-calculated and corresponding to a given boundary condition. The air temperature distribution is then calculated from the energy equation and is based on the given boundary condition and the pre-determined flow field. He then compared the uniform air room temperature with his methodology to determine the air conditioning load. He concluded that the uniform model is not a suitable approach for the tested cases and that his methodology predictions are corroborated by experimental data.

However, when compared to these two cases, the present work is more comprehensive since it tries to embody several aspects of building simulation such as fluid flow, plant and control systems, lighting, etc within one computational environment, as described in the following chapters.

2.5 MODELS CHOSEN TO CONDUCT THE PROJECT

The development of simulation tools to model the phenomena explained above is a complicated task demanding a substantial time investment (some simulation environments have been under developed for the last 20 years) and effort. Therefore, starting the tool development from scratch does not seem a reasonable option since many tools have already reached a high degree of sophistication. For this reason, it was decided to base the current work on an existing tool.

The BTS environment, ESP-r, which has been under development for more than 20 years at the University of Strathclyde is the system adopted to conduct the present work. The fact that such a system is now being used throughout the world with constant feedback from several institutions and the fact that it has been subjected to various international validation programmes (Jensen 1994 and Lomas *et al* 1994) confer increasing confidence in the program.

These are some characteristics of the system which justify its choice regarding, simultaneity, integrity, rigour, user interface (ease of use) and multi-disciplinarity:

- It is a state-of-the-art research environment which aims to simulate the real world as rigorously as possible. First principle approaches are invoked to reproduce the reality integrity.
- The system embodies simple and detailed approaches, offering the possibility to combine them.
- Multi-disciplinary works have been carried out within the program (as mentioned in section 2.3).
- Advanced numerical techniques are used to treat the simultaneous energy/flow interactions among building and plant systems.

- The system offers a user interface with extensive graphical facilities.

- The system is well documented: training instructions with comprehensive exemplars and an inbuilt tutorial are available which are regularly updated as the system evolves.

Regarding the integration of BTS and CFD these are some of the advantages of the ESP-r system:

- The program is available at source code level and well commented. This makes the understanding of the code easy and allows modifications in order to interact with the CFD model.

- The program offers a highly modular structure which facilitates its comprehension and development. A CFD model can thus be included within the system as a new module without damaging the system integrity.

- Fluid flow simulation is described by means of a unified flow network within the combined building and plant systems which makes the integration with a CFD domain a simple task.

- The system employs the finite volume technique to discretise conservation equations of mass and energy flow as some CFD models.

In order to perform the conflation work, two CFD programs were considered: the commercial package PHOENICS (Rosten and Spalding 1987) and the public domain code TEACH (Gosman and Ideriah 1976). PHOENICS is a robust system which is able to model different kinds of fluid flow in complex geometries (using body fitted coordinates) with a highly graphical interface. As the source code is not available, no modification to the program is allowed. Therefore, the conflation possibilities are restricted: the program must run in parallel with the BTS program. ESP-r must thus be modified to invoke PHOENICS (providing the necessary information) to obtain the required data. On the other hand, TEACH is a two-dimensional, steady-state program which has the basic requirements of interest to CFD modelling: 2-D, mass momentum and energy transport, including turbulence modelled by the $k - \varepsilon$ transport equations. TEACH is available at the source code level and modifications are allowed in order to interact with ESP-r. The second alternative was chosen for been more attractive for the current work.

A new ESP-r CFD module, *dfs* (domain flow solver), was then develop to solve the three-dimensional, turbulent, transient air flow encountered within buildings. *Dfs* offers some graphical capabilities and user interface. Generic grid generation is also available. Some routines of this new program make use of TEACH's original structure: the coefficient generation and the SIMPLE algorithm. Some characteristics of *dfs* are listed:

- The program is available at source code level. This facilitates its proliferation and diffusion into the research community and other sectors and also its integration with a BTS environment.

- It is a relatively small code which can be incorporated within a larger system such as ESP-r. Any change necessary to cope with the interaction of the two systems can be made without a major effort.

- It employs cartesian coordinates which is appropriate to the usually rectilinear geometries of building.

- Reasonable documentation is available.

- The source code is well structured and self explanatory. This facilitates understanding and makes the development process an easy task.

- The discretisation technique employed is the finite volume approach as in ESP-r.

Not only was *dfs* developed to model the air flow encountered within buildings but also its elaboration envisaged the integration of the simulation applications discussed in later chapters.

The current chapter emphasised the importance of numerical simulation within the context of building design. The evolution of simulation/design tools and the course these tools are taking towards an integrated computational environment were described. The present work, which consists of combining a Building Thermal Simulation model with a Computational Fluid Dynamics model, and how this adds to the integrity of simulation tools was also discussed. Finally, the two simulation models chosen to perform the work were introduced, and their characteristics and commonalities pointed out.

The next two chapters describe in detail the ESP-r simulator, *bps*, and the ESP-r CFD module, *dfs*, by explaining their mathematical models, numerical techniques and the system's capabilities. Chapter 5 explains how the two techniques are merged into a single computational environment. Chapters 6 and 7 demonstrates the validity and applicability of the proposed technique.

REFERENCES

Andre, P. and Nicolas, J., 1994, Use of an Integrated Software for Building Design and System Simulation, *Pre-Prints of the Proc. 4th Int. Confer. System Simulation in Buildings*, Liege, Dec.

Chen, Q., 1988, *Indoor Airflow, Air Quality and Energy Consumption of Buildings*, PhD thesis, Delft University of Technology, Delft, The Netherlands.

Clarke, J. A., 1985, *Energy Simulation in Building Design*, Adam Hilger Ltd, Bristol, UK.

Clarke, J. A., 1993, Assessing Building Performance by Simulation, *Building and Environment*, Vol. 28, No. 4, pp. 419-427.

Clarke, J. A., Hand, J. W., MacRandal, D. F. and Strachan, P., 1995, The Development of an Intelligent, Integrated Building Design System within the European COMBINE Project, *Proc. of Building Simulation '95*, Madison, Wisconsin.

Clarke, J. A. and MacRandal, D. F., 1993, Implementation of Simulation Based Design Tools in Practice, *Proceedings of Building Simulation '93* (Adelaide, Aug.), IBPSA, pp. 93-98, Ghent, Belgium.

Clarke, J. A. and Maver, T. W., 1991, Advanced Design Tools for Energy Conscious Building Design: Development and Dissemination, *Building and Environment*, Vol. 28, No. 4, pp. 419-427.

Gosman, A. D. and Ideriah, F. J. K., 1976, *TEACH-2E: A General Computer Program for Two-Dimensional, Turbulent, Recirculating Flows*, Imperial College, London.

Janak, M., 1995, *MPhil Thesis (to be published)*, ESRU, University of Strathclyde.

Jensen, S. O. (ed), 1994, *Validation of Building Energy Simulation Programs*, Part I and II, Research Report PASSYS Subgroup Model Validation and Development, Commission of the European Communities, Directorate General XII for Science, Research and Development, Brussels, EUR 15115 EN.

Kelly, N., 1995, *PhD Progress Report*, ESRU, University of Strathclyde.

Lomas, K., J., Eppel, H., Martin, C. and Bloomfield, D., 1994, *Empirical Validation of Thermal Building Simulation Programs Using Test Room Data*, Volume 1: Final Report, IEA Annex 21.

MacQueen, J., 1995, *PhD Thesis (to be published)*, ESRU, University of Strathclyde.

Morel, N. and Faist, A., 1993, Design Tools for Building Thermal Analysis: The Significance of Integration, *Building and Environment*, Vol. 28, No. 4, pp. 465-473.

Nakhi, A. E., 1995, *PhD Thesis (to be published)*, ESRU, University of Strathclyde.

Patankar, S. V., 1980, *Numerical Heat Transfer and Fluid Flow*, Hemisphere Publishing Corporation.

Rosten, H. I. and Spalding, D. B., 1987, The PHOENICS Beginner's Guide, CHAM Report Number TR/100.

Sahlin, P., Bring, A. and Sowell, E. F., 1992, *The Neutral Model Format for Building Simulation*, Final Report, Department of Building Services Engineering, Stockholm, Sweden.

Schaelin, A., Dorer, V., Van der Maas, J., Moser, A., 1993, Improvement of Multizone Model Predictions by Detailed Flow Path Values from CFD Calculations, *ASHRAE Transactions*, Vol. 99, Part 2, pp. 709-720.

Ward, G., 1992, *The RADIANCE 2.1 Synthetic Imaging System*, Lawrence Berkeley Laboratory.

Wright, A. J., Bloomfield, D. and Wiltshire, T. J., 1992, Building Simulation and Building Representation: Overview of Current Developments, *Building Services Engineering Research and Technology*, Vol. 13, No. 1, pp. 1-11.

The ESP-r Simulator, bps

3.1 INTRODUCTION

A description of the ESP-r system chosen to conduct the present work is now discussed. Since the work focuses on building ventilation processes, the present chapter is mainly devoted to the analysis of energy flowpaths taking place inside zones. The purpose is to introduce the basic requirements necessary to understand the conflation of BTS and CFD as described in Chapter 5.

A brief description of ESP-r's capabilities is given in the next section. Section 3.3 introduces the overall system mathematical model (although special attention is given to inside surface heat balances, air volume heat balance and air flows). The numerical procedure applied to the governing equations is introduced in Section 3.4. Section 3.5 shows how the boundary conditions are established. The numerical solution applied to a single zone heat balance equations and also to the mass flow equations are explained in Section 3.6. Finally, Section 3.7 describes how a problem can be defined in the ESP-r system.

3.2 DESCRIPTION OF THE SYSTEM

ESP-r has a modular structure essentially composed of three main modules: *prj* (project manager), *bps* (simulator) and *res* (results analyser). The first module supports interactive definition of the building, its plant network and its control systems. This is done by accessing satellite modules relating to databases (climate, event profiles, plant components, window properties, etc.) and shading and insolation prediction and view factors, etc.). *Prj* subjects all input data to a legality check and provides building and plant perspective views. It also controls the user's access to the other two main modules. *Bps* performs the simulation of building/plant heat and fluid flows according to the problem defined. Several modules, which are responsible for individual technical aspects of the simulation, comprises *bps*. These correspond to control, fluid flow, plant system, etc. This modular structure allows each module to evolve independently, allowing specialists to be committed only to the development of those modules which are related to their research field. This preserves the integrity of the system when a model is modified or a new model is included, since the modifications can be verified separately from the whole system. The third main module is responsible for the analysis of the results stored by *bps*. Different forms of results are available: perspective visualisations, results interrogation, statistical analysis, graphical display, tabulations, etc. The interaction between the three

modules can be continuous in order to help the building designer make decisions. In other words, the user analyses the results, changes some parameters of the problem and executes new simulations in a iterative loop.

As the current work is concerned with the combination of the simulator (*bps*) with the CFD model discussed in the next chapter, the remainder of this chapter is concerned with the description of *bps*.

Bps presents some graphical facilities, as for example the graphic shown in Figure 3.1. This figure illustrates the monitoring of variables during the simulation process. This capability allows the user to supervise the behaviour of zone air temperatures and heat injections during the solution. This provides the user with an impression of the system performance without having to analyse the complete set of results. If the user is not satisfied with the system's behaviour, he/she can re-set some parameters and run another simulation before analysing the results.
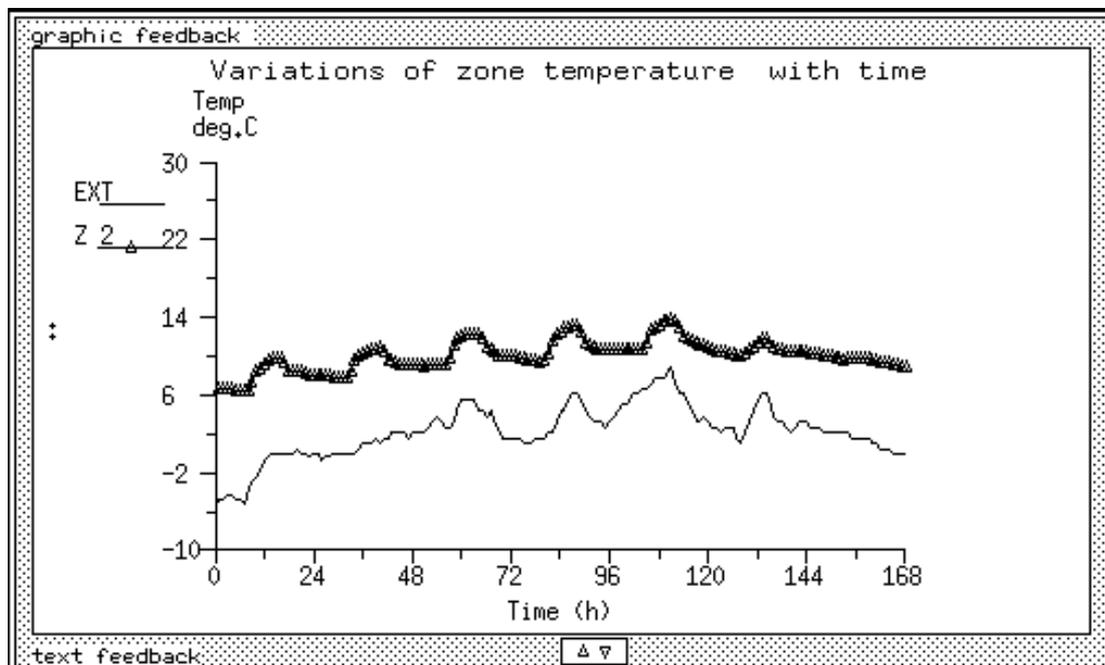

Figure 3.1 Monitoring of external and zone temperatures during a *bps* simulation.

According to Clarke (1985), *bps* seeks to include the different dynamic energy flowpaths taking place in combined building and plant systems which are illustrated in Figure 3.2 and are summarised as:

• Natural (infiltration and inter-zone air flow) and mechanical ventilation.

- Internal and external surface convection.

- Longwave radiation exchanges between internal surfaces.

- Shortwave radiation impinging on internal and external surface as caused by the sun's path.

- Shading (caused by buildings, trees, overhangs, etc.) and insolation on solid surfaces.

- External surface longwave exchanges.

- Moisture transfer through porous media (such as constructions), by ventilation or infiltration or moisture produced by internal sources.

- Casual gains (internal heat sources) as caused by people, lighting and equipment.

- Building/Plant interaction in the form of convective, radiant or mixed heat exchange.

- The control system acting over the combined building and plant system.

- Energy interaction (fluid flow, convection, conduction and radiation) among plant components, such as heat exchangers, boilers, ducts, fans, etc.

Although the principles of heat and mass conservation can be applied to all energy flowpaths described in the previous paragraph, each subsystem (plant network, fluid flow, etc) presents a particular characteristic of energy transfer processes and governing equations. Different solvers are then employed for the subsystem matrices according to their specific features. The *bps* mathematical models and solutions are described by Clarke (1985) and Hensen (1991). The following sections are devoted only to the energy flowpaths taking place inside zones.

3.3 MATHEMATICAL MODEL

The simultaneous presence of multiple energy transfer processes such as conduction, convection, radiation, fluid flow and heat generation imposes certain restrictions on the establishment of a general mathematical model for the whole energy system. An alternative is to apply energy balance techniques to control volumes representing some finite regions, while ensuring that conservation principles are observed within each volume. Consider Figure 3.3 where a control volume (CV) is bounded by a control surface (CS) which is in energetic contact with several other regions. The conservation of any transport process within the volume can be interpreted as ensuring that the rate of storage of a transport property within the CV is equal to the net flux of such a property across the CS plus the portion of the property generated within the volume:

$$[storage\ rate]_{CV}\ =\ [net\ flux]_{CS}\ +\ [generation\ rate]_{CV} \tag{3.1}$$
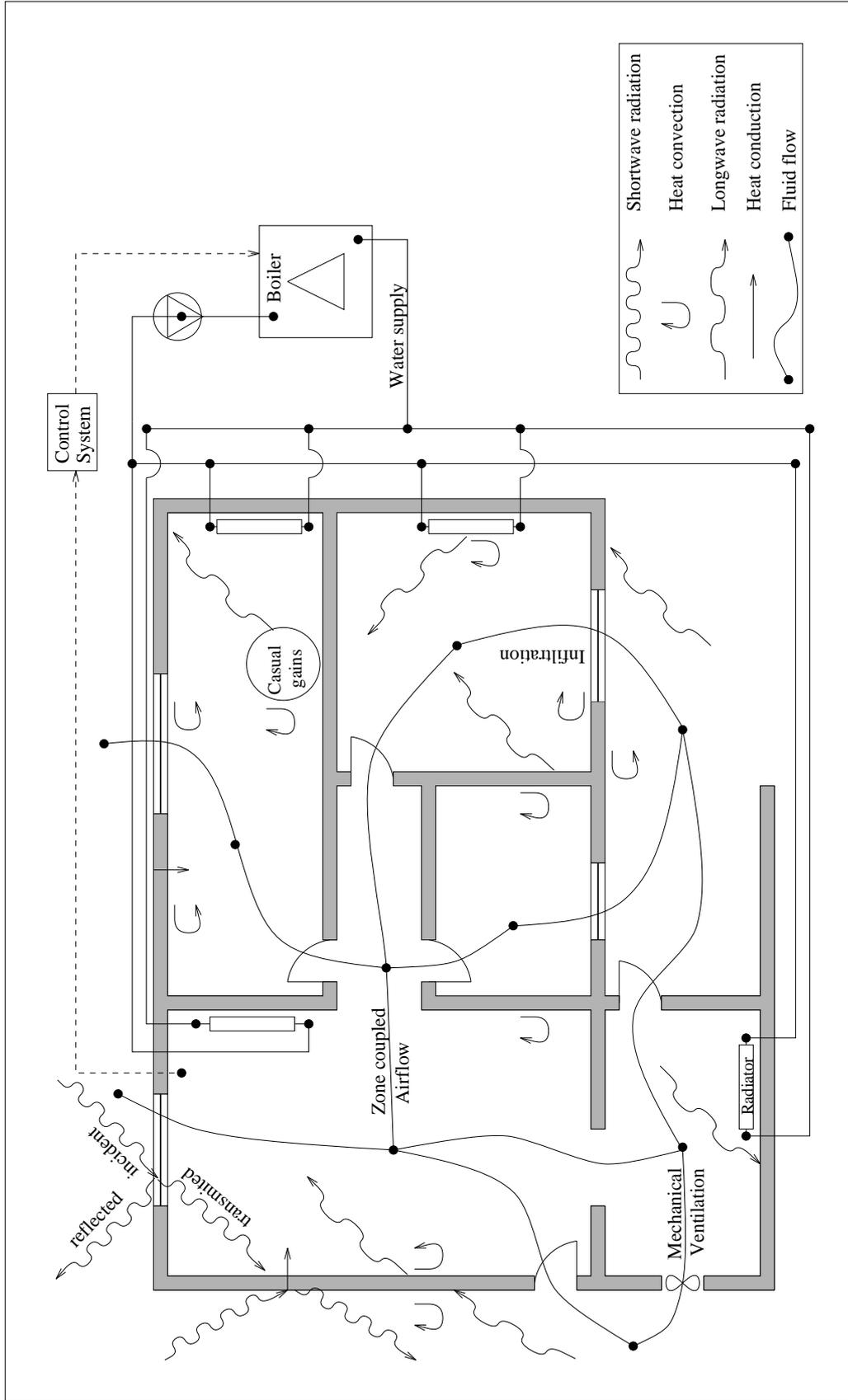
Figure 3.2 Building/plant energy flow paths as modelled within ESP-r
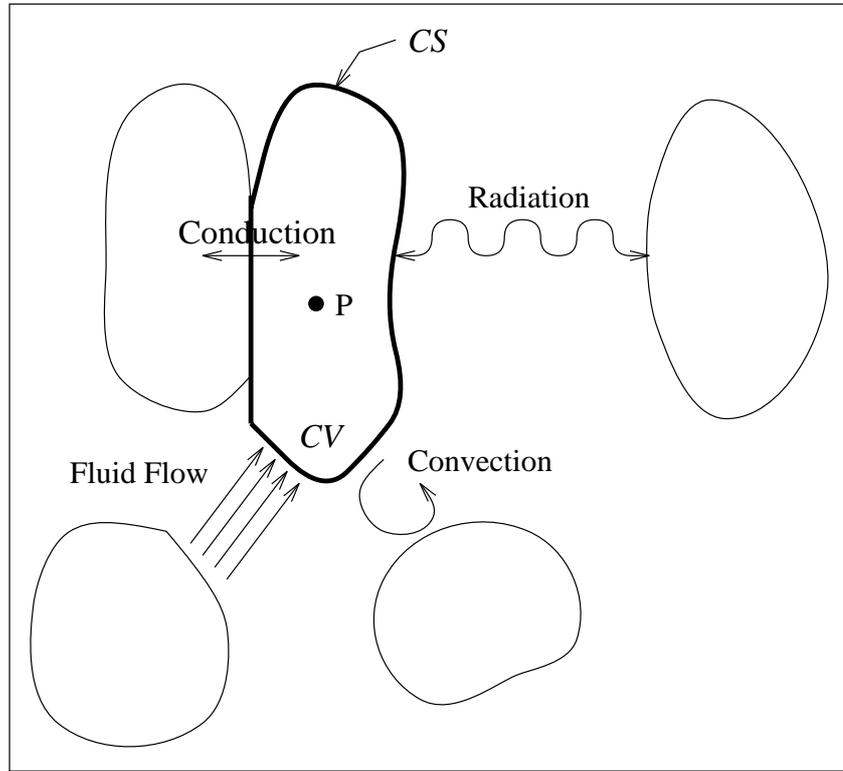
Figure 3.3 Thermal energy transfer in a control volume.

In this context, *bps* suggests that building and plant systems are composed of a number of inter-connected finite regions holding uniform properties. These regions correspond to constructional materials, internal and external zone surfaces, room air volumes, working fluids, plant component interfaces, etc. A conservation equation when written for each finite region gives rise to a set of equations which represents the state of the whole system in time and space. The conservation equation (3.1) for the finite region *P* of Figure 3.3 can be written in the following mathematical form:

$$\frac{\partial}{\partial t}\left(\rho_P \upsilon_P \phi_P\right) = (J_\phi A)_{CS} + S_{\phi_P} \upsilon_P \tag{3.2}$$

where ϕ represents a transport property such as temperature, moisture content, etc, ρ_P is the density of the region P (kg/m^3), υ_P is the volume of the region P (m^3), $(J_\phi)_{CS}$ is the flux of the transport property ϕ through the control surface per unit of area ($kg/m^2 s$ multiplied by the transport property unit), A_{CS} represents the control surface area and S_{ϕ_P} is any energy or mass injected directly to the finite region ($kg/m^3 s$ multiplied by the transport property unit). The transport property flux through the control surface is the result of the energy exchange mechanisms between the finite regions in energetic contact, through conduction, convection, radiation and fluid flow (as illustrated by Figure

3.3). As the flux at the control surface is usually difficult to estimate, it is treated as a function of the transport property differences. Therefore, the product $(J_\phi A)_{CS}$ is expressed as the sum of all inter-volume interactions concerning control volume P:

$$(J_\phi A)_{CS} = \sum_{j=1}^{n} K_{j,P}(\phi_j - \phi_P) \tag{3.3}$$

where j is a finite volume in contact with the volumes P, n is the total number of finite volumes in contact with P, $K_{j,P}$ is the conductance coefficient (representing conduction, convection coefficients, mass flow rates, etc.) between volumes j and P (kg/s). The flux through the control surface can now be expressed as the energy interactions between finite regions. The technique necessary to obtain all conductance coefficients related to the different energy transfer process (conduction, convection, radiation, etc) is described by Clarke (1985). Even the radiation process, which is proportional to temperature to the power of four, can be expressed by equation (3.3), since the non-linearities of the process are accounted for in the conductance coefficient.

Now, because they are used in the integrations presented in Chapter 5, a more specific description of three types of conservation equations are discussed relating to inside surface energy balance, the zone air energy balance and the mass balance. The remaining balances are described by Clarke (1985).

Inside surface energy balance

The dynamic heat conduction taking place inside a multi-layered construction is modelled by dividing the layers into a number of finite regions. These regions are distributed along the internal and external surfaces in order to represent the surface temperatures while the remaining regions are located within the constructional layers as illustrated by Figure 3.4. Special attention is focussed on the convection heat transfer at the inside zone surfaces because this plays a major role on the integrations discussed later. Considering the energy balance for the inside surface, equation (3.2) can be rewritten in the following form:

$$\frac{\partial}{\partial t}(\rho_f v_f T_f) = \sum_{j=1}^{nf-1} K_{j,f}(T_j - T_f) + \frac{h_{f,a}A_f}{c_{p,f}}(T_a - T_f) + S_f v_f \tag{3.4}$$

where T is the temperature, h is the convection coefficient between the surface and the adjacent air layer ($W/m^2 K$) which is a function of the geometry, surface temperature and air temperature and $c_{p,f}$ is the surface material specific heat (J/kgK). A is the surface area, nf is the number of inter-volume interactions with the surface f and the subscripts f and a indicate inside surface and air layer in

contact with the inside surface respectively. The conductance coefficient, K, accounts for conduction and longwave radiation between surfaces. The source term, S_f, for such a balance equation relates to shortwave radiation impinging on the surface and heat injections caused by plant, etc. Many correlations for internal convection coefficients are available in the literature. They are usually defined for specific geometries, range of applications and type of convections (natural or forced) (Alamdari and Hammond 1983).

Zone air energy balance

    The zone air volume is usually in contact with several inside surface layers, adjacent zone air volumes, ambient conditions or plant components. These interactions may cause advection and convection. Equation (3.2), when applied to the zone air energy balance, results in the following expression:

$$\frac{\partial}{\partial t}(\rho_a \upsilon_a T_a) = \sum_{j=1}^{na-ns} K_{j,a}(T_j - T_a) + \sum_{i=1}^{ns} \frac{h_{i,a} A_i}{c_{p,a}}(T_i - T_a) + S_a \upsilon_a \qquad (3.5)$$

where *ns* is the number of surfaces in contact with the air volume, *na* is the number of intervolume interactions with the air volume, the subscript *a* represents the air zone volume and $K_{j,a}$ indicates the other conductance coefficients (advection). The source term represents, for example, plant heat injection at the air node, casual gain, etc.
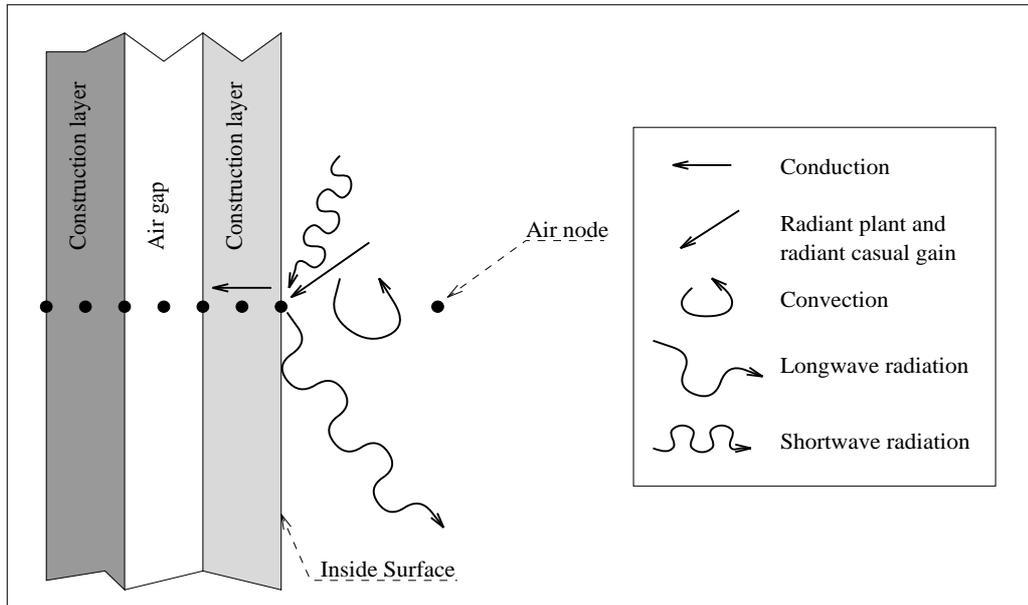

Figure 3.4 Energy interactions at inside zone surface.

Mass balance

The exchange of mass between finite regions can still be represented by the conservation equation (3.2), although it is not explicitly evident. The conservation of mass can then be obtained by making ϕ_P equal to 1 and $K_{j,P}$ equal to the mass flow rates. The potential difference $(\phi_j - \phi_P)$, which governs the transfer process, indicates, in this case, only the direction of flow; positive if flow is entering or negative if flow is leaving the region. Considering that the flow is incompressible, the mass conservation equation based on equation (3.2) assumes the following form (observe Figure 3.5)

$$\sum_{j=1}^{n} \dot{m}_{j,P} = S_{\dot{m}_P} v_P \tag{3.6}$$

where, $\dot{m}_{j,P}$ is the mass flow rate between the region j and P and $S_{\dot{m}_P}$ is the source of mass at the region P. Although the continuity equation is necessary it is not sufficient to determine mass flow rates. Since momentum equations are not required in such an approach, the flow is considered to be governed by pressure and/or temperature differences. The flow connecting the finite regions can be described by a nonlinear relationship between mass flow rate, pressure and temperature differences:

$$\dot{m}_{j,P} = f(\Delta P_{j,P}, \Delta T_{j,P}) \tag{3.7}$$

where $\dot{m}_{j,P}$ represents the mass flow rate through the flowpaths, such as doorways, cracks, ducts, fans, etc., $\Delta P_{j,P}$ and $\Delta T_{j,P}$ are respectively the pressure and temperature differences across the flowpaths. P accounts for static pressure, dynamic losses and stack effect. The temperature difference is included to assess possible bidirectional flow taking place at large openings such as doorways. The $f(\Delta P, \Delta T)$ function representing different flow components is usually an empirical correlation and a collection of them are available in the literature (e.g. Hensen 1991). Although equation (3.7) is not a multi-dimensional equation its functionality is similar to the momentum equations which consider flow directions. The flow direction in the present model must be *a priori* known by the user.

Control schedules (in the form of equations or algorithms) are added to the set of conservation equations to impose conditions on the system's behaviour.

3.4 NUMERICAL APPROACH

Because of the complexities (most of them associated with estimating values of conductance coefficients and boundary conditions) involved in the energy transfer processes mentioned above, an analytical solution for the set of equations (3.2) is restricted to special cases. On the other hand, a numerical solution can be applied to any transfer process represented by equation (3.2). Although it is

an approximation, the degree of reliability of the numerical solution is in most applications satisfactory.
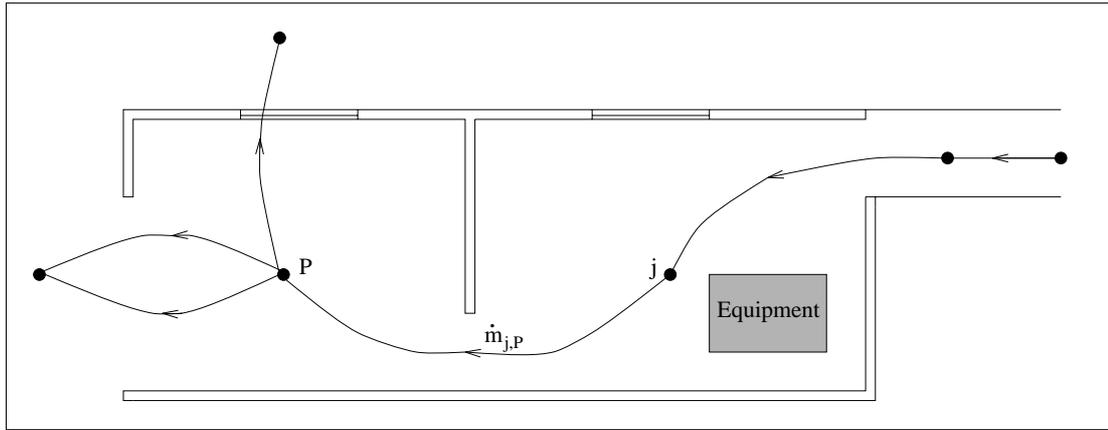
Figure 3.5 Mass flow interactions at a finite region.

A discretisation technique is always necessary to make possible the use of a numerical approach. As can be noticed, the conservation equations above were already introduced in their spatial discretised form. This discretisation technique is usually referred to as the finite volume method (FVM). The complete discretised form, in time and space, is obtained by integrating equation (3.2) over a finite time interval, δt:

$$\upsilon_P[\rho_P\phi_P - \rho_P^-\phi_P^-] = \sum_{j=1}^{n} K_{j,p}^{\xi}(\phi_j^{\xi} - \phi_P^{\xi})\delta t + S_{\phi_P}^{\xi}\upsilon_P\delta t \tag{3.8}$$

where the superscript $-$ represents the property at the beginning of some time interval (present values) and the superscript ξ indicates the values within the time interval. The symbols without superscript are the values at the end of the time interval (future values). Since the variations of the properties over the time interval is unknown, an approximation for the values at ξ must be assumed. Usually, those values are approximated by present values, characterising the explicit formulation, or future values (implicit formulation). An alternative is a combination of the two schemes, as suggested by Patankar (1980):

$$\theta^{\xi} = \gamma\theta + (1 - \gamma)\theta^- \tag{3.9}$$

where θ is any value at time ξ, γ is a weighting factor accepting values between 0 (explicit formulation) and 1 (fully implicit formulation). Although a default value of $\gamma = 0.5$ (Crank-Nicolson

scheme) is assumed in *bps*, the user has control over the degree of implicitness and can change γ whenever necessary. The effects of implicitness in *bps* are discussed elsewhere (Hensen and Nakhi 1994). Substituting equation (3.9) into equation (3.8) gives an expression in terms of present and future values. Dividing equation (3.8) by δt results in the expression:

$$\frac{\upsilon_P}{\delta t}(\rho_P\phi_P - \rho_P^-\phi_P^-) = \gamma \sum_{j=1}^{n} K_{j,P}(\phi_j - \phi_P) +$$

$$(1-\gamma)\sum_{j=1}^{n} K_{j,P}^-(\phi_j^- - \phi_P^-) + \gamma S_{\phi_P}\upsilon_P + (1-\gamma)S_{\phi_P}^-\upsilon_P \quad . \tag{3.10}$$

Finally, the set of conservation equations are rearranged and expressed only in terms of future values (unknowns) and source terms (known values) before they are solved. The general equation (3.10) results in the following expression:

$$a_P\phi_P - \sum_{j=1}^{n} a_j\phi_j = b_P \tag{3.11}$$

where

$$a_P = \gamma \sum_{j=1}^{n} K_{j,P} + \frac{\upsilon_P\rho_P}{\delta t}, \qquad a_j = \gamma K_{j,P}$$

and

$$b_P = \gamma S_{\phi_P}\upsilon_P + (1-\gamma)\left[\sum_{j=1}^{n} K_{j,P}^-(\phi_j^- - \phi_P^-) + S_{\phi_P}^-\upsilon_P\right] + \frac{\upsilon_P\rho_P^-\phi_P^-}{\delta t} \quad .$$

This algebraic equation is the basic form for the solution procedure introduced in Section 3.5. This equation suggests that only transport properties are unknown and must be computed, however the equation can still be rearranged in order to determine the future source term as a function of the transport property: for example, what is the heat that should be injected at an inside surface to keep the zone air temperature constant over some control period?

3.5 BOUNDARY CONDITIONS

Before the set of equations, represented by equation (3.11), can be solved, the boundary conditions of the problem must be defined; these are necessary for both building and plant systems.

For simplicity, the building conditions are introduced in this section. These conditions must be established for the transport equations of temperature and pressure. They are usually imposed at inside and outside zone surfaces, openings and zone air nodes and can be classified as follows.

Climate

The dynamic behaviour of the building system is dictated by the weather variations. In numerical simulation, the discretised nature of the equations require that the climatic conditions be in the form of time-series data. These data are generally collected at frequencies of one hour or greater at meteorological stations around the world. The climate variables necessary to support *bps* simulations are diffuse horizontal solar intensity (W/m^2), dry bulb temperature (^oC), direct normal or global horizontal solar intensity (W/m^2), wind speed (m/s), wind direction (^{o} from north, clockwise) and relative humidity (%). ESP-r has available a number of annual data collections containing hourly values of the climatic variables. These data collections also contain the year to which the climate relates, a description of the site and the site latitude and longitude difference from the reference meridian.

Ground conditions

Normally at least one of the constructions in a *bps* simulation will have contact with the ground. Thus, the outside surface of such a construction will be exposed to the ground temperature. ESP-r offers a set of temperature profiles representing the annual variation of the ground temperature for different geographical locations (in the form of 12 values describing each month's average temperature). The user can also specify alternative temperature profiles which suit the building location under analysis.

Known conditions

This type of condition is usually employed when part of the building is not involved in the simulation. For instance, a zone is in contact with a zone which is not participating in the simulation. An estimate of the non-participating zone's air temperature, and of any radiation impinging on the outside surface of the participating zone, can be provided. Another possibility is to establish an adiabatic condition at the outside surface of the participating zone.

When modelling mass flows such conditions can also be employed. If pressure and temperature are known, or guessed, then these can be assigned to certain finite volumes (nodes) of the network.

Identical environments

In this case, some non-participating zone is assumed to have identical conditions to the participating one.

The above types of boundary conditions can be applied to different finite volumes depending on the problem defined. An explanation of how to introduce these boundary conditions to the finite volumes follows.

Exterior nodes

Within *bps*, external conditions are represented by finite volumes to which are assigned temperature and pressure. The temperature is directly obtained from the climate collection. Pressure, if declared to be wind induced, is dependent on the local wind speed and facade obstructions. As reported by Hensen (1991), pressure coefficients which account for the effects of obstructions are employed to compute the wind induced pressure. ESP-r has several sets of pressure coefficients available with each set referring to alternative exposures, dimensions and inclinations of the facade. The local wind speed is a fraction of the wind speed read from the climate collection. The ratio between the two speeds being defined as a wind reduction factor which is evaluated from a power law profile, a logarithmic law profile, or some other suitable profile.

Surface nodes

Three different conditions can be defined at outside surfaces (transparent or opaque): the surface can be in contact with the exterior node, with a ground node or with some constant condition. In the first case, convection takes place between the exterior node and the outside surfaces as a function of the external temperature, wind speed and surface geometry. Also, shortwave radiation impinges on the surface in the form of an energy source term. The temperature of the sky, the ground and the neighbouring buildings are estimated in order to compute exchanges of longwave radiation flux between the outside surface and the surrounding environment. In the second case, the ground temperature profile is established at the outside surface. Lastly, a constant condition may be imposed at the surface.

The zone inside surfaces can be subjected to shortwave radiation transmitted through transparent surfaces. Such heat loads are injected at the surfaces as a source term of the energy conservation equation.

Inside node

At certain nodes of the mass flow network (representing, for example, a non-participant zone air condition or the flow condition at a plant component) a constant condition can be established. Pressure and temperature are, thus, fixed at those nodes.

3.6 SOLUTION PROCEDURE

After establishing the conservation equations which represent energy and mass flow paths between all communicating finite regions of the system within some finite period of time, the set of algebraic equations must be solved. While the final set of equations were presented in a linear form, the coefficients representing the processes of conduction, convection, radiation and fluid flow are non-linear functions of the transport variable. In order to increase the solution efficiency, two different procedures are applied according to the nature of the conservation equations and of the coefficients. The first procedure is employed to solve the set of energy balance equations (3.2) and the second one is directed to the solution of the mass conservation equations (3.6).

Solution of the energy equations

At each finite period of time the algebraic energy conservation equations derived from equation (3.11) are established and are written in matrix notation as,

$$[A(T)][T] = [B(T)] \tag{3.12}$$

where T is the vector of unknown nodal temperatures and heat injections, A is a non-homogeneous sparse matrix containing the future time-row coefficients which are time dependent. The matrix holding the present values and the known boundary excitations at the present and future time-rows is represented by the column matrix B. Because of the implicitness of the equations, the set of equations (3.12) must be solved simultaneously at each simulation time-step. However, A is a sparse matrix holding many non-zero coefficients and its inversion by a direct method is computationally expensive. Since the matrix A is composed of clusters of equations referring to different sub-systems, an efficient solution process consists of partitioning A into a series of sub-system matrices (representing each building zone and the plant system). Each partitioned matrix is then processed separately and information is exchanged between each solution stream in order to allow the global solution to evolve. The overall solution procedure, which consists of the direct solution of each building zone and plant submatrix independently, and the integration of these sub-solutions, is explained by Clarke (1985). In this section, only the solution method for the equations involved in a single zone is introduced as this is employed in the method derived in Chapter 5.

In order to exemplify the solution scheme, consider the single zone shown in Figure 3.6a which is bounded by six multi-layered constructions. The air is completely mixed inside the zone and a control schedule is not applied. The dynamic, one-dimensional heat conduction within constructions, as explained in this section, is the default model installed within ESP-r[#]. Figure 3.6b illustrates how

---

[#] A multi-dimensional heat conduction analysis is also available within ESP-r (Nakhi 1995).

the single zone problem can be discretised into finite regions in which one finite volume represents the totally mixed zone air and several others are distributed along the normal axis of each constructional element. It should be noticed in Figure 3.6b that two of the constructional nodes represent the internal and external surfaces and the others are placed within the constructional element. Each internal surface node may interact with other surface nodes through longwave radiation exchanges and with the zonal air node through heat convection processes. Adjacent zone conditions are assumed to be known at the future time-row. The resulting set of equations, written in the form of equation (3.12), is illustrated by the matrix equation shown in Figure 3.7. The derivation of the a coefficients is explained by Clarke (1985). $T_{f,A}$, $T_{f,B}$, ... represent the inside surface temperatures, T_a is the zone air temperature, $T_{1,A}$, $T_{1,B}$, ... are outside surface temperatures and the other T are intra-construction node temperatures. The constructional energy balance equations are located in sequence in the matrix of Figure 3.7. The three equations, one for each node of construction 1, are located at rows 1 to 3, the five balance equations of the second construction are placed at rows 4 to 8, and so on. They are also located from outside to inside for each construction such that row 1 is the outside surface balance, row 2 is the intra-construction balance and row 3 is the inside surface balance of the first construction. The intra-construction balance equations hold three coefficients (the self-coupling and the adjacent nodes coupling coefficients) to represent the transient heat conduction. The inside surface energy balance equations are placed at rows 3, 8, 13, 16, 23, 26 of Figure 3.7, row 27 is the zone air energy balance and the remaining rows are the intra-construction and outside surface heat balances. The coefficients coupling the inside surface node equations express the longwave radiation exchanges.

As can be seen, the single zone matrix is sparse, suggesting an approach based on partitioning. The matrix is decomposed into a series of sub-matrices, each one representing a multi-layered construction. These matrices, which hold the coefficients relating to the intra-construction heat conduction and storage, can be seen in Figure 3.8. Figure 3.9 displays the surface and air point equations grouped in another sub-matrix. The matrix coefficients of Figure 3.9 represent the zone inter-surface radiation exchanges, surface convection, fluid flow and heat storage. Notice that the linkages between the construction sub-matrices and the zone balance sub-matrix are maintained by the coefficients $a_{2,3}$, $a_{7,8}$, $a_{12,13}$, $a_{15,16}$, $a_{22,23}$ and $a_{25,26}$ of Figure 3.8 and by the coefficients $a_{3,2}$, $a_{8,7}$, $a_{13,12}$, $a_{16,15}$, $a_{23,22}$ and $a_{26,25}$ of Figure 3.9. Those coefficients are connections between the inside surface nodes and the intra-construction, next-to-inside surface nodes.

The solution is achieved by a direct method. A forward reduction process is performed on each construction submatrix of Figure 3.8, eliminating all coefficients below the main diagonal. Figure 3.10 shows the reduced matrices. This process modifies the diagonal coefficients and the source coefficients. The last row of each reduced matrix of Figure 3.10 (which is the modified, energy balance equation related to the next-to-inside surface node) now holds only the coefficients related to the next-to-inside and inside surface temperatures. These equations are now employed to eliminate the coefficients related to the next-to-inside surface nodes of Figure 3.9; coefficients $a_{3,2}$, $a_{8,7}$, $a_{13,12}$,

$a_{16,15}$, $a_{23,22}$, $a_{25,26}$. This is achieved by multipling the modified equations by the ratios $-a_{3,2}/a_{2,2}^x$, $-a_{8,7}/a_{7,7}^x$, $-a_{13,12}/a_{12,12}^x$, $-a_{16,15}/a_{15,15}^x$, $-a_{23,22}/a_{22,22}^x$, $-a_{25,26}/a_{25,25}^x$ and adding them to the matrix of Figure 3.9. This results in the matrix of Figure 3.11. As can be seen, the diagonal coefficients and the right-hand side terms *b* are modified and the next-to-inside surface coefficients have been removed. The zone balance matrix of Figure 3.11 now holds only surface and air node coefficients and therefore can be solved for the related variables. A forward reduction is conducted and the coefficients below the diagonal of this modified matrix are eliminated, resulting in the reduced matrix of Figure 3.12. At this point, the inside surface and air node temperatures can be obtained from backward substitution. Finally, the values of the inside surface temperatures are substituted in the reduced constructional matrices of Figure 3.10 and the intra-construction node temperatures are obtained from a backward substitution in the reduced construction matrices. In conclusion, all energy equations representing the flow paths in a single zone are solved simultaneously by employing a direct method for one time-step. The complete solution for a certain simulation period is accomplished by re-establishing the matrix coefficients and solving for each subsequent time-step.
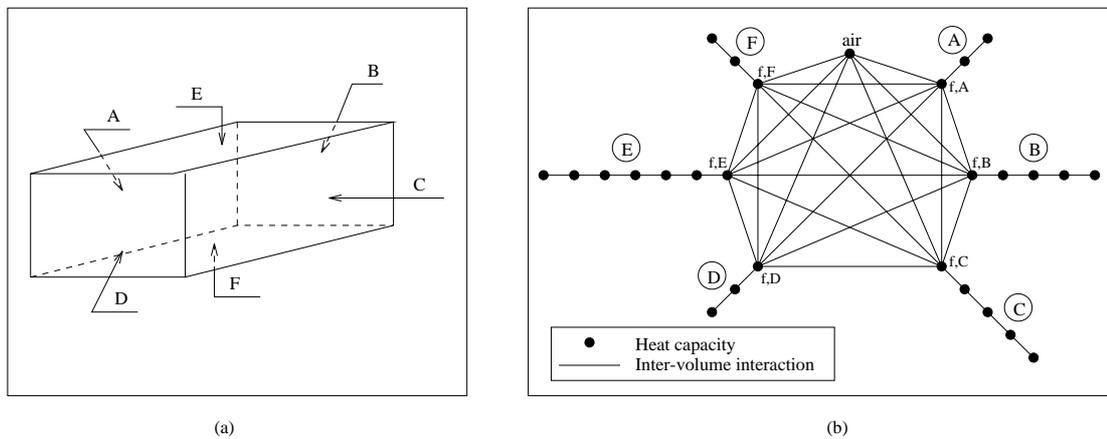
Figure 3.6 (a) a single zone system and (b) the equivalent volume discretisation.

For multi-zone systems two options exist for the solution: either each zone can be solved independently as above, inter-zone processes being imposed one time-step in arrears or the solution process can be made to iterate across all zones to achieve an overall simultaneous solution.
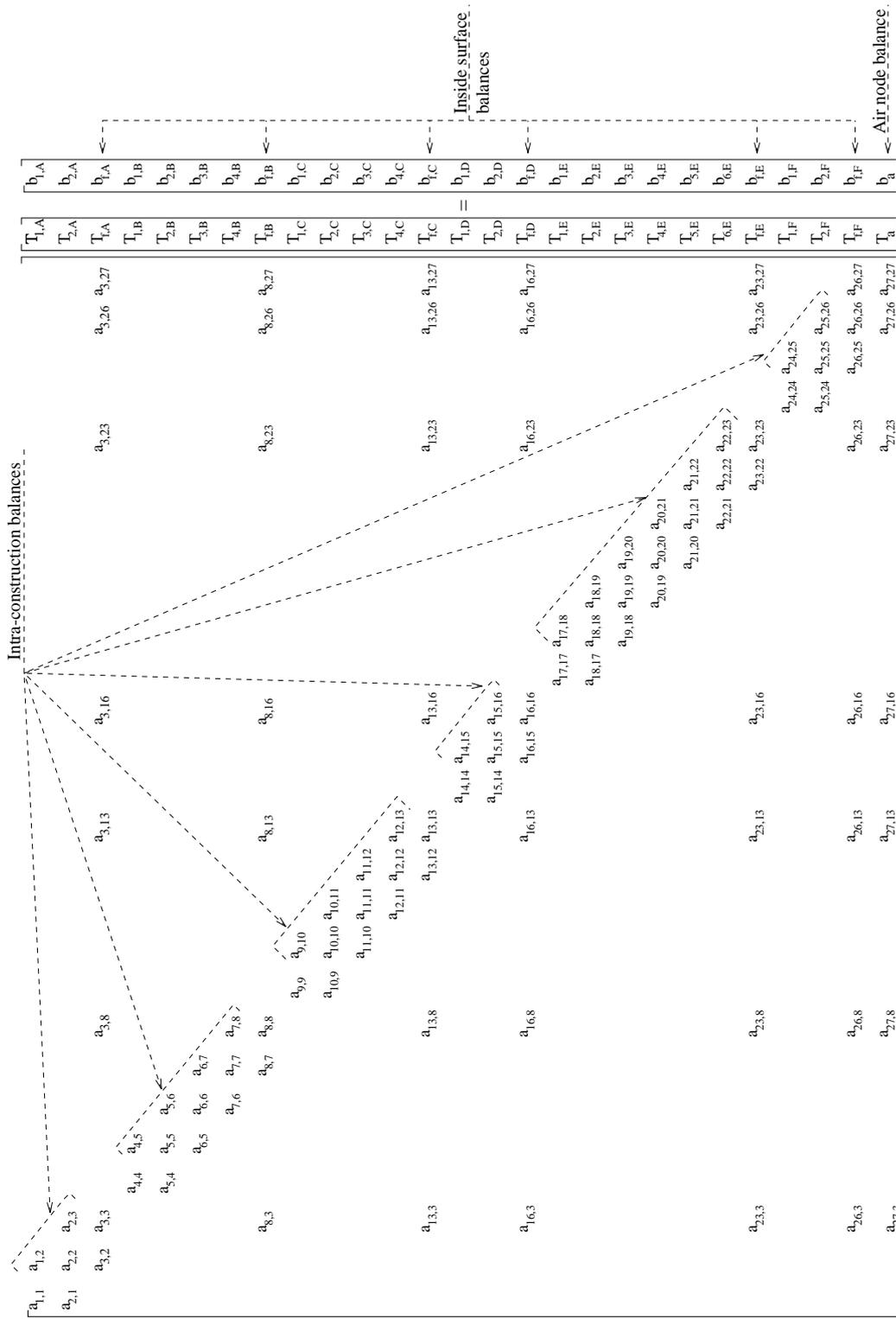
Figure 3.7 Overall single zone matrix (from Clarke 1985).

$$
\begin{bmatrix} a_{1,1} & a_{1,2} \\ a_{2,1} & a_{2,2} & a_{2,3} \end{bmatrix}
\begin{bmatrix} T_{1,A} \\ T_{2,A} \\ T_{f,A} \end{bmatrix} =
\begin{bmatrix} b_{1,A} \\ b_{2,A} \end{bmatrix}
\qquad
\begin{bmatrix} a_{4,4} & a_{4,5} \\ a_{5,4} & a_{5,5} & a_{5,6} \\ & a_{6,5} & a_{6,6} & a_{6,7} \\ & & a_{7,6} & a_{7,7} & a_{7,8} \end{bmatrix}
\begin{bmatrix} T_{1,B} \\ T_{2,B} \\ T_{3,B} \\ T_{4,B} \\ T_{f,B} \end{bmatrix} =
\begin{bmatrix} b_{1,B} \\ b_{2,B} \\ b_{3,B} \\ b_{4,B} \end{bmatrix}
$$

$$
\begin{bmatrix} a_{9,9} & a_{9,10} \\ a_{10,9} & a_{10,10} & a_{10,11} \\ & a_{11,10} & a_{11,11} & a_{11,12} \\ & & a_{12,11} & a_{12,12} & a_{12,13} \end{bmatrix}
\begin{bmatrix} T_{1,C} \\ T_{2,C} \\ T_{3,C} \\ T_{4,C} \\ T_{f,C} \end{bmatrix} =
\begin{bmatrix} b_{1,C} \\ b_{2,C} \\ b_{3,C} \\ b_{4,C} \end{bmatrix}
\qquad
\begin{bmatrix} a_{14,14} & a_{14,15} \\ a_{15,14} & a_{15,15} & a_{15,16} \end{bmatrix}
\begin{bmatrix} T_{1,D} \\ T_{2,D} \\ T_{f,D} \end{bmatrix} =
\begin{bmatrix} b_{1,D} \\ b_{2,D} \end{bmatrix}
$$

$$
\begin{bmatrix} a_{17,17} & a_{17,18} \\ a_{18,17} & a_{18,18} & a_{18,19} \\ & a_{19,18} & a_{19,19} & a_{19,20} \\ & & a_{20,19} & a_{20,20} & a_{20,21} \\ & & & a_{21,20} & a_{21,21} & a_{21,22} \\ & & & & a_{22,21} & a_{22,22} & a_{22,23} \end{bmatrix}
\begin{bmatrix} T_{1,E} \\ T_{2,E} \\ T_{3,E} \\ T_{4,E} \\ T_{5,E} \\ T_{6,E} \\ T_{f,E} \end{bmatrix} =
\begin{bmatrix} b_{1,E} \\ b_{2,E} \\ b_{3,E} \\ b_{4,E} \\ b_{5,E} \\ b_{6,E} \end{bmatrix}
\qquad
\begin{bmatrix} a_{24,24} & a_{24,25} \\ a_{25,24} & a_{25,25} & a_{25,26} \end{bmatrix}
\begin{bmatrix} T_{1,F} \\ T_{2,F} \\ T_{f,F} \end{bmatrix} =
\begin{bmatrix} b_{1,F} \\ b_{2,F} \end{bmatrix}
$$

Figure 3.8 Partitioned construction matrices (from Clarke 1985).

$$
\begin{bmatrix}
a_{3,2} & a_{3,3} & & a_{3,8} & & a_{3,13} & & a_{3,16} & & a_{3,23} & & a_{3,26} & a_{3,27} \\
 & a_{8,3} & a_{8,7} & a_{8,8} & & a_{8,13} & & a_{8,16} & & a_{8,23} & & a_{8,26} & a_{8,27} \\
 & a_{13,3} & & a_{13,8} & a_{13,12} & a_{13,13} & & a_{13,16} & & a_{13,23} & & a_{13,26} & a_{13,27} \\
 & a_{16,3} & & a_{16,8} & & a_{13,13} & a_{16,15} & a_{16,16} & & a_{16,23} & & a_{16,26} & a_{16,27} \\
 & a_{23,3} & & a_{23,8} & & a_{23,13} & & a_{23,16} & a_{23,22} & a_{23,23} & & a_{23,26} & a_{23,27} \\
 & a_{26,3} & & a_{26,8} & & a_{26,13} & & a_{26,16} & & a_{26,23} & a_{26,25} & a_{26,26} & a_{26,27} \\
 & a_{27,3} & & a_{27,8} & & a_{27,13} & & a_{27,16} & & a_{27,23} & & a_{27,26} & a_{27,27}
\end{bmatrix}
\begin{bmatrix} T_{2,A} \\ T_{f,A} \\ T_{4,B} \\ T_{f,B} \\ T_{4,C} \\ T_{f,C} \\ T_{2,D} \\ T_{f,D} \\ T_{6,E} \\ T_{f,E} \\ T_{2,F} \\ T_{f,F} \\ T_a \end{bmatrix} =
\begin{bmatrix} b_{f,A} \\ b_{f,B} \\ b_{f,C} \\ b_{f,D} \\ b_{f,E} \\ b_{f,F} \\ b_a \end{bmatrix}
$$

Figure 3.9 Partitioned inside zone energy balance matrix (from Clarke 1985).

$$\begin{bmatrix} a_{1,1} & a_{1,2} \\ & a_{2,2} & a_{2,3} \end{bmatrix} \begin{bmatrix} T_{1,A} \\ T_{2,A} \\ T_{f,A} \end{bmatrix} = \begin{bmatrix} b_{1,A} \\ b_{2,A}^x \end{bmatrix}$$

$$\begin{bmatrix} a_{4,4} & a_{4,5} \\ & a_{5,5}^x & a_{5,6} \\ & & a_{6,6}^x & a_{6,7} \\ & & & a_{7,7}^x & a_{7,8} \end{bmatrix} \begin{bmatrix} T_{1,B} \\ T_{2,B} \\ T_{3,B} \\ T_{4,B} \\ T_{f,B} \end{bmatrix} = \begin{bmatrix} b_{1,B} \\ b_{2,B}^x \\ b_{3,B}^x \\ b_{4,B}^x \end{bmatrix}$$

$$\begin{bmatrix} a_{9,9} & a_{9,10} \\ & a_{10,10}^x & a_{10,11} \\ & & a_{11,11}^x & a_{11,12} \\ & & & a_{12,12}^x & a_{12,13} \end{bmatrix} \begin{bmatrix} T_{1,C} \\ T_{2,C} \\ T_{3,C} \\ T_{4,C} \\ T_{f,3} \end{bmatrix} = \begin{bmatrix} b_{1,C} \\ b_{2,C}^x \\ b_{3,C}^x \\ b_{4,C}^x \end{bmatrix}$$

$$\begin{bmatrix} a_{14,14} & a_{14,15} \\ & a_{15,15}^x & a_{15,16} \end{bmatrix} \begin{bmatrix} T_{1,D} \\ T_{2,D} \\ T_{f,D} \end{bmatrix} = \begin{bmatrix} b_{1,D} \\ b_{2,D}^x \end{bmatrix}$$

$$\begin{bmatrix} a_{17,17} & a_{17,18} \\ & a_{18,18}^x & a_{18,19} \\ & & a_{19,19}^x & a_{19,20} \\ & & & a_{20,20}^x & a_{20,21} \\ & & & & a_{21,21}^x & a_{21,22} \\ & & & & & a_{22,22}^x & a_{22,23} \end{bmatrix} \begin{bmatrix} T_{1,E} \\ T_{2,E} \\ T_{3,E} \\ T_{4,E} \\ T_{5,E} \\ T_{6,E} \\ T_{f,E} \end{bmatrix} = \begin{bmatrix} b_{1,E} \\ b_{2,E}^x \\ b_{3,E}^x \\ b_{4,E}^x \\ b_{5,E}^x \\ b_{6,E}^x \end{bmatrix}$$

$$\begin{bmatrix} a_{24,24} & a_{24,25} \\ & a_{25,25}^x & a_{25,26} \end{bmatrix} \begin{bmatrix} T_{1,F} \\ T_{2,F} \\ T_{f,F} \end{bmatrix} = \begin{bmatrix} b_{1,F} \\ b_{2,F}^x \end{bmatrix}$$

where superscript 'x' is related to coefficients modified once.

Figure 3.10 Reduced construction matrices (from Clarke 1985).

$$\begin{bmatrix} a_{3,3}^x & a_{3,8} & a_{3,13} & a_{3,16} & a_{3,23} & a_{3,26} & a_{3,27} \\ a_{8,3} & a_{8,8}^x & a_{8,13} & a_{8,16} & a_{8,23} & a_{8,26} & a_{8,27} \\ a_{13,3} & a_{13,8} & a_{13,13}^x & a_{13,16} & a_{13,23} & a_{13,26} & a_{13,27} \\ a_{16,3} & a_{16,8} & a_{13,13} & a_{16,16}^x & a_{16,23} & a_{16,26} & a_{16,27} \\ a_{23,3} & a_{23,8} & a_{23,13} & a_{23,16} & a_{23,23}^x & a_{23,26} & a_{23,27} \\ a_{26,3} & a_{26,8} & a_{26,13} & a_{26,16} & a_{26,23} & a_{26,26}^x & a_{26,27} \\ a_{27,3} & a_{27,8} & a_{27,13} & a_{27,16} & a_{27,23} & a_{27,26} & a_{27,27} \end{bmatrix} \begin{bmatrix} T_{f,A} \\ T_{f,B} \\ T_{f,C} \\ T_{f,D} \\ T_{f,E} \\ T_{f,F} \\ T_a \end{bmatrix} = \begin{bmatrix} b_{f,A}^x \\ b_{f,B}^x \\ b_{f,C}^x \\ b_{f,D}^x \\ b_{f,E}^x \\ b_{f,F}^x \\ b_a \end{bmatrix}$$

where superscript 'x' is related to coefficients modified once.

Figure 3.11 Adjusted inside zone energy balance matrix (from Clarke 1985).

$$\begin{bmatrix} a_{3,3}^{x} & a_{3,8} & a_{3,13} & a_{3,16} & a_{3,23} & a_{3,26} & a_{3,27} \\ & a_{8,8}^{xx} & a_{8,13}^{x} & a_{8,16}^{x} & a_{8,23}^{x} & a_{8,26}^{x} & a_{8,27}^{x} \\ & & a_{13,13}^{xx} & a_{13,16}^{x} & a_{13,23}^{x} & a_{13,26}^{x} & a_{13,27}^{x} \\ & & & a_{16,16}^{xx} & a_{16,23}^{x} & a_{16,26}^{x} & a_{16,27}^{x} \\ & & & & a_{23,23}^{xx} & a_{23,26}^{x} & a_{23,27}^{x} \\ & & & & & a_{26,26}^{xx} & a_{26,27}^{x} \\ & & & & & & a_{27,27}^{x} \end{bmatrix} \begin{bmatrix} T_{f,A} \\ T_{f,B} \\ T_{f,C} \\ T_{f,D} \\ T_{f,E} \\ T_{f,F} \\ T_{a} \end{bmatrix} = \begin{bmatrix} b_{f,A}^{x} \\ b_{f,B}^{xx} \\ b_{f,C}^{xx} \\ b_{f,D}^{xx} \\ b_{f,E}^{xx} \\ b_{f,F}^{xx} \\ b_{a}^{x} \end{bmatrix}$$

x	- coefficient modified once.
xx	- coefficient modified twice.

Figure 3.12 Reduced inside zone energy balance matrix (from Clarke 1985).

The time-dependent conductance coefficients of matrix **A** are dependent on future time-row quantities which are unknown until the solution has been achieved (i.e the problem is non-linear). To overcome this non-linear problem, the future time-row coefficients are computed on the basis of the present nodal information and the present time-row coefficients are derived from the immediate past information. This procedure has no major consequences on the results since nodal quantity changes between time-steps are usually not significantly large. However, the accuracy can be improved by reducing the time-step or iterating as mentioned above.

This example elucidated only on the free floating (no control schedule imposed) condition. Other solution schemes for user-imposed control cases can be found elsewhere (Clarke 1985).

Solution of the mass conservation equations.

Although the mass conservation equation (3.6) do not include the dynamic term (the temporal derivative of density), since the flow was considered incompressible, the flows between finite volumes and the nodal pressures must be determined dynamically because of the transient nature of the boundary conditions (climatic variations). Due to the non-linear relationship between flow rates and pressures, the solution of the set of simultaneous equations requires an iterative process. The technique, explained in detailed elsewhere (Cockroft 1979, Clarke 1985 and Hensen 1991), consists of attributing an arbitrary value for all unknown nodal pressures. Equation (3.7) is then employed to compute the flow rates based on the guessed values. Since the pressures are guessed, the flow rates do not satisfy the nodal conservation of mass and nodal flow residuals arise. The residuals are then calculated from equation (3.6) as,

$$R_{j,P} = \sum_{j=1}^{n} \dot{m}_{j,P} - S_{\dot{m}_{P}} v_{P} \tag{3.13}$$

where $R_{j,P}$ is the nodal mass flow residuals (kg/s). The nodal pressures are then corrected in subsequent iterations until the nodal residuals satisfy some convergence criteria.

The pressures are corrected based on the Newton-Raphson technique which consists of adding a vector of the last iteration nodal pressures to a vector of pressure corrections. The pressure correction vector is the product of the nodal residuals vector and the inverse of the Jacobian matrix of the mass residuals. The solution of the Jacobian matrix is obtained by LU decomposition with scaling and implicit pivoting.

Mass flow simulations are performed in tandem with energy balance calculations. However, as the mass flow rates are not strongly dependent on the nodal temperatures and vice-versa, the temperatures are previously evaluated by the solution of the energy equations and are assumed known in the computation of equation (3.7). On the other hand, if buoyancy driven flow plays a major role on the determination of bidirectional flows in large openings, two possibilities exists: either a small time-step must be employed or iterations between the solutions of the mass and energy equations must take place.

3.7 PROBLEM DEFINITION

A brief description of the information necessary to define a problem in ESP-r is provided in this section. This is the basic requirements to understand the definition of a combined problem discussed in Chapter 5. The complete set of instructions are, however, described by Aasem *et al* (1992) or within the "on-line" ESP-r tutorial.

The building system, which can represent a building in whole or in part, is composed of several zones and individual components form the plant system. The user defines each building zone, specifying its three-dimensional geometry and fabric and also its operational profiles. The zones are then connected to each other in order to form the building and, optionally, a mass flow network is defined to represent the leakage distribution. Available plant components are then inter-connected to create a plant network. Finally, the building and plant are coupled and appropriate control strategies are imposed. Existing or user-defined databases help in the definition of constructions, event profiles and plant components.

As the present work is mostly concerned with coupling models within a zone, particular attention is given to the definition of zones. In order to exemplify the description, consider the two zone problem illustrated in Figure 3.13[#]. The Kitchen, which is a rectangular parallelepiped (cuboid) bounded by 6 opaque constructions (Part_kit, Right, Front, Back, Ceiling and Floor) and one transparent (Window) construction, can be seen in detailed in Figure 3.14.

_____

This problem is used throughout this thesis and has been kept deliberately simple.
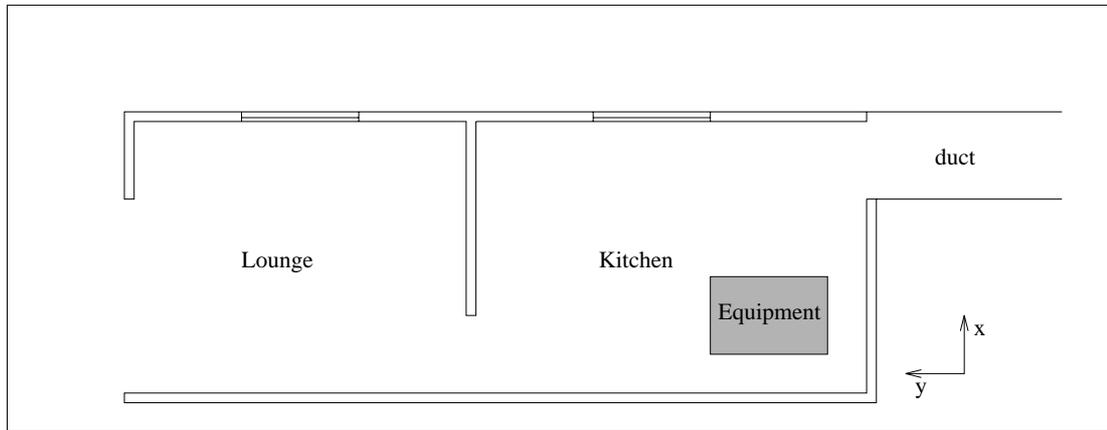
Figure 3.13 Two zone problem.
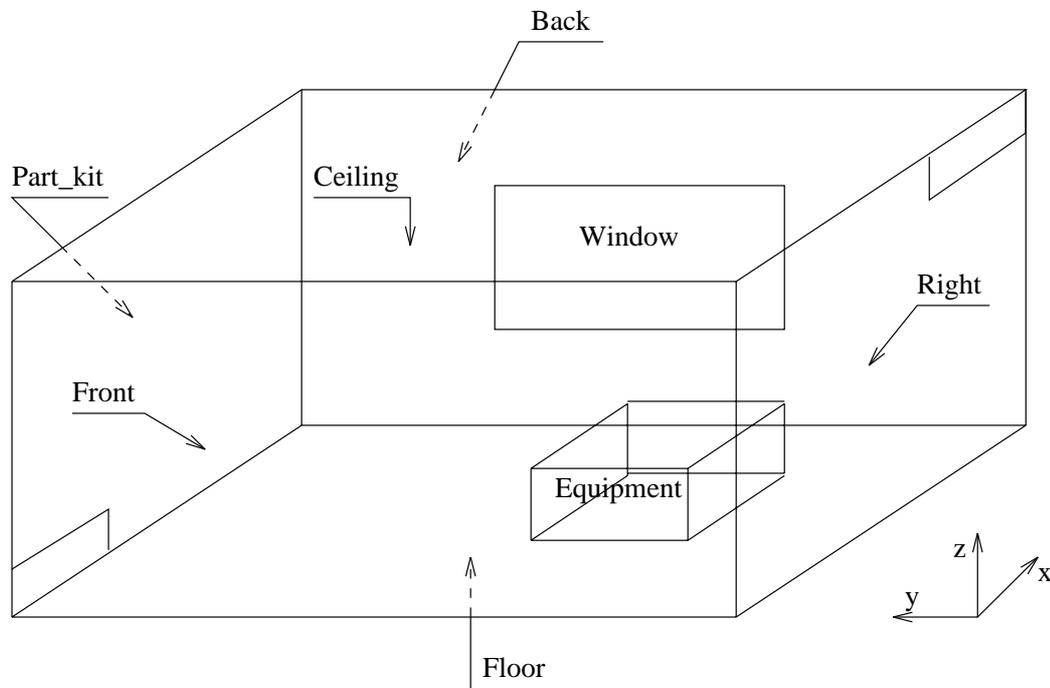
Figure 3.14 Kitchen of the problem of Figure 3.13.

The problem is defined in an ESP-r's "system configuration file"[*] as shown in Figure 3.15. Most of the information contained in this file is self-explanatory. The lines followed by the symbol # are comment lines. The index 1 in the first information line indicates that a building system is being simulated (index 2 and 3 signify plant only and plant and building simulations, respectively), and the

_____

[*] Users interact with ESP-r's project manager and will not be aware of this file and have no need to adjust its contents.

next two lines are related to the site location. In the sequence, information about the database and job notes location is provided. After that, the file names containing information regarding zone operation, geometry construction and optional features (utilities) for the Lounge and Kitchen are provided. The information of each zone's boundary condition (how the zones are connected to each other or to other kinds of environments) are then given (this is the most important information regarding the definition of a combined problem which will be discussed in Chapter 5). This information is supplied as: zone name, surface name, connection type and supplementary data. The connection type indicates the boundary condition outside the construction and the supplementary data are given according to the connection type. In this case, the partition wall in the Kitchen, Part_kit, is linked to another participating zone. The supplementary data describe the connected zone (Lounge) and the surface in the coupled zone which corresponds to Part_kit (Part_lou). The surfaces Right and Back and also the window (Window) are connected to outside; climatic data are taken as boundary condition. The Ceiling is connected to an environment whose temperature (10^oC) and the radiation ($0W/m^2$) impinging at the outside surface are constant and known. The Front wall is adiabatic and the Floor is connected to the ground pointing to an annual temperature profile (profile number 1) within *bps*. The Lounge is defined similarly and therefore the whole information regarding the building connections is provided.

Infiltration, ventilation (natural or forced) rates are determined by simulation. Building and/or plant fluid flow is described by means of a flow network. The user defines several nodes representing the air condition outside the building, within zones and within plant components. These nodes are inter-connected by means of components which are chosen from a list representing pipes/ducts, pumps, openings, cracks, doorways, valves, etc.

The presence of the flow network is indicated by the last three lines in the system configuration file, as shown in Figure 3.15. The penultimate line indicates the flow network description file name and the last line contains the nodes in the mass flow network which correspond to the Kitchen and Lounge (this relates to the link between flow simulation and thermal simulation). The flow network of this problem is illustrated in Figure 3.16 and its description is defined in Figure 3.17. As can be seen, the first line in the flow network file indicates how many nodes (six), components (four) and connections (five) are in the network and also a wind reduction factor (1 - power law profile). The next lines hold information about the nodes. Nodes Kitche and Lounge (which represent the air pressure and temperature within the corresponding zones) and node Duct_1 (which represent the air condition at the outlet of the duct), are internal nodes (node type 0). This signifies that pressures at such nodes are unknown and must be determined. The fluid type (1 - air), height and temperature of the nodes are also specified. In the case of the outside (type 3) nodes, Out_w and Out_n, temperature is not required to be specified but two additional data are necessary. The first additional item denotes the wind pressure coefficients (1 - vertical wall with ratio length/width equal to 1.0) and the second one provides the surface azimuth (^{o} clockwise from North). At node Duct_2 (which represents the air

condition at the inlet of the duct), the total pressure is known (node type 2) and is provided via the first data item (50Pa). The second data item (1.0) indicates that the node temperature equals the outside air temperature.

The next lines in the file describe the components which link the nodes. Two lines are necessary to define a component. In the first line, the component name, component index (identification in the component library), number of component data items, number of connection supplementary nodes and a description of the components are defined. In the second line, the component data items (regarding geometry, power law coefficients, etc.) are specified.

The rest of the information in the network file is related to the connection of nodes by components. The information contained in each line describing a connection is: name of the first node, height of linkage point relative to the first node, the second node name, height of linkage point relative to the second node and the linking component. Two additional supplementary nodes may also be required for some components, but are not relevant in the current case.

Energy casual gains due to occupancy, lighting and equipment for each zone can be defined as a time-series for each zone. Each time-step *bps* reads a file containing the total sensible conductive, sensible radiant and latent heat gains (all in Watts) for the zone. This is particular useful, for example, if the heat input of the equipment placed in the Kitchen is known hourly.

Control strategies are specified in terms of control functions (associated with building zones or flow components) or control loops (associated with plant components). A control function/loop is comprised of sensor and actuator locations, sensing and actuating properties, control laws and periods during which actuation is active. The control law establishes the relation between the sensed and actuated properties. A series of building, plant and mass flow control laws are available, such as, ideal control, free-floating, on-off control, PID controller, etc.

In the case of the example of Figure 3.13, the air temperature of the Kitchen could be controlled during some period of the day, say from 8:00 to 17:00. A certain amount of heat could be injected to a surface, which may represent a radiator. Control laws such as an on-off or PID controller could be invoked during such periods.

3.8 REMARKS

The ESP-r system was introduced in this chapter to provide a brief description about its architecture. The mathematical models, numerical techniques, solution procedures of the ESP-r simulation module, *bps*, were discussed. The boundary conditions and the system configuration, which are necessary to define a problem in ESP-r, was also presented. This material was mostly introduced in a manner which will help the reader understand the BTS and CFD conflation mechanisms introduced in Chapter 5. The reader should notice that the energy balance on the surfaces and in the air volume, the mass balance equations and the problem definition are the main

requirements for such integration.

```
* CONFIGURATION
# ESRU system configuration defined by file
# Two_zone.cfg
       1           # Building only
 50.000    0.000    # Latitude & Longitude
       1    0.200   # Site exposure & ground refl
* DATABASES
*prm  /usr/esru/esp-r/databases/constr.db1
*mlc  /usr/esru/esp-r/databases/multicon.db1
*opt  /usr/esru/esp-r/databases/optics.db1
*prs  /usr/esru/esp-r/databases/pressc.db1
*evn  /usr/esru/esp-r/databases/profiles.db1
*clm  /usr/esru/esp-r/climate/clm67
*pdb  /usr/esru/esp-r/databases/plantc.db1
* PROJ LOG
job.notes
* Building
Two zone problem
       2  # no of zones
       1    # reference for kitchen
kitchen.opr     # schedules
kitchen.geo     # geometry
kitchen.con     # constructions
       0
       2    # reference for lounge
lounge.opr      # schedules
lounge.geo      # geometry
lounge.con      # constructions
       0
      13    # number of connections
#   ZONE      SURFACE     CONNECTION        SUPPLEMENTARY  DATA
#
  Kitche    Right      External
  Kitche    Back       External
  Kitche    Part_kit   Another zone        Lounge     Part_lou
  Kitche    Front      adiabatic
  Kitche    Ceiling    Constant            10.0       0.0
  Kitche    Floor      Ground profile       1
  Kitche    Window     External
  Lounge    Part_lou   Another zone        Kitche     Part_kit
  Lounge    Surf-2     External
  Lounge    Surf-3     External
  Lounge    Surf-4     External
  Lounge    Surf-5     Constant            10.0       0.0
  Lounge    Surf-6     Ground profile       1
#
       1    # no mass flow analysis
flow.mfn    # leakage description
  Kitche  Lounge
```

Figure 3.15 Configuration file of the problem shown in Figure 3.13.
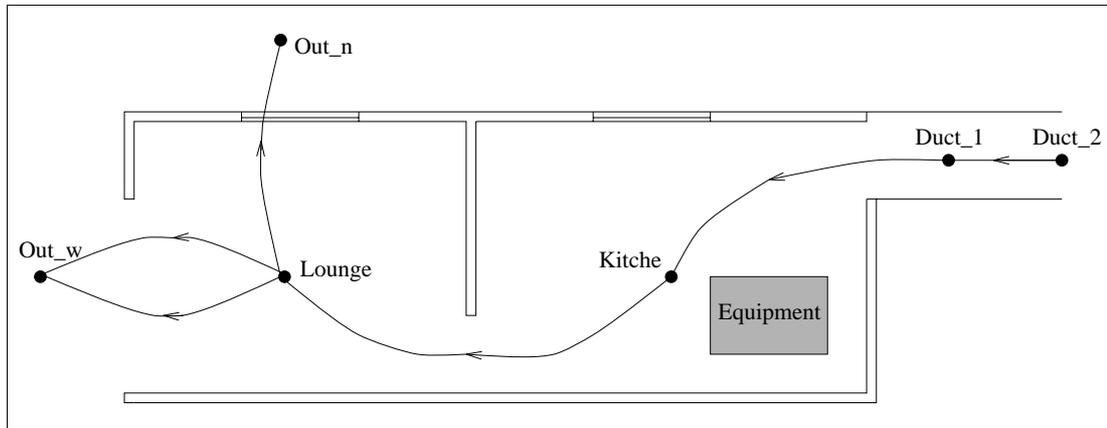
Figure 3.16 Flow network of the problem of Figure 3.13.

```
    6     4     5      1.000     (nodes, components, connections, wind reduction)
Node   Fld. Type    Height      Temperature      Data_1        Data_2
Duct_1   1    2    2.9000            0.          50.000        1.0000
Duct_2   1    0    2.9000          20.000           0.            0.
Kitche   1    0    1.5000          20.000           0.            0.
Lounge   1    0    1.5000          20.000           0.            0.
Out_n    1    3    1.5000            0.          1.0000           0.
Out_e    1    3    1.5000            0.          1.0000         270.
Comp    Type C+ L+ Description
duct      50   3  0 Laminar pipe vol. flow rate comp.    m = rho.f(L,R,mu,dP)
    1.00000     5.00000     2.50000E-02
open      40   3  0 Common orifice vol. flow rate comp. m = rho.f(Cd,A,rho,dP)
    1.00000     2.00000E-02   0.650000
window    35   2  0 Constant mass flow rate component    m = a
    1.00000     0.500000
door     130   5  0 Specific air flow door              m = rho.f(W,H,dP)
    1.00000     0.800000    2.10000    1.00000    0.650000
+Node   dHght    -Node    dHght    Comp      Snod1  Snod2
Duct_1  0.000    Duct_2   0.000    duct
Duct_2  0.000    Kitche  -0.700    open
Kitche  0.700    Lounge   0.700    open
Lounge  0.000    Out_n    0.000    door
Lounge  0.000    Out_e    0.000    window
```

Figure 3.17 Description of the flow network of the Figure 3.16.

REFERENCES

Aasem, E., Clarke, J. A., Hand, J., Hensen, J., Pernot, C. and Strachan, P., 1992, *ESP-r The European Reference Program for Building Energy Simulation*, ESRU Manual, Version 8 series, Glasgow, UK.

Alamdari, F. and Hammond, G. P., 1983, Improved Data Correlation for Buoyancy-Driven Convection in Rooms, *Rep. SME/J/83/01*, Cranfield Institute of Technology, Applied Energy Group, Cranfield.

Clarke, J. A., 1985, *Energy Simulation in Building Design*, Adam Hilger Ltd, Bristol UK.

Cockroft, J. P., 1979 Heat Transfer and Air Flow in Buildings, *PhD Thesis*, University of Glasgow.

Hensen, J. L. M., 1991, *On the Thermal Interaction of Building Structure and Heating and Ventilation System*, PhD thesis, Technische Universiteit, Eindhoven.

Hensen, J. L. M. and Nakhi, A. E., 1994, Fourier and Biot Numbers and the Accuracy of Conduction Modelling, *Proc. of Building Environmental Performance '94*, York, UK.

Nakhi, A., 1995, *PhD Thesis (to be published)*, ESRU University of Strathclyde.

Patankar, S. V., 1980, *Numerical Heat Transfer and Fluid Flow*, Hemisphere Publishing Corporation.

The New ESP-r CFD Simulator, dfs

4.1 INTRODUCTION

As illustrated in Chapter 3 many different types of indoor air flows can be modelled as uniform mixtures, for example when the air property fields (such as, temperature, concentration, etc) inside rooms are uniform or nearly so. In some cases, however, the presence of flow property gradients cannot be neglected because they play a major role in the estimation of building energy consumption and comfort conditions. Therefore, an approach which removes the assumption of a mixed volume is necessary to address these types of circumstances. Such rigorous analysis can be performed by CFD in order to predict the distribution of indoor air flow properties.

In this chapter, the *dfs* CFD system is described. The next section presents the general description of the model. A mathematical description of the transport processes is introduced in Section 4.3. In Section 4.4, the numerical method and the discretisation technique employed are presented. Section 4.5 describes the types of boundary conditions available in *dfs*. The solution technique applied to solve the discretised conservation equations is then discussed in Section 4.6 and, finally, Section 4.7 demonstrates how a problem is defined for simulation. This material comprises the requisites necessary to follow the integration approach discussed later.

4.2 DESCRIPTION OF THE SYSTEM

The *dfs* system was developed to address building air flows. It is a menu-driven program similar to, and compatible with, the other ESP-r modules. Because of its modular structure, maintenance and further developments are enabled. The *dfs* module is able to perform transient analysis of indoor air flows which are incompressible, three-dimensional, turbulent or laminar. The pressure and buoyancy driven flow is numerically evaluated by solving the conservation equations of mass, momentum, energy and turbulent transport equations. The procedure allows the prediction of local flow properties such as velocity, pressure, temperature, concentration of the air constituents (for example, moisture content, contaminants) and turbulent properties.

Since the conservation equations are solved iteratively, the program enables graphic monitoring of the convergence process. The residuals of the equations and the monitoring values (velocity components, pressure, etc) at a nominated grid cell can be visualised as the solution takes place. Figure 4.1 shows an example of such a graph after convergence is reached[*]. Although in this solution

---

[*] The left hand side graph shows the sum of the residuals of all cells in the domain for each individual equation (in this case mass, momentum in y and z directions) and the right hand side one presents the values of pressure and velocity

the residuals always decrease and the monitoring values stabilise at the end of the solution process, there are many cases where convergence is never achieved. In these situations the continual observation of the graphs permits a judgement as to whether a solution will be obtained or not. The process may be stopped, if necessary, and re-initialised with, for example, new relaxation factors. The code is also able to generate, automatically, the cell grid according to a user defined power law equation. Since the power law coefficient is randomly chosen, the user cannot imagine how cells are distributed and thus, a grid visualisation facility is provided in order to observe how the cells are placed in the domain.

(a)   (b)
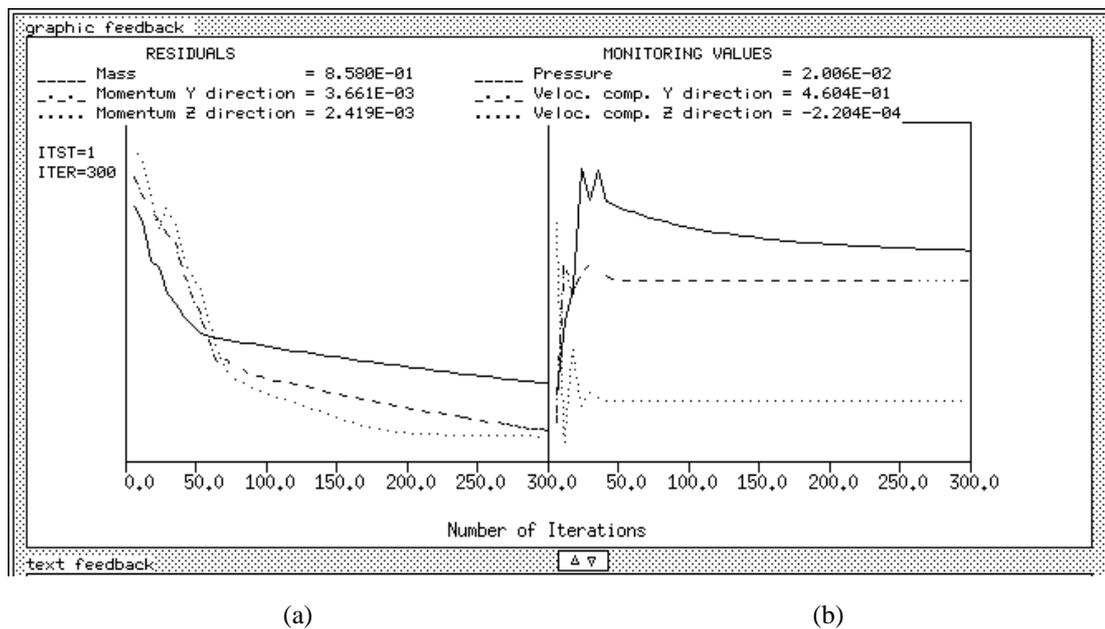
Figure 4.1 Evolution of the *dfs* convergence process: (a) sum of residuals. (b) monitoring values.

The analysis of the air flow over the whole domain may become prohibitive because of the extensive computational effort. However, in most cases the need to evaluate the gradients of the flow properties is limited only to a few zones, or even a single zone in the whole building. The air flow in the remaining zones can be reasonably estimated by applying the assumption of mixed flow.

The different energy transfer processes taking place inside a zone, which can be modelled by *dfs*, are summarised as:

_____

components in a particular cell. The residuals in the y axis are plotted using a logarithmic scale and the monitoring values are shown using a linear scale. During the monitoring both graphs are constantly re-scaled according to maximum and minimum values. The current residuals and monitoring values are always displayed.

- convection heat transfer between a solid surface and the air layer in contact with the surface[#].

- buoyancy effect caused by air temperature and air constituent gradients.

- convection heat/contaminant source placed in a specific position inside the zone (eg. equipment, people, lighting, etc.).

- the influence of furniture obstructing the air flow inside the zone.

- plant interaction in the form of convective heat exchange.

- control of zone air temperature/concentration at a specific position.

Heat sources in rooms are not all convective and significant radiative heat transfer occurs between walls and between heat sources and walls. As with many CFD models, *dfs* is not able to compute radiation between surfaces and/or heat sources. Additionally, internal surface shortwave gain caused by the sun can only be considered if previously known and then included at the surface as a source of heat (recall that these deficiencies provide the estimate for the *bps/dfs* conflation as described in Chapter 5).

4.3 MATHEMATICAL MODEL

The air flow and temperature distribution within enclosures involve the solution of the mass conservation equation, momentum transport equations and the energy transport equation. However, the characteristics of indoor air motion are always difficult to identify whether it is locally induced turbulent, transitional or fully turbulent. This fact introduces an additional complexity into the problem because of the chaotic state of turbulence: flow properties at certain points in the space always fluctuate at a very high frequency. From the three different approaches for turbulent flows discussed in Appendix A (direct simulation, large-eddy simulation and turbulence transport models), the third one is the most appropriate for the present work since it is the most computationally economical. The $k - \varepsilon$ model, the most extensively used turbulence transport model, is able to describe the complexities of the indoor turbulent motion with acceptable accuracy for engineering purposes (Chen and Jiang 1992, Jones and Whittle 1992).

In the case of turbulence models, there is no interest in the highly fluctuating motion and the governing equations are time-averaged. The resulting mean conservation equations derived in Appendix A can be written in the following format:

$$\frac{\partial}{\partial t}(\rho \phi) = \frac{\partial}{\partial x_j}\left(\Gamma_\phi \frac{\partial \phi}{\partial x_j} - \rho U_j \phi\right) + S_\phi \tag{4.1}$$

\# This is true if the validity of wall functions is accepted (refer to Sections 4.5 and 5.4.1).

where ϕ (= 1 (continuity), U, V, W, T, C, etc.) represents any mean scalar variable or velocity component. The diffusion coefficient, Γ_ϕ, and the source terms, S_ϕ, are given in Table 4.1. As can be seen from Table 4.1, time-averaged turbulent equations have the same form as the laminar flow equations, but the laminar diffusion coefficients, such as molecular viscosity and diffusivity, are replaced by effective (molecular plus eddy) diffusion coefficients. In the case of turbulent flow, the eddy diffusivity is added to the molecular diffusivity in order to absorb the fluctuating motion and therefore only the average values are estimated.

Table 4.1 The dynamic three-dimensional governing equations.

Equation	ϕ	Γ_ϕ lam.	Γ_ϕ turb.	S_ϕ
Continuity	1	-	-	-
U - mom.	U	μ	μ_{ef}	$-\dfrac{\partial P}{\partial x} + \dfrac{\partial}{\partial x}\left(\mu_{ef}\dfrac{\partial U}{\partial x}\right) + \dfrac{\partial}{\partial y}\left(\mu_{ef}\dfrac{\partial V}{\partial x}\right) + \dfrac{\partial}{\partial z}\left(\mu_{ef}\dfrac{\partial W}{\partial x}\right)$
V - mom.	V	μ	μ_{ef}	$-\dfrac{\partial P}{\partial y} + \dfrac{\partial}{\partial x}\left(\mu_{ef}\dfrac{\partial U}{\partial y}\right) + \dfrac{\partial}{\partial y}\left(\mu_{ef}\dfrac{\partial V}{\partial y}\right) + \dfrac{\partial}{\partial z}\left(\mu_{ef}\dfrac{\partial W}{\partial y}\right)$
W - mom.	W	μ	μ_{ef}	$-\dfrac{\partial P}{\partial z} + \dfrac{\partial}{\partial x}\left(\mu_{ef}\dfrac{\partial U}{\partial z}\right) + \dfrac{\partial}{\partial y}\left(\mu_{ef}\dfrac{\partial V}{\partial z}\right) + \dfrac{\partial}{\partial z}\left(\mu_{ef}\dfrac{\partial W}{\partial z}\right) - \rho g$
Energy	T	$\dfrac{\mu}{Pr}$	Γ_T	$\dfrac{q'''}{c_{p,a}}$
Concent.	C	$\dfrac{\mu}{Sc}$	Γ_C	$\dot{m}'''$
Turb. E.	k	-	$\dfrac{\mu_{ef}}{\sigma_k}$	$G - C_D\rho\varepsilon - G_b$
E. dissip.	ε	-	$\dfrac{\mu_{ef}}{\sigma_\varepsilon}$	$C_1\dfrac{\varepsilon}{k}G - C_2\rho\dfrac{\varepsilon^2}{k} - C_3\dfrac{\varepsilon}{k}G_b$

$$\Gamma_T = \frac{\mu}{Pr} + \frac{\mu_t}{\sigma_T} \quad ; \quad \Gamma_C = \frac{\mu}{Sc} + \frac{\mu_t}{\sigma_C} \quad ; \quad \mu_{ef} = \mu_t + \mu \quad ; \quad \rho = \rho(T,C)$$

$$G_b = g\beta_T\frac{\mu_t}{\sigma_T}\frac{\partial T}{\partial z} \quad ; \quad G = \mu_t\left(\frac{\partial U_i}{\partial x_j} + \frac{\partial U_j}{\partial x_i}\right)\frac{\partial U_i}{\partial x_j}$$

$$C_D = 1.0 \quad ; \quad C_1 = 1.44 \quad ; \quad C_2 = 1.92 \quad ; \quad C_3 = 1.44$$

$$\sigma_k = 1.0 \quad ; \quad \sigma_\varepsilon = 1.3 \quad ; \quad \sigma_T = 0.9 \quad ; \quad \sigma_C = 1.0$$

For the $k\text{-}\varepsilon$ model, the eddy viscosity is related through scaling arguments to the ratio of the square of the kinetic turbulent energy, k, and its rate of dissipation, ε:

$$\mu_t = C_\mu \rho \frac{k^2}{\varepsilon} \tag{4.2}$$

where C_μ is an empirical value equal to 0.09. In order to compute the eddy viscosity two additional transport equations are introduced to evaluate k and ε. These equations are also derived from the momentum equation. The complete derivation of k and ε equations can be found elsewhere (Rodi 1984). The resulting transport equations for k and ε assume the same form of equation (4.1) and the diffusion coefficients and source terms for a fully turbulent flow can be found in Table 4.1. The G term represents the production of k by interaction of the Reynolds stress and mean-velocity gradients,

$-\rho\varepsilon$ is the viscous dissipation and G_b is the production or destruction of turbulence due to buoyancy. In stable stratification, G_b is negative and thus reduces the production of turbulence. In unstable stratification the opposite takes place. Notice that such terms are always generation minus destruction in either turbulence energy or energy dissipation equations.

To summarise, all transport equations have the same format as equation (4.1) and their different terms are generally described as storage, diffusion, convection and source terms. If the sum of diffusion and convection terms are defined as J, and can be interpreted as the inter-volume interactions described in the previous chapter, equation (4.1) becomes similar to equation (3.2):

$$\frac{\partial}{\partial t}(\rho\phi) = \frac{\partial J_j}{\partial x_j} + S_\phi \qquad (4.3)$$

where J_j is equal to $\Gamma_\phi \dfrac{\partial \phi}{\partial x_j} - \rho U_j \phi$.

The problem now is reduced to a set of 8 time-averaged conservation laws (expressed by equation (4.3)) and 8 unknowns (P, U, V, W, T, C, k, ε) constituting a closed set of differential equations which can be solved. However, the conservation equations are highly non-linear and analytical solutions are only possible in very simplified cases with limited practical application. Numerical techniques are employed to integrate the digital form of the conservation equations.

4.4 NUMERICAL APPROACH

The technique used to discretise the conservation equations is the same method employed in the previous chapter: the finite volume (FV) approach. The FV method is characterised by the integration of the transport equations (in their conservative form as given by equation (4.3)) over a finite volume in the space. Since the method preserves flux inside each FV, it is designated a conservative method. This means that mass, momentum, heat, etc. are conserved inside the domain independently of the number of cells applied.

In building applications, zone geometries are generally not complex and most of them can be reduced to simple shapes. Therefore, for simplicity, only cartesian coordinates are used to tackle the problem and consequently the flow domain is restricted to rectilinear forms.

In order to discretise the conservation equations, consider the schematic representation of a finite volume as given in Figure 4.2. The control volume, P, is bounded by six neighbouring volumes (W, E, S, N, L and H) and the interfaces between P and its neighbours are symbolised by the small letters, w, e, s, n, l and h. Integrating the general transport equation (4.3) over the control volume P and the time interval δt (time-step) results in the discretised finite volume equation (Patankar 1980):

$$v_P[\rho_P\phi_P - \rho_P^-\phi_P^-] = \sum_j J_j^\xi A_j \delta t + S_{\phi_P}^\xi v_P \delta t \qquad j = w, e, s, n, l, h \qquad (4.4)$$
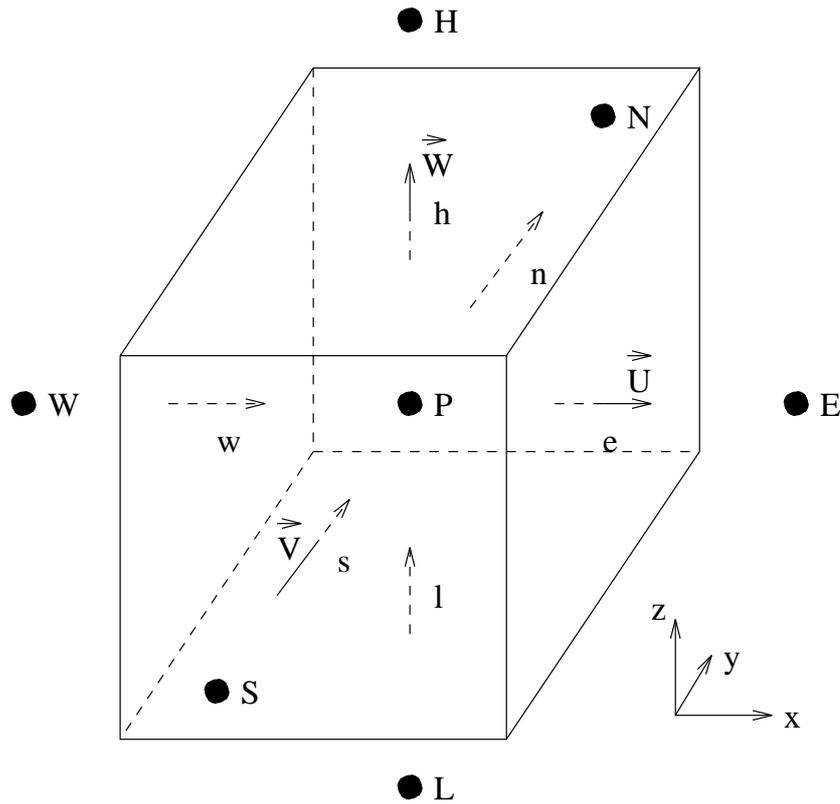

Figure 4.2 Schematic representation of a finite volume.

where v_P ($\delta x \delta y \delta z$) is the finite volume ($m^3$), J_j is the net flux (diffusion plus convection) through each boundary surface (w, e, s, n, l, h) per unit of area (kg/m^2s multiplied by the transport property unit) and A_j is the surface area of each boundary surface (m^2). The superscript $-$ refers to values at the start (present values) of the time interval, the superscript ξ denotes the values within the time interval and the symbols without superscripts are future time values. The finite volume equation (4.4) is identical to the mathematical formulation suggested in Chapter 3 and it can be interpreted as the rate of storage of ϕ inside the control volume (CV) equal to the net flux of ϕ through its boundaries (control surface) plus the generation of ϕ within the CV (equation (3.1)). Usually J_j are unknown at the finite volume boundaries and they are expressed as a function of the transport property differences evaluated at the centre of the volumes:

$$J_j^\xi A_j = a_i^\xi(\phi_i^\xi - \phi_P^\xi) \qquad j = w, e, s, n, l, h \qquad i = W, E, S, N, L, H \qquad (4.5)$$

where a_i are the conductance coefficients representing diffusion and convection. Substituting expression (4.5) into (4.4) and dividing it by δt, gives the following equation

$$\frac{\upsilon_P}{\delta t} [\rho_P \phi_P - \rho_P^- \phi_P^-] = \sum_i a_i^\xi (\phi_i^\xi - \phi_P^\xi) + S_{\phi_P}^\xi \upsilon_P \qquad i = W, E, S, N, L, H \qquad . \qquad (4.6)$$

Notice that this equation is similar to the formulation presented the Chapter 3 and can be understood as "the rate of storage of ϕ's equal to the inter-volume interactions plus a source of ϕ".

As can be seen from Figure 4.2, the components of the velocity vector are placed at the boundaries of the control volume P (position of all scalar variables). This configuration characterises a staggered grid which was chosen to avoid pressure solution oscillation, known as the *chequerboard* pattern (Shaw 1992). Even though, the discretised equation derived for the velocity components is identical to equation (4.6).

The symbols with the superscript ξ of equation (4.6) must be expressed in terms of known present and future values. Because it is unconditionally stable, the fully implicit scheme is implemented into equation (4.6) rather than the interpolation between explicit and fully implicit method as employed in equation (3.10). All terms on the right hand side are thus represented by their future values and the following expression results

$$\frac{\upsilon_P}{\delta t} (\rho_P \phi_P - \rho_P^- \phi_P^-) = \sum_i a_i (\phi_i - \phi_P) + S_{\phi_P} \upsilon_P \qquad i = W, E, S, N, L, H \qquad . \qquad (4.7)$$

In order to evaluate the conductance coefficients, a hybrid scheme is applied. This scheme is an approximation of convection and diffusion effects by combining the central difference and up-wind approaches (Patankar 1980). This scheme consists of applying the upwind approach if the cell's Reynolds number, given by $\rho \phi \delta x_i / \Gamma_\phi$, is greater than 2 and the central differences if the number is 2 or less. The conductance coefficients , a_i, take the following form

$$a_W = \max\left[|0.5(\rho UA)_w| , \left(\frac{\Gamma_\phi}{\delta x} A\right)_w \right] + 0.5(\rho UA)_w \qquad (4.8a)$$

$$a_E = \max\left[|0.5(\rho UA)_e| , \left(\frac{\Gamma_\phi}{\delta x} A\right)_e \right] - 0.5(\rho UA)_e \qquad (4.8b)$$

$$a_S = \max\left[|0.5(\rho VA)_s| , \left(\frac{\Gamma_\phi}{\delta y} A\right)_s \right] + 0.5(\rho VA)_s \qquad (4.8c)$$

$$a_N = \max\left[|0.5(\rho VA)_n| , \left(\frac{\Gamma_\phi}{\delta y} A\right)_n \right] - 0.5(\rho VA)_n \qquad (4.8d)$$

$$a_L = \max\left[\, |0.5(\rho WA)_l| \, , \left(\frac{\Gamma_\phi}{\delta z} A\right)_l \right] + 0.5(\rho WA)_l \qquad (4.8e)$$

$$a_H = \max\left[\, |0.5(\rho WA)_h| \, , \left(\frac{\Gamma_\phi}{\delta z} A\right)_h \right] - 0.5(\rho WA)_h \qquad (4.8f)$$

where max is the maximum value between the terms in brackets. Moreover, the source term S_{ϕ_P} is linearised and written as

$$S_{\phi_P} = S_c + S_P \phi_P \qquad . \qquad (4.9)$$

Finally, rearranging the a_i and S coefficients the equation (4.4) can be rewritten as

$$a_P \phi_P - \sum_i a_i \phi_i = b_P \qquad i = W, E, S, N, L, H \qquad (4.10)$$

where

$$a_P = \sum_i a_i \phi_i - S_P + \frac{v_P \rho_P}{\delta t} \qquad i = W, E, S, N, L, H$$

$$b_P = S_c + \frac{v_P \bar{\rho_P}}{\delta t} \bar{\phi_P} \qquad .$$

The discretisation equations were derived in general terms and are applicable to any regular grid distribution. According to Patankar (1980) there are two possibilities for locating control volume faces: cells faces are located midway between the grid points or grid points are situated at the centres of the control volumes. For convenience of conforming cell faces with the domain contours, the second option was adopted. The faces of the control volumes are drawn first and then the grid points are placed at the centres of the cells, as shown by Figure 4.3. Another benefit of this approach is the fact that discontinuities (in material properties, in geometry or in boundary conditions) can be placed at control volume faces avoiding discontinuities lying *within* cells.

The cuboid grid may acquire uniform or non-uniform forms. The definition of uniformity is related to a particular direction. In the uniform distribution, a specific dimension (length, width or height) is exactly the same for all cells. The non-uniform grid, on the other hand, is generated by employing a power law. This formulation evaluates the cell face positions in each direction of a region according to the equation,

$$x_i = L \left[\frac{i}{n} \right]^c \tag{4.11}$$
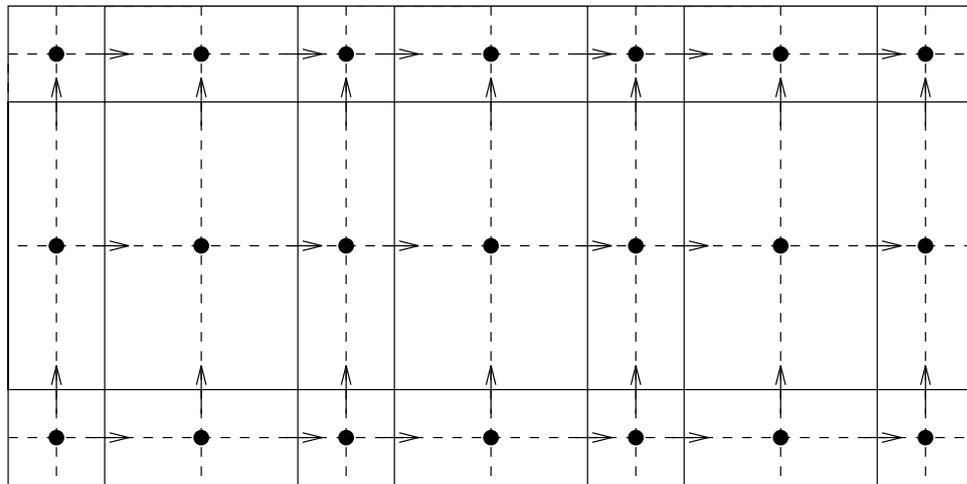
Figure 4.3 Example of grid points placed at the centres of the cells.

where x_i is the coordinate of the face of the cell, i is the cell index, L is the dimension of the region in a specific direction, n is the number of cells in the specific direction and c is the power law coefficient. Figure 4.4 shows examples of grids produced from equation (4.11) with two different values of c. Basically, if the c coefficient is greater than one the grid starts fine for small values of x, becoming coarser as x increases. The opposite happens if c is smaller than unity. Different arrangements, such as a fine grid at the edges and coarse at the middle, can be produced using variations of equation (4.11). In this case, the domain is divided into two and the equation is used in each part (for the left hand side, the cells are defined from right to left).


(a)   (b)
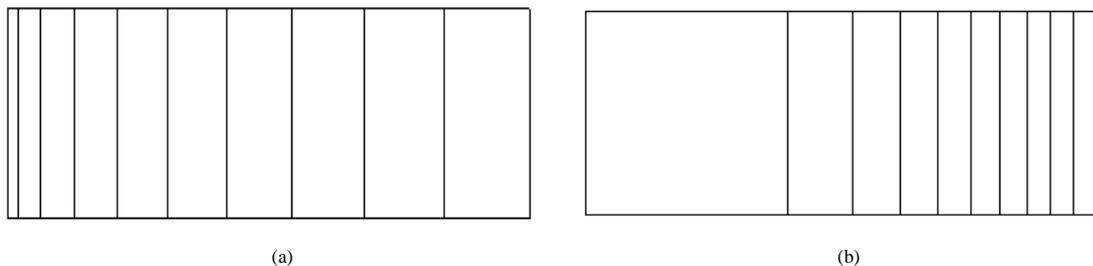
Figure 4.4 Examples of grids generated by equation (4.11).

Although *dfs* can only consider rectilinear geometries, furniture, equipment, etc., inside a zone, and also different room shapes, can still be modelled. Since the cartesian grid was adopted, the

programing algorithm to handle such geometries must be specific for each situation. To avoid such complexities the solution domain is kept as a cuboid but some cells are blocked in order to conform with the desired form. The blocking is achieved by setting the viscosity at some cells to a high value[#]. Finally, the solution takes place for the whole domain. Figure 4.5 shows an example of how different room geometries can be included in a rectilinear grid. Although this procedure will result in higher than necessary computational times and memory requirements, it provides a general solution to the treatment of different geometries within a rectilinear grid and has been found to be appropriate for the shapes occurring within buildings.


(a)

(b)
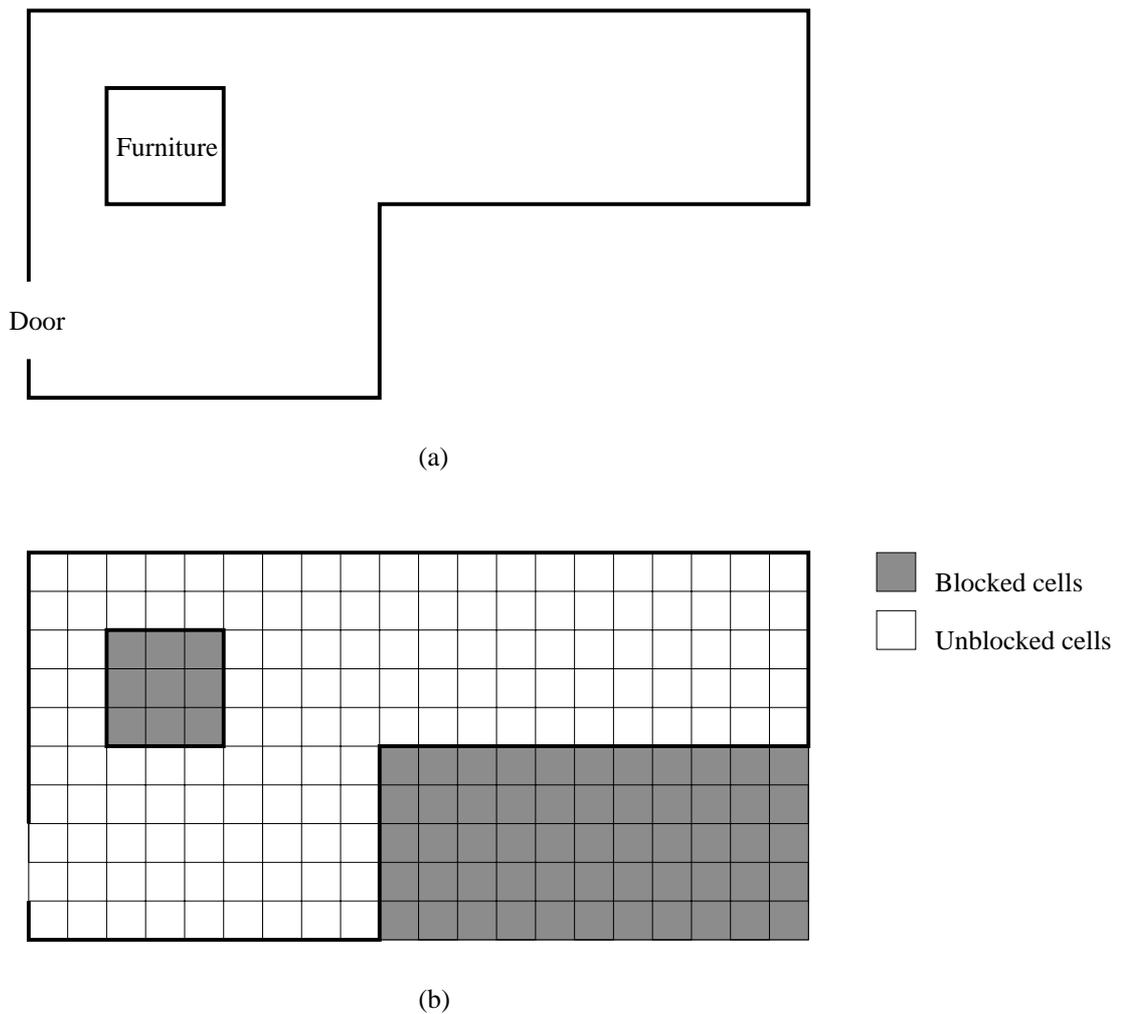
Figure 4.5 Example of *dfs* domain for a non-cubical or non-rectangular shape.

\# Fluid with infinite viscosity corresponds to a solid since the diffusion effect is much larger than the convection. As a result, the velocities to be calculated at such positions are equal to zero.

4.5 BOUNDARY CONDITIONS

Before the set of equations (4.10) is solved the boundary conditions of the system to be simulated must be established. Since a *dfs* analysis over the entire building is prohibited by computational restrictions, all boundary conditions of the limited domain (coupled zones or a single zone) must be provided. In the case of a single zone bounded by several surfaces (opaque or transparent) and openings (windows, doors, cracks, etc.), the temperatures or heat fluxes at the surfaces and the condition of the air entering or leaving the zone must be supplied. Moreover, the system is a dynamic one and consequently the boundary conditions must be known during the period of interest. Such dynamic conditions are always difficult to estimate unless they are measured. This lack of information usually restricts the problem to a steady state analysis.

The boundary conditions for the transport variables are generally established as follow,

- Velocity components are commonly given at the boundaries. If this is not done, their gradients normal to the boundary are usually zero.

- Pressure or mass flow may be specified at different points in the domain. However the fluid pressure needs to be defined at least in one point in the flow (reference pressure).

- Temperature and concentration or their fluxes are required to be established at the boundaries.

- Turbulence variables (k and ε are also defined at the boundaries, but a special treatment is considered for solid boundaries.

These conditions are applied at a variety of boundaries such as the following:

Solid boundaries

Internal surfaces of opaque and transparent constructions, and also the contours of furniture, machinery, etc., can be classified as solid boundaries. For the case of laminar flow, the velocity components are set to the velocity of the surface (in this case zero). The situation is more complex with turbulent flow. Close to the surface, molecular viscosity becomes as significant as eddy viscosity due to the damping effect of the walls. In such regions, the standard $k - \varepsilon$ model is not applicable and wall functions (Launder and Spalding 1974) are employed in order to evaluate the velocity component parallel to the boundaries and the heat transfer at the surfaces. Within the laminar sublayer viscous effects prevail and the air flow is described by the Couette flow expressions. According to the nomenclature of Figure 4.6, the wall shear stress at a cell adjacent to a surface, f, and the heat transfer through the surface are approximated as,

$$\tau_f = \mu \, \frac{U_P - U_f}{y_P} = \mu \, \frac{U_P}{y_P} \qquad (4.12)$$

$$\frac{q_f''}{c_{p,a}} = \mu \frac{(T_P - T_f)}{Pr\ y_P} \tag{4.13}$$

for $y^+ \le 11.63$
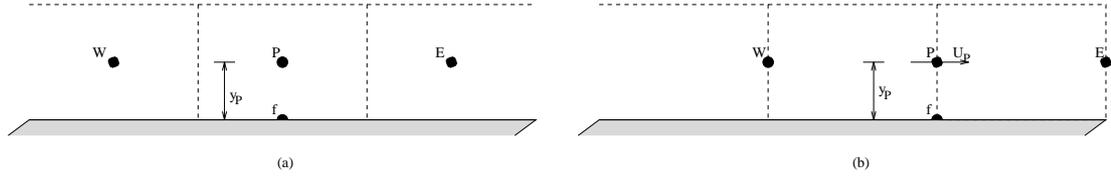
Figure 4.6 Grid nodes adjacent to the wall. (a) scalar cells and (b) velocity cells.

where $y^+ = C_\mu^{1/4} \rho_P k_P^{1/2} \frac{y_P}{\mu}$, U_P indicates the velocity component at the cell position P, U_f is the velocity at the surface (identically zero), q_f'' is the heat transfer through surface f per unit area, $c_{p,a}$ is the specific heat of the air and T_P is the temperature at the cell parallel to the wall. Outside the laminar sublayer turbulent shear becomes noticeable and generation and dissipation of turbulent energy is assumed to be in balance: $\tau_f/\rho_P = C_\mu^{1/2} k_P$. Thus, the following logarithmic distribution arises for momentum and heat flux:

$$\tau_f = \frac{\kappa C_\mu^{1/4} \rho_P k_P^{1/2}}{\ln(Ey^+)} (U_P - U_f) = \frac{\kappa C_\mu^{1/4} \rho_P k_P^{1/2}}{\ln(Ey^+)} U_P \tag{4.14}$$

$$\frac{q_f''}{c_p} = \frac{C_\mu^{1/4} \rho_P k^{1/2}(T_P - T_f)}{\sigma_T \left[\frac{1}{\kappa} \ln(Ey^+) + f\left(\frac{Pr}{\sigma_T}\right) \right]} \tag{4.15}$$

for $y^+ > 11.63$,

where k_P is the turbulent energy at cell P, κ is the von Karman constant (= 0.4187), E is the logarithm constant (= 9.793) and $f\left(\frac{Pr}{\sigma_T}\right)$ given by Gosman and Ideriah (1976) is equal to $9.24\left[\left(\frac{Pr}{\sigma_T}\right)^{3/4} - 1\right]e^{-0.007(\frac{Pr}{\sigma_T})}$. Shear force and heat flux can now be computed from the above expressions:

$$F_f = \tau_f A_f = M_{P,f} U_P \tag{4.16}$$

$$\frac{Q_f}{c_p} = \frac{q_f''}{c_P} A_f = N_{P,f}(T_P - T_f) \tag{4.17}$$

where A_f is the wall surface area, $M_{P,f} = \dfrac{\mu A_f}{y_P}$, $N_{P,f} = \dfrac{\mu A_f}{Pr \, y_P}$ for $y^+ \le 11.63$ and

$$M_{P,f} = \frac{\kappa C_\mu^{1/4} \rho_P k_P A_f}{\ln(Ey^+)}, N_{P,f} = \frac{C_\mu^{1/4} \rho_P k_P^{1/2} A_f}{\sigma_T\left[\dfrac{1}{\kappa}\ln(Ey^+) + f\left(\dfrac{Pr}{\sigma_T}\right)\right]}$$ for $y^+ > 11.63$. The shear force and the heat

transfer are then linearised and incorporated into the discretised equation (4.10) as a source term for the wall neighbouring cells. Also, the a_f of equation (4.10) is set equal to zero. Note that the format of equation (4.17) will help the understanding of the coupling mechanisms explained in Chapter 5.

Boundary conditions for k and ε must also be specified at solid boundaries. The generation and dissipation of turbulent energy are introduced as the source term of equation (4.10). According to Gosman and Ideriah (1976), the k source term for the cells adjacent to the walls may be represented by the following expression,

$$S_k = \tau_f \frac{U_P}{y_P} \ - \ C_D C_\mu^{3/4} \rho_P k_P^{3/2} \frac{u^+}{y_P} \tag{4.18}$$

where $u^+ = y^+$ for $y^+ < 11.63$; $u^+ = 1/\kappa ln(Ey^+)$ for $y^+ > 11.63$ and τ_f is computed by expression (4.16). The a_f coefficient is set to zero and equation (4.18) is linearised and introduced within the coefficients S_P and S_c of equation (4.9). In contrast, ε reaches its highest value for the flow close to the walls (much higher than in a free stream). A fixed value for ε is thus assumed for the P cell based on equilibrium relations (Gosman and Ideriah 1976):

$$\varepsilon_P = \frac{C_\mu^{3/4} k_P^{3/2}}{\kappa \, y_P} \tag{4.19}$$

To introduce this value at the boundary cell the linearised source coefficients are written as

$$S_P = -10^{30} \quad ; \quad S_c = 10^{30} \varepsilon_P \quad . \tag{4.20}$$

As the walls are considered impermeable, the pollutant flux is zero at the surface. In some special cases, for example if a substance is evaporating, the concentration flux could be defined at the wall. Thus, the pollutant flux is always known and a wall function to approximate the concentration

gradient is not necessary.

Openings

Open windows, doorways, cracks, air supply and return ducts, etc. are examples of openings. They are classified as inlets if the flow is entering the zone, or outlets if the flow is exiting the zone. Apart from pressure, all scalar variables are assumed uniform and they must be fixed at the inlets. Turbulent kinetic energy and energy dissipation rate are based on the following relationship (Gosman and Ideriah 1976),

$$k_{in} = IU_{in}^2 \qquad \varepsilon_{in} = \frac{k_{in}^{3/2}}{\lambda H} \qquad (4.21)$$

where subscript *in* indicates inlet condition, λ is the length scale factor (0.005), $H^{\#}$ is the height of the room and I, which is equal to 0.03, is the turbulence intensity. Additionally, the momentum (velocity intensity and direction) is generally supposed to be known at inlets when it has a major influence on the zone air flow. Nevertheless, in some cases, e.g. cracks, the cell dimension is considerably larger than the crack size and the intensity of the momentum does not alter the main flow. In such cases, the pressure is fixed at the inlet and a specified source of mass is injected to the domain. At the outlets, a set of options are available for the momentum equations boundary conditions: fixed velocity according to mass balance, fixed pressure or normal velocity gradient equal to zero. One of them should be chosen in accordance with the application. A zero stream wise gradient was imposed for the remaining scalar variables considering that the outside air condition has no effect on the inside condition.

Symmetry condition

This is mainly useful when a domain is symmetric to a certain plane. In such situations, the solution is carried out in just one half of the enclosure and consequently the computational burden is reduced. Also, for the case of free shear stresses (free boundary), a symmetry condition is assumed. At these planes zero gradient (no-flux) is imposed for all variables in the direction normal to the boundary. Considering Figure 4.6, the flux of the variable ϕ is

$$\left.\frac{\partial \phi}{\partial y}\right|_f = \frac{\phi_P - \phi_f}{y_P} = 0 \qquad \phi_P = \phi_f \qquad . \qquad (4.22)$$

_____

\# Some other authors employ the dimension of the opening rather than the height of the room to estimate ε_{in}. The use of height is also supported by Awbi (1991).

4.6 SOLUTION PROCEDURE

Compliant with equation 4.10, a set of algebraic equations is established which must be solved for each time-step. Although the equations are written in a linear form they are highly nonlinear due to the nature of the convective terms and source terms and due to the dependence of the flow properties (e.g. eddy viscosity) on the unknown state variables. In other words, the coefficients and source terms are dependent on the solution itself. The system of equations for one variable originating from equation (4.10) is written in matrix notation as[#]

$$A(\phi)\phi = B(\phi) \tag{4.23}$$

where ϕ is the vector of unknown nodal values, A contains the algebraic coefficients arising from discretisation and is dependent on the solution ϕ, B is made up of algebraic coefficients associated with the discretisation and may also depend on ϕ. The matrix $A(\phi)$ is typically sparse (few non-zero elements) and these non-zero terms are distributed in seven diagonals for the three-dimensional case, as shown by the schematic representation of Figure 4.7.

$$\begin{bmatrix} \cdot & \cdot & & \cdot & & \cdot & \\ \cdot & \cdot & \cdot & & \cdot & & \cdot \\ & \cdot & \cdot & \cdot & & \cdot & & \cdot \\ & & \cdot & \cdot & \cdot & & \cdot & & \cdot \\ & & & \cdot & \cdot & \cdot & & \cdot & & \cdot \\ & & & & \cdot & \cdot & \cdot & & \cdot & & \cdot \\ -a_L & & -a_S & a_P & -a_E & & -a_N & & -a_H \\ & & & \cdot & \cdot & \cdot & \cdot & \cdot & & \cdot \\ & & & & \cdot & \cdot & \cdot & \cdot & \cdot \\ & & & & & \cdot & \cdot & & \cdot & \cdot & \cdot \\ & & & & & & \cdot & & \cdot & \cdot & \cdot \end{bmatrix} \begin{bmatrix} \cdot \\ \cdot \\ \cdot \\ \cdot \\ \cdot \\ \cdot \\ \phi_P \\ \cdot \\ \cdot \\ \cdot \\ \cdot \end{bmatrix} = \begin{bmatrix} \cdot \\ \cdot \\ \cdot \\ \cdot \\ \cdot \\ \cdot \\ b_P \\ \cdot \\ \cdot \\ \cdot \\ \cdot \end{bmatrix}$$

Figure 4.7 Representation of the *dfs* matrix for the variable ϕ.

Considering the fact that A is not a dense matrix, its inversion using direct methods (i.e. those requiring no iteration) can be complicated and can require large amounts of computer storage and time. For a linear problem, which requests the solution of the algebraic equations only once, a direct method may be acceptable. In nonlinear problems, on the other hand, the equations have to be solved

[#] Note here the similarity with the BTS equivalent matrix of previous chapter.

repeatedly, since the algebraic coefficients (**A** and **B**) are dependent on ϕ and therefore, direct methods are usually not economical. Iterative methods are attractive for handling nonlinearities and generally involve minimal computer storage. Initially, the field of ϕ is guessed and the equations are manipulated in some manner in order to obtain an improved field estimate. The algorithm is repeated successively leading to a result which is sufficiently close to the exact solution of the algebraic equations. In nonlinear problems, the coefficients **A** must be re-evaluated, according to the new values of ϕ, as the solution procedure takes place.

The *dfs* solver consists of a convenient combination of a direct method; Thomas algorithm (or TDMA - Tri-Diagonal Matrix Algorithm) and an iterative Gauss-Siedel method (Patankar 1980). In one-dimensional problems, the matrix of the coefficients has a tri-diagonal format, similar to the construction sub-matrices of Chapter 3. A direct solution of such matrices can be obtained using a derivation of the Gaussian elimination method. Assume that the matrix of Figure 4.7 can be re-ordered with just three diagonals (the main diagonal and two adjacent diagonals). In such a case, the ϕ_S's ϕ_N's, ϕ_L's and ϕ_H's are considered known and are added to the b coefficient on the right hand side of Figure 4.7. Equation (4.23) is then re-written and the matrix acquires the one-dimensional format of Figure 4.8.

$$\begin{bmatrix} \cdot & \cdot & & & & & \\ \cdot & \cdot & \cdot & & & & \\ & \cdot & \cdot & \cdot & & & \\ & & -a_W & a_P & -a_E & & \\ & & & \cdot & \cdot & \cdot & \\ & & & & \cdot & \cdot & \cdot \\ & & & & & \cdot & \cdot \end{bmatrix} \begin{bmatrix} \cdot \\ \cdot \\ \cdot \\ \phi_P \\ \cdot \\ \cdot \\ \cdot \end{bmatrix} = \begin{bmatrix} \cdot \\ \cdot \\ \cdot \\ b_P{}' \\ \cdot \\ \cdot \\ \cdot \end{bmatrix} \quad where \ \ b_P{}' = b_P + a_S\phi_S + a_N\phi_N + a_L\phi_L + a_H\phi_H$$

Figure 4.8 One-dimensional *dfs* submatrix for variable ϕ.

Supposing that the submatrix of Figure 4.8 is for the x direction, a submatrix for each discretised value of y and z exists. The one-dimensional matrix of Figure 4.8 is directly solved for a fixed y and z position, employing the TDMA algorithm. The solution procedure for the overall matrix of Figure 4.7 takes place solving each x-direction submatrix for each y value and then for each z value. As the operation evolves from one x-row to the next, the most updated value of ϕ_P's neighbours are used as known values characterising the Gauss-Siedel method. The present scheme consists of a forward sweep (from the lower values of y and z to their higher values) and a backward sweep (from higher values to lower ones). After the sweeps take place a_i and b_i coefficients are re-evaluated based on the new ϕ_i's and again the solution is performed. The procedure is valid for each ϕ variable which is independent from the others. However, all ϕ variables are inter-dependent and they must be solved simultaneously. Thus, the overall practice is firstly to evaluate the coefficients and finally to obtain the

solution for each of the ϕ variables in sequence. This operation progresses until the converged solution is achieved according to some criteria. The whole solution procedure, which is carried out for each simulation time-step, is summarised in Figure 4.9.

Figure 4.9 Summary of the overall *dfs* solution procedure.

Apart from continuity, all other conservation equations lead to a discretised equation for U, V, W, T, C, k, ε, but an explicit equation for pressure does not exist. Since the discretised equations are not solved together, the pressure cannot be obtained from the procedure of the previous paragraph . A modified form of the continuity equation is then produced in order to compute the pressure. This is performed on the basis that the velocity components computed from the momentum equations do not satisfy continuity until the convergence has been achieved. In fact, a pressure correction equation is

derived from the continuity assuming the same form of equation (4.10). This equation is solved in the same manner as the others resulting in a pressure correction field. The pressure is then evaluated from its previous iteration with the pressure correction added. The pressure correction equation and the solution are based on the SIMPLE (Semi-Implicit Method for Pressure-Linked Equations) algorithm (Patankar 1980).

Convergence is reached when the maximum value amongst the sum of mass and momenta residuals is below a value specified by the user. The residuals are computed separately for each equation and are written as

$$R_k = \sum_{j=1}^{N}(a_j\phi_j - \sum_{i}^{n} a_{i,j}\phi_{i,j} - b_j) \quad ; \quad k = m, x, y, z \quad ; \quad i = W, E, S, N, L, H \qquad (4.24)$$

For the case of inlet openings in the occupied space, the residuals of the continuity equation are made relative to the inlet flow,

$$R_m = \frac{\sum_{j=1}^{N}(a_j\phi_j - \sum_{i}^{n} a_{i,j}\phi_{i,j} - b_j)}{\dot{m}_{in}} \quad ; \quad i = W, E, S, N, L, H \qquad (4.25)$$

and the residuals of the momentum equations is made relative to the inlet momentum,

$$R_k = \frac{\sum_{j=1}^{N}(a_j\phi_j - \sum_{i}^{n} a_{i,j}\phi_{i,j} - b_j)}{\dot{m}_{in}U_{in}} \quad ; \quad k = x, y, z \quad ; \quad i = W, E, S, N, L, H \qquad (4.26)$$

where R is the absolute or relative sum of all cell residuals, $\dot{m}_{in}$ is the inlet mass flow rate, U_{in} is the inlet velocity, the indices m, x, y and z are respectively related to mass, x, y and z momentum, N is the total number of cells in the domain and n is the number of "P" neighbours. The convergence criteria is then attained if an inequality is true:

$$\max[R_m , R_x , R_y , R_z] < \psi \qquad (4.27)$$

where ψ is the maximum admissible value for R.

The iterative scheme introduced to handle the nonlinearities may produce divergence, or convergence is never reached (in which case oscillations around a certain value occurs). To overcome

the presence of such phenomena, underrelaxation methods are applied to the discretised equations. These prevent large changes of ϕ from one iteration to the next by holding the new iteration value closer to the previous one. Two kinds of underrelaxation are considered: inertia and linear. The former is inserted into equation (4.10) in the form of a transient term:

$$a_P \phi_P - \sum_i^n a_i \phi_i + \frac{\rho_P \upsilon_P (\phi_P - \phi_P^o)}{\delta t_f} = b_P \qquad i = W, E, S, N, L, H \qquad (4.28)$$

where ϕ_P^o is ϕ value at the previous iteration and δt_f is the relaxation factor (fictitious time-step). The smaller δt_f, the higher the dependence of the new value on the previous one and the lower the influence of the other terms on the equation. When the solution takes place, the ϕ_P fictitious time-step coefficient is added to a_P and the previous iteration term is appended to the source term b_p. The latter is included in the discretised equation as a weighed average between current and previous iteration values (Patankar 1980):

$$\frac{a_P}{\alpha} \phi_P - \sum_i^n a_i \phi_i = b_P + (1 - \alpha) \frac{a_P}{\alpha} \phi_P^o \qquad i = W, E, S, N, L, H \qquad (4.29)$$

where α is the linear under-relaxation factor (weighing factor). Again the previous iteration term is added to b_P. At convergence, the current and previous values are virtually the same and the effect of inertia and linear relaxation factors vanishes. Inertia under-relaxation factor can be applied to all transport variables but pressure, in which case only the linear under-relaxation can be used. Although the process is referred to as under-relaxation, they both can be used to overrelax the equation and speed up the convergence if the process is not subjected to numerical instabilities. In case of over-relaxation, δt_f assumes negative values, and values greater than one are expected for α. In contrast, δt_f is positive and α adopts values between zero (totally underrelaxed, no changes between iterations) and one (no under-relaxation) for the under-relaxation procedure.

4.7 PROBLEM DEFINITION

The information necessary to define the air flow problem to *dfs* is introduced in this section. Such information is subjected to a range of validity and if an input value lies outside such a range, a warning message is produced. The input data are provided via a configuration file which contains instructions about the zone geometry, grid distribution, boundary conditions and some simulation control parameters.

Geometry and grid

An automatic grid generation could locate, for example, an interface between a solid surface and an opening occurring inside some cells. A fraction of the volume of such cells would then be made solid and some fluid. In order to avoid this, and to conform the cell distribution with solid

boundaries, openings, furniture, etc., grid and geometry are defined together. This procedure consists of dividing each dimension of the cuboid domain into a certain number of regions. For each region, the direction, the length and the grid distribution is defined. The cells are independently distributed in each region according to a power law equation (4.11) and the parameters necessary are shown in Table 4.2. To illustrate the process, consider the case where a door is located on a surface (as shown in Figure 4.10) and a grid must be distributed over the surface in the longitudinal direction. Three regions in such a direction are identified; one region located left of the door, one at the doorway and the last one placed to the right of the door. At the left region, the power law parameters are set to: $n > 0$, $|c| > 1$ and $c > 0$ in order to make the cell sizes increase from left to right. The cells are uniformly distributed at the doorway ($c = 1$) and the cells sizes decrease from right to left on the last region using the parameters $n > 0$, $|c| > 1$ and $c < 0$.

Table 4.2 Grid and geometry definition.

Direction	Number of cells in the region		Dimension of the region (m)	Power law coefficient
X	$n > 0$	Cells distributed over the whole region.		$c = 1$ Uniform distribution
Y			$L > 0$	$\|c\| > 1$ Grid size $\begin{bmatrix} \text{increase* if } c > 0 \\ \text{decrease* if } c < 0 \end{bmatrix}$
Z	$n < 0$	Cells distributed symmetrically over the region.		$\|c\| < 1$ Grid size $\begin{bmatrix} \text{decrease* if } c > 0 \\ \text{increase* if } c < 0 \end{bmatrix}$

* Increase/decrease from the beginning to the end (or middle if $n < 0$) of the region.

The grid can be specified in one, two or three dimensions depending on the type of air flow to be analysed.
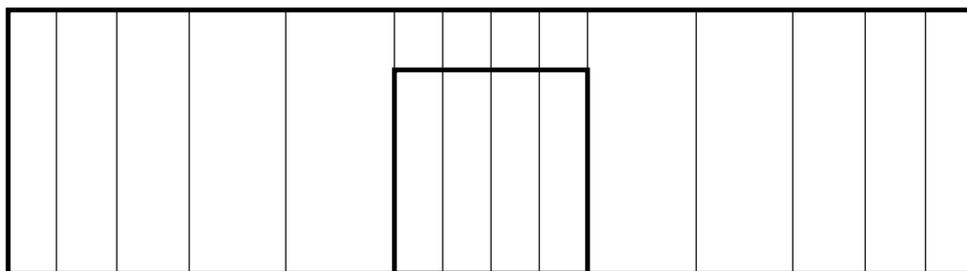
Figure 4.10 Example of *dfs* grid definition.

Equations

The user is able to define the nature of the flow (laminar or turbulent, two or three-dimensional) by choosing the equations to be solved. Energy and concentration equations and buoyancy effect are included or not in the simulation depending on the problem. The z direction is assumed to be vertical (direction of gravity) and buoyancy is only considered in this direction. If a two-dimensional simulation is running in the x-y plane no buoyancy is taken into account. For example, if U, V, T, k and ε are specified, the flow is two-dimensional turbulent, the energy equation is solved but no buoyancy is involved.

Openings

Four types of boundary conditions are available to represent openings: pressure, mass flow rate, velocity and zero velocity gradient. They must be chosen according to the situation (usually velocity is fixed at the inlets and pressure, mass flow or zero velocity gradient at outlets). Six planes, designated "West" and "East" (normal to x), "South" and "North" (normal to y) and "Low" and "High" (normal to z), are used to define the cell faces. The openings are then located at one of the six planes according to the grid definition in a certain number of cells. In other words, the plane name and the indices of the first and last cells inserted in the opening (in each direction) are specified. The definition of the plane is only relevant for velocity and zero gradient boundary types. For pressure and mass flow types this information becomes redundant. If an opening is introduced in a certain plane (say West) the indices of the initial and final cells in the direction normal to the plane (say x-direction) must be the same. Additionally, the air condition at openings must be provided in terms of mass flow rate (mass flow, velocity boundary type) or pressure (pressure boundary type). In the case of velocity boundary types, the velocity at the opening is based on the specified mass flow rate, air density at the opening and opening area. A positive mass flow rate indicates that the flow is entering the domain and an outlet flow is denoted by a negative value. Also, temperature and concentration only are defined, if necessary, at the inlets, since at the outlet it is assumed that the diffusive terms are overcome by the convective terms and the gradients of such properties can be made equal to zero. To clarify the opening definition, consider the following example

$$\text{Vel} \quad \text{West} \quad 5 \quad 5 \quad 3 \quad 7 \quad 5 \quad 8 \quad 1.0 \quad 20.0 \quad 0.1 \quad .$$

This indicates that velocity is fixed at the WEST face of the 5th cell in the x-direction. The opening is located at five cells (3rd, 4th, 5th, 6th and 7th cells) in the y-direction and at four cells (5th, 6th, 7th, and 8th cells) in the z-direction. $1 kg/s$ of air is entering the domain at 20°C and with a 10% pollutant concentration. Table 4.3 presents the information necessary to describe an opening and the air condition at such a position.

For transient simulations, dynamic boundary conditions can also be specified. In such a situation, the air condition in Table 4.3 is substituted by an identifier (a word or a number). The identifier points to three different files where time-series of mass flow (or pressure), temperature and concentration for each opening are defined. Each time-step, during the simulation, *dfs* reads the corresponding files and up-dates the boundary conditions.

Table 4.3 Opening definition

Type	Location	Initial and final cells in x-axis	Initial and final cells in y-axis	Initial and final cells in z-axis	Air condition		
- Pressure - Mass flow - Velocity - Zero Vel. gradient	- West - East - South - North - Low - High	IX_i IX_f	IY_i IY_f	IZ_i IZ_f	- Mass flow rate (kg/s) - Pressure (Pa)	- Temp. (°C)	- Conc. (-)

Solid boundaries

The boundary conditions for solid surfaces are characterised by three types: fixed temperature, fixed heat flux or symmetric plane. For the first two types, only temperature or heat flux are specified and for the symmetric plane type no condition is specified since the gradient normal to the plane for all variables is assumed zero. The solid boundaries are positioned by applying the same procedure as for an opening. The information required to describe a solid boundary is introduced in Table 4.4. If a dynamic simulation is performed, an identifier (which can be a surface name or an index) substitutes the boundary condition in Table 4.4. Similarly to the openings, a file containing time-series of temperature or heat fluxes must be created.

Table 4.4 Solid boundary definition

Type	Location	Initial and final cells in x-axis	Initial and final cells in y-axis	Initial and final cells in z-axis	Boundary condition
- Temper. - Heat flux - Symmetry	- West - East - South - North - Low - High	IX_i IX_f	IY_i IY_f	IZ_i IZ_f	- Temperature (°C) - Heat flux (W)

Heat/concentration sources

Solid objects, partitions, solid or non-solid heat or concentration sources can be inserted in the domain at this point. Four types of sources can be chosen: fixed temperature, heat flux, concentration and concentration flux. The sources are characterised as a group of cells with a cuboid shape and are defined exactly as for openings except that the boundary planes are not specified. Furthermore, the sources can be blocked (representing furniture or a partition, for example) or not. Table 4.5 shows how sources can be specified inside the domain. Again, in transient simulations, an identifier indicates that temperatures and concentration are read from two different files.

Table 4.5 Heat/concentration source definition

Type	Initial and final cells in x-axis	Initial and final cells in y-axis	Initial and final cells in z-axis	Boundary condition	Blocked Cells ?
- Temperature - Heat flux - Concentration - Concentration Flux	$IX_i \quad IX_f$	$IY_i \quad IY_f$	$IZ_i \quad IZ_f$	- Temperature(^{o}C) - Heat flux(W) - Concentration (-) - Concentration Flux(kg/s)	- Yes - No

Iteration process control

The convergence process is controlled by the user specified number of iterations and the maximum source of residuals allowed. The simulation stops when the tolerance of residuals or the defined number of iterations is reached, whichever occurs first.

The user has also the control over the relaxation factors. Linear and fictitious time-step relaxation factors can be selected for each of the transport variables (U, V, W, T, C, k, ε) and also a linear relaxation can be chosen for turbulent viscosity (μ_t). If a relaxation factor is not specified, a default value is assumed.

Convergence is also a function of the initial values of the variables. A solution can be achieved or not depending on the values assumed at the beginning of the iteration process. Initial values (uniform for the whole field) for each transport variable can be selected in order to speed up the convergence.

A previously converged solution saved to file can also be used to initiate variable values for a new simulation. This facility is named re-initialisation because after being partially run, the simulation can be re-started. For example, a zone may be subjected to a one day simulation and after 12 one hour time-steps the solution process diverges. To achieve convergence the relaxation factors can be reset and the simulation re-started, but instead of beginning from the first time-step it can be started from the last converged time-step without repeating the already converged hours. This is possible because

both present and future values are set to the initialised values. Initialisation fields are only feasible at the first simulation time-step since after that the initial values for a certain time-step are the converged solution of the last time-step.

Results

The velocity component and scalar variable fields are saved to file for post-processing. *dfs* uses 3rd party codes to provide visualisation of the temperature and pressure fields and velocity profiles (Rosten and Spalding 1987). The results can be selected to be stored at specific time-steps to avoid uninteresting results from overloading the disk.

The values of pressure and velocity components at monitored positions, and the corresponding residuals, can be observed graphically as the simulation progresses or through a monitoring file after the simulation has taken place. The user is able to choose a cell inside the domain where the variables are monitored.

All the information introduced in this section is provided for *dfs* via a configuration file. To clarify the definition process, the zone Kitchen (Figure 3.14), which was used to exemplify the problem definition in Chapter 3, is chosen to be defined for a *dfs* simulation. The configuration file for this problem is presented in Figure 4.11[#]. Compare this file with Figure 4.12 and observe that the grid is defined to conform with the openings (one inlet and one outlet), the equipment and the window. The non-isothermal (indicated by T), turbulent (denoted by the variables k and ε), three-dimensional flow (expressed by the grid definition in X, Y and Z and by the three velocity components, U, V and W) is solved including buoyancy (indicated by Buoyancy). Two types of boundaries were used to define the inlet (near the ceiling) and the outlet (near the floor): Velocity at the inlet and Mass flow at the outlet. Since the problem is dynamic, the air condition at the inlet and outlet are supplied in a file as a time-series (the identifiers Open_1 and Open_2 indicates that).

Unlike the *bps* problem where all conditions were defined at the <u>outside</u> surface in the *dfs* problem, the boundary conditions are defined at the <u>inside</u> surface. Apart from the West wall where heat flux is imposed, all surface temperatures are fixed. Observe that all surface conditions are denoted by an identifier. Deliberately, the identifiers are the surface names shown in Figure 4.12 and 3.13 (this makes the problem definition introduced in Chapter 5 easier to understand). Those temperature are obtained from a time-series included in a file. Note that 4, 2 and 2 surface boundaries were necessary to define the Back, the Part_kit and West walls, respectively. That is because the window and the openings are located at those walls.

_____

Again it should be noted that users are offered a facility by the ESP-r project manager for the creation of this file.

```
#    Simulation Title
  Kitchen mechanical ventilated.
#    N. of x-Regions      N. of y-Regions      N. of z-Regions
        1                    3                     1
#    Grid X-direction    N. of cells    Length    Pow. law coefficient
        X                    7           3.00           1.0
#    Grid Y-direction    N. of cells    Length    Pow. law coefficient
        Y                    4           1.50           1.0
        Y                   -3           1.00           1.2
        Y                    3           1.00           1.1
#    Grid Z-direction    N. of cells    Length    Pow. law coefficient
        Z                    9           2.80           1.2
#    Variables:
        U    V    W    T    k    Epsilon    Bouyancy
#    Number of openings
        2
#    Opening type    location   Ii  If  Ji  Jf  Ki  Kf    P(Pa) or m(kg/s)   T('C)   C(-)
        Vel           South       1   1   6   7   8   9       open_1
        Mas           North      10  10   1   2   1   2       open_2
#    Number of solid boundaries
        12
#    Solid  Bnd. type     location   Ii  If  Ji  Jf  Ki  Kf    T('C) or Q(W)
        Heat             West       1   1   1  10   1   9        Front
        Temp             East       7   7   1   4   1   9        Back
        Temp             East       7   7   5   7   1   3        Back
        Temp             East       7   7   5   7   4   6        Window
        Temp             East       7   7   5   7   7   9        Back
        Temp             East       7   7   8  10   1   9        Back
        Temp             North      3   7  10  10   1   9        Part_kit
        Temp             North      1   2  10  10   2   9        Part_kit
        Temp             South      1   5   1   1   1   9        Right
        Temp             South      1   7   1   1   1   8        Right
        Temp             High       1   7   1  10   9   9        Ceiling
        Temp             Low        1   7   1  10   1   1        floor
#    Number of heat/concentration sources
            1
#    Source type      Ii  If  Ji  Jf  Ki  Kf    T('C) or Q(W) or C(-) or CF(kg/s)    Yes(blocked) or No
        Heat           2   3   2   4   1   3              Equipment                          Yes
#    Max. n. of iterations          Max. source of residues
        200                             0.01
#    Number of relaxation factors
        5
#    Relaxation factor type         variable        value
        Linear                      U               0.5
        Linear                      V               0.5
        Linear                      W               0.5
        Inertia                     k               1.0
        Inertia                     E               0.1
#    Number of variables to be initiated
        2
#    Initial conditions variable          initial value
            V                              0.10
            T                              20.0
#    Time-step interval to print results            result file name
            4                                        Kitchen.res
#    Monitoring position IMON  JMON  KMON           monitoring file name
                         3     1     3              Kitchen.mon
#    Re-initialize simulation ?  Yes or No
                            No
Kitchen.flw
Kitchen.otp
Kitchen.wtp
Kitchen.eqp
```

Figure 4.11 Example of a *dfs* configuration file.

Differently from the previous chapter, the equipment can be placed geometrically within the Kitchen and the heat released more precisely located. Additionally, as the equipment is a piece of furniture, some cells of the domain are blocked to represent it. The identifier Equipment in the configuration file indicates that a time-series of convective heat is resident in a file.

The simulation stops after 200 iterations or if the sum of the residuals is less than 1% of the inlet momentum or mass flow rate. Five relaxation factors are specified: linear for velocity components and inertia for turbulent variables. The velocity component in the y direction is made equal to 0.1m/s for all cells in the domain and the temperature field is initialised equal to 20°C. The variable fields are stored every four time-steps within the file Kitchen.res. The monitoring position is located at the cell 3,1,3 and the monitoring results, consisting of simulation residuals and monitoring values, are saved to the file Kitchen.mon. The re-initialisation facility is not invoked in this case.
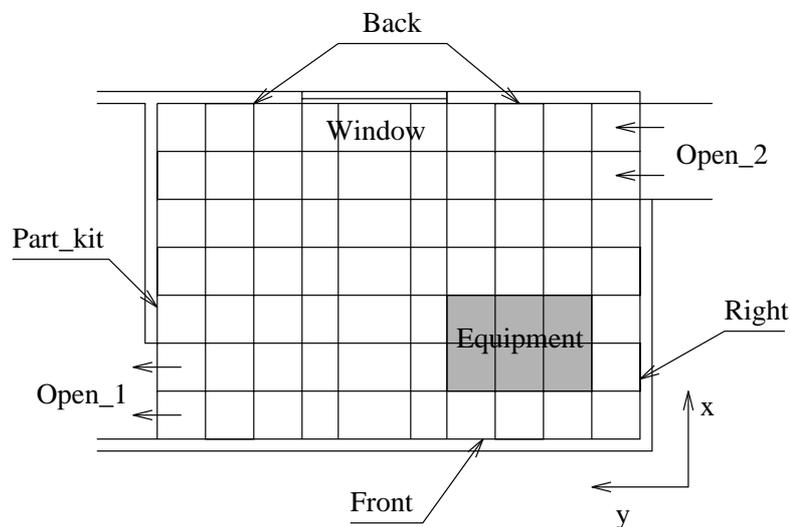
Figure 4.12 Geometry for the configuration file of Figure 4.11.

The last four lines in the file supplies the file names of the time-series of flow rates (kitchen.flw) at the openings, inlet temperatures (kitchen.otp), surface temperatures (kitchen.tmp) and Equipment heat sources (kitchen.wtp). The time-series of surface temperatures contained in the file Kitchen.wtp are shown in Figure 4.13. Observe that the first line in such a file indicates the surface name which must match the names provided as boundary conditions. Each column, therefore, contains the surface temperatures or heat fluxes (in the case of Front wall) at each simulation time-step. At each time-step (in this case 1h), the file is read and the surface temperatures up-dated. The other time-series files have the same format as the surface temperature file.

Time(h)	Front	Back	Window	Part_kit	Right	Ceiling	Floor
1.0	0.0	11.0	10.0	15.0	10.0	15.0	9.0
2.0	0.0	11.5	10.4	15.2	10.5	15.3	10.0
3.0	0.0	12.1	11.0	15.5	11.0	15.7	11.0
4.0	0.0	13.0	11.7	15.8	11.9	15.9	12.0

Figure 4.13 Time-series of surface temperatures.

4.8 REMARKS

This chapter discussed the ESP-r module, *dfs*, which was developed for the simulation of indoor air flow. Its main capabilities, the mathematical model, numerical technique, solution procedure, boundary conditions and problem definition were discussed. Although air flow properties within occupied spaces can be predicted by using such a simulation tool, the development of this program was addressed to the integration discussed in Chapter 5. As the reader will notice, the boundary conditions and the problem definition will mostly serve this purpose.

REFERENCES

Awbi, H. B., 1991, *Ventilation of Buildings*, E & FN SPON.

Chen, Q. and Jiang, Z., 1992, Significant Questions in Predicting Room Air Motion, *ASHRAE Transactions*, vol. 98, part 1, pp. 929-939

Gosman, A. D. and Ideriah, F. J. K., 1976, *TEACH-2E: A General Computer Program for Two-Dimensional, Turbulent, Recirculating Flows*, Imperial College, London.

Jones, P. J. and Whittle, G. E., 1992, Computational Fluid Dynamics for Building Air Flow Prediction - Current Status and Capabilities, *Building and Environment*, vol. 27, n. 3, pp. 321-338.

Launder, B. E. and Spalding, D. B., 1974, The Numerical Computation of Turbulent Flow, *Computer Methods in Applied Mechanics and Engineering*, vol. 3, pp. 269-289.

Patankar, S. V., 1980, *Numerical Heat Transfer and Fluid Flow*, Hemisphere Publishing Corporation.

Rodi, W., 1984, *Turbulence Models and Their Applications in Hydraulics - A State of the Art Review*, University of Karlsruhe, Karlsruhe, Federal Republic of Germany.

Rosten, H. I. and Spalding, D. B., 1987, *The PHOENICS Beginner's Guide*, CHAM Limited, UK.

Shaw, C. T., 1992, *Using Computation Fluid Dynamics*, Prentice Hall.

5.1 INTRODUCTION

The previous chapters described two ESP-r modules for complementary building simulation applications. As the reader will have noticed, these chapters were intentionally given the same structure. The objective of this approach was to draw attention to each system's similarities which suggest possibilities for combining Building Thermal Simulation (as represented by ESP-r *bps*) and Computational Fluid Dynamics (as represented by ESP-r *dfs*).

In the next section the commonalities between *bps* and *dfs* are emphasised. During the process of conflation, the functionalities of both systems were extended and this work is explained in Section 5.3. Section 5.4 introduces three possible conflation mechanisms at different levels. Section 5.5 discusses how a problem is defined for a combined simulation and finally, the capabilities of the combined system are introduced in Section 5.6.

5.2 COMMONALITIES BETWEEN THE bps AND dfs MODULES

The main commonality between the two systems lies in the fact that both are able to undertake transient thermal energy and mass flow simulations. Although *dfs* is usually employed to simulate air flows within a single zone (or within a small part of a building), there is no inherent restriction to use the system for the thermal energy analysis of the entire building. The limitation in practice is more associated with the computer capabilities than the physical model. Theoretically, *dfs* can be used to perform simulations of the thermal processes taking place within plant components and constructions. On the other hand, *bps* generally considers the air within zones as homogeneously mixed although a zone can be subdivided into a small number of volumes and gradients of indoor air flow properties can be predicted. This is however problematic because insufficient information is usually known about the correlation between inter-volume mass flow rates and pressures, and the convection coefficients at inside surfaces.

Both *bps* or *dfs* could be made to apply the conservation of mass and energy principles to predict temperature, flow rates, humidity, etc in several components of the building and plant systems. Although *bps* does not employ momentum equations to describe the air flow, equation (3.7) acts as a substitute for momentum equations since pressure difference is the driving force of the flow. Despite equation (3.7) being a one dimensional expression, the flow can be applied to many directions by

defining various flow paths in the space.

It must be noted that the boundaries of the *dfs* model coincide with the internal surfaces defined for the *bps* model. *Bps* assigns energy balances in the internal surfaces from which the surface temperatures are computed. Although, a non-structured grid can be defined in the flow network approach, the nodes in this network represents <u>similar</u> air volumes in the *dfs* mesh.

Unlike other simulation models which employ combinations of numerical and analytical methods (such as response factor and the frequency response method) both *bps* and *dfs* apply a numerical solution to the set of conservation equations. Additionally, they make use of the conservative finite volume method to discretise the differential equations resulting in an equivalent set of algebraic conservation equations. Clearly the algebraic equations differ only by the inter-volume interaction coefficients and source terms which are specific for each system of equations. As the originated equations are non-linear algebraic expressions, they can both be solved applying the same numerical solution technique. However, in the present work distinct solvers were implemented since the nature of the equations and non-linearities are different.

As described in Sections 3.7 and 4.7, both systems present a general structure and were conceived to deal with different geometries which are subjected to distinct boundary conditions. For example, casual gains can be introduced inside a room in the form of source of heat and/or mass and different control schedules can be imposed on the air condition by both systems.

As explained, *bps* has the potential to predict the thermal performance of buildings including uniform air flow properties within rooms. The system can also compute individual processes of internal longwave radiation, shortwave radiation and conduction. The important point is that the system is usually restricted to compute only uniform air conditions inside zones which may not be adequate for predictions of local comfort levels. On the other hand, *dfs* is capable of modelling gradients of air flow properties within zones for a range of problems. The *dfs* boundary conditions, by contrast, are generally unknown or difficult to estimate, unless they are measured for the specific case.

From the examination of the commonalities, a combination of the two systems emerges as a way to reduce the short-falls of each. A combined technique would eliminate problems with the *dfs* boundary conditions, make possible evaluation of air flow property distribution and model all other energy transfer mechanisms such as intra-construction conduction, internal and external surface longwave exchanges, shortwave radiation impinging on internal and external walls, interaction with plant components, etc. Also, the number of finite volumes (equations) involved is reasonably small, demanding an accessible computational power. The present chapter proposes a conflation technique, with the purpose of computing indoor air property distribution where judged relevant. As illustrated by Figure 5.1, *dfs* assesses air flow properties gradients within zones of interest and the rest of the building (including its nodal flow network) is represented by the *bps* methodology.
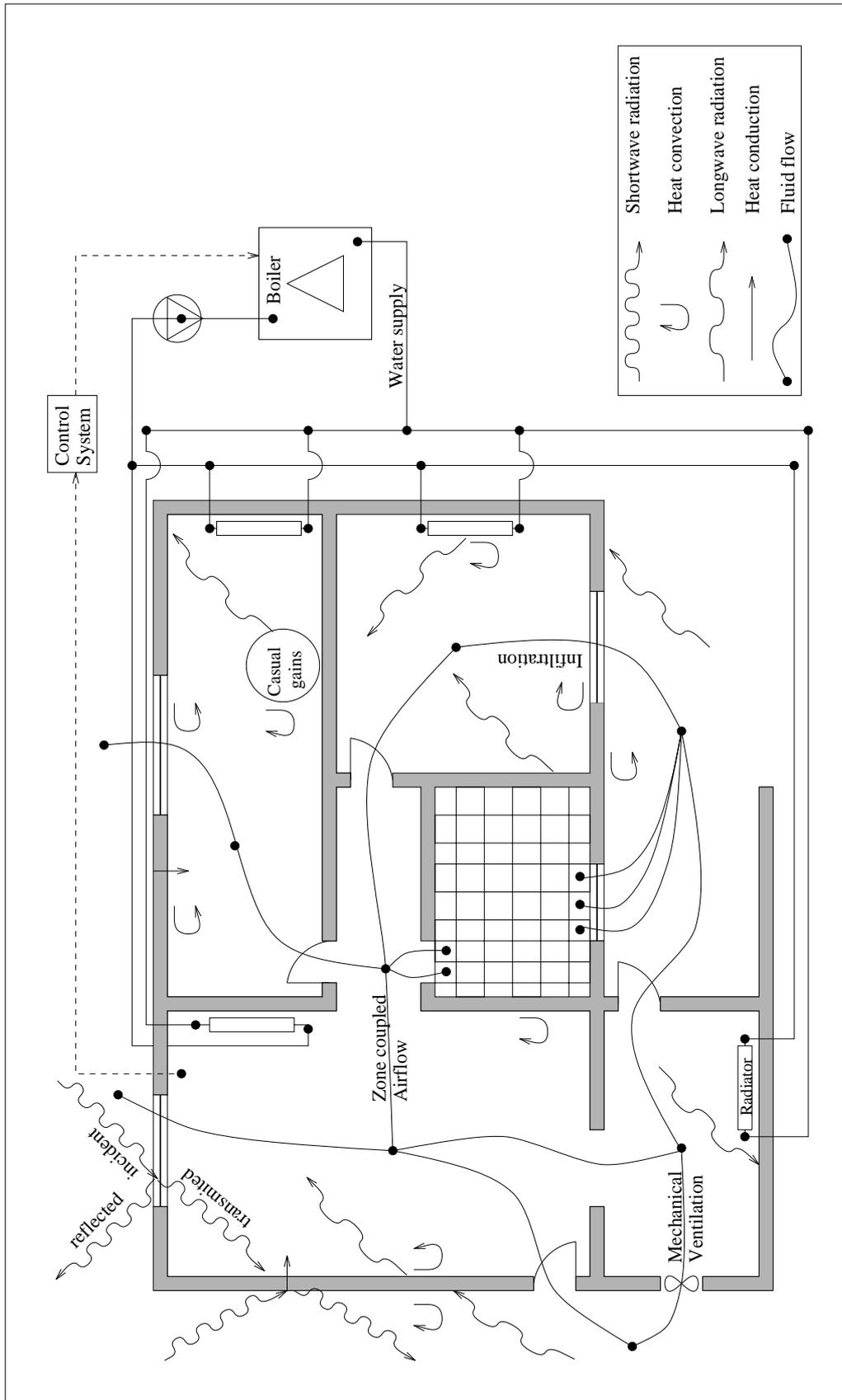
Figure 5.1 Building/plant energy flow paths

5.3 EXTENDING THE FUNCTIONALITIES OF bps AND dfs

Some modifications to the systems were introduced in order to improve their potential to better represent reality. The *bps* capabilities to control mass flow through components were enhanced, and the three-dimensional, transient module, *dfs*, developed.

bps flow control enhancements

The *bps* mass flow control was originally performed by exclusive flow control components which could only manage pressure driven flows (Aasem 1992). A general procedure was introduced to allow the flow control over any component of the network. The control of temperature driven flows through large openings is now also possible. This is done by multiplying the mass flow through a component by a control variable. The control variable assumes values between zero (component closed) and one (component completely open) allowing a fraction of the total mass flow rate to cross the component for a given pressure and/or temperature difference. The control variable values are attributed through the control algorithm according to some user defined control law (free-floating, on-off and linear control with hysteresis). A control law establishes a relation between the sensing property (mass flow rate, zone temperature, ambient temperature, wind speed, etc.) and the actuating property (mass flow rate). The law can be imposed during different periods of the day and can be prescribed on a weekly, monthly or seasonal basis. This development task not only served the purpose of enhancing *bps*' capabilities but also encouraged familiarity with the system's air flow model, structure and source code was increased.

dfs module development

The original TEACH program was written to solve two-dimensional, steady flows. Since the air flow within buildings is rarely two-dimensional and it is always dynamic, a new, *dfs* code was developed to compute transient, three-dimensional flows, where possible code re-use from TEACH was undertaken. *Dfs* also deals with buoyancy driven flows because this plays a major role in most building applications. In addition to the linear relaxation, the inertia relaxation factor was introduced to help the user with the control of the *dfs* iterative solution process. The TEACH algorithm for the solution of the algebraic equations, which was re-used, was modified to deal with the three-dimensionality of the equations; an alternative algorithm which consists of sweeping forward and backwards (as explained in Section 4.6) was introduced. The concentration equation was added to the set of conservation equation to take into account dispersion of pollutants (Elsen 1994)[#]. A relatively generic procedure to generate the mesh, which is based on a power law distribution, was included to help the user to define the problem.

––––––––––––––––

This work comprised part of the final year project of the first degree in Mechanical Engineering of the student Jan ten Elsen.

A user interface was implemented into *dfs* to assist with the specification of different geometries, grid distributions, heat source intensities and positions and boundary conditions. The interface also provides the user with a choice of different variable initial values, relaxation factors and dynamic boundary conditions. A graphic visualisation of the equation residuals and some monitoring values during the solution process is also available. This facility allows a continuous observation of the iteration process. Visualisation of the generated grid is also offered with the possibility to observe how the cells are distributed over the discretised domain.

5.4 CONFLATION MECHANISMS

As illustrated by Figure 5.1, the combination of the two systems consists of substituting a *bps* zone air volume by a *dfs* domain. The two systems thus need to communicate to each other in a certain manner. The conflation problem is essentially concerned with *dfs* boundary conditions or in other words, what takes place at the interface between the two domains. The interaction between the two systems occurs at the inside zone surfaces and at openings (doorways, windows, ducts, cracks, etc). In terms of conservation principles, the energy, momentum and mass balance equations must be connected.

At the solid interface a number of *dfs* cells are in contact with an internal surface. Figure 5.2 illustrates the energy interaction of the surface node with other nodes and with *dfs* cells. It should be noticed that convection heat transfer between the *bps* air node and inside surface node is substituted by the interaction between the surface node and *dfs* cells. Inside surface temperature and convection heat transfer are thus the parameters involved in the exchange mechanism.

At the openings, *dfs* cells can be in contact with some other zone air node, exterior air nodes, or some plant component nodes. Mass flow rates, pressures, velocities and other scalar variables (such as temperature, humidity, etc.) are, in this case, the quantities to be inter-changed.

Three different conflation mechanisms have been investigated corresponding to increasing degrees of complexity and sophistication. Firstly, a simple scheme involving no direct interaction between the two systems was investigated. This scheme accounts concurrently for the interactions at the internal surface (convection heat transfer) and at the openings. Secondly, direct interactions of the thermal coupling at inside zone surfaces are considered and finally, a direct integration of the momentum and mass equations at the openings are taken into account.
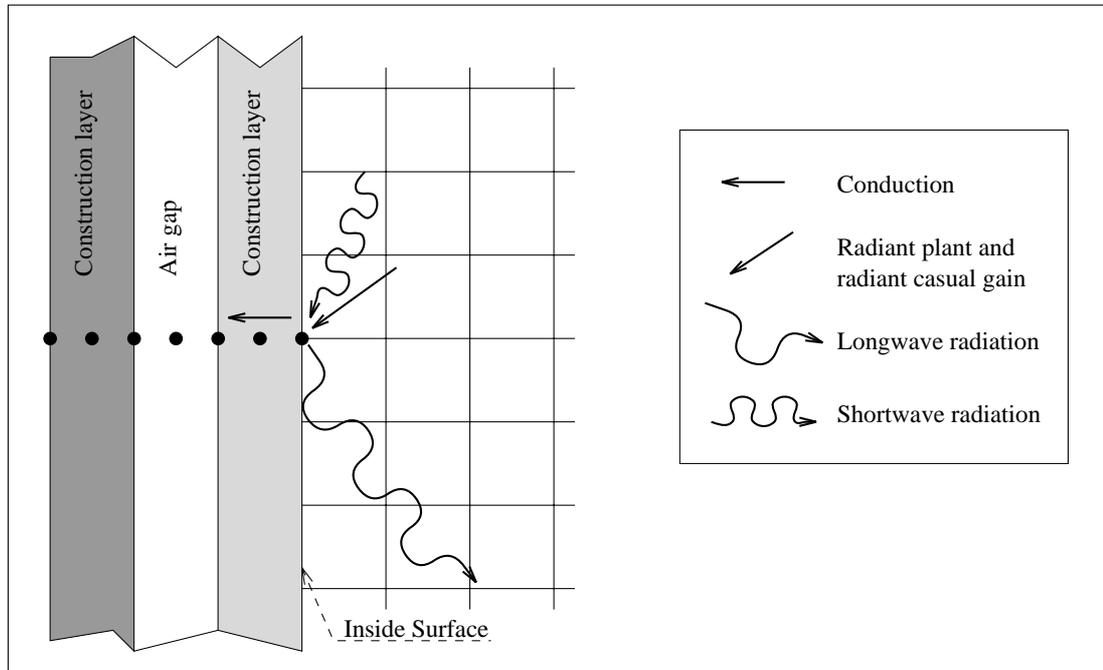
Figure 5.2 Inside zone surface heat flow paths.

5.4.1 Simple Scheme

The first approach investigated is the most obvious, simplest and least expensive. It involves an exchange of information between the two systems without any direct interaction. In other words, their domain of analysis are simulated independently. *Bps* simulates the whole building (including the zones in which the property gradients are critical) using its own models. In addition, *dfs* performs the analysis of the air flow within the zones where the gradients are required.

The input requirements for *dfs* are the domain boundary conditions. These include inside zone surface temperatures and the air condition at inlet openings, such as mass flow rate, flow direction, temperature, humidity, etc. Moreover, *bps* requests the air properties distribution, the convection heat transfer at inside zone surfaces and the air condition at the outlet openings of the *dfs* domain (which may affect the air condition in other zones) to compute the building total energy consumption and the local comfort conditions.

The conflation technique, which comprises the exchange of the aforementioned information, is summarised in Figure 5.3. Firstly, the simulation of the whole thermal system under analysis (e.g. as exemplified by Figure 3.2) is performed during a certain period of time by *bps*. A time-series of inside zone surface temperatures and inlet air conditions are then obtained from the *bps* simulation. Secondly, *dfs* is run with the boundary conditions obtained from the *bps* output time-series. The *dfs* simulation can be performed over the same *bps* period of time or only at specific time-steps, depending on the interest of the user. The *dfs* outputs are a time-series of convection heat transfers at

internal surfaces, outlet air conditions and air property distributions. Finally, *bps* is run once again taking into account the *dfs* outputs. At this last execution, the building energy consumption and local comfort levels are evaluated based on the parameters calculated by *dfs*.

For the case where *dfs* convergence with CFD models is problematic, this approach does not compromise the *bps* integrity since the programs run separately. Of course the user may have to take time and effort to obtain a *dfs* solution before being able to progress to the second *bps* run.

The *dfs* velocities at inlet openings are computed on the basis of mass flow rates supplied by *bps*, inlet air density and opening areas. For the case of cracks, where an opening area is not defined, the mass flow rate is fixed at the inlet cells rather than the velocity. In other words, a pressure level is imposed in order to provide the required source of mass. The convection heat transfer evaluated by *dfs* is based on the inside surface temperature (produced by *bps*) and the temperature of the cells adjacent to the inside surfaces. The total convection heat transfer is calculated as a sum of the fluxes from the surface to each *dfs* cell in contact with the surface. Equation (4.17) derived from wall functions is thus invoked to calculate the inside surface convection heat flux:

$$Q_{f,tot} = \sum_{i=1}^{n} c_{p,a} N_{i,f} (T_{a,i} - T_f) \tag{5.1}$$

where $Q_{f,tot}$ is the total heat transferred from the surface to the adjacent *dfs* cells, n is the total number of *dfs* cells in contact with the surface f, $N_{i,f}$ is a wall function coefficient (kg/s), $T_{a,i}$ is the cell temperature, T_f is the surface temperature and $c_{p,a}$ is the specific heat of the air.

Although equation (5.1) is an empirical correlation it provides a more refined approximation for the convection heat transfer than the convection coefficients since information on the localised flow is available. Such correlations are employed because of the nature of the flow near solid objects: laminar or turbulent. However, if more appropriate correlations are developed in the future, the wall function coefficient, $N_{i,f}$, can be up-graded. This suggests that the convection heat transfer at the wall is always a function of the difference between the surface and cell temperatures, as in the case of laminar flow where no approximation regarding the model is performed. In laminar flow, the heat transfer at the wall ($-\lambda \frac{\partial T}{\partial y} A$ - i.e. only conductive flux) can still be represented by equation (5.1). In such a case $N_{i,f}$ is approximated by the product of the conductivity of the air (λ) and the interface cell area (A_i divided by the distance from the center of the cell to the wall (y_P)), as in expression 4.15.
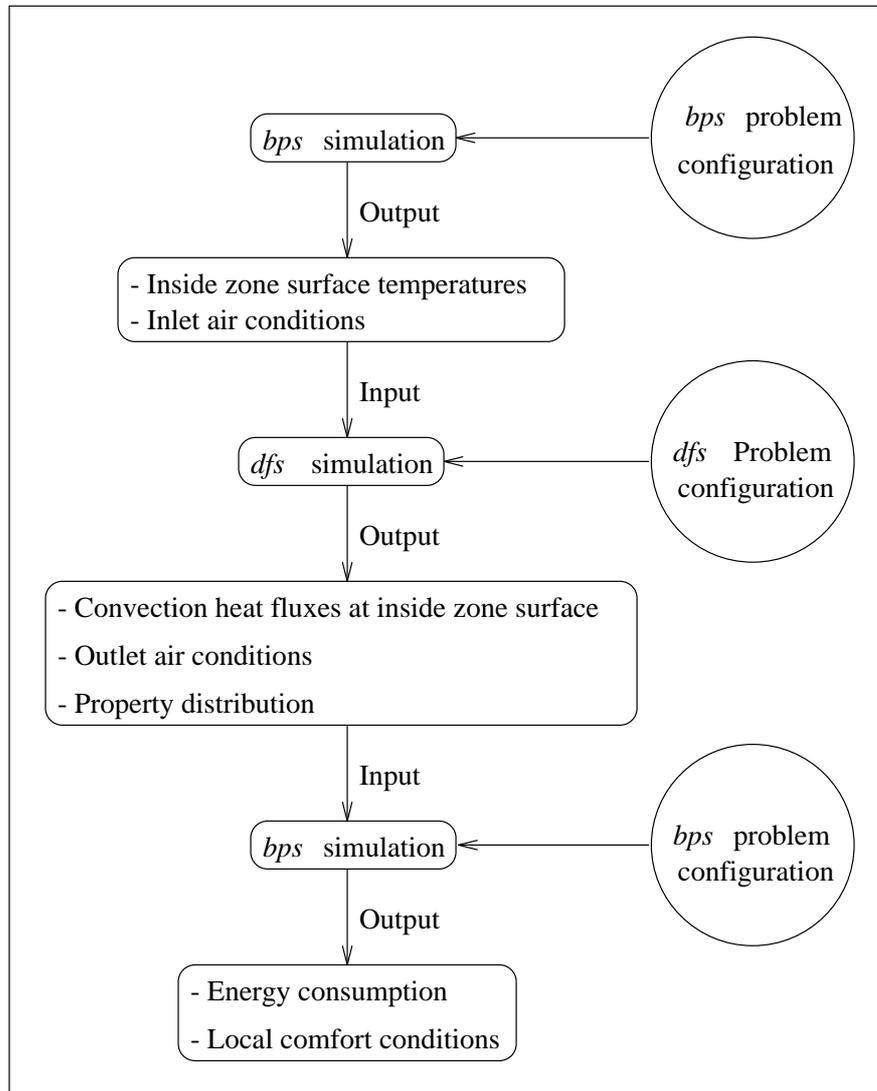
Figure 5.3 Simple approach.

5.4.2 Thermal Coupling

This section addresses only the thermal coupling of the inside zone surface interface. In contrast with the simple approach where the solution of each system takes places sequentially, in this approach the simulations of *bps* and *dfs* are concurrent. Three different approaches, comprising direct interaction of the energy equations of the two systems, are introduced. In the first approach, the equations are linked by means of convection coefficients, in the second approach, the interactions of the equations take place one time-step in arrears and in the last approach, a simultaneous solution of the *bps* and *dfs* energy equations involved in a single zone is enabled.

Convection coefficient scheme

In terms of complexity, this procedure is the next step after the simple approach. In this case, the two systems run at the same time but there is no change to their original models. Basically, the convection coefficient needed to link the *bps* surface node and air node is now calculated by *dfs* rather than by an empirical correlation. Meanwhile, the *dfs* solution takes place assuming the inside surface temperatures computed by *bps* as its known boundary conditions.

Consider now the *bps* internal surface energy balance equation (3.4) and air node energy balance equation (3.5) which are unchanged:

$$\frac{\partial}{\partial t}(\rho_f v_f T_f) = \sum_{j=1}^{nf-1} K_{j,f}(T_j - T_f) + \frac{h_{f,a} A_f}{c_{p,f}}(T_a - T_f) + S_f v_f \qquad . \tag{3.4}$$

$$\frac{\partial}{\partial t}(\rho_a v_a T_a) = \sum_{j=1}^{na-ns} K_{j,a}(T_j - T_a) + \sum_{i=1}^{ns} \frac{h_{i,a} A_i}{c_{p,a}}(T_i - T_a) + S_a v_a \tag{3.5}$$

The convection coefficients for the above equations are now evaluated from the following equation

$$h_{f,a} = \frac{Q_{f,tot}}{(T_f - T_a)A_f} \tag{5.2}$$

where $Q_{f,tot}$ is the convection heat transfer at an internal surface computed from equation (5.1). Notice that by substituting equation (5.2) in equations (3.4) and (3.5), the convection heat transfer term reduce to $Q_{f,tot}/c_{p,f}$ and $Q_{i,tot}/c_{p,a}$ respectively. When equations (3.4) and (3.5) are discretised in time, the present and future values of the convection coefficients need to be evaluated.

Within the method, at every time-step *bps* invokes *dfs* to calculate the convection coefficients for each internal surface. The inside surface temperatures must then be provided to *dfs* to obtain the air flow solution and consequently the convection coefficients. Nevertheless, inside zone surface temperatures are not known at the future time-step because they are dependent on the convection coefficients. An iteration between the two systems would then be required to compute convection coefficients and surface temperatures simultaneously. In order to avoid this computationally expensive scheme, an alternative approach is suggested: *bps* supplies to *dfs* the most up-dated surface temperatures, the present values. This is similar to evaluating conductance coefficients one time-step in arrears as mentioned in chapter 3. However, the effects of non-simultaneity are lessened if the time-step is reduced. The complete approach is exemplified in the diagram of Figure 5.4. The future and present values of the convection coefficients are then calculated from the expressions

$$h_{f,a} = \frac{\sum_{i=1}^{n} c_{p,a} N_i (T_{a,i} - T_f^-)}{(T_f^- - T_a^-) A_f} \tag{5.3}$$

$$h_{f,a}^- = \frac{\sum_{i=1}^{n} c_{p,a} N_i^- (T_{a,i}^- - T_f^{-1})}{(T_f^{-1} - T_a^{-1}) A_f} \tag{5.4}$$

where the superscript -1 indicates the time-step immediately before the present time-step and the superscript $-$ is the present time-step. Future values are those without a superscript.
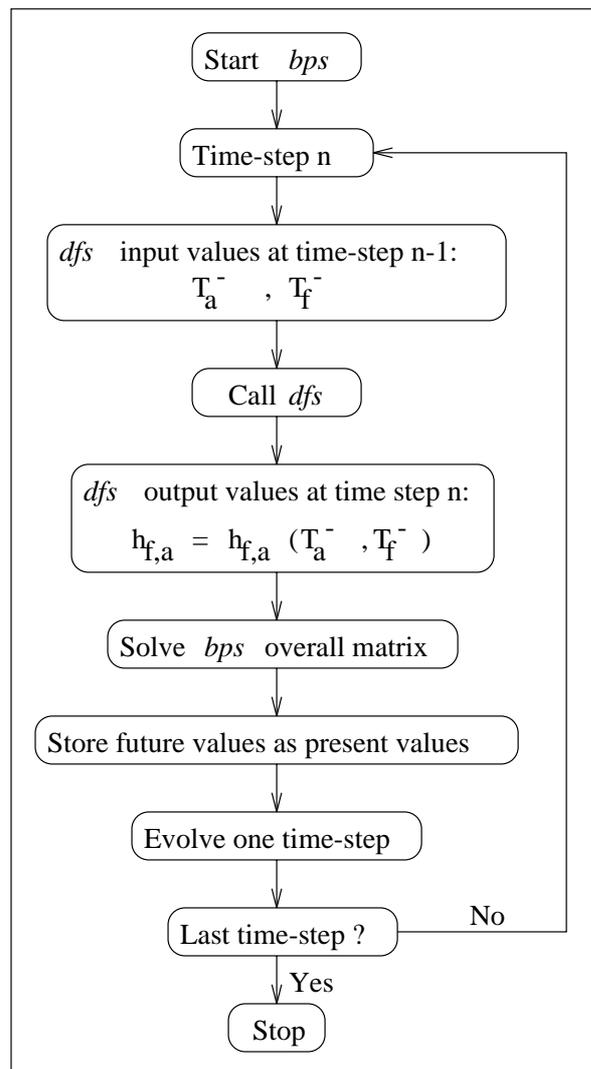
Figure 5.4 Thermal coupling involving convection coefficients.

Unlike the simple approach, only one *bps* simulation is performed and energy consumption and local comfort levels are now evaluated every time-step as the solution evolves and they can be recovered later within the results analysis. In the present approach, the convection coefficients do not need to be evaluated by *dfs* every time-step. The user has the option to dictate when it should be done.

Sequential approach

In order to bring the solution to a more accurate approach within the same time-step, this approach is suggested as an evolution when compared with the previous approach. In this case the air volume energy balance equation is substituted by the *dfs* equations and expression (5.1) for $Q_{f,tot}$ replaces the heat convection term in the inside surface energy balance (see Figure 5.5 and compare with Figure 3.6b):

$$\frac{\partial}{\partial t}(\rho_f v_f T_f) = \sum_{j=1}^{nf-1} K_{j,f}(T_j - T_f) + \frac{\sum_{i=1}^{n} c_{p,a} N_i(T_{a,i} - T_f)}{c_{p,f}} + S_f v_f \quad . \qquad (5.5)$$

When equation (5.5) is discretised, the term $h_{f,a} A_f$ is superseded within the coefficient a_P and source term b_P by the terms $c_{p,a} \sum_{i=1}^{n} N_i$ and term $c_{p,a} \sum_{i=1}^{n} N_i T_{a,i}$ respectively.
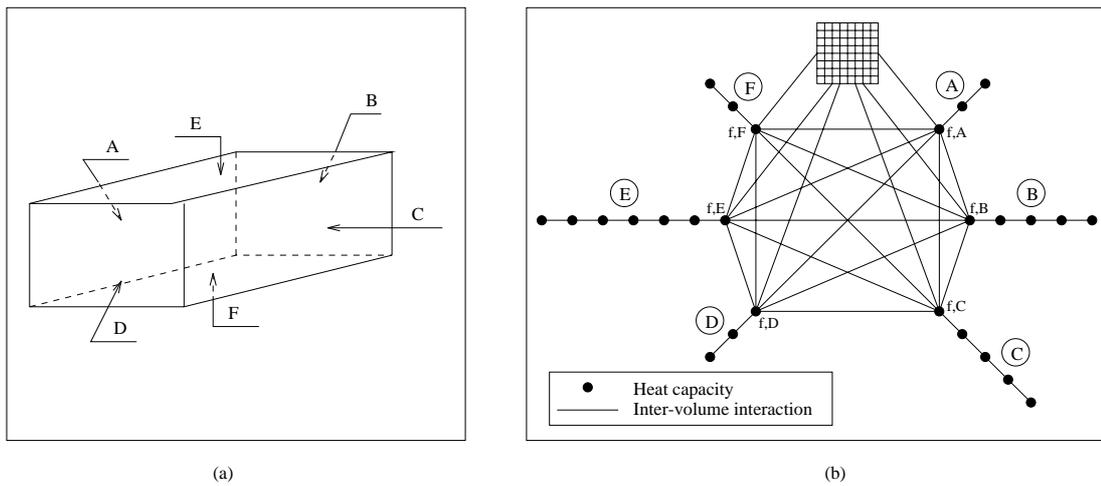
Figure 5.5 Volume discretisation of the combined domain.

Since N_i and $T_{a,i}$ are dependent on the values of T_f's and vice-versa, iterations between *bps* and *dfs* solutions must take place. In order to avoid the high computation time involved in such an approach, one model solution takes place after the other at every time-step considering the most updated parameters of the other approach. This procedure is illustrated in Figure 5.6 where *bps*

incorporates *dfs*. As can be seen, a simulation is initiated by *bps* and the values for $\sum_{i=1}^{n} N_i$ and $\sum_{i=1}^{n} N_i T_{a,i}$ are assumed. After that, the overall constructional matrix is solved in a procedure similar to that introduced in Chapter 3 (with the air volume energy balance equation excluded from the overall matrix) and the surface temperatures, $T_{f,?}$ values, are obtained. *Dfs* is now invoked considering the calculated $T_{f,?}$ values as its boundary condition. As a result, new values for $\sum_{i=1}^{n} N_i$ and $\sum_{i=1}^{n} N_i T_{a,i}$ are calculated. After the new computed values are stored the simulation evolves to the next time-step until the simulation period is completed.
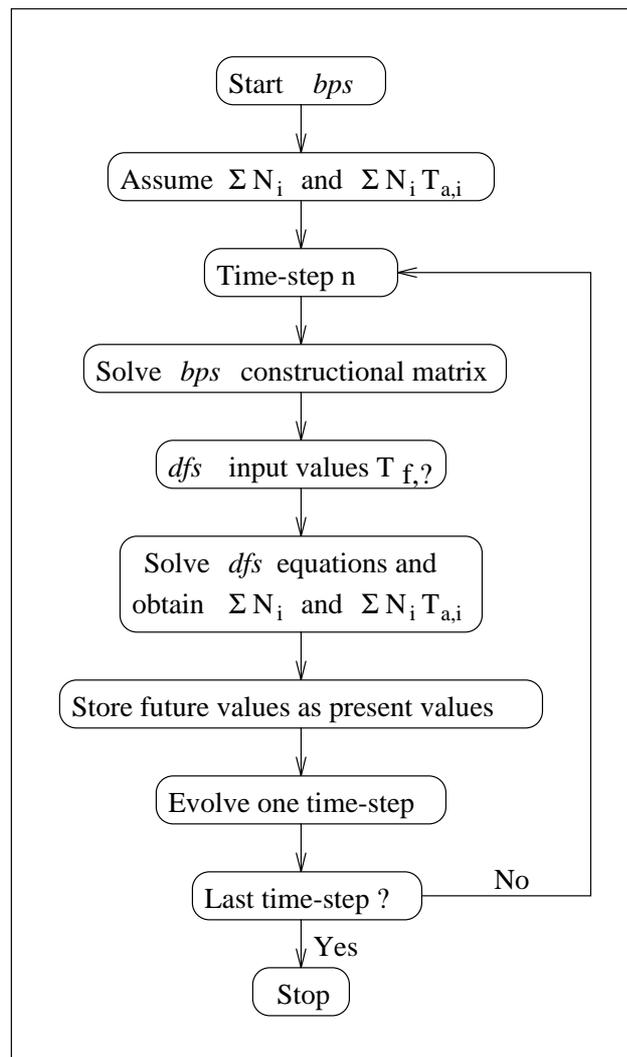
Figure 5.6 Thermal coupling involving the sequential approach.

Although this approach is more computationally accurate than the convection coefficient approach, its implementation is more complex since changes in the *bps* model are necessary.

Simultaneous solution scheme

The third thermal coupling approach is more sophisticated mathematically. All energy equations describing the heat fluxes within a zone are iteratively solved within a time-step; with the surface and intra-constructional energy balances computed by *bps* and the inside zone energy balances calculated by *dfs*. Considering the *bps* partitioning solution procedure and the *dfs* iterative solution, the proposed technique combines the two solution methods. *Bps*' energy balance zone matrix is partitioned and processed as far as possible and then an iterative process is carried out between *dfs* and a *bps* sub-matrix.

As in the previous approach, the *bps* air volume energy equation is substituted by the *dfs* air flow energy equations and therefore, a direct interaction between the two systems of equations must exist. The convection heat transfer in equation (3.4) is now estimated directly by equation (5.1) and the inside surface temperatures computed by *bps* are established at the *dfs* domain boundaries. Substituting equation (5.1) into equation (3.4), the following expression arises:

$$\frac{\partial}{\partial t}(\rho_f v_f T_f) = \sum_{j=1}^{nf-ns} K_{j,f}(T_j - T_f) + Q_{f,tot} + S_f v_f \qquad . \tag{5.6}$$

To illustrate the solution procedure, the same single zone problem used to exemplify the solution method applied to *bps*' energy equations is again referenced. However, the discretisation scheme presented in Figure 3.6b is now replaced by the scheme of Figure 5.5b. Control strategies are not invoked and the *bps* energy balance equations are again related to zone surface and intra-constructional nodes, excluding the inside zone surface nodes. Instead, equation (5.6) is applied to the inside zone surfaces. Thus, a system of equations, similar to the matrix of Figure 3.7, emerges. This equations-set can be seen in Figure 5.7. Observe that row 27 of Figure 3.7, representing the air zone balance, was withdrawn from the set of equations. Also, the last column of the matrix of coefficients, which connected the inside surface equations to the air volume equation, has been removed. In compensation, the convection heat fluxes ($Q_{f,?}$, where ? is the surface indicator) at the future time-row are included on the right hand side of the inside surface equations and their present values are added to the source terms.

If convection heat fluxes are assumed to be known at the future time-row (noting that they depend on the solution of the *dfs* domain), the matrix of Figure 5.7 can be processed in the same way as the matrix of Figure 3.7. A similar partition to the one proposed in Chapter 3 is then performed and the resulting partitioned construction matrices are exactly the same as the matrices of Figure 3.8. As the inside surface balances were modified, the inside zone balance matrix is slightly different from the matrix of Figure 3.9 and now it has the format of the Figure 5.8 matrix.

The linkages between the construction sub-matrices and the inside zone sub-matrix are again held by the coefficients $a_{2,3}$, $a_{7,8}$, $a_{12,13}$, $a_{22,23}$ and $a_{25,26}$ of Figure 3.8 and $a_{3,2}$, $a_{8,7}$, $a_{13,12}$, $a_{23,22}$ and $a_{26,25}$ of Figure 5.8. As the construction sub-matrices are the same, they can be forward reduced exactly as they were in the original *bps* approach. This process results in the matrices of Figure 3.10. Once more, the last row of all Figure 3.10 matrices are used to eliminate $a_{3,2}$, $a_{8,7}$, $a_{13,12}$, $a_{23,22}$ and $a_{26,25}$ of Figure 5.8 resulting in the adjusted matrix of Figure 5.9.

In addition to the main diagonal coefficients and the source terms, the convection heat fluxes are also modified in the operation. Instead of altering the $Q_{f,?}$ terms, the $d_?$ coefficients multiplying the convective fluxes are introduced in Figure 5.9. This procedure represents the change of the unity multiplying the heat fluxes (Figure 5.8) and is as effective as the modification of $Q_{f,?}$.

Since the convection heat fluxes are assumed known values, the only unknowns of the adjusted inside zone sub-matrix are the inside surface temperatures. Therefore, the matrix of Figure 5.9 can be solved in order to obtain the inside surface temperatures. A forward reduction is then applied to the sub-matrix and the matrix of Figure 5.10 arises. The $d_?$ coefficients were modified in this forward reduction operation keeping the convection heat fluxes unchanged.

A backward substitution can now take place to obtain the inside surface temperatures. However, the $Q_{f,?}$ terms are computed based on the inside surface temperatures which are unknown values. Besides, the convection heat transfer is a function of the temperature and the flow within the cells adjacent to the inside surface. The flow and cell temperatures are evaluated by *dfs* based on the inside surface temperatures as boundary conditions. As the inside surface temperatures and the inside zone air flow are dependent on each other, they must be determined simultaneously employing an iterative procedure. This solution process consists of iterations between the matrix of Figure 5.10 and *dfs*.

A possible solution procedure comprises the following sequence: firstly, $T_{f,?}$ are computed by backward substitution of the Figure 5.10 matrix considering that $Q_{f,?}$ are known values; secondly, the *dfs* domain is solved considering $T_{f,?}$ as its boundary conditions; thirdly, $Q_{f,?}$ are calculated based on the most recent values of $T_{f,?}$ and adjacent-to-surface cell temperatures; fourthly the inside surface temperatures are again evaluated by backward substitution, and so on. Such an operation proceeds continually until changes on the inside surface temperatures and the *dfs* property values satisfy some convergence criteria (this is equivalent to the previous approach if iterations between the two systems take place). Since the *dfs* iterative solution for a fixed set of boundary conditions demands a significant computation effort and must be performed several times, such a procedure can be considerably time consuming.

Inside zone surface balances

Intra-construction balances

$Q_{f,A}$
$Q_{f,B}$
$Q_{f,C}$
$Q_{f,D}$
$Q_{f,E}$
$Q_{f,F}$

$+$

$b_{1,A}$, $b_{2,A}$, $b_{f,A}$, $b_{1,B}$, $b_{2,B}$, $b_{3,B}$, $b_{4,B}$, $b_{f,B}$, $b_{1,C}$, $b_{2,C}$, $b_{3,C}$, $b_{4,C}$, $b_{f,C}$, $b_{1,D}$, $b_{2,D}$, $b_{f,D}$, $b_{1,E}$, $b_{2,E}$, $b_{3,E}$, $b_{4,E}$, $b_{5,E}$, $b_{6,E}$, $b_{f,E}$, $b_{1,F}$, $b_{2,F}$, $b_{f,F}$

$=$

$T_{1,A}$, $T_{2,A}$, $T_{f,A}$, $T_{1,B}$, $T_{2,B}$, $T_{3,B}$, $T_{4,B}$, $T_{f,B}$, $T_{1,C}$, $T_{2,C}$, $T_{3,C}$, $T_{4,C}$, $T_{f,C}$, $T_{1,D}$, $T_{2,D}$, $T_{f,D}$, $T_{1,E}$, $T_{2,E}$, $T_{3,E}$, $T_{4,E}$, $T_{5,E}$, $T_{6,E}$, $T_{f,E}$, $T_{1,F}$, $T_{2,F}$, $T_{f,F}$

$$a_{1,1}\ a_{1,2}$$
$$a_{2,1}\ a_{2,2}\ a_{2,3}$$
$$a_{3,2}\ a_{3,3}\ a_{3,8}\ a_{3,13}\ a_{3,16}\ a_{3,23}\ a_{3,26}$$
$$a_{4,4}\ a_{4,5}$$
$$a_{5,4}\ a_{5,5}\ a_{5,6}$$
$$a_{6,5}\ a_{6,6}\ a_{6,7}$$
$$a_{7,6}\ a_{7,7}\ a_{7,8}$$
$$a_{8,7}\ a_{8,8}\ a_{8,3}\ a_{8,13}\ a_{8,16}\ a_{8,23}\ a_{8,26}$$
$$a_{9,9}\ a_{9,10}$$
$$a_{10,9}\ a_{10,10}\ a_{10,11}$$
$$a_{11,10}\ a_{11,11}\ a_{11,12}$$
$$a_{12,11}\ a_{12,12}\ a_{12,13}$$
$$a_{13,12}\ a_{13,13}\ a_{13,3}\ a_{13,8}\ a_{13,16}\ a_{13,23}\ a_{13,26}$$
$$a_{14,14}\ a_{14,15}$$
$$a_{15,14}\ a_{15,15}\ a_{15,16}$$
$$a_{16,15}\ a_{16,16}\ a_{16,3}\ a_{16,8}\ a_{16,13}\ a_{16,23}\ a_{16,26}$$
$$a_{17,17}\ a_{17,18}$$
$$a_{18,17}\ a_{18,18}\ a_{18,19}$$
$$a_{19,18}\ a_{19,19}\ a_{19,20}$$
$$a_{20,19}\ a_{20,20}\ a_{20,21}$$
$$a_{21,20}\ a_{21,21}\ a_{21,22}$$
$$a_{22,21}\ a_{22,22}\ a_{22,23}$$
$$a_{23,22}\ a_{23,23}\ a_{23,3}\ a_{23,8}\ a_{23,13}\ a_{23,16}\ a_{23,26}$$
$$a_{24,24}\ a_{24,25}$$
$$a_{25,24}\ a_{25,25}\ a_{25,26}$$
$$a_{26,25}\ a_{26,26}\ a_{26,3}\ a_{26,8}\ a_{26,13}\ a_{26,16}\ a_{26,23}$$

Figure 5.7 Overall single zone matrix.

$$
\begin{bmatrix}
a_{3,2} & a_{3,3} & & a_{3,8} & & a_{3,13} & & a_{3,16} & & a_{3,23} & & a_{3,26} \\
 & a_{8,3} & a_{8,7} & a_{8,8} & & a_{8,13} & & a_{8,16} & & a_{8,23} & & a_{8,26} \\
 & a_{13,3} & & a_{13,8} & a_{13,12} & a_{13,13} & & a_{13,16} & & a_{13,23} & & a_{13,26} \\
 & a_{16,3} & & a_{16,8} & & a_{13,13} & a_{16,15} & a_{16,16} & & a_{16,23} & & a_{16,26} \\
 & a_{23,3} & & a_{23,8} & & a_{23,13} & & a_{23,16} & a_{23,22} & a_{23,23} & & a_{23,26} \\
 & a_{26,3} & & a_{26,8} & & a_{26,13} & & a_{26,16} & & a_{26,23} & a_{26,25} & a_{26,26}
\end{bmatrix}
\begin{bmatrix}
T_{2,A} \\ T_{f,A} \\ T_{4,B} \\ T_{f,B} \\ T_{4,C} \\ T_{f,C} \\ T_{2,D} \\ T_{f,D} \\ T_{6,E} \\ T_{f,E} \\ T_{2,F} \\ T_{f,F}
\end{bmatrix}
=
\begin{bmatrix}
b_{f,A} \\ b_{f,B} \\ b_{f,C} \\ b_{f,D} \\ b_{f,E} \\ b_{f,F}
\end{bmatrix}
+
\begin{bmatrix}
Q_{f,A} \\ Q_{f,B} \\ Q_{f,C} \\ Q_{f,D} \\ Q_{f,E} \\ Q_{f,F}
\end{bmatrix}
$$

Figure 5.8 Inside zone balance sub-matrix.

$$
\begin{bmatrix}
a_{3,3}^{x} & a_{3,8} & a_{3,13} & a_{3,16} & a_{3,23} & a_{3,26} \\
a_{8,3} & a_{8,8}^{x} & a_{8,13} & a_{8,16} & a_{8,23} & a_{8,26} \\
a_{13,3} & a_{13,8} & a_{13,13}^{x} & a_{13,16} & a_{13,23} & a_{13,26} \\
a_{16,3} & a_{16,8} & a_{13,13} & a_{16,16}^{x} & a_{16,23} & a_{16,26} \\
a_{23,3} & a_{23,8} & a_{23,13} & a_{23,16} & a_{23,23}^{x} & a_{23,26} \\
a_{26,3} & a_{26,8} & a_{26,13} & a_{26,16} & a_{26,23} & a_{26,26}^{x}
\end{bmatrix}
\begin{bmatrix}
T_{f,A} \\ T_{f,B} \\ T_{f,C} \\ T_{f,D} \\ T_{f,E} \\ T_{f,F}
\end{bmatrix}
=
\begin{bmatrix}
b_{f,A}^{x} \\ b_{f,B}^{x} \\ b_{f,C}^{x} \\ b_{f,D}^{x} \\ b_{f,E}^{x} \\ b_{f,F}^{x}
\end{bmatrix}
+
\begin{bmatrix}
d_{1}Q_{f,A} \\ d_{2}Q_{f,B} \\ d_{3}Q_{f,C} \\ d_{4}Q_{f,D} \\ d_{5}Q_{f,E} \\ d_{6}Q_{f,F}
\end{bmatrix}
$$

where superscript 'x' is related to coefficients modified once.

Figure 5.9 Adjusted inside zone balance sub-matrix.

$$
\begin{bmatrix}
a_{3,3}^{x} & a_{3,8} & a_{3,13} & a_{3,16} & a_{3,23} & a_{3,26} \\
 & a_{8,8}^{xx} & a_{8,13}^{x} & a_{8,16}^{x} & a_{8,23}^{x} & a_{8,26}^{x} \\
 & & a_{13,13}^{xx} & a_{13,16}^{x} & a_{13,23}^{x} & a_{13,26}^{x} \\
 & & & a_{16,16}^{xx} & a_{16,23}^{x} & a_{16,26}^{x} \\
 & & & & a_{23,23}^{xx} & a_{23,26}^{x} \\
 & & & & & a_{26,26}^{xx}
\end{bmatrix}
\begin{bmatrix}
T_{f,A} \\ T_{f,B} \\ T_{f,C} \\ T_{f,D} \\ T_{f,E} \\ T_{f,F}
\end{bmatrix}
=
\begin{bmatrix}
b_{f,A}^{x} \\ b_{f,B}^{xx} \\ b_{f,C}^{xx} \\ b_{f,D}^{xx} \\ b_{f,E}^{xx} \\ b_{f,F}^{xx}
\end{bmatrix}
+
\begin{bmatrix}
d_{1}\,Q_{f,A} \\ d_{2}^{x}\,Q_{f,B} \\ d_{3}^{x}\,Q_{f,C} \\ d_{4}^{x}\,Q_{f,D} \\ d_{5}^{x}\,Q_{f,E} \\ d_{6}^{x}\,Q_{f,F}
\end{bmatrix}
$$

x - coefficient modified once.
xx - coefficient modified twice.

Figure 5.10 Reduced inside zone balance sub-matrix.

As the backward substitution within the Figure 5.10 matrix is relatively fast compared to the *dfs* solution, an alternative iterative procedure is suggested. This consists of computing the inside surface temperatures after each *dfs* iteration. In other words, backward substitution operation is processed after all *dfs* variables are obtained at each *dfs* sweep. This means that the *dfs* boundary conditions are modified each sweep. The solution evolves until *dfs* has achieved convergence. In this case, the convergence of the inside surface temperatures are not necessarily checked since their changes are considerably smaller when compared to the flow variations. Therefore, once *dfs* has achieved convergence, the criteria for the inside surface temperatures must have been satisfied.

The size of the inside zone sub-matrix depends only on the number of inside zone surfaces involved, consequently the effort to process a backward substitution ever time-step is not extensive. A possibility to reduce the computation further is to calculate the inside surface temperatures every *n dfs* sweeps, since the change per sweep is not large during the iterative process.

Finally, after the inside surface temperatures are obtained, they are substituted in the matrices of Figure 3.10 and the intra-construction temperatures are determined by backward substitution. Thus, all energy balance and air flow equations describing one zone are solved simultaneously. This complete procedure is explained in Figure 5.11.

In principle, this approach and the previous two methodology are identical: only the integration of the transient term of the conservation equation defines the difference. For a specific time-step, the current procedure presents a more accurate solution of the overall set of equations than the convection coefficients and sequential schemes. Certainly, if the time-step is reduced, the results of these two techniques will tend towards the results from a simultaneous scheme. Of course, the simultaneous scheme is more CPU demanding due to the backward substitution operation being performed at each iterative sweep, however, no comparisons have yet been carried out to quantify the difference.

In order to deal with ideal control strategies, the simultaneous solution is subjected to variations. If, for example, an internal surface temperature is controlled (kept at a constant value) the heat injected at the surface (or at any construction layer) is calculated instead. If the air temperature at some cells is controlled, the heat injection is determined directly from the energy balance at the cells. However, if the heat is injected at a surface, it must be computed iteratively during the *dfs* iteration process. Such a heat injection is based on the difference between the cell's temperatures and the set point. The iteration must proceed until the set point is reached at the controlled cells.

In the case of more realistic control schemes, such as PID or on-off controllers, the control action is based on sensed properties calculated one time-step in arrears. In other words, if the air temperature at certain cells is controlled by injecting heat in a surface, the relation between air temperature (sensed variable) and the heat flux (control variable) is based on the present value of the sensed variable. The sensed value is computed as an average of the temperatures of the cells.
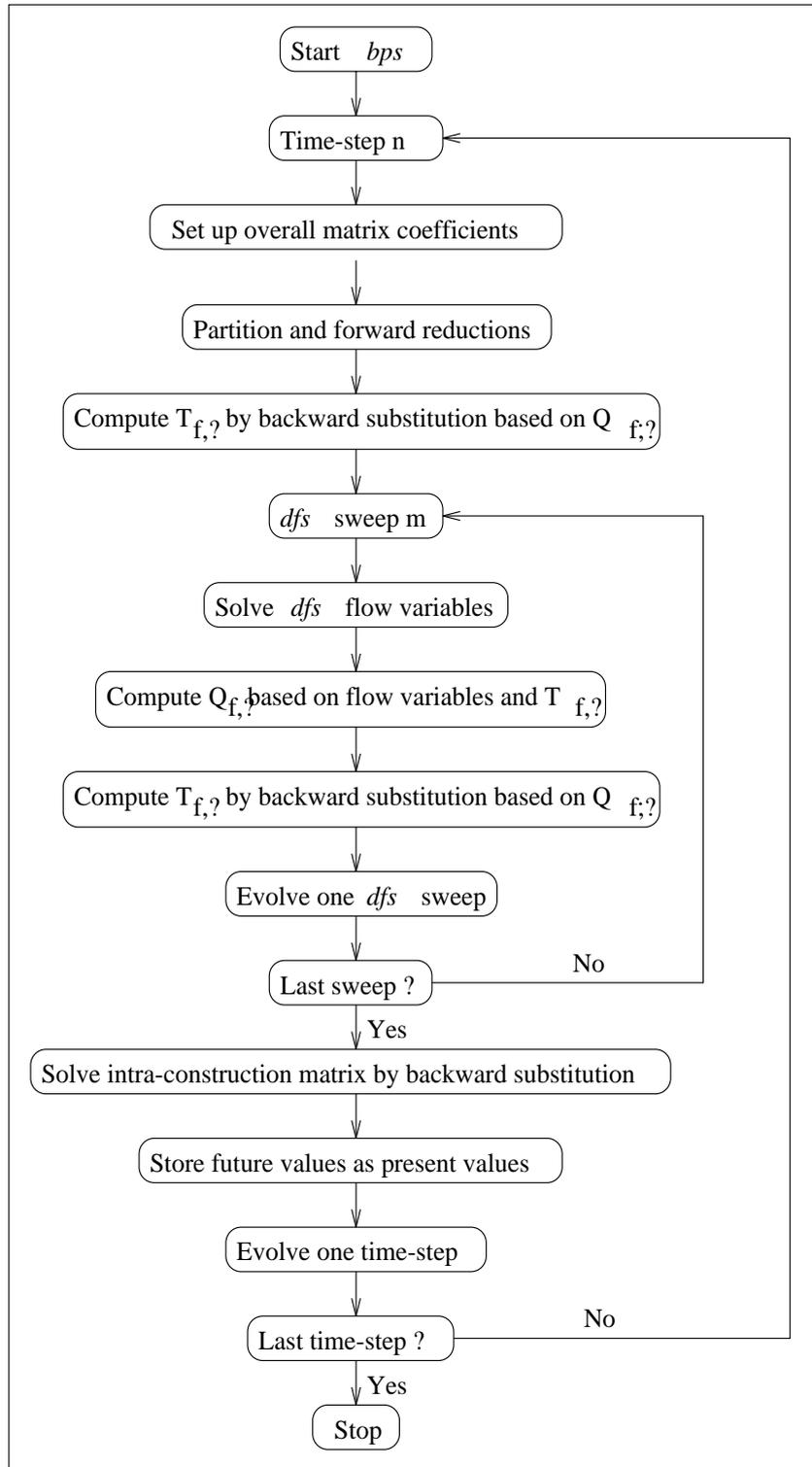
Figure 5.11 Simultaneous solution of one zone energy equations.

5.4.3 Momentum Coupling

This approach consists of combining the *bps* mass flow equations with the *dfs* momentum equations at inlet and outlet openings. This approach is complementary to the thermal coupling previously described. Unlike the simple approach, which assumes that the mass flow network (mass flow rate) is unaffected by the inside zone air flow, the present coupling supposes that both domains are dependent on each other, and therefore a direct interaction between the two systems must exist. This means that the air flow within the zone influences the flow in other parts of the building and vice-versa. The zone air node is substituted by the *dfs* domain, and the *dfs* cells at the openings are linked to other zone air nodes (as defined in the original nodal flow network), the ambient air node and/or plant component nodes, as can be seen in Figure 5.1. The common variables at the interface between the two domains are mass flow rates and pressures at inlet or outlet openings.

The combination proposed is a simultaneous solution of the mass flow network equations (3.6) and the *dfs* equations. To elucidate the solution process, consider the mass flow network coupled to the *dfs* domain of Figure 5.12a. As can be seen, the Kitchen node of Figure 3.13 is replaced by the *dfs* domain. The previous two connections in Figure 3.13 were substituted by three connections representing the link between the two domains. The first connection attaches the node Lounge to two *dfs* cells. The second and third join a plant component node (node Duct_1) and a *dfs* cell at an air supply duct. The nodes A, B and C represent the effect of the *dfs* cells on the network. Pressure and temperature are known at the boundary nodes Out_n, Out_w and Duct_2 and therefore they are the complete set of boundary conditions of the coupled domain. As each system solution is performed separately, the mass flow network must be decoupled from the *dfs* domain in order to be solved. Figure 5.12b shows how the network of Figure 5.12a is detached from the *dfs* mesh. In Figure 5.12b, the vectors at the boundary of the *dfs* cells connected to the decoupled network represent the air flow entering or leaving the zone. Such air flow can be understood as sources or sinks of mass at the network nodes A, B and C. If these sources or sinks of mass obtained from the *dfs* solution are considered to be known values ($\dot{s}_A$, $\dot{s}_B$ and $\dot{s}_C$ in Figure 5.12c), the mass flow network can be solved. Pressure at Lounge, A, B, C and Duct_2 and the remaining flow rates in the network are then determined.

The $\dot{s}_A$, $\dot{s}_B$ and $\dot{s}_B$ terms, as evaluated by *dfs*, are the net flow rates entering or exiting the zone. The flow rate is the product of the velocity component crossing the interface of the cell, density and interface cell area. The source/sink terms $\dot{s}_A$, $\dot{s}_B$ and $\dot{s}_C$ are thus computed by the following expression:

$$\dot{s}_k = \sum_{j}^{m} \sum_{i}^{n} (\rho u A)_{i,j,k} \qquad k = A, B, C \qquad (5.7)$$

where m is the number of cells which are connected to a mass flow network node, n is the number of interfaces of each cell, ρ is the air density at the cell interface, u is the velocity component at the cell interface and A is the interface cell area. The direction of the velocity component is considered in the above equation: if the flow is entering a cell, it is considered positive and if it is exiting, it is negative. Hence, $\dot{s}_k$ is the net flow rate at the considered cells which can be positive (source of mass) or negative (sink of mass).

(a)

(b)

(c)
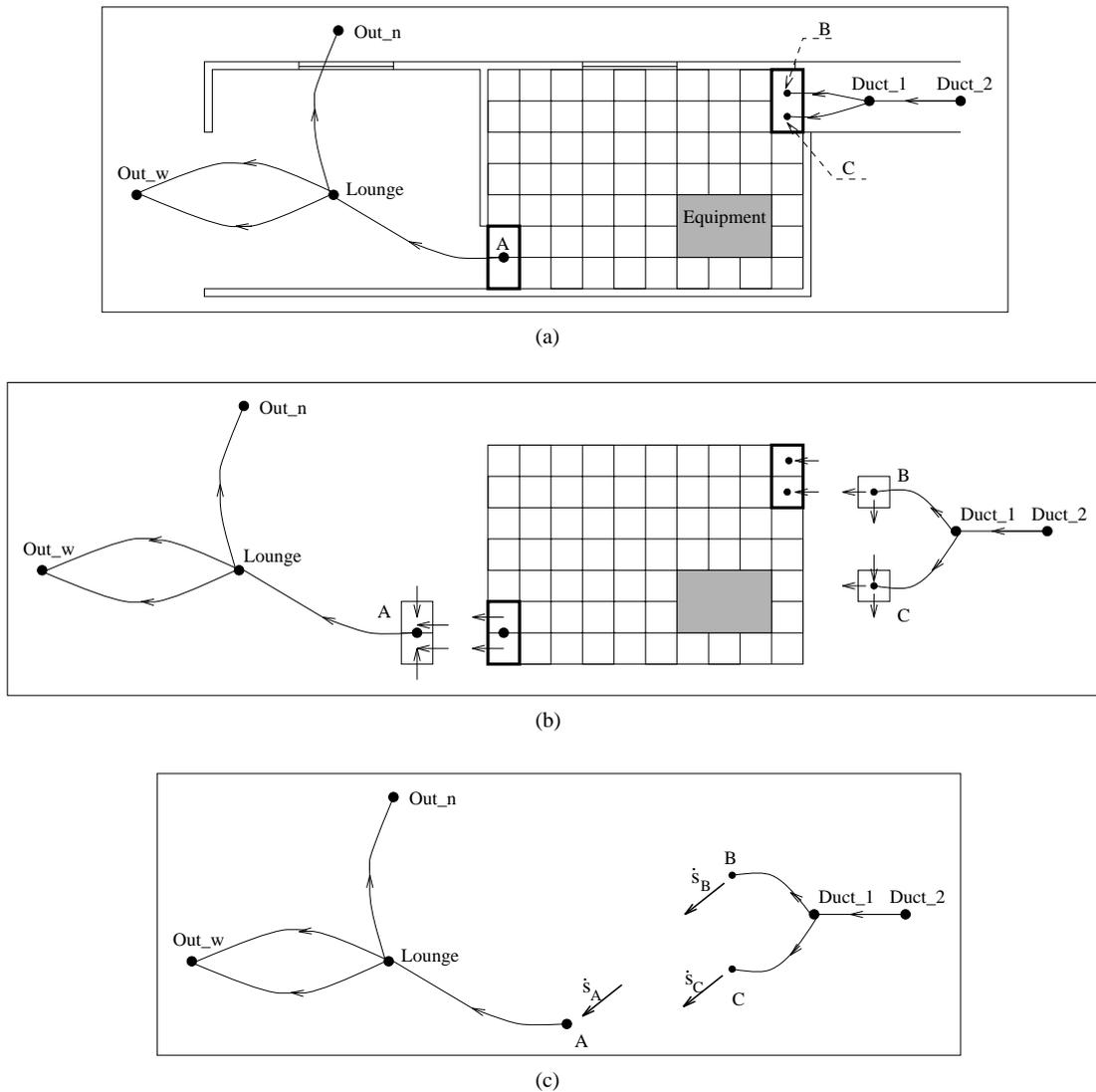
Figure 5.12 Example of how a mass flow network is decoupled from a *dfs* domain.

On the other hand, the solution of the disconnected *dfs* domain is performed assuming the boundary conditions evaluated by the mass flow network solution. These boundary conditions are sources/sinks of mass to/from the *dfs* domain through the connections *Lounge − A*, *Duct_1 − B* and *Duct_2 − C* (see Figure 5.12). Two different ways of imposing such flow rates are investigated:

- a known pressure at the boundary cells (cells represented by the nodes A, B and C);

- a known speed and direction (momentum) at the interface of the opening cells.

The pressure type boundary condition is applicable to cases where the inlet momentum changes the flow locally but does not affect substantially the zone air flow pattern. This, for instance, is the case with a crack whose dimension is much smaller than the size of the cells. In such a situation, the pressures calculated by the mass flow network at the nodes A, B and C are fixed at the *dfs* cells which they represent. The velocity type condition is appropriate to inlet openings where the momentum magnitude can significantly modify the zone air flow pattern and must be known in advance. Usually the effect of the outlet momentum on the zone air flow pattern is not so significant and either pressure or velocities can be fixed at such positions. The velocities are obtained from mass flow rates through the openings (air flow through the connections *Lounge* − *A*, *Duct*_1 − *B* and *Duct*_2 − *C* divided by the air density and opening areas.

Since air flow through the connections *Lounge* − *A*, *Duct*_1 − *B* and *Duct*_2 − *C* are dependent on the *dfs* solution, and the pressure or momentum at the boundary cells are calculated by *bps*, an iterative operation must take place between the two systems until a convergence criteria is satisfied. An iteration procedure, in which one solution is carried out after another up to the convergence of the two systems, is very time consuming. As the number of *dfs* equations to be solved for a single zone can be considerably higher than the number of mass flow network equations representing a whole building, a less expensive scheme is applied. In this procedure, the *dfs* solution process evolves considering that its boundary conditions are re-established at each sweep. This means that the mass flow network solution is computed as the *dfs* boundary conditions at each *dfs* sweep. Mass flow network convergence should be reached every *dfs* iteration. The convergence of the whole system is accomplished when the *dfs* solution is obtained. This iterative procedure is performed at each time-step during the simulation period as explained by Figure 5.13.

However, the present algorithm does not allow velocity alone to be fixed at openings because this would cause an inconsistency in the solution of the integrated domain. In other words, the mass flow rate obtained from the mass flow network (through connections *Lounge* − *A*, *Duct*_1 − *B* and *Duct*_2 − *C*) cannot be imposed (in the form of momentum) at the *dfs* cells because this is the flow already computed from *dfs* (the net flow rate entering or leaving the zone; $\dot{s}_A$, $\dot{s}_B$, and $\dot{s}_C$). The alternative is to fix pressure at nodes A, B and C and velocity at opening faces at the same time. Although this practice may seem conflicting since the momentum to be imposed corresponding to the fixed pressure is not known, an iteration procedure takes place between the two approaches, and consequently pressures and mass flow evaluated by the mass flow network are equivalent to each other. Also, as the pressures at the *dfs* boundaries are not affected by the changes on the momentum, the inlet velocity can be interpreted only by the way mass flow is established on the *dfs* domain.
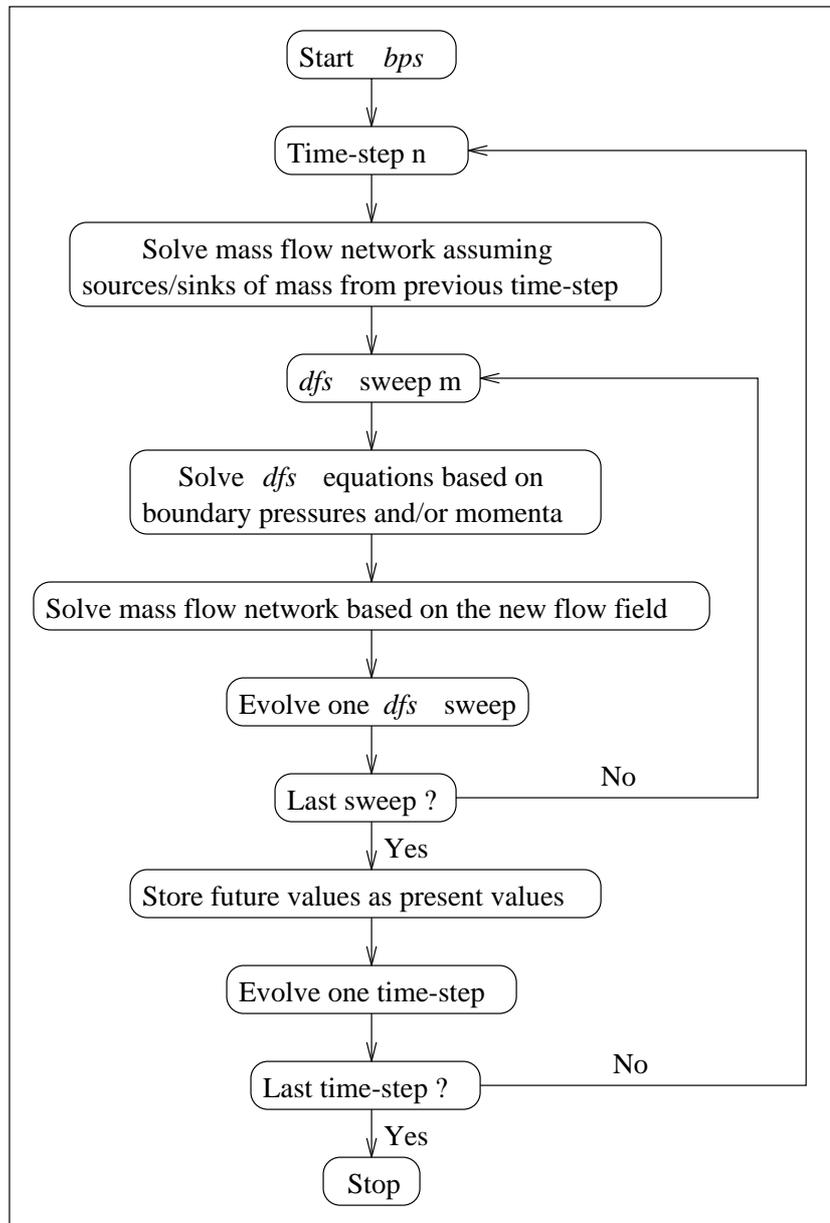
Figure 5.13 Momentum coupling.

The *dfs* inlet condition for the scalar variables (temperature, humidity, etc.) is the property condition at the connected mass flow network node, in this case node Duct_1. The inlet scalar property is multiplied by the mass flow rate and introduced in the corresponding cell's transport equation. At the outlets, no condition is imposed on the scalar variables because it is assumed that inside zone air flow is not influenced by those values. That is to say, diffusion is not considered at the outlets. These outlet values are thus assumed at the nodes which represent the *dfs* cells in the network, in this case node A. The values are then employed in the mass flow analysis to compute the effect of the discretised *dfs* domain in other parts of the building.

In order to diminish the computational time, the frequency of the mass flow network solution could be reduced; for example, the mass flow network computations could take place every ten *dfs* sweeps. However, this may cause divergence problems because of the large changes of the flow properties during the iteration process.

5.5 PROBLEM DEFINITION

After the discussion of the problem definition of *bps* and *dfs* and the previous chapters, the problem definition of a combined domain becomes an easy task. Regarding the thermal coupling and momentum coupling approaches, the combined method runs as an optional feature and is activated during specified time-steps.

Considering the definition of zones, the problem can be specified in the same manner as introduced in Sections 3.7 and 4.7. However, instead of specifying the boundary conditions in the *dfs* required configuration, the identifier, which is employed for dynamic simulations, must be defined as surface names, connection names and source names in order to match the names specified in the *bps* configuration, as the example used in Sections 3.7 and 4.7. In the case of the simple approach, *bps* creates a time-series of flow rates, inlet temperatures, surface temperatures, heat sources, etc. in the format of Figure 4.13. If one of the thermal coupling technique is invoked, surface names and source identifiers are matched within the simulation and the models exchange information accordingly.

In the case of momentum coupling, some other nodes, components and connections in the flow network must be defined. These new connections represent the link between the flow nodal network and the CFD domain. Considering the combined domain as in the diagram of Figure 5.12a, the new network file assumes the format of Figure 5.14. It should be noted that the two connections in the network file of Figure 3.17 are not replaced by the new connections but are added to the connection list. In the *dfs* file, on the other hand, each connection is represented by one opening. Instead of defining one identifier as the opening boundary condition, two identifiers are required: one for the connection which represents the opening, and one for the connection in the original network (Figure 3.17) which is replaced. As can be seen, connections in the network file are defined by five items (two nodes, one component and two heights). Each identifier in the *dfs* file comprises three items (two nodes and one component). The first node of the first connection must always be the node which represents the *dfs* cells in the network (see Figure 5.15). No order is required for the definition of the second identifier.

The approach of replacing original connections only during the coupling allows switching between the network and combined approaches during the simulation. In other words, if the combined approach is requested only at specific time-steps during the simulation, the original network can be employed before and after the required steps. Outside the requested time-steps, the replaced network nodes are reactivated and the coupling connections between *dfs* and the flow network are de-activated. Within the required time-steps the opposite takes place. Also, if at the specified time-steps the *dfs*

calculations does not converge, the combined network is switched back to the original nodal network and the simulation can proceed without damaging the whole solution. This is also valid for the thermal couplings, although, the replacing mechanism is not necessary because each linkage between surface temperatures and air nodes is substituted by just one join of surface temperature and *dfs* cells.

Although the definitions of the approaches were introduced separately, it is entirely possible for the thermal coupling to be simulated together with the momentum coupling.

```
    9     5     8     1.000     (nodes, components, connections, wind reduction)
  Node   Fld. Type   Height      Temperature       Data_1          Data_2
  Duct_1   1     2   2.9000             0.          50.000          1.0000
  Duct_2   1     0   2.9000         20.000             0.              0.
  Kitche   1     0   1.5000         20.000             0.              0.
  Lounge   1     0   1.5000         20.000             0.              0.
  Out_n    1     3   1.5000             0.          1.0000             0.
  Out_e    1     3   1.5000             0.          1.0000           270.
  A        1     0   0.3000         20.000             0.              0.
  B        1     0   2.9000         20.000             0.              0.
  C        1     0   2.9000         20.000             0.              0.
  Comp    Type C+ L+ Description
  duct      50   3   0 Laminar pipe vol. flow rate comp.    m = rho.f(L,R,mu,dP)
     1.00000     5.00000     2.50000E-02
  open      40   3   0 Common orifice vol. flow rate comp. m = rho.f(Cd,A,rho,dP)
     1.00000     2.00000E-02   0.650000
  open1     40   3   0 Common orifice vol. flow rate comp. m = rho.f(Cd,A,rho,dP)
     1.00000     1.00000E-02   0.650000
  window    35   2   0 Constant mass flow rate component   m = a
     1.00000     0.500000
  door     130   5   0 Specific air flow door              m = rho.f(W,H,dP)
     1.00000     0.800000   2.10000     1.00000     0.650000
  +Node   dHght   -Node   dHght   Comp        Snod1  Snod2
  Duct_2  0.000   Duct_1  0.000   duct
  Duct_1  0.000   Kitche -0.700   open
  Kitche  0.700   Lounge  0.700   open
  Lounge  0.000   Out_n   0.000   door
  Lounge  0.000   Out_e   0.000   window
  B       0.000   Duct_1 -0.700   open1
  C       0.000   Duct_1 -0.700   open1
  A       0.000   Lounge -0.700   open
```

Figure 5.14 Flow network file for a combined approach simulation.

```
#    Simulation Title
  Kitchen mechanical ventilated.
#    N. of x-Regions      N. of y-Regions      N. of z-Regions
     1                    3                    1
#    Grid X-direction    N. of cells    Length    Pow. law coefficient
     X                   7              3.00          1.0
#    Grid Y-direction    N. of cells    Length    Pow. law coefficient
     Y                   4              1.50          1.0
     Y                  -3              1.00          1.2
     Y                   3              1.00          1.1
#    Grid Z-direction    N. of cells    Length    Pow. law coefficient
     Z                   9              2.80          1.2
#    Variables:
     U     V     W     T     k     Epsilon     Bouyancy
#    Number of openings
     3
#    Opening type    location    Ii  If  Ji  Jf  Ki  Kf   P(Pa) or m(kg/s)    T('C)    C(-)
     Vel             South        1   1   6   6   9   9   C   Duct_1  Open1   Duct_1  Kitche  Open
     Vel             South        1   1   7   7   9   9   B   Duct_1  Open1   Duct_1  Kitche  Open
     Mas             North       10  10   1   2   1   1   A   Lounge  Open            Kitche  Lounge  Open
#    Number of solid boundaries
         12
#    Solid  Bnd. type    location    Ii  If  Ji  Jf  Ki  Kf    T('C) or Q(W)
     Heat                West         1   1   1  10   1   9        Front
     Temp                East         7   7   1   4   1   9        Back
     Temp                East         7   7   5   7   1   3        Back
     Temp                East         7   7   5   7   4   6        Window
     Temp                East         7   7   5   7   7   9        Back
     Temp                East         7   7   8  10   1   9        Back
     Temp                North        3   7  10  10   1   9        Part_kit
     Temp                North        1   2  10  10   2   9        Part_kit
     Temp                South        1   5   1   1   1   9        Right
     Temp                South        1   7   1   1   1   8        Right
     Temp                High         1   7   1  10   9   9        Ceiling
     Temp                Low          1   7   1  10   1   1        Floor
#    Number of heat/concentration sources
         1
#    Source type    Ii  If  Ji  Jf  Ki  Kf   T('C) or Q(W) or C(-) or CF(kg/s)    Yes(blocked) or No
     Heat            2   3   2   4   1   3                 Equipment                      Yes
#    Max. n. of iterations           Max. source of residues
     200                                 0.01
#    Number of relaxation factors
         5
#    Relaxation factor type    variable    value
     Linear                    U           0.5
     Linear                    V           0.5
     Linear                    W           0.5
     Inertia                   k           1.0
     Inertia                   E           0.1
#    Number of variables to be initiated
         2
#    Initial conditions variable        initial value
         V                                  0.10
         T                                  20.0
#    Time-step interval to print results            result file name
                 4                                  Kitchen.res
#    Monitoring position IMON   JMON   KMON         monitoring file name
                 3      1      3                     Kitchen.mon
#    Re-initialize simulation ?  Yes or No
                            No
Kitchen.flw
Kitchen.otp
Kitchen.wtp
Kitchen.eqp
```

Figure 5.15 *dfs* file for a combined approach simulation.

5.6 CAPABILITIES OF THE COMBINED SYSTEM

The proposed combination is a contribution to the integration of building design elements in order to improve the potential of analysis of energy and fluid flow within the built environment. This allows the investigation of inter-related parameters which are usually, because of the complexities involved, analysed separately. Essentially, the conflation can be employed to estimate more appropriate boundary conditions for *dfs* simulations and to study the influence of zone property distribution on the building comfort and pollution conditions, and the building's total energy consumption.

The ever present difficulty to assess *dfs* boundary conditions can now be evaluated in the transient domain rather than the usual steady-state one. Convection heat transfer (or convection coefficients), longwave exchanges, shortwave radiation, plant interactions, heat conduction and inlet air flow conditions are integrated with the analysis of the discretised air flow domain. Also, the influence of *dfs* outlet conditions on the energy and air flow analysis of the rest of the building and plant systems can be better investigated. As concluded by Schaelin *et al* (1993) the concentration of pollutant at outlets can be largely different from the averaged value computed by the mixed air approach.

The present model can be employed to enhance the efficiency of building/plant systems in terms of comfort and energy requirements. Several design parameters concerned with spatial property distribution can be examined in order to improve system performance. For example, the optimum geometries and positions for the air supplies and exhausts within a mechanically ventilated zone to provide a uniform air flow distribution is possible; the effect of the radiator position on the uniformity of the zone air flow, comfort levels or energy consumption; the influence of changes to the mechanical supply on the local air flow properties; the best position of heat or contaminant sources to reduce the global or local zone heating or pollution.

The overall control capabilities were also strengthened. Sensors can now be located at a specific zone spatial position to perceive local air flow properties. This could not be performed by *bps* itself. On the other hand, the actuator can be placed in any building section or plant component, and this was not possible within *dfs*. Such improvements allow simulations of more realistic control systems.

Considering the larger size of *bps* and the fact that it already covers different areas of the energy flow analysis, *dfs* was incorporated into *bps* to accomplish the integrated conflation mechanisms explained in sections 5.3.2 and 5.3.3. The *bps* user, in such cases, can define his whole problem embodying building and plant systems as usual. The simulation of the defined problem can be performed employing the standard mixed air approach or, optionally, by invoking *dfs* for the analysis of the air flow within a particular zone. This allows comparisons between the mixed air approach and the combined approach. The comparisons can, for instance, be used to investigate the range of

applicability of the mixed air approach. As the computational time can often be extensive, the user does not necessarily need to employ the combined method during the whole simulation period. The combined approach may only be invoked during specific time-steps of the simulation period. This means that a blend of the combined and mixed air approach is allowed within a single simulation. When convergence problems occur with the integrated approach, the *dfs* domain is abandoned and the previously removed *bps* standard model is re-established. This allows the simulation to proceed, albeit with a simplified model of the *dfs* domain.

Comparing the three thermal coupling mechanisms introduced, the convection coefficient and sequential schemes can be numerically less accurate than the simultaneous scheme for a specific time-step. However, as the time-step is reduced the results of the three solution approaches tend to converge. On the other hand, the simultaneous scheme is possibly more time consuming for a given time-step because of the iteration involved with the internal surface temperatures. Therefore, comparisons between the three methodology must be carried out in future to investigate accuracy and the computational time involved.

The intra-construction heat conduction considered on the thermal coupling was assumed one-dimensional. Sometimes, a two or three-dimensional analysis of such heat conduction is necessary, as suggested by Nakhi (1995). Nevertheless, the thermal coupling described early can be applied irrespectively of the type of heat conduction.

In the simple approach, the simultaneous effect of one system on the other is not observed. This could only happen if a sequence of *bps* and *dfs* simulation was performed, but this is probably too time consuming. Also, the mass flow network is decoupled from the *dfs* domain (the pressure changes on the *dfs* domain do not affect the network flow) and the influence of the discretised domain on the network is never perceived. This can only be noticed when the integrated approach is applied.

At the present moment, only the convection coefficient, simultaneous schemes and momentum coupling are implemented within *bps*. Also, the simple approach is only partially implemented since the second independent *bps* run does not account for the *dfs* calculations.

5.7 REMARKS

The current chapter discussed the combination of Building Thermal Simulation and Computational Fluid Dynamics. The two simulation applications introduced in the previous chapters, *bps* and *dfs*, were used to perform the combination. Several coupling mechanisms were described with different degrees of complexity and sophistication. The conflation is mostly concerned with the *dfs* boundary conditions (convection heat transfer and momentum, mass flow and pressures at openings) where the interaction of the models take place. The advantages and disadvantages of the conflation mechanisms regarding implementation, integrity, accuracy and computational requirements were discussed. An explanation of how the user can define a combined problem, making use of the problem

definitions introduced in the previous chapters, was presented. Finally, the capabilities of the combined system were described.

REFERENCES

Aasem, E., Clarke, J. A., Hand, J., Hensen, J., Pernot, C. and Strachan, P., 1992, *ESP-r The European Reference Program for Building Energy Simulation*, ESRU Manual, Version 8 series, Glasgow, UK.

Elsen, J. t., 1994, *Development of a Optimisation Design Tool Using the CFD code TEACH*, ERASMUS Student Exchange Programme.

Nakhi, A., 1995, *PhD Thesis (to be published)*, ESRU,University of Strathclyde.

Schaelin, A., Dorer, V., Van der Maas, J., Moser, A., 1993, Improvement of Multizone Model Predictions by Detailed Flow Path Values from CFD Calculations, *ASHRAE Transactions*, Vol. 99, Part 2, pp. 709-720.

6.1 INTRODUCTION

The basic theory and numerical techniques introduced in Chapters 3 and 4, have been shown to be adequate for modelling building and plant systems. However, the overall accuracy of simulation models depends on many factors. Judkoff *et al* (1983) identified seven source of inaccurate predictions in building simulation programs which were also mentioned by Hensen (1991) and here they are summarised in four categories:

•   Input uncertainties;

•   Inappropriate translation of the real physical phenomena into a mathematical model;

•   Unsuitable representation of the mathematical model in a computer understandable form;

•   Incorrect software implementations.

Hensen (1991) also classifies the first category as *external* sources of errors as they are independent of the working performance of the program. The other three categories are classified as *internal* sources since they are under the control of the developer and are directly responsible for the internal program operation. Some candidates for external source of errors are: inadequate user assumptions of actual system behaviour, errors within input files, uncertainties in physical parameters (geometry, thermophysical properties, etc.) and of boundary conditions. Lomas *et al* (1994a) identify some examples of the second category: physical phenomena not included in the modelling because they are incorrectly thought to be unimportant; approximation of relevant complex phenomena; simplification of physical processes to ease or speed up calculations. Errors on the model derivation, such as unit conversions, can be added to this list. Under the third category lies the adoption of a computer model and solution algorithms which may not be appropriate for the representation of the mathematical model (such as discretisation techniques, relaxation factors, linear equation solvers, etc), though these may be the best approaches available.

Some of the external source of errors can be eliminated by the use of a knowledge-based interface which checks that all input parameters are within a legal range and can supply intelligent defaults. However, most errors are outwith the developer's control and depend on the user's judgement and skill, and on the specification of boundary conditions (for instance climate conditions).

Hence, this chapter is mostly concerned with those sources of inaccuracy classified as internal errors.

A validation methodology must be established in order to increase confidence in simulation programs. The purpose of this methodology is to test the applicability of the model by determining the range of its results validity and by identifying the possible sources of inaccurate predictions. An example of a validation procedure from the PASSYS project (Jensen 1994) comprises the following steps:

- Critical evaluation of the theory;

- Check of the source code;

- Analytical validation;

- Inter-model comparison;

- Empirical validation;

- Sensitivity and statistical analysis.

Theory checking involves an examination of existing models to represent the physical phenomena and a meticulous investigation of the employed approach. The process of documentation production, as suggested by Van der Laan (1994), is considered as part of the theory checking; for instance the publication of the present work. In this phase of the project, the literature is revised, the concepts and assumptions are examined and sources of potential inaccuracies documented. As part of this task, three PhD progress report (Negrão 1993, Negrão 1994a and Negrão 1994b) and two publications (Clarke *et al* 1995a and Clarke *et al* 1995b) were produced. The second step consists of a systematic inspection of the source code to ensure that the algorithms are properly implemented. If the code is reasonably well commented and modularly structured, this helps to identify sources of errors, which is assumed to be the case for the code being developed. Elsen (1994) and Loomans (1995) during the development of their projects have contributed to this part of the work. Both authors have questioned some sections of *dfs* code and made suggestions for changes some of which were adopted. Also, during the program development process, the code was thoroughly inspected by the use of checking (for syntax errors) and *debugging* (for logic errors) tools. Some bugs and mistakes were found and corrected. Considering that a sensitivity analysis is usually concerned with the influence of input parameter variations on simulation predictions, such a task was not undertaken in the present study and it is suggested as a future investigation.

The remaining three procedures (analytical validation, inter-model comparison and empirical validation) consists of comparing the model under analysis to another, usually well known method. Each of these three procedures have advantages and disadvantages in terms of the consolidation of a simulation model. The analytical solution is usually free of uncertainties but its application is restricted to given simple cases. With inter-model comparison any level of complexity can be tested

and also no input uncertainties are present. However, a standard of absolute correctness cannot be identified. Although the case chosen for empirical validation is generally a reasonable representation of the reality, it is limited to a number of cases due to economic reasons. Furthermore, a certain degree of input uncertainty is involved and only an approximation of "truth" is attainable in terms of the accuracy of the data acquisition system.

The main purpose of the following sections is to consolidate the combined method. However, as the accuracy of the combined approach depends on the validity of the two simulation systems, some effort is devoted to validate the separate models. Also, the current chapter does not intend to be comprehensive in order to cover all the coupling mechanisms discussed in the previous chapter. Only the simultaneous scheme (thermal coupling) and the momentum coupling will be checked. Validation of the other approaches are left for the future.

In Section 6.2, the momentum coupling and *dfs* are checked against analytical solutions. Section 6.3.1 employs a natural convection situation to compare *dfs* and the simultaneous scheme with PHOENICS. In Section 6.3.2, a forced ventilation case is used to validate *dfs* and the momentum coupling against other numerical models. Finally, results of an empirical validation carried out in test cells are employed to compare the simultaneous scheme with measured values.

6.2 ANALYTICAL VERIFICATION

As mentioned, the overall potential of the model under investigation cannot be checked using analytical validation because only tests for simplified sub-sets can be analysed. However, these are usually the only *truth* standard available to corroborate simulation predictions. To fulfill such requirements, a predominantly two-dimensional, steady flow is analysed.

The purpose of this analysis is to check the validity of the *dfs* system when connected to a *bps* mass flow network and when the two approaches are considered separately. The case studied comprises the air flow through three horizontal parallel-plate ducts connected in series, as illustrated in Figure 6.1. The whole circuit is investigated by firstly employing only a mass flow network and, secondly, by the same network but where the duct B is modelled by the *dfs* system. Since an analytical turbulent solution does not exist for such an internal flow, only the laminar situation is evaluated. The intermediate duct is 3m long and the other two are each 1m long.

Analytical solution

The two-dimensional flow within the parallel plates as a result of a uniform stream U_{in} at the inlet is shown in Figure 6.2. At the entrance to the channel, two separate boundary layers are formed on both walls. The layers grow to a thickness D/2, merging with each other after an *entrance* length. The channel flow can be thought of as a succession of two distinct flow regions. In the first (the entrance or developing region), two boundary layers coexist with a core zone that has not yet been

influenced by the viscous forces associated with the walls. In the second (the fully developed region), the core zone no longer exists and the boundary layers have joined.
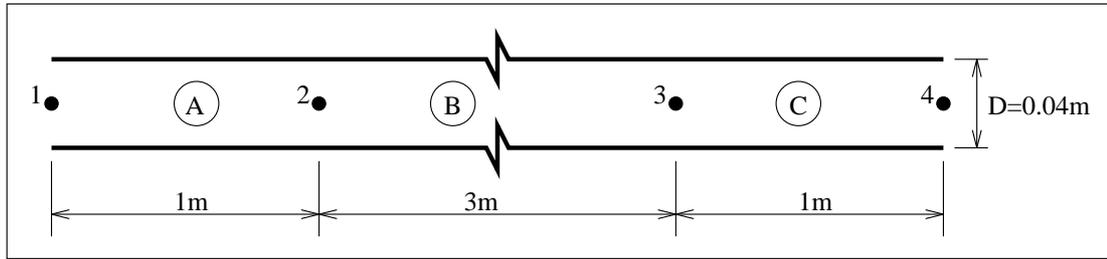
Figure 6.1 Three parallel-plate ducts connected in series.
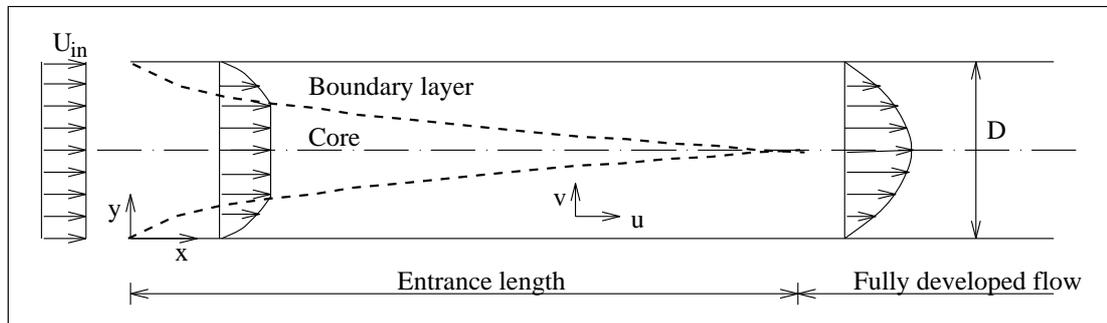
Figure 6.2 Fluid flow through a parallel-plate duct.

Developing region

Two solutions are suggested for this region. The first one consists of an approximate solution which was derived by Bejan (1984). The second one is another approximate solution derived by Schlichting (1979), which is supposed to be more accurate.

As the boundary layers grow, Bejan suggested that the flow on the core zone must accelerate in order to obey the conservation of mass. The core flow is expected to be inviscid and can be modelled by the Bernoulli equation:

$$\frac{\rho U_c^2}{2} + p = constant \tag{6.1}$$

where U_c is the velocity of the core flow. On the other hand, the velocity on the viscous zone is assumed to have a boundary layer profile shape. This profile is given by

$$u(x, y) = U_c(x)\left[2\left(\frac{y}{\delta(x)}\right) - \left(\frac{y}{\delta(x)}\right)^2\right]$$ (6.2)

where δ is the boundary layer thickness. An integration of the boundary layer equation gives an approximate solution for the core velocity and boundary layer thickness:

$$\frac{3}{160}\left(9\frac{U_c}{U_{in}} - 2 - 7\frac{U_{in}}{U_c} - 16\ln\frac{U_c}{U_{in}}\right) = \frac{x/D}{\text{Re}_D}$$ (6.3)

$$\frac{\delta}{D/2} = 3\left[1 - \frac{U_{in}}{U_c}\right]$$ (6.4)

where U_{in} is the imposed uniform velocity at the entrance of the channel and Re_D is the Reynolds number based on U_{in} and the distance between plates, D. The velocity on the developing region can be completely determined by equations (6.2), (6.3) and (6.4).

At the location where the two boundary layers merge ($\delta = D/2$), the combination of equation (6.3) and (6.4) yields $U_c = \frac{3}{2}U_{in}$, with the entrance length found from

$$\frac{X/D}{\text{Re}_D} = 0.0065$$ (6.5)

where X is the laminar entrance length. Applying the Bernoulli equation (6.1) through the entrance region, an approximated expression for the pressure drop at the developing region arises:

$$\Delta p = \frac{\rho}{2}\left[\left(\frac{3}{2}U_{in}\right)^2 - U_{in}^2\right] = \frac{5}{8}\rho U_{in}^2 \quad .$$ (6.6)

Schlichting (1979) solved the same problem by obtaining a series solution for the accelerated boundary layer flow at the beginning of the entrance length, and by matching this series to a second series solution valid near the end of the laminar entrance length. The velocity profile is obtained from Schlichting (1979), Chapter IX, Figure 9.15, which will be shown later in this section. The distance from the inlet where the two layers merge is estimated by Schlichting:

$$\frac{X/D}{\text{Re}_D} = 0.04 \qquad . \tag{6.7}$$

Fully developed region

The fully developed region is considered to be situated far enough from the channel entrance and therefore the scale of the velocity component parallel to the y direction is negligible. Such an assumption leads to the result that the flow profile no longer changes with x and that the pressure gradient is constant (the pressure varies linearly in the x direction). This reduces the analysis to a simplified form of the x momentum equation which can be effortlessly solved. Assuming no-slip conditions at the walls, a solution for such an equation is achieved (Bejan 1984):

$$u(y) = \frac{3}{2} U_{in}\left[1 - \left(\frac{y}{D/2}\right)^2\right] \tag{6.8}$$

where,

$$U_{in} = \frac{D^2}{12\mu}\left(-\frac{\partial p}{\partial x}\right) \tag{6.9}$$

and y is, in this case, measured from the centre line. This is known as the Hagen-Poiseuille solution for fully developed flow between parallel plates. The pressure gradient can be represented by $-\partial p/\partial x = \Delta p/L$ since it is constant in the longitudinal direction. Δp is the pressure drop along the length L. The relation between mass flow and pressure drop can then be obtained from equation (6.9):

$$\dot{m} = \frac{\rho D^3 \Delta p}{12\mu L} \qquad . \tag{6.10}$$

For the solution of the energy equation on the fully developed region, the flow is assumed to be hydrodynamically fully developed: in other words, $v = 0$ and $u = u(y)$. Also, the axial diffusion is considered to be negligible. The differential energy equation is then solved by adopting a Hagen-Poiseuille velocity profile. The solution for a constant heat flux at the duct wall acquires the following form

$$\frac{T_o(x) - T(x, y)}{T_o(x) - T_m(x)} = \frac{3}{4} Nu\left\{\frac{5}{24} - \left(\frac{y^*}{2}\right)^2\left[1 - \frac{2}{3}\left(\frac{y^*}{2}\right)^2\right]\right\} \tag{6.11}$$

where T_o is the duct wall temperature, y^* is the dimensionless y position ($= \frac{y}{D/2}$) and Nu is the Nusselt number, which for this case is a constant equal to 1260/153 (Bejan 1984). T_m is the bulk flow

temperature computed from the following expression

$$T_m(x) = \frac{2}{\rho_{in} U_{in} D} \int\limits_{0}^{D/2} \rho(x, y) u(x, y) T(x, y) dy \qquad (6.12)$$

where ρ_{in} is the density at the duct inlet. The total heat transferred from the walls to the air flow along the whole duct is computed from

$$Q = \dot{m} c_p [T_m(L) - T_{in}] \qquad (6.13)$$

where $T_m(L)$ is the air bulk temperature at the duct outlet and T_{in} is the inlet air temperature.

Network solution

Given the complexity involved at the entrance region, the network method is only concerned with the solution of the fully developed flow. Mass flow rate and pressure drop are related by the following power law expression

$$\dot{m} = e_1 (\Delta p)^{e_2} \quad . \qquad (6.14)$$

The coefficients e_1 and e_2 are derived from the analytical solution (equation (6.10)):

$$e_1 = \frac{\rho D^3}{12 \mu L} \qquad e_2 = 1.0 \quad .$$

dfs solution

The flow comprising the developing and fully developed region can be completely solved by the *dfs* system if all boundary conditions are provided. At the duct inlet a uniform velocity profile is imposed. A no-slip condition is assumed at the walls and a parabolic boundary condition is taken at the duct outlet (pressure = 0). Because the flow is symmetric with the x axis, only half of the domain is solved. 20 cells and 15 cells are distributed in the x and y directions respectively and placed non-uniformly in both directions according to the power law equation (4.11). The grid size increases with x or y and the power law coefficient c is equal to 1.5.

To compare the temperature profile within the fully developed region with the analytical solution, the bulk temperature at each cross section is approximated by *dfs*, from equation (6.12), as

$$T_m(x) = \frac{2}{\rho_{in}U_{in}D} \sum_{i=1}^{Nc} \rho_P u_P T_P \Delta y_p \qquad (6.15)$$

where u_P and T_P are respectively the velocity and temperature at cell P and Nc is the total number of cells in the y direction.

Results

In the first instance, the flow is considered isothermal at a constant temperature of 20^oC. In order to solve the problem of Figure 6.1, pressures at nodes 1 and 4 are assumed equal to 0.51794Pa and 0.0Pa respectively. The mass flow rate through the ducts and pressures at nodes 2 and 3 are computed by employing the network approach. The pressure drop in each duct and the mass flow rate are presented in Table 6.1. The differences between such values and the analytical solution are insignificant. This is expected since the mass flow equation (6.14) is derived from the analytical solution. However, such agreement improves confidence in the network method. A more complete validation process of the network approach is provided by Hensen (1991).

Table 6.1 Mass flow network results.

Mass flow (kg/s)	Δp_{1-2} (Pa)	Δp_{2-3} (Pa)	Δp_{3-4} (Pa)
0.035643	0.10359	0.31076	0.10359

The flow through duct B of Figure 6.1 is solved by *dfs* assuming the uniform velocity of 0.75m/s (corresponding to a mass flow rate of 0.035643kg/s) at the inlet of duct B. The following linear under-relaxation factors were employed, $\alpha_u = 0.5$, $\alpha_v = 0.5$ and $\alpha_p = 0.7$, and convergence is achieved after approximately 400 iterations when the source of residuals is below 0.1% of the inlet flow or momentum.

Initially, only Bejan's solution on the developing region was invoked to compare with *dfs* solution. Figure 6.3 shows the air velocity (normalised through the inlet velocity - u/U_{in}) in the duct cross section ($\frac{y}{D/2}$). Although the *dfs* solution behaves similarly to Bejan's solution there is a certain discrepancy between the models. As the agreement was not satisfactory, the cause of discrepancy was mostly attributed to the analytical solution. A comparison with Schlichting's solution[#], which is supposed to be more accurate, was thus performed. As can be seen in Figure 6.3, Schlichting's and *dfs* solutions agree reasonably well. According to equation (6.5) and (6.7), the entrance length is 0.5m

―――――――――
  [#] This solution is a reproduction of Figure 9.15 shown in Schlichting (1979).

and 2.6m respectively, and therefore the flow at such *x* positions is within the developing region. The entrance length estimated from the *dfs* results is the distance where the velocity at the centre line reaches 99% of the velocity at the outlet, In this case the length is approximately 2.1m which is in the same order of magnitude as the value estimated by Schlichting.
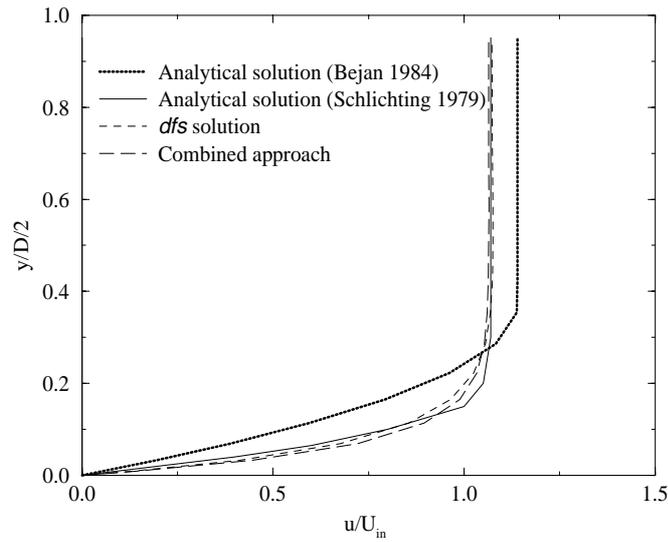
(a)
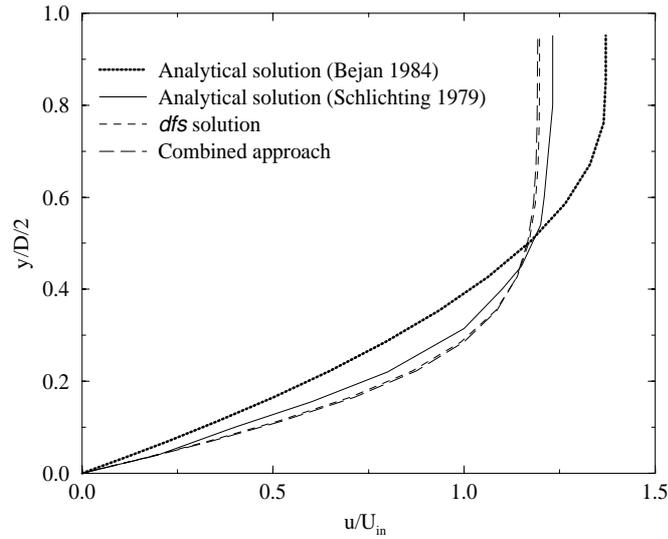
(b)

Figure 6.3 Velocity distribution at the duct cross section in the developing region. (a) $x = 0.034m$ and (b) $x = 0.268m$.

The discrepancy which remains can be assigned to either the analytical or numerical solutions. Additional to the fact that Schlichting's solution is an approximation, it is obtained from an interpolation on a graphic. This process may introduce certain uncertainties in the results. The hypothesis of parabolic flow, assumed at the outlet of the duct by *dfs*, may not be satisfactory since the entrance length (from Schlichting or *dfs*) has the same order of magnitude as the duct length. To certify if this is correct, the duct length should be increased and the parabolic condition assumed at the outlet. The results of this new situation should thus be compared with the original case at a distance approximately equal to 2.0m. Due to lack of time, this task was however not performed here and is left for the future.

The above case was tested by *dfs* in different combinations of planes, such as $x - y$, $y - z$ and $x - z$. The same results were obtained for each combination, demonstrating the reliability of the numerical solution in different planes. Such comparisons are important to identify possible mistakes in the source code.

The comparison between the numerical and analytical results in the fully developed region is presented in Figure 6.4. In this case, the analytical result is the exact solution of the differential equation (against the stated simplifications for the fully developed region). The numerical solution is taken at a position far from the entrance region. As can be seen, the two curves are close, with the simulated curve within the sensitivity band associated with the analytical solution. The source of discrepancies can be attributed to either the assumptions within the analytical method or to problems in the numerical solution. The latter can be attributed to the fact that the flow may not be fully developed within such a region.
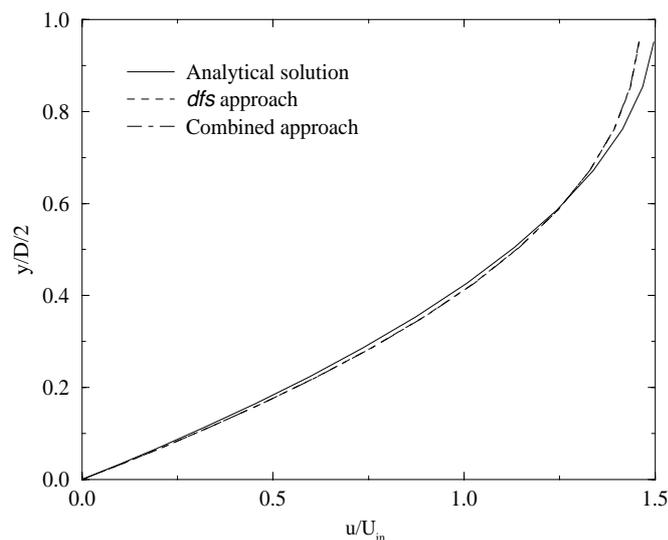
Figure 6.4 Velocity distribution at the duct cross section in the fully developed region.

A comparison with PHOENICS was also carried out. PHOENICS and *dfs* results are only slightly different in both the entrance and developed regions.

Dfs produces a pressure gradient in the *y* direction at a region closer to the inlet which tends to zero as *x* increases. On the other hand, the pressure gradient in the *x* direction decreases with *x*. At a region considered fully developed, the pressure drop only takes place in the *x* direction and is proportional to the distance. This is consistent with the analytical solution. The total pressure drop along the duct is approximately equal to 0.50Pa. The corresponding analytical pressure difference is the sum of equations (6.6) and (6.9) which is 0.68Pa. Although the difference is significant, it should be reminded that the analytical value is derived from Bejan's solution which is an approximate solution. A value derived from Schlichting's solution should provide a better comparison with the numerical result, but this is left for future investigation.

In a second *dfs* run, the energy equation was also solved with a prescribed constant heat flux of 700W at the duct walls. Analytical and numerical temperature profiles in the fully developed region are compared in Figure 6.5. As can be seen, only small discrepancies between the two results are perceived along the cross section, indicating a reasonable performance of *dfs* in the fully developed regime. Also, the estimated outlet bulk temperature from the *dfs* results (equation (6.15)) is 39.25^{o}C which is comparable with the analytical value of 39.52^{o}C as calculated from equation (6.13).
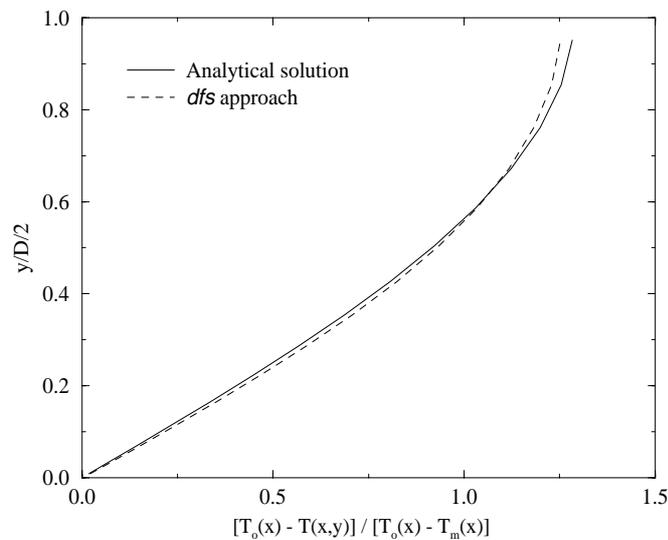
Figure 6.5 Temperature distribution at the duct cross section in the fully developed region.

The three ducts shown in parallel in Figure 6.1 were then simulated by the combined method. Figure 6.6 shows the discretised combined domain. As can be seen, node 1 is connected to node 2,

and node 3 is linked to node 4 by a mass flow component. Node 2 in this case represents all inlet cells and node 3 outlet cells in the CFD domain.
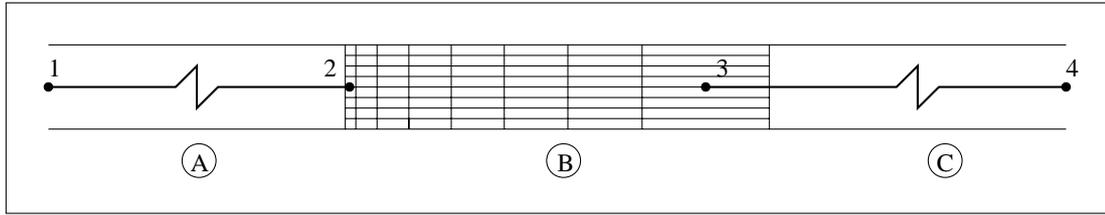
Figure 6.6 Discretised combined domain.

In order to obtain almost the same mass flow rate as the network only case, a higher pressure difference between nodes 1 and 4 was supplied: $p_1 = 1.05$Pa and $p_4 = 0.00$Pa. The reason is because duct B is now modelled as a CFD domain and the entrance region (where a higher pressure drop occurs) is now considered in duct B. At the inlet of duct B, pressure and momentum (uniform profiles) computed by the network approach were imposed, and at the outlet only pressure was fixed. The number of iterations necessary to achieve convergence was smaller than the *dfs* only case with the same under-relaxation factors.

The calculated mass flow rate and the duct pressure differences are indicated in Table 6.2. The mass flow rate and the pressure drops at ducts 1 and 3 are in agreement with the results of equation (6.10). However, the pressure drop along duct B is higher than with the *dfs* only case. The possible reason is the zero transverse pressure gradient at the duct inlet caused by the pressure imposition. The fact that only one node in the nodal network represents all inlet cells leads to the uniform pressure imposed. This condition prevents a two-dimensional flow from taking place and a higher pressure drop is necessary at the beginning of the duct entrance region. The consequence on the velocity distribution can be observed in Figures 6.3 and 6.4. A slight difference between the combined and *dfs* results can be seen at the beginning of the entrance region which tends to vanish as *x* increases. To avoid the uniform pressure at the inlet, one connection should be specified for each inlet cell. In other words, 15 cells should be linked to node 1 by 15 parallel connections.

Table 6.2 Combined approach results

Mass flow (kg/s)	Δp_{1-2} (Pa)	Δp_{2-3} (Pa)	Δp_{3-4} (Pa)
0.035836	0.10415	0.84171	0.10415

6.3 INTERMODEL COMPARISON

For the intermodel comparison, the degree of complexity involved in the case study is higher than that of the analytical validation. However, such comparison usually cannot cover the whole potential of the developed model. The purpose of the current section is to validate *dfs* and, whenever possible, the combined *bps/dfs* approach. PHOENICS (Rosten and Spalding 1987), a well known generic CFD program, is the elected reference standard model to compare with *dfs*. In some cases, other sources are utilised. The ability of the developed system to predict both natural and forced ventilation is investigated. The comparison of natural ventilation consists of laminar and turbulent, two and three-dimensional, steady and transient cavity flow; the forced ventilation comparison comprises a steady turbulent two-dimensional case.

6.3.1 Natural Ventilation

This section tests the reliability of *dfs* to predict heat transfer and air flow in natural ventilated systems. The two and three-dimensional fluid flow inside a sealed cubic cavity (3mx3mx3m), as shown in Figure 6.7, was the configuration adopted for the analysis.

Two-dimensional case

The flow originated by the buoyancy effect was initially tested in a laminar steady state regime. The left hand side vertical wall was heated to 30^oC whereas the opposite side was cooled to 0^oC. The horizontal walls (bottom and top) were adiabatic as illustrated in Figure 6.7a. The air flow regime for such a geometry and conditions is possibly transitional: the Rayleigh number (Ra)[#] is in the order of $1.0x10^9$ to $1.0x10^{10}$. In order to ensure a laminar flow, the fluid viscosity was conveniently adjusted to reach three different Rayleigh numbers: $1.0x10^3$, $2.5x10^4$ and $1.0x10^5$. 20 grid cells were symmetrically distributed in each direction according to the power law equation (4.11) (*c* coefficient equal to 1.5). Linear under-relaxation factors for pressure, v and w were necessary and were respectively 0.7, 0.5 and 0.5.

Figures 6.8 and 6.9 show the flow streamlines and isotherms computed by *dfs* and PHOENICS for $Ra = 1.0x10^5$. As can be seen, the results are in reasonable agreement with each other. The streamlines exhibit a large recirculation in the cavity, where the flow rises close to the hot wall and moves downwards near the opposite surface. Additionally, all isotherm curves are perpendicular to the adiabatic top and bottom surfaces, and the heat flux (3376W for *dfs* and 3402W for PHOENICS) gained by the air at the hot surface is delivered to the cold surface. These are perfectly consistent with the physical conservation principles. Moreover, Arpaci and Larsen (1984) present a numerical solution which agrees with Figures 6.8 and 6.9 and hence corroborates the *dfs* predictions. The same

---

[#] $Ra = \rho g \beta_T \Delta T \dfrac{H^3}{\alpha \mu}$, where ΔT is the temperature difference between vertical surfaces and H is the cavity height.

degree of similarity between PHOENICS and *dfs* results occurs for the other Rayleigh numbers although they are not shown here.
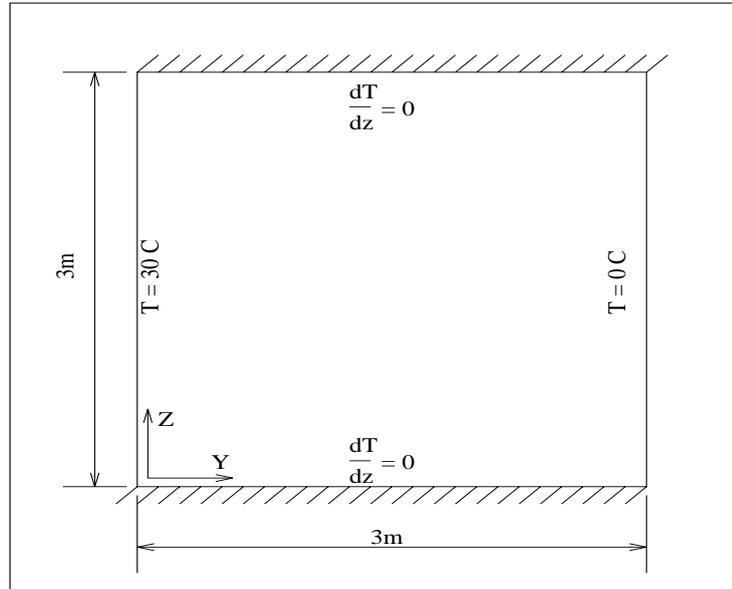
(a)
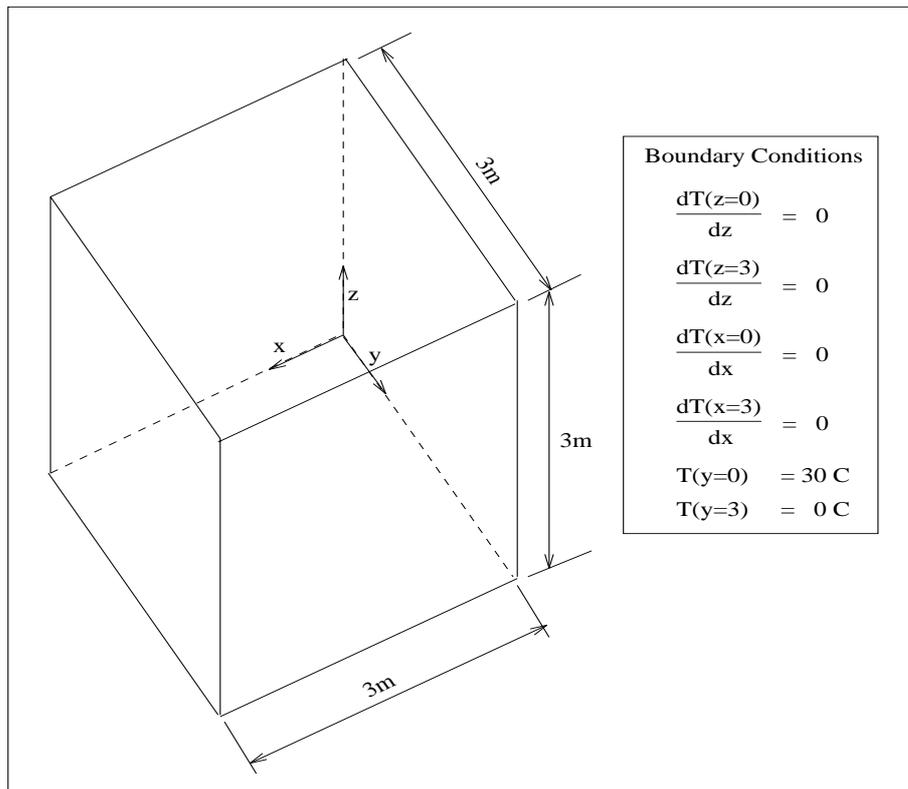
(b)

Figure 6.7 (a) Two and (b) three-dimensional sealed cavity.

To demonstrate the *dfs* capability to predict transient flows, the following situation was analysed: stagnant air at a temperature of 15^oC was instantly exposed to a hot and a cold vertical wall (30^oC and 0^oC respectively). A simulation was then performed for a period of 1s with a 0.2s time-step. Although it is usually not employed in building applications, such a time scale was used to observe the beginning of the air motion. During the whole simulation period the isotherms are essentially vertical and highly concentrated near the hot and cold walls. The reasons are twofold: firstly, a high temperature gradient appears between the wall and the adjacent air layer. Thus, a high amount of heat is transferred diffusively from the wall to the air causing the concentration of isotherms. Secondly, the flow velocities are still low and therefore the convective terms have no major influence on the energy conservation equation. Consequently, the heat transferred from one surface to the other is predominantly diffusive. PHOENICS and *dfs* results are much the same for the whole simulation period and Figure 6.10 is an example of how close their flow patterns are.

(a)   (b)
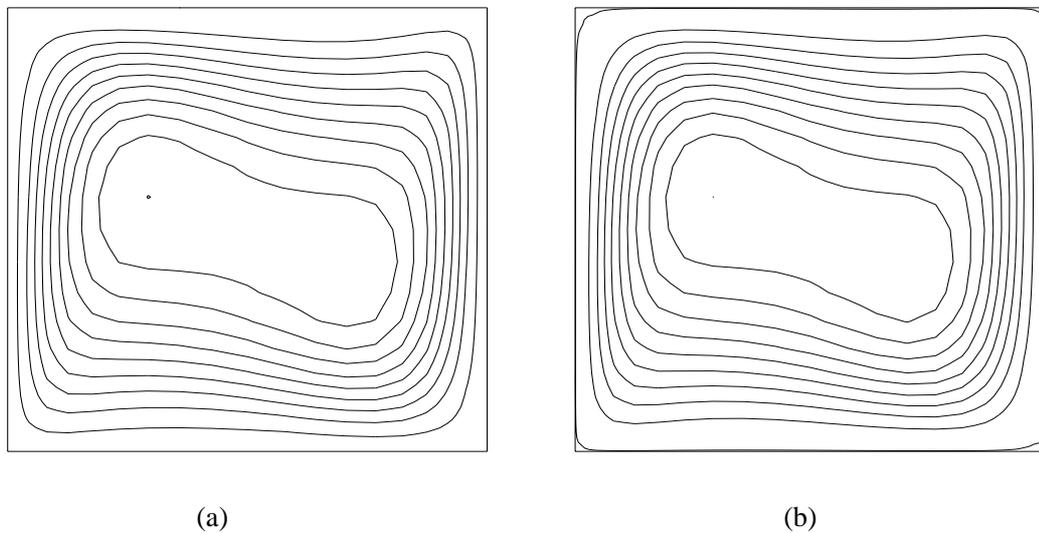
Figure 6.8 Streamlines for the two-dimensional laminar cavity flow: (a) *dfs* and (b) PHOENICS results.

In order to validate the thermal coupling (simultaneous scheme) between *dfs* and *bps*, constructional elements were added externally to the surfaces. The purpose was to evaluate the conjugate phenomena of conduction within the constructions (modelled by *bps*) and the natural convection inside the cavity (modelled by *dfs*).

<center>(a)   (b)</center>
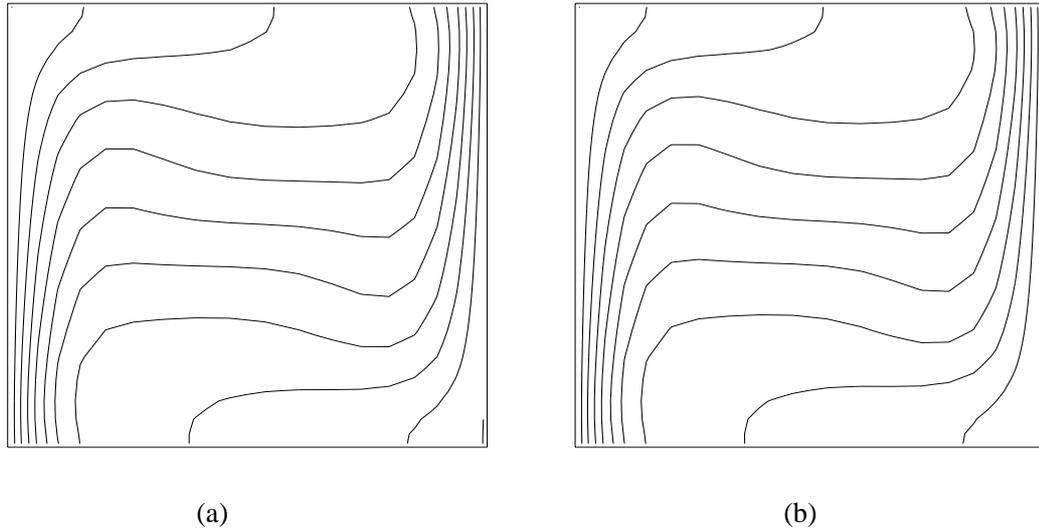
Figure 6.9 Isotherms of the two-dimensional laminar cavity flow: (a) *dfs* and (b) PHOENICS results.

<center>(a)   (b)</center>
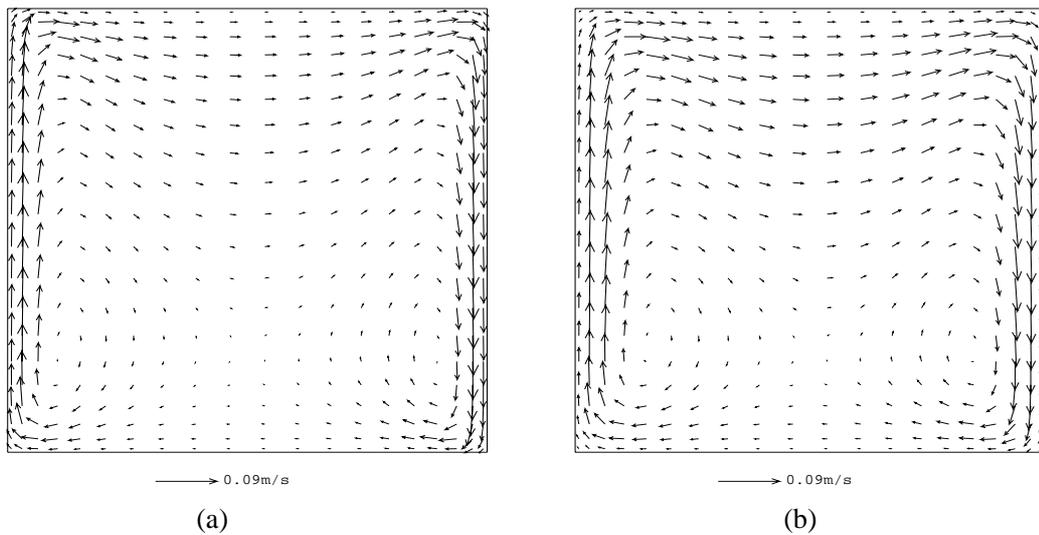
Figure 6.10 Laminar transient flow pattern within a two-dimensional cavity: After 0.6s of simulation. (a) *dfs* and (b) PHOENICS.

In this situation, no surfaces were specified adiabatic and constructional elements were added to all surfaces, as shown in Figure 6.11. The temperatures were fixed at adjacent outside air layers and constant convection coefficients equal to $4W/m^2K$ were specified. The environment adjacent to the left hand side wall was at 33.0^oC and to the opposite wall was equal to 0^oC. The top and bottom

external air layers were both kept at 15^oC. The constructions comprised a $200mm$ layer of a material with the following thermophysical properties: $\lambda = 0.27W/m\ K$, $c_p = 200J/kg\ K$ and $\rho = 200Kg/m^3$. The λ value corresponds to the conductivity of brick and the specific heat and density were conveniently adjusted to provide a short transient period, as the interest was predominantly on the steady behaviour. The fluid specific heat $(5.25J/kg\ K)$ was adjusted to correspond to a fluid conductivity in the order of $0.026W/mK$ (the conductivity of the air) and therefore to maintain the same Rayleigh number (10^5). As this exercise was only concerned with conduction and convection, *bps*'s radiation exchange mechanism between solid surfaces was de-activated by choosing surface emissivities and absorptivities equal to zero. As explained in Chapter 3, the standard *bps* model treats the intra-constructional heat conduction as one-dimensional.
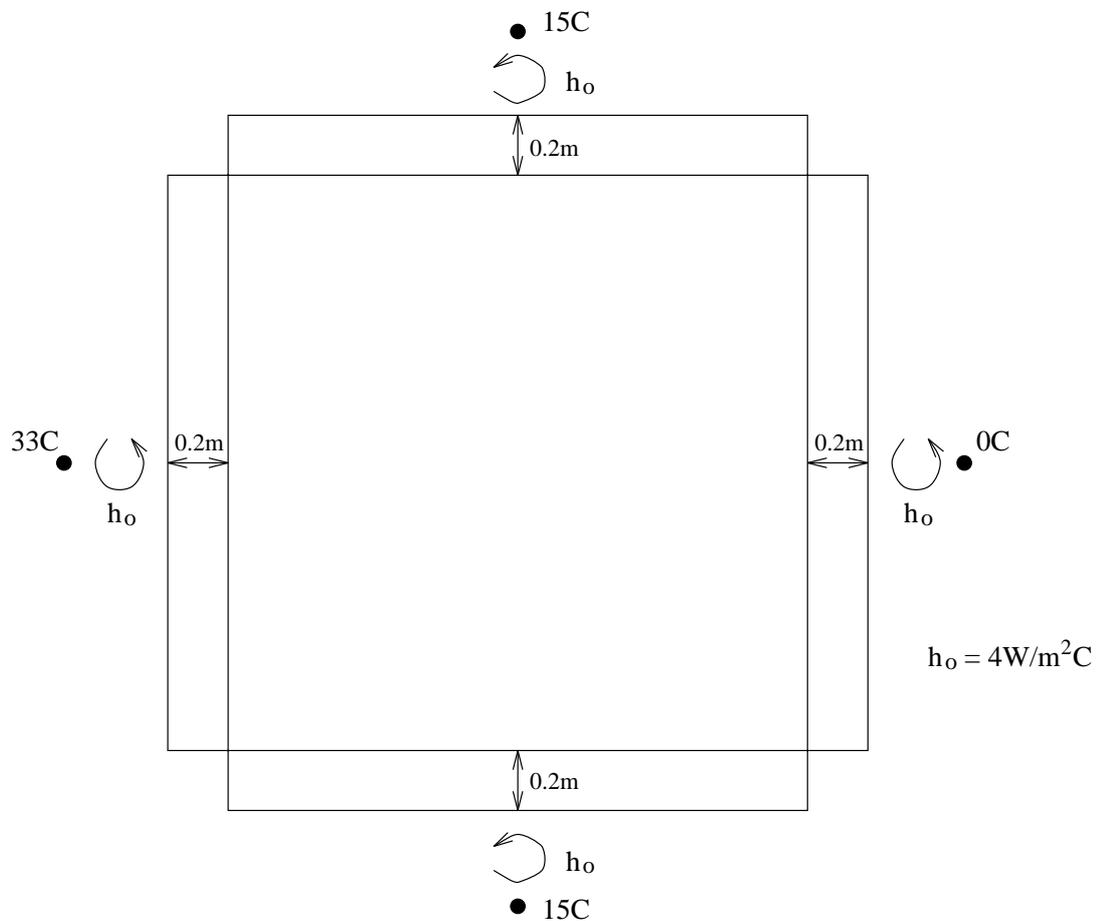
Figure 6.11 Geometry of the cavity with constructions.

The simultaneous thermal coupling scheme was employed to solve the steady laminar problem. The results show that the heat flux produced by the *dfs* calculations at each internal surface is equal to the corresponding one-dimensional intra-constructional heat conduction flux. Moreover, the heat loss

at the hot boundary is the sum of the heat gained at the other boundaries, demonstrating the agreement with the energy conservation principle. PHOENICS was then used assuming the internal surface temperatures obtained from the combined approach results (the heat conduction is not modelled by PHOENICS since this is not considered one-dimensional). Once again, the flow patterns produced by the two models agree well.

Although this section is mainly concerned with intermodel comparisons, an analytical solution is now given to analyse the one-dimensional heat transfer. The steady heat flux from the external air layer to the internal surface can be calculated from

$$Q_f = UA\Delta T = \left(\frac{1}{1/h_o + W/\lambda}\right)A\Delta T \tag{6.16}$$

where, Q_f is the heat flux, U is the overall heat transfer coefficient, A is the heat transfer area, ΔT is temperature difference between the outside air layer and the internal surface, h_o is the outside convection coefficient, W is the construction thickness and λ is the conductivity of the construction. If the internal surface temperature evaluated by the combined approach is assumed, the one-dimensional heat flux can be calculated by equation (6.16). The result is the same value obtained from the combined approach solution. This demonstrates the accuracy of the combined approach results when handling the conjugate one-dimensional heat conduction and heat convection.

The two-dimensional turbulent steady case is now considered. The flow within the cavity of Figure 6.7a was examined, invoking the $k - \varepsilon$ model by *dfs* and PHOENICS. The fluid viscosity and specific heat were reset to the values for air; in this case, the flow is possibly transitional. The $k - \varepsilon$ model was thus invoked. Again, the internal surface temperatures of the vertical walls were made equal to 30^oC and 0^oC respectively, and the top and bottom walls were adiabatic. This situation corresponds to $Ra = 2.8 x 10^{10}$. 40 cells were placed in both directions using a power law distribution with the c coefficient equal to 1.5. In this situation, it was extremely difficult to obtain a converged solution with both CFD programs. Several combinations of under-relaxation factors were used and they were changed as the solution process progressed. The necessary number of iterations is uncertain since the programs were run several times and the variables were initialised with values of the previous run. Figures 6.12 and 6.13 present the final streamlines and isotherms of the problem. Although PHOENICS and *dfs* behave similarly, the boundary layer computed by *dfs* is thinner than the PHOENICS one. This can possibly be attributed to the difference in the wall function models since in PHOENICS a large region is sensitive to the presence of the wall (diffusion effect). Nevertheless, both solutions obey the energy conservation principle: the heat delivered at the hot wall (125W for *dfs* and 120W for PHOENICS) is convected to the cold wall. The results presented by Ben Yedder and Bilgen (1995) show flow patterns very similar to Figures 6.12 and 6.13 which also help to

legitimise the *dfs* and PHOENICS predictions.

Comparing the turbulent results with their laminar counterpart, it can be observed that the turbulent boundary layers (near the vertical walls) are thinner, resulting in a high concentration of isotherms close to the vertical walls. This implies that the turbulent heat transfer flux is greater than the laminar one. This conclusion cannot, however, be taken from the comparison of the heat transfer values since the laminar case was computed with a higher conductivity. If the air conductivity is considered in the laminar case, the heat flux is in the order of 10 times smaller than the turbulent heat flux.

Three-dimensional case

This situation is an extension of the two-dimensional laminar case where the two additional surfaces are also adiabatic (see Figure 6.7b). 20 grid cells are distributed in each direction employing the power law equation 4.11 with the power law coefficient equal to 1.5. A comparison between *dfs* and PHOENICS was carried out for such a case and again the results are similar. The heat flux at the hot wall calculated by *dfs* differs 0.8% from the value computed by PHOENICS. The air flow is essentially two-dimensional on the $y - z$ planes since the only surfaces to transfer heat are the vertical surfaces in the $x - z$ planes. However, the main flow at small and large x values is influenced by the presence of the walls. The flow pattern and isotherms on the middle $y - z$ plane are similar to the two-dimensional results of Figures 6.8 and 6.9 and, as expected, the isotherms are normal to the adiabatic surfaces. The difference between the total incoming heat flux and the total heat lost is less than 0.02%.

(a)   (b)
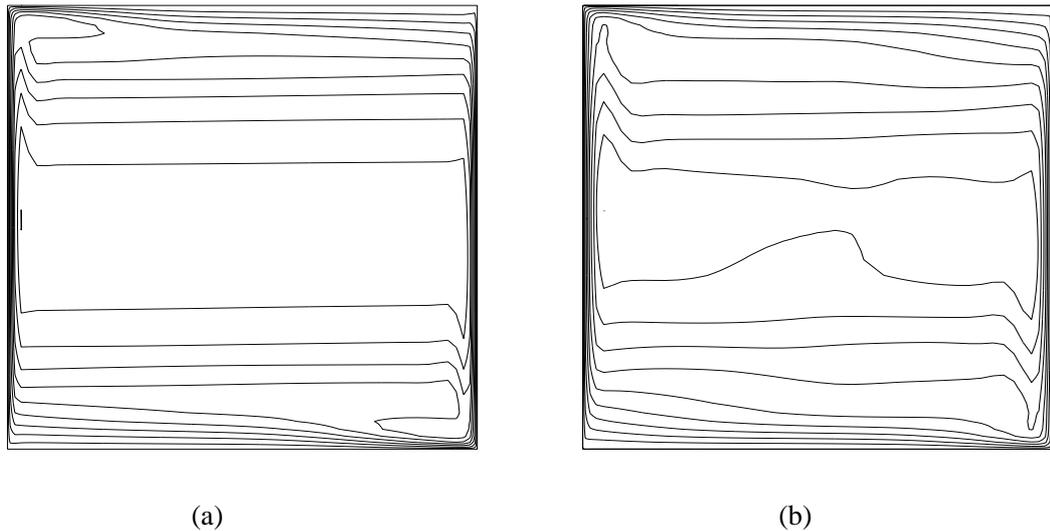
Figure 6.12 Streamlines of the turbulent two-dimensional cavity flow. (a) *dfs* and (b) PHOENICS.

<center>(a)</center> <center>(b)</center>
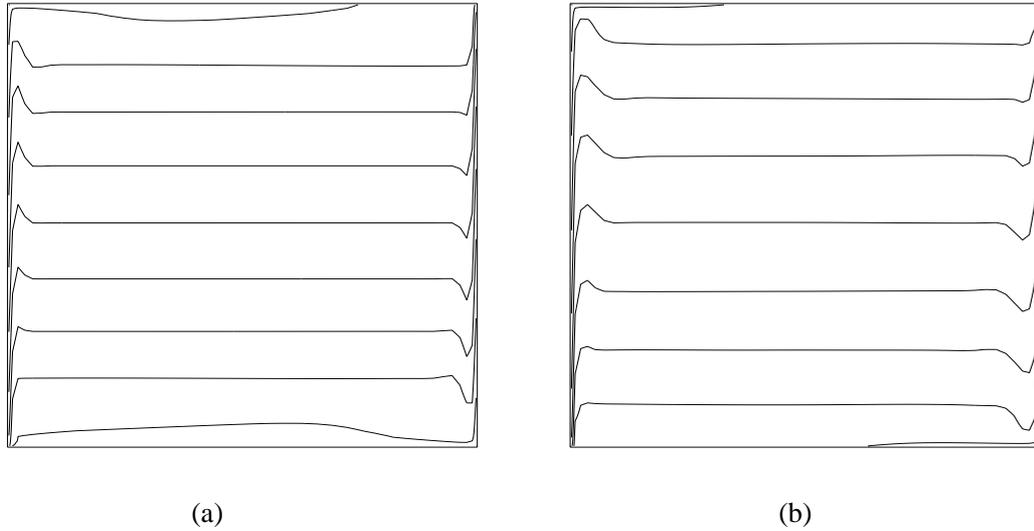
Figure 6.13 Isotherms of the turbulent two-dimensional cavity flow. (a) *dfs* and (b) PHOENICS.

6.3.2 Forced Ventilation

Isothermal case

In this section, a turbulent forced convection situation is examined by four different models, *dfs*, PHOENICS, the nodal network approach and a combination of *dfs* and the nodal network method. Their results are compared. The case under investigation originated from the 2D test case which was adopted by an international research team for the validation of numerical models and was described in the IEA Annex 20 final report (Lemaire 1992). The experiment consisted of a steady two-dimensional isothermal flow within the room of Figure 6.14. The air was supplied from a high-level slot adjacent to the ceiling with a fixed height of 0.168m and an inlet Reynolds number of 5000. A non-uniform grid of 20x20 nodes was placed in the x and y directions respectively. Two and four cells in the y direction were located at the inlet and outlet respectively. Such a grid configuration was adopted in PHOENICS and *dfs* since both handle a similar power law distribution. Momentum was fixed at the inlet in the direction normal to the left hand side vertical wall and pressure was fixed at the outlet cells. The $k - \varepsilon$ model was required and the standard model available in PHOENICS was employed. In *dfs*, linear under relaxation was considered for the momentum equations (under relaxation factor equal to 0.5) and inertia under relaxation was necessary for the turbulent energy and energy dissipation (under relaxation factor equal to 0.1 and 1.0 respectively). In PHOENICS, only inertia type relaxation was used: 10.0 for the momentum equations and 1.0 for the turbulent energy and energy dissipation. The converged solution in both programs was accepted when the sum of the residuals fell below 0.5% of the inlet flow rate or momentum.
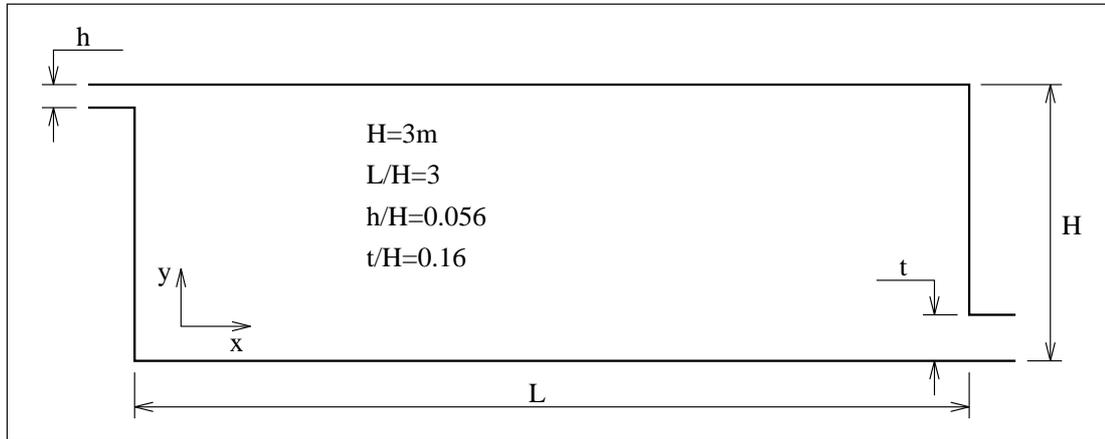
Figure 6.14 Two-dimensional room with forced ventilation.

Firstly, *dfs* and PHOENICS streamlines are compared in Figure 6.15. Both flow patterns show a main stream which takes place close to the top and right hand side vertical walls and also a secondary flow recirculating inside the room. Similar results obtained from different author and programs are presented in the IEA report. However, there are small discrepancies in the magnitude of the velocity vectors as can be observed in Figure 6.16. The intensity of the velocity at the cells close to the top and bottom walls calculated by *dfs* is slightly smaller than its counterpart computed by PHOENICS. This difference causes different momentum diffusion on the main and secondary flows as can be observed on the stream lines. This is possibly due to some differences between the wall function models. Such a difference should be investigated in the future but, of course, its relevance must also be judged.

Recently, Loomans (1995)[#] also tested this example by comparing the results predicted by *dfs* and the measured data. The measurements were obtained by Laser Doppler Anemometry and were taken from Nielsen (1990). Although he used zero velocity gradient at the outlet and prescribed different turbulent kinetic energy and energy dissipation at the inlet, the predictions are similar to those presented in Figures 6.15a and 6.16a. Two grid distributions were used, one with 20x20 cells (similar to the above) and another with 30x20 cells, in order to investigate the grid independence. The predictions and the measurements are reproduced in Figures 6.17 to 6.20. The results are normalised through the inlet velocity U_o. The normalised horizontal mean velocity and the normalised root square velocity (or the turbulence intensity) are shown in two different normalised *x* and *y* positions. Additional to the fact that the predictions agree well with the measurements, *dfs* results are similar to the several predictions presented in the IEA report. Moreover, the small differences between the two predictions indicate that the results obtained with 20x20 cells is already independent from the grid.

The work was the result of a four week visit, by the author, to the Energy Systems Research Unit at the University of Strathclyde.

Loomans concludes that *dfs* is performing well for the prediction of two-dimensional isothermal flow problems.
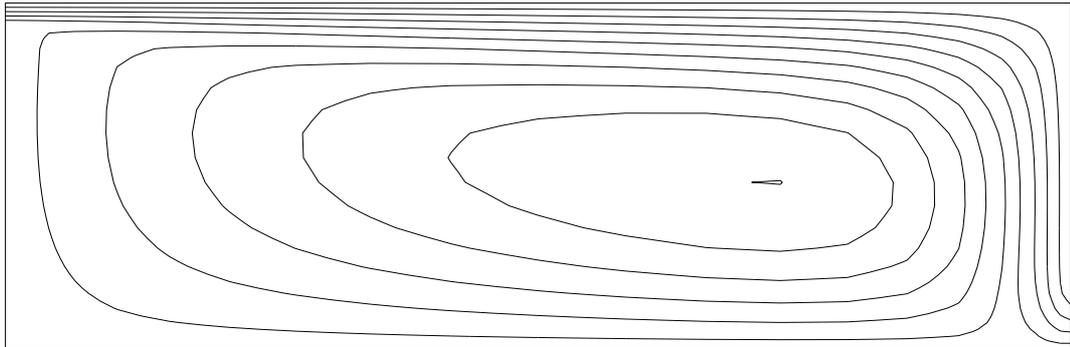
(a)
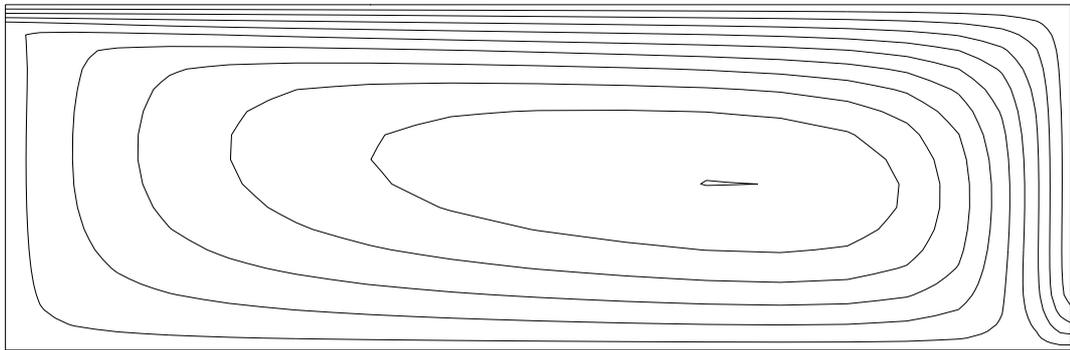
(b)
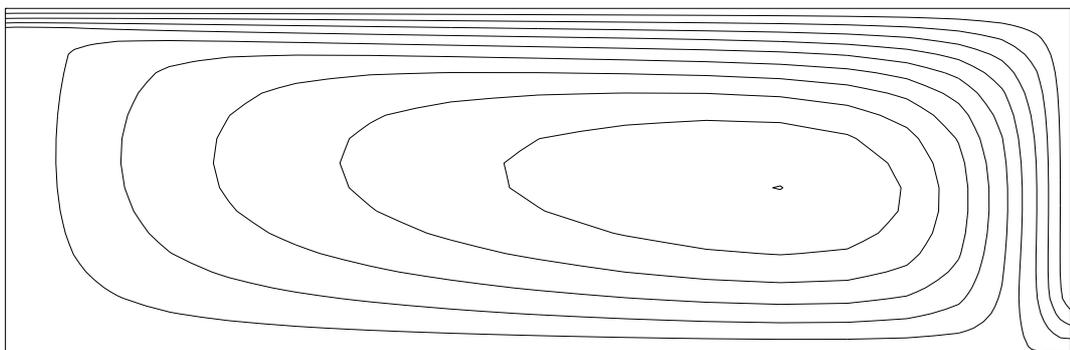
(c)

Figure 6.15 Streamlines inside a two-dimensional ventilated room. (a) *dfs*, (b) PHOENICS and (c) combined approach.
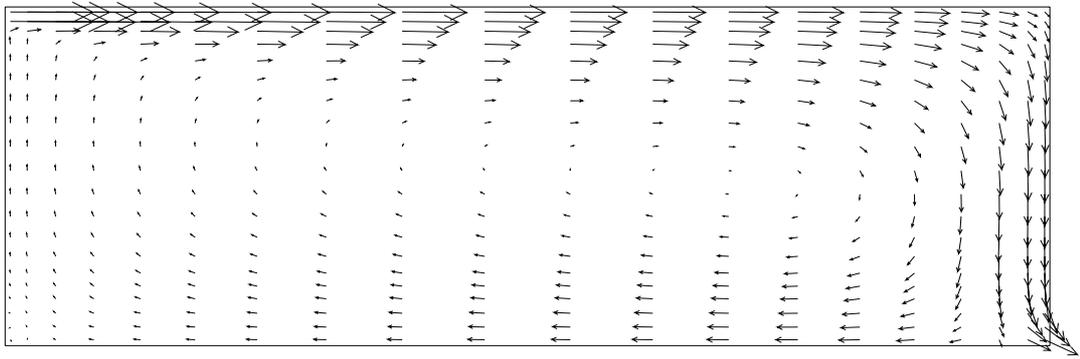
(a)
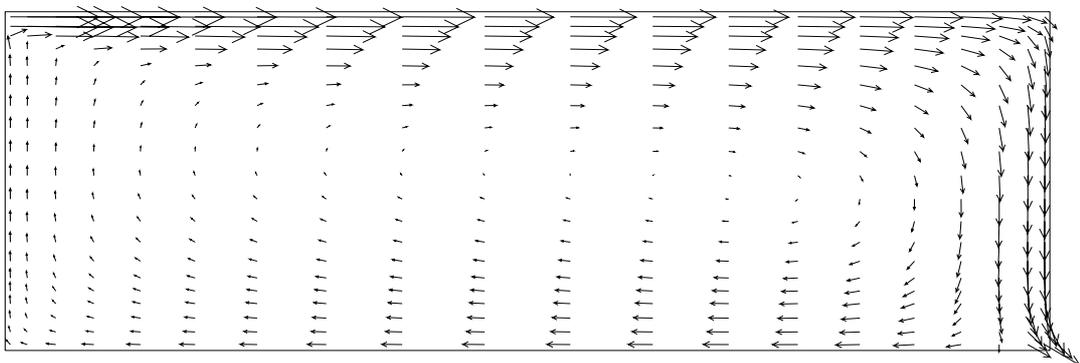
(b)
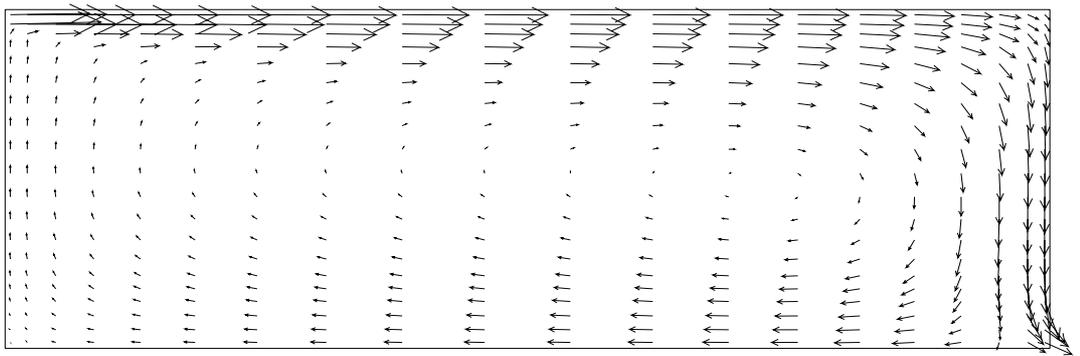
$\longrightarrow$ 0.50m/s

(c)

Figure 6.16 Flow pattern inside a two-dimensional ventilated room. (a) *dfs*, (b) PHOENICS and (c) combined approach.
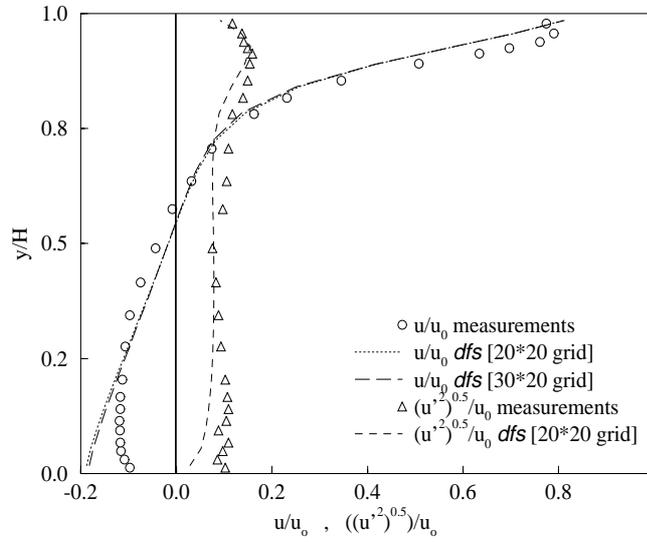
Figure 6.17 Horizontal mean velocity u/u_o and turbulent intensity $\sqrt{u'^2/u_o}$ (from $\sqrt{k} = 1.1\sqrt{u'^2}$) at $x/H = 1$ (Loomans 1995).
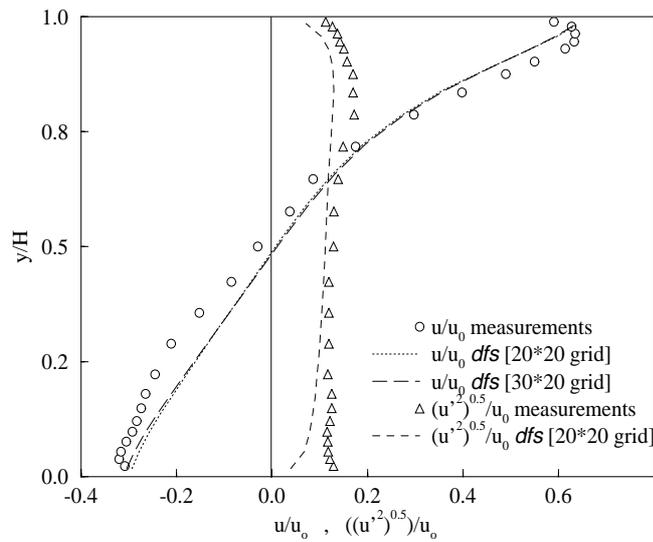
Figure 6.18 Horizontal mean velocity u/u_o and turbulent intensity $\sqrt{u'^2/u_o}$ at $x/H = 2$ (Loomans 1995).
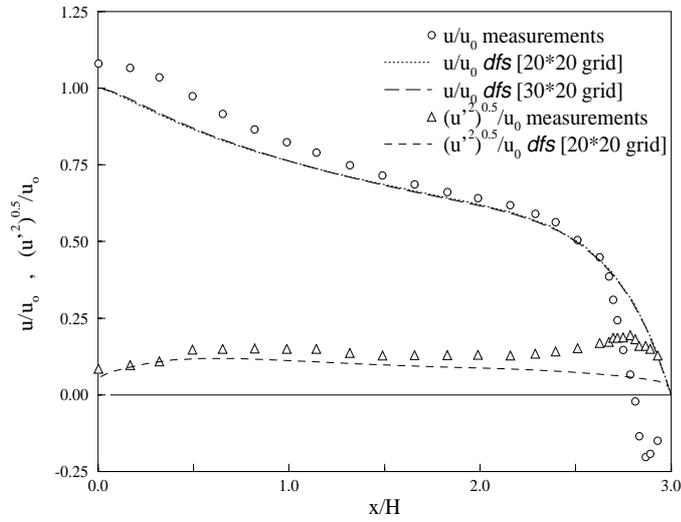
Figure 6.19 Horizontal mean velocity u/u_o and turbulent intensity $\sqrt{u'^2/u_o}$ near the top wall at $y = H - h/2$ (Loomans 1995).
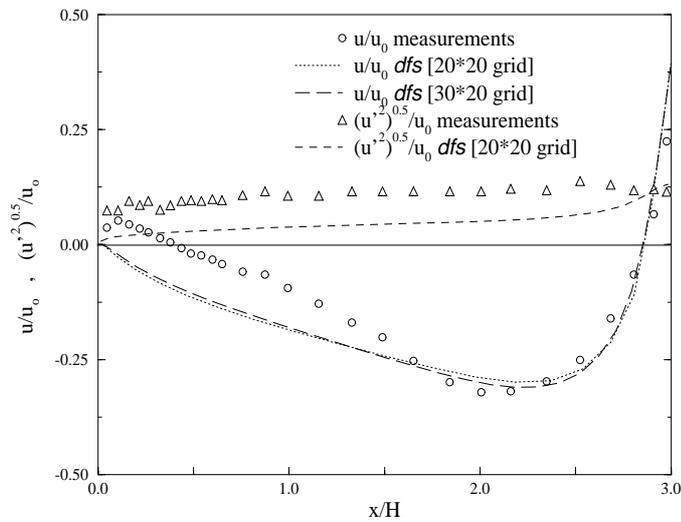
Figure 6.20 Horizontal mean velocity u/u_o and turbulent intensity $\sqrt{u'^2/u_o}$ near the bottom wall at $y = h/2$ (Loomans 1995).

A minimum network of three nodes was also established to characterise the flow of Figure 6.14. The nodes were connected according to the diagram of Figure 6.21a. The node "I" represents the flow pressure before entering the zone and node "O" represents the condition immediately after the flow leaves the zone. The node "Z" denotes the whole pressure field of the zone; stack effect is not considered. The following expression is used to describe the relationship between pressure differences and mass flow at the connections

$$\dot{m} = e\sqrt{\Delta p} \qquad (6.17)$$

where e is the resistance of the opening which is equal to 0.1853185 in the case of the inlet and equal to 0.5294815 in the case of the outlet. The pressures at nodes "I" and "O" were conveniently fixed at 0.2839098Pa and 0.0Pa in order to provide a Reynolds number equal to 5000 at the inlet. The network was then solved and yielded the results of Table 6.3, which corresponds to the above Reynolds number. The summation of the pressure drops at the outlet, and at the inlet, is equal to the total pressure difference. This is another quick check with the network approach.

Additionally, the nodes "I" and "O" were connected to the CFD domain of Figure 6.21b. The two cells at the inlet were linked to the node "I" by means of two connections and the four cells at the outlet to the node "O" by means of four connections. Since parallel flow resistances are equivalent to a single resistance whose coefficient is equal to the summation of the coefficients of the parallel resistances, the above e coefficients was divided by two in the case of the inlet and divided by four in the case of the outlet. The same pressures were then fixed at nodes "I" and "O" to verify the combined approach. For such a configuration, the combined method produced flow rates through the two inlet and four outlet connections as shown in Table 6.3. The results are presented from the top to bottom according to the diagram of Figure 6.21b. As can be seen, the higher flow rate takes place near the solid surface (top and bottom) where the higher pressure gradients occur. The total flow rate through the inlet and outlet are the summation of the flow rates through the individual connections. This flow rate is slightly smaller than the network only method. Such small differences are attributed to the modest pressure drop inside the room (the higher pressure drop inside the room is not larger than 5×10^{-2}Pa) which is considerably smaller than the total pressure drop. To understand this, the *dfs* domain can be thought of as an additional resistance included in the mass flow network, which in this case has a small influence on the incoming flow. Such a conclusion could have been made previously, considering the zone and opening dimensions and also the almost homogeneous pressure field yielded by the *dfs* only results.

The agreement between the two methods demonstrates the good performance of the network only approach for such applications. However, the same result would be produced from the network approach for a different zone configuration. If, for example, the opening areas are placed on different

surfaces, the same mass flow would be calculated. Besides, the combined method provides additional information regarding the internal zone flow which cannot be obtained from the network approach. Figure 6.15c and 6.16c shows the flow pattern computed by the combined approach. This is much the same as the *dfs* only pattern since the boundary conditions to the zone domain (inlet momentum and outlet pressure) are very similar.

(a)

(b)
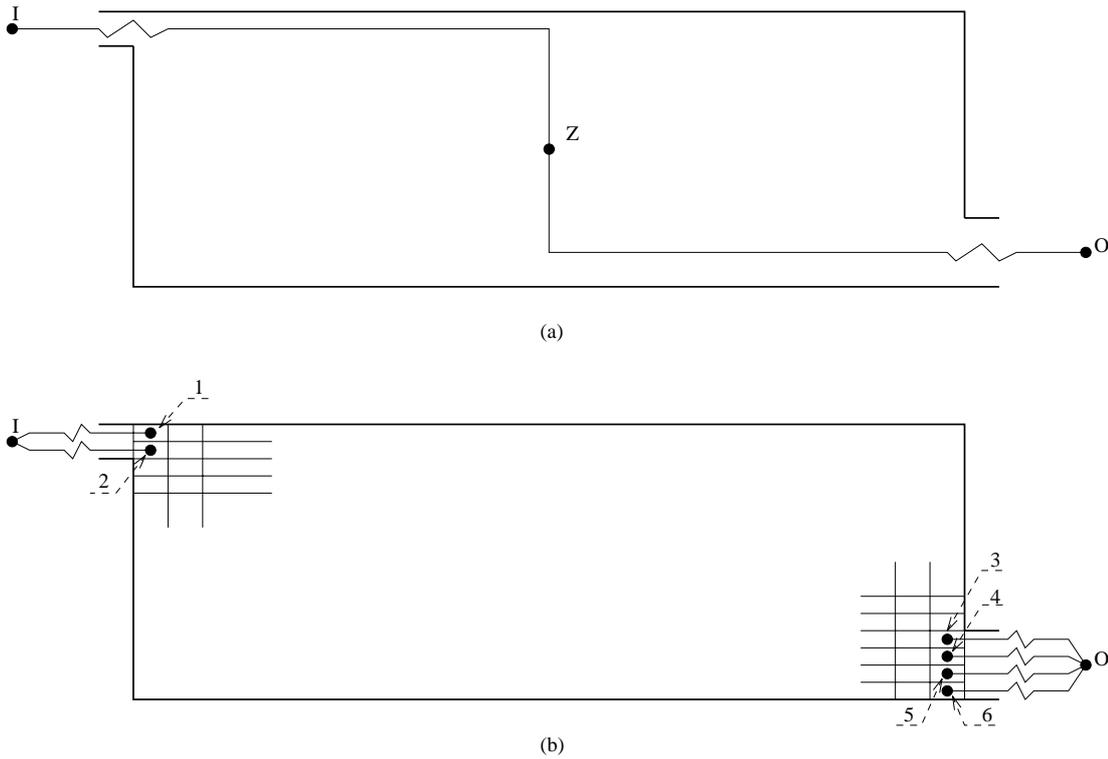
Figure 6.21 (a) Network and (b) combined approach diagrams of the flow domain of Figure 6.14.

Table 6.3 Mass flow and pressure differences through the zone openings.

	Network approach			Combined method		
	ΔP (Pa)	$\dot{m}$ (kg/s)		ΔP (Pa)	$\dot{m}$ (kg/s)	Total mass flow (kg/s)
inlet	2.5293×10^{-1}	9.3200×10^{-2}	1	2.5323×10^{-1}	4.6628×10^{-2}	9.2932×10^{-2}
			2	2.4972×10^{-1}	4.6304×10^{-2}	
outlet	3.0983×10^{-2}	9.3200×10^{-2}	3	2.1391×10^{-2}	1.9360×10^{-2}	9.2931×10^{-2}
			4	2.9930×10^{-2}	2.2901×10^{-2}	
			5	3.3937×10^{-2}	2.4385×10^{-2}	
			6	3.9429×10^{-2}	2.6285×10^{-2}	

Non-isothermal case

Loomans (1995) also investigated the case above for a non-isothermal situation using *dfs*. This case was also part of the Annex 20 work, but no measurements are available.

In order to account for the buoyancy effect, cold air was introduced through the inlet opening at the same flow rate. A heat flux was imposed at the floor and the other surfaces were made adiabatic. Situations with different Archimedes numbers were tested to identify the critical Archimedes number. The critical value represents the situation where the jet penetration depth does not correspond to the room length. The Archimedes number is defined as

$$Ar = \frac{g \Delta T h}{T u_{in}^2} \tag{6.18}$$

where g is the gravitational acceleration (m/s^2), u_{in} is the inlet velocity m/s, T is the temperature level (K) and ΔT is the temperature difference between exhaust and inlet (^oC).

Loomans reports that his results are qualitatively comparable with Chen's results which are presented in the Annex 20 report. He concludes that the critical Archimedes number lies between 0.12 and 0.14 which is also similar to the value found by Chen.

6.4 EMPIRICAL VALIDATION

Empirical validation is always necessary to substantiate model predictions as it is the most obvious technique for establishing a 'truth' model, although it is the most difficult to accomplish. The collaborative validation exercise conducted by the International Energy Agency (IEA) to assess the performance of building simulation programs (Lomas *et al* 1994a) is an example. This conducted a comprehensive exercise involving 25 result sets from 17 genuinely different programs. The work consisted of both empirical and inter-model validations and, as reported, there was a considerable difference among the predictions. Also, few model predictions lay within the error bands for all measured data. The internal heat transfer coefficient was identified as one major source of result uncertainty. In Appendix F11 of the IEA Final Report, a sensitivity analysis of different approaches to estimate the internal convection coefficient was presented and it was shown that the predicted energy consumption was markedly affected by such a parameter. The empirical validation work under the PASSYS programme (Jensen 1994) also indicated the choice of convection coefficients as a main source of discrepancy.

Within this section, the IEA study is adopted as a reference model in order to evaluate the combined approach predictions. Also, the impact of the combined approach on the evaluation of convection coefficients and consequently on the room air temperature is investigated. The *bps* results, which are computed employing the Alamdari and Hammond convection correlations for buoyancy driven flow (Alamdari and Hammond 1983), are compared with the combined thermal coupling results.

The test site comprising eight semi-detached rooms with roof spaces is located on the edge of Cranfield airfield in Bedfordshire, approximately 70km northwest of London. The experiments were conducted in only three rooms operating in a heating condition in October and in a free floating condition in May. The windows of the test rooms had three different configurations: opaque, single glazed and double glazed. The test rooms, whose geometry is shown in Figure 6.22, were very tightly sealed and therefore infiltration was assumed to be zero. The tests were conducted over a 10 day period. However, the first three days were considered as a simulation start-up period in order to lessen the effects of initial conditions. The complete geometric and operational information of the test site is provided by Lomas *et al* (1994b).
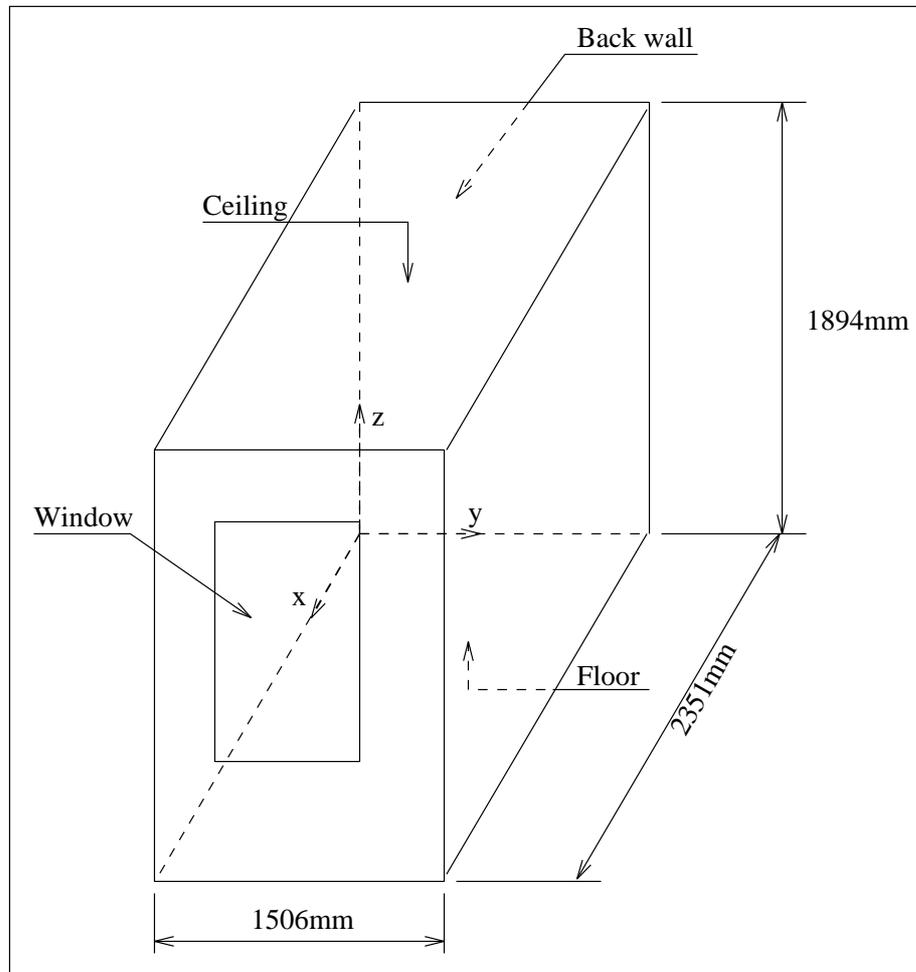
Figure 6.22 IEA test room geometry.

In the present work, only the double glazing, unheated case was tested. A grid composed of 35x23x32 (25760) cells was non-uniformly distributed within the test room. Since the combined method is very time consuming, the *bps* standard algorithm was employed during the start-up period

and only a one day simulation is performed using the combined approach. For the same reason, only the simultaneous scheme was tested since over 168 hours were necessary to solve the problem on a Sun Sparc 10 workstation. Instead of establishing a convergence criterion, the maximum number of iterations was made equal to 1000. The purpose was to allow the simulation to proceed every time-step independent of whether the convergence had been reached or not. The level of residuals reached every time-step were reasonably low although the results were not totally converged; some oscillations of the monitoring values remained.

The air temperature computed by the combined approach, as expected, is not uniform, but its variation (the difference between the highest and lowest temperature within the room) is never higher than 1^oC. For instance, the air temperature distribution in two vertical planes at 12:00 can be seen in Figure 6.23. The air temperature is almost uniform in the zone centre region whereas the higher gradients occurs closer to the walls.

In the IEA exercise, air temperature is measured in three different positions (classified as top, middle and bottom). These values do not differ much from each other, indicating that air temperature is uniformly distributed in the core region of the test room which agrees with the combined method predictions. This suggests that a uniform approach, like the *bps* standard technique, can be reasonably applied to this situation. A comparison of measured and predicted air temperatures is shown in Figure 6.24. The measured value is considered in the middle of the test room. In order to compare with the experimental values, the predicted air temperature is considered at the position (1061mm, 699mm, 1069mm). As can be seen, the combined approach shows better agreement with the measurements than *bps* standard results. In the first few hours, it is even closer to the experimental results than the standard technique curve.

Figures 6.25, 6.26 and 6.27 show comparisons of the three methods for surface temperatures. In all three cases, the dynamic behaviour of the combined method is similar to the other two. Observing the extreme points, it can be seen that near the minimum value, that both the standard result and combined result are close to the measured data. Although the result of the combined approach is closer to the measurements than the standard *bps* result in the neighbourhood of the maximum value, discrepancies in the order of 2.0^oC are observed. These discrepancies can be attributed to the calculation of solar radiation since this has great impact on temperatures at this time of the day. A comparison of *bps* standard approach using two different solar models (Klucher[#] and Perez models) was carried out. It was observed that the *bps* standard approach is sensitive to the solar model. Also, it should be noted that the measured floor temperature shows a tendency toward a high maximum value and suddenly at 13:00 this tendency changes to a lower maximum temperature. This non-continuous characteristic gives an indication of problems with the measurements.

––––––––––––––––––

[#] Klucher model current default model within *bps*.

(a)

(b)

Figure 6.23 Temperature distribution within the test room at 12:00. (a) x=1061mm (b) y=699mm.
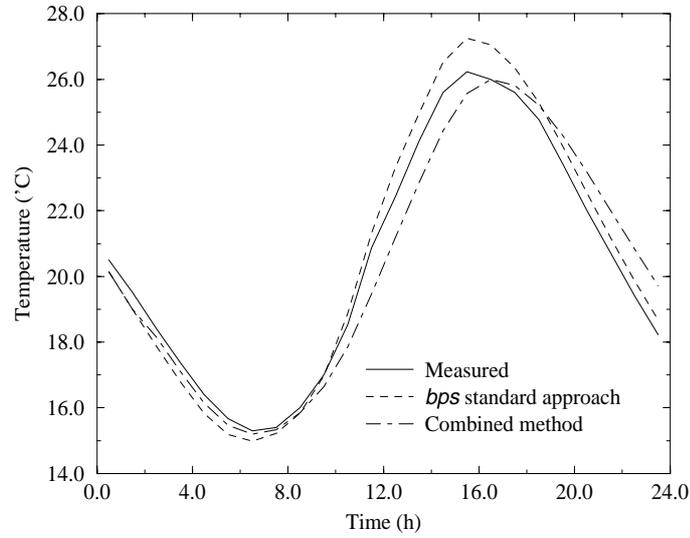
Figure 6.24 Air temperature of the test room.
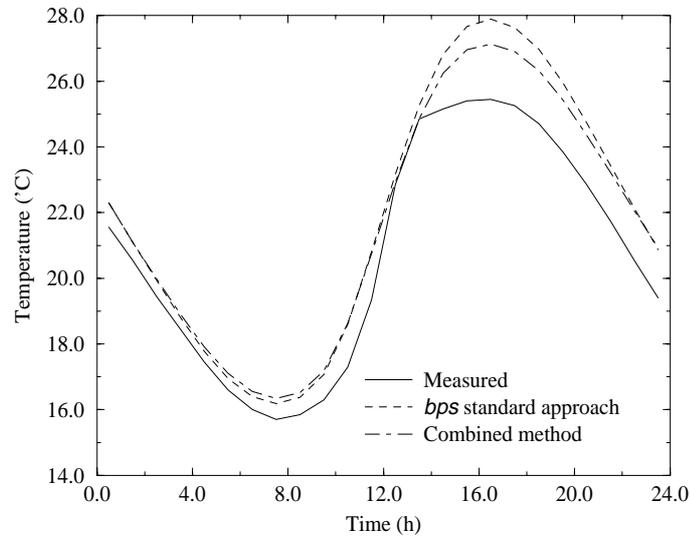
Figure 6.25 Internal surface temperature of the floor.

Predictions of internal convection heat fluxes are presented in Figures 6.28 to 6.31[*]. It can be seen that at the floor and at the window, both predictions behave similarly. Although the two approaches show different behaviour for the calculated fluxes at the other surfaces, the values have the same order of magnitude. If the window flux is not considered, it can be noticed that the combined

_____

    [*] Measured convection heat fluxes are not available.

approach predicts lower heat fluxes near 12:00 and higher fluxes at the other hours. This behaviour corresponds to the surface temperatures (Figures 6.25 to 6.27), where the combined method computes lower temperatures close to the maximum value and higher temperatures near the minimum value. Of course, temperature and fluxes are shifted but that is probably because of the heat storage.
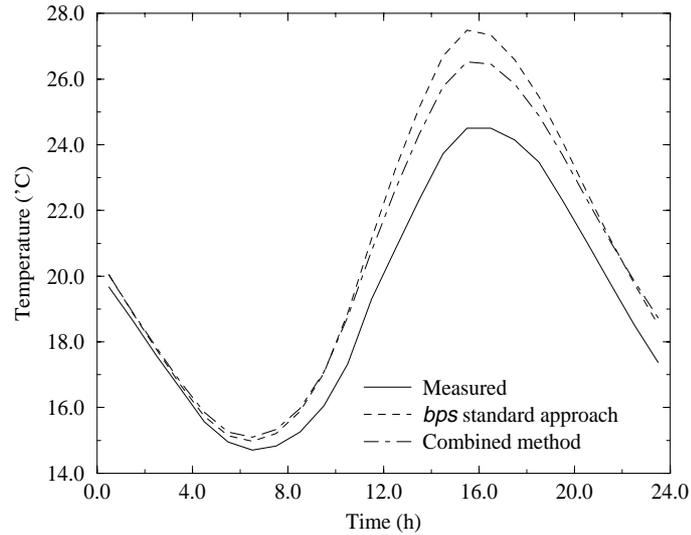
Figure 6.26 Internal surface temperature of the back wall.
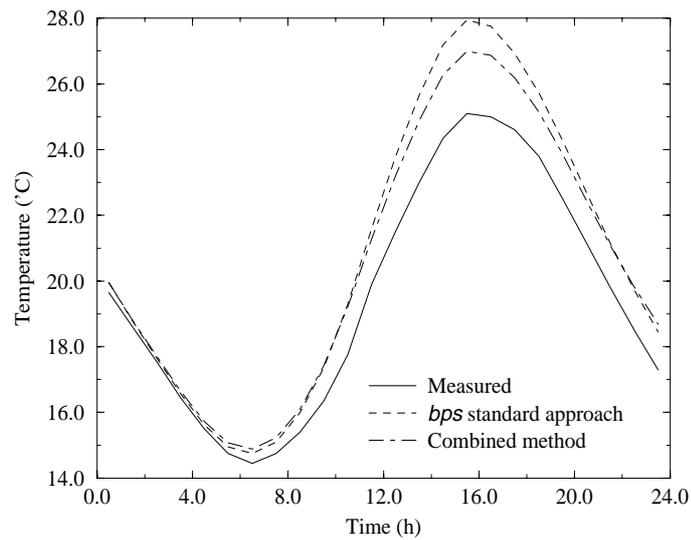
Figure 6.27 Internal surface temperature of the ceiling.
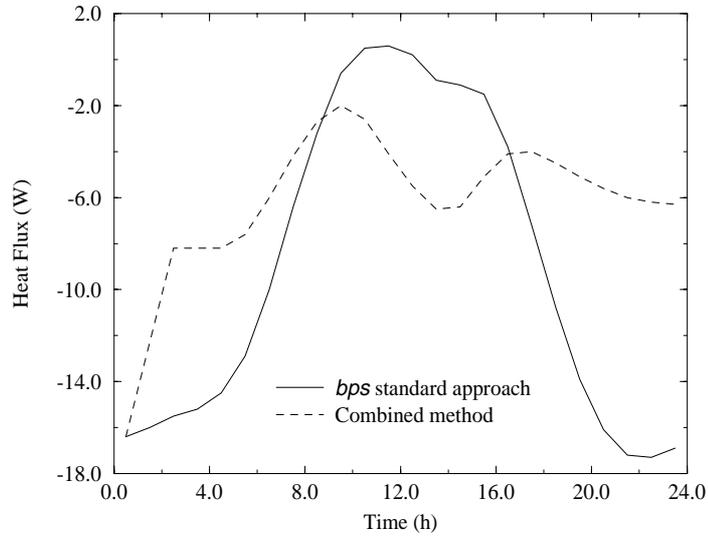
Figure 6.28 Internal convection heat flux at the floor.
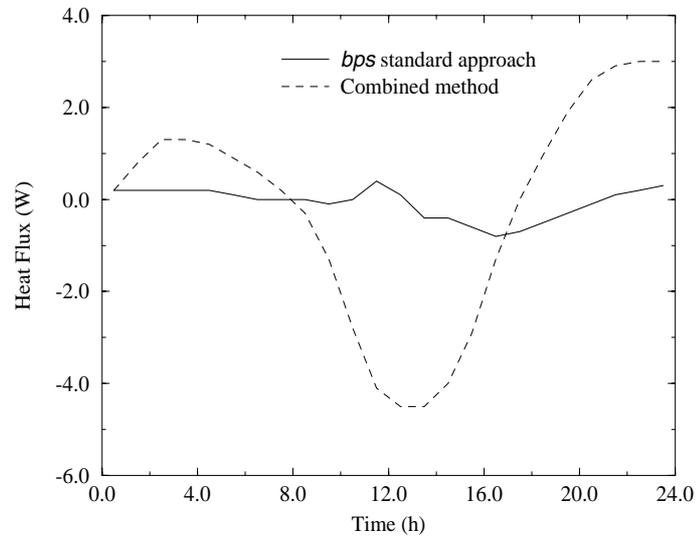
Figure 6.29 Internal convection heat flux at the back wall.
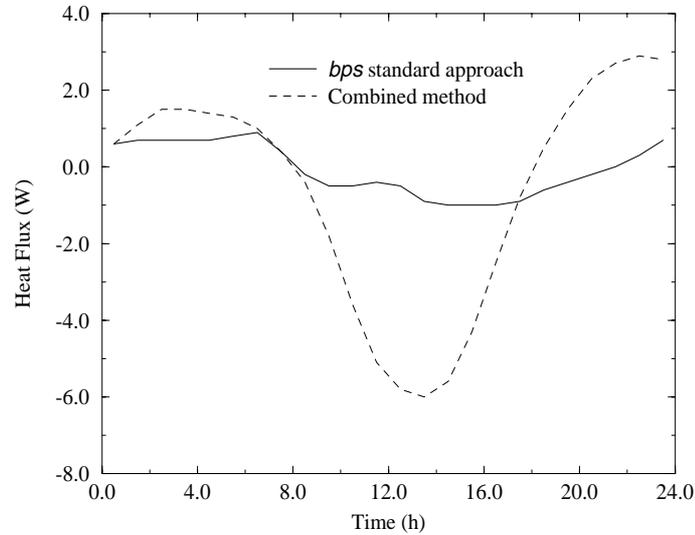
Figure 6.30 Internal convection heat flux at the ceiling.
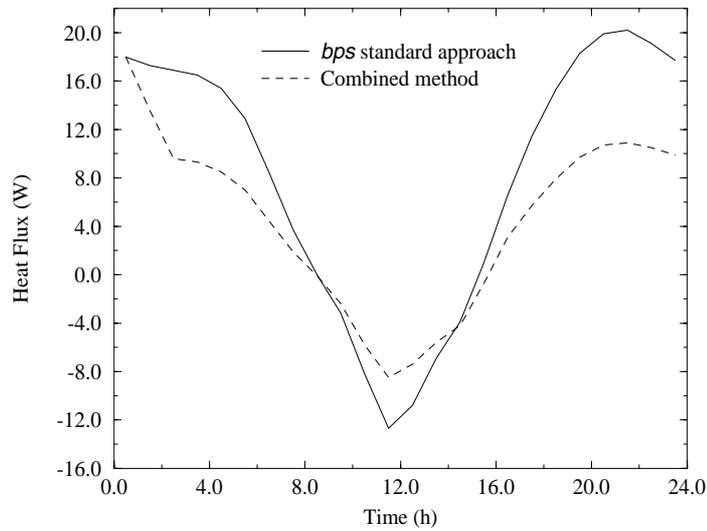
Figure 6.31 Internal convection heat flux at the window.

A comparison of the convection coefficients computed by the *bps* standard approach and by the combined technique is now presented. The combined convection coefficients are computed based on the difference of surface and air temperatures (air temperature computed at 1061mm, 699mm, 1069mm). It can be seen from Figures 6.32, 6.33 and 6.34 that there is a certain discrepancy between the two methods but their orders of magnitude are comparable. The variation of the convection coefficients computed by the combined approach is usually smaller than that calculated by the

www.manaraa.com

standard technique.

The basic difference between the combined and *bps* standard approaches lies on the evaluation of the convection heat transfer. If the convection coefficients generated by the combined approach are used in the *bps* standard approach, the performance of the *bps* standard approach within the IEA exercise is expected to be improved, as the combined approach results are closer to the measurement than the *bps* standard results.

6.5 CONCLUSION AND FUTURE WORK

The validation work undertaken showed the potential of *dfs* and the combined approach to predict the indoor air flow and helped to increase confidence in the approach. The results obtained are comparable with those from other methods or programs. However, some discrepancies have been identified and their causes should be investigated in the future. For example, the discrepancies between PHOENICS and *dfs* turbulent results are possibly caused by the different turbulence models.

The combined approach show certain improvement in relation to the *bps* standard approach when compared with the measurements from the IEA exercise. However, some discrepancies still exist which can be attributed to measurements fault or the solar model. Other investigations should be devised in order to consolidate the method: for instance, the heating situation presented in the IEA report.
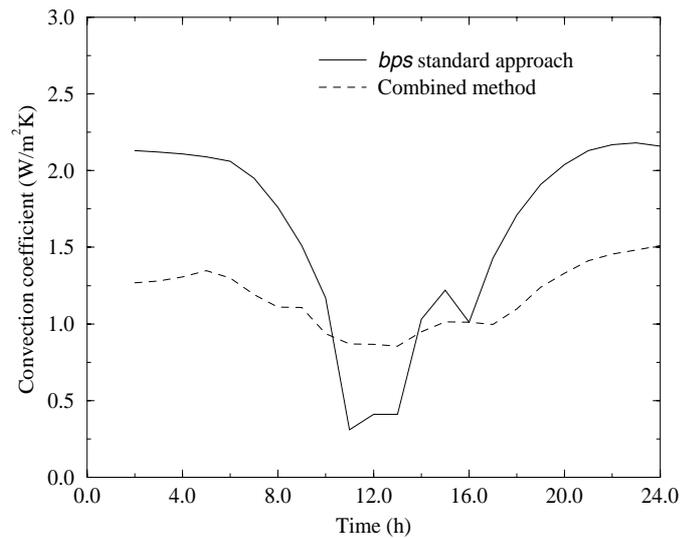
Figure 6.32 Inside surface convection coefficient at the floor.
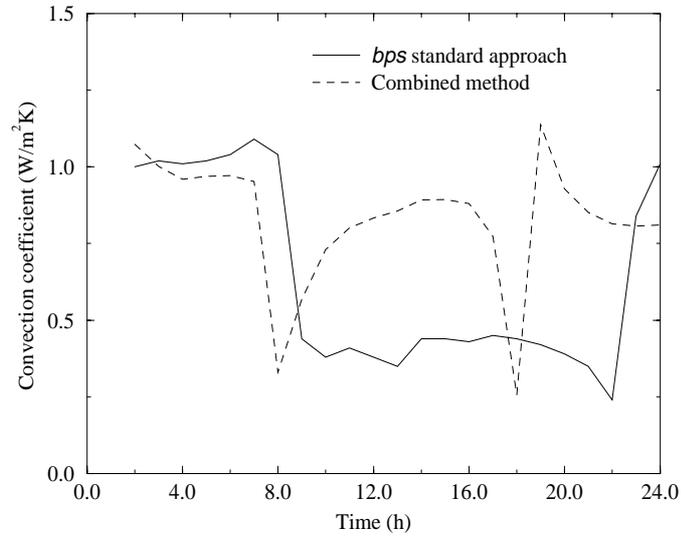
Figure 6.33 Inside surface convection coefficient at the ceiling.
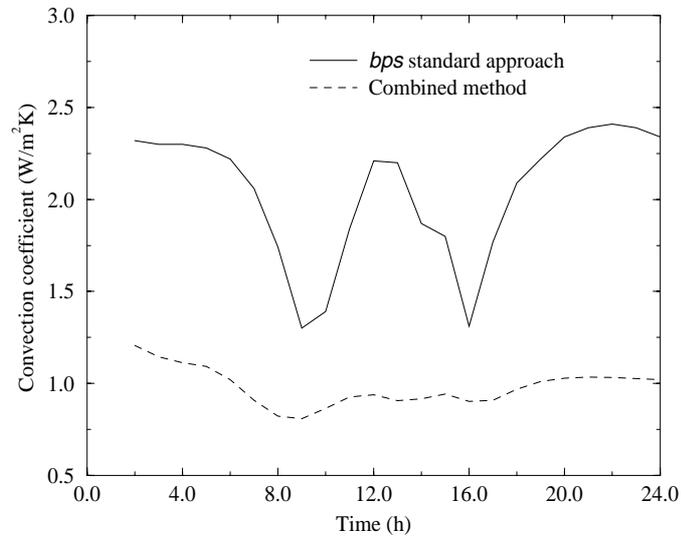
Figure 6.34 Inside surface convection coefficient at the window.

REFERENCES

Alamdari, F. and Hammond, G. P., 1983, Improved Data Correlation for Buoyancy-Driven Convection in Rooms, *Rep. SME/J/83/01*, Cranfield Institute of Technology, Applied Energy Group, Cranfield.

Arpaci, V. S. and Larsen, P. S., 1984, *Convection Heat Transfer*, Prentice Hall.

Bejan, A., 1984, *Convection Heat Transfer*, John Wiley & Sons.

Ben Yedder, R. and Bilgen, E., 1995, Turbulent Natural Convection in Enclosures Bounded by a Massive Wall, *Inter. J. Heat Mass Transfer*, Vol 38, No. 10, pp. 1879-1891.

Clarke, J. A., 1985, *Energy Simulation in Building Design*, Adam Hilger Ltd, Bristol, UK.

Clarke, J. A., Dempster, W. M. and Negrão, C. O. R., 1995a, The implementation of a Computational Fluid Dynamics Algorithm within the ESP-r System, *Proc. of Building Simulation 95*, Madson, Wisconsin.

Clarke, J. A., Hensen, J. L. M. and Negrão, C. O. R., 1995b, Predicting Indoor Air Flow by Combining Network Approach, CFD and Thermal Simulation, *Proc. of 16th AIVC Conference 95*, Palm Springs CA, (to be published).

Hensen, J. L. M., 1991, *On the Thermal Interaction of Building Structure and Heating and Ventilation System*, PhD thesis, Technische Universiteit, Eindhoven.

Jensen, S. O. (ed), 1994, *Validation of Building Energy Simulation Programs*, Part I and II, Research Report PASSYS Subgroup Model Validation and Development, Commission of the European Communities, Directorate General XII for Science, Research and Development, Brussels, EUR 15115 EN.

Judkoff, R., Wortman D., O'Doherty B. and Burch, J., 1983, *A Methodology for Validating Building Energy Analysis Simulations*, SERI/TR-254-1508, Solar Energy Research Institute, Golden, CO.

Lemaire, A.D. et.al., 1992, *Room Air and Contaminant Flow, Evaluation of Computational Methods*, IEA Annex 20, Subtask-1 Summary Report, Delf.

Lomas, K., J., Eppel, H., Martin, C. and Bloomfield, D., 1994a, *Empirical Validation of Thermal Building Simulation Programs Using Test Room Data*, Volume 1: Final Report, IEA Annex 21.

Lomas, K., J., Martin, C., Eppel, H., Watson, M. and Bloomfield, D., 1994b, *Empirical Validation of Thermal Building Simulation Programs Using Test Room Data*, Volume 2: Empirical Validation Package, IEA Annex 21.

Loomans, M. G. L. C., 1995, Comments on and Simulations with the Domain Flow Solver, a CFD Program Implemented in the ESP-r Building Simulation Environment, FAGO-report 95.45.W, Eindhoven University of Technology, Eindhoven.

Negrão, C. O. R., 1993, *A Proposal to Conjoin Building Thermal Simulation and Computational Fluid Dynamics*, PhD Progress Report, University of Strathclyde, Glasgow.

Negrão, C. O. R., 1994a, *Combining Mass Flow Network and CFD Approaches*, PhD Progress Report, University of Strathclyde, Glasgow.

Negrão, C. O. R., 1994b, *A Possibility of Conflating Building Thermal Simulation and Computational Fluid Dynamics*, PhD Progress Report, University of Strathclyde, Glasgow.

Nielsen, P.V., 1990, *Specification of a two-dimensional test case*, IEA Annex 20, Research item 1.45, Technical Report, University of Aalborg, Aalborg.

Rosten, H. I. and Spalding, D B, 1987, The PHOENICS Beginner's Guide, CHAM Report Number TR/100.

Schlichting, H., 1979, *Boundary Layer Theory*, McGraw-Hill.

Elsen, J. t., 1994, *Development of a Optimisation Design Tool Using the CFD code TEACH*, ERASMUS Student Exchange Programme.

Van der Laan, M. J., 1994, *A Model for Combined Heat and Vapor Transfer in Building Construction*, PhD Progress Report, Technische Universiteit, Eindhoven.

7.1 INTRODUCTION

In this chapter, the capabilities of the combined methodology are introduced by means of examples. The purpose is to demonstrate the potential of analysis of the developed methodology. Not only are the results for the combined *bps/dfs* method shown, but comparisons with each tool in stand-alone mode are also made. Considering the combined technique as standard, the individual tools will be judged by the extent to which they can be used separately. Firstly, a three zone problem, in which one room is ventilated by displacement, is analysed. Secondly, a small building, in which a large room is heated by a radiator, is studied. And finally, a mixing ventilation system is modelled.

These three problems cover a range of different types of air flows encountered within buildings and also demonstrate the applicability of the thermal and momentum coupling methods separately. In the first two examples, the functionality of the combined approach regarding the thermal coupling is shown. In the last example, the operation of the conflation of the flow network and the CFD technique is analysed.

All the situations in this chapter were subjected to the annual weather data as collected in 1967 at Kew, latitude 52^oN, and longitude 0°.

7.2 DISPLACEMENT VENTILATION SYSTEM

The insulation of buildings has greatly increased in recent years and therefore the heat to be extracted (cooling systems) from the indoor environment is smaller. From the viewpoint of energy savings, it is more economical to reduce the amount of air supplied rather than the air temperature differences between the inlet and outlet condition. As a consequence, the indoor air becomes more polluted and a non-uniform temperature distribution is produced. Displacement ventilation, which is an attempt to remove more efficiently the indoor pollutants, has been developed and is becoming widely used in Scandinavian countries (Davidson 1989, Chen and Van der Kooi 1990). The system consists of supplying cool air (at a low velocity) into a room through a large opening (often via distributed nozzle injection) at the floor level. The cool air is heated by a source of heat within the room and a plume is formed above the heat source due to buoyancy (see Figure 7.1). At a certain z-level, the flow in the plume is equal to the total ventilation flow (above this level the flow is higher and below it is smaller). Consequently, two zones are created: a lower zone with clean cool air and an

upper zone with recirculation, contaminated, heated air.

Level where the flow is equal
to the total ventilation flow
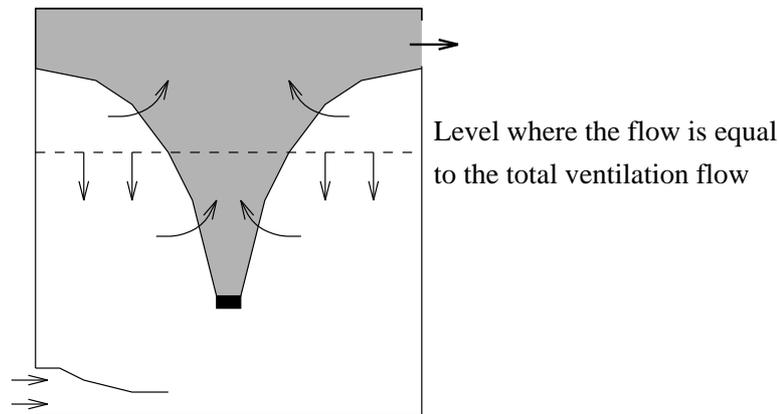
Figure 7.1 Principle of displacement ventilation system.

The problem to be analysed comprises three zones as shown in Figure 7.2. The "roof_space" is sealed but is subjected to 800W of sensible casual gains. An infiltration rate of 0.3 air changes per hour is entering the "reception". The "reception" is also subjected to 1590W of sensible heat (due to occupancy, lighting and equipment) from 8:00 to 17:00 and to 800W (due to equipment) during the whole day. The "office" is ventilated by displacement at a constant flow rate of 2 air changes per hour. Cool air at 13°C is supplied to the "office" at the slot near the floor. A constant convective heat source of 250W is located at the centre of the "office" ($0.697x0.294x0.528m^3$). A grid of 10x20x20 (4000) cells is employed with one, two and five cells used to represent the heat source in the x, y and z directions respectively. The number of cells defined in y and z directions are larger because the flow is mainly two-dimensional in these directions.

Initially, the whole building is simulated using the *bps* standard approach[#]. A control schedule is applied to the "reception" to maintain the air temperature controlled at 25°C during the working hours (08:00h to 17:00h). No control conditions is imposed on the "office" and the air temperature is allowed to fluctuate over the simulation period. The simulation was performed during a spring day (6th of June) employing a one hour time-step. A three-day start-up period was necessary to eliminate the effects of the initial conditions. The computed air temperature within the "office" and the "reception" over the 24h period is presented in Figure 7.4. Note that the air temperature variation within the "office" is not larger than 1.2^{o}C during the simulation period. On the other hand, the air temperature inside the "reception" is held constant during the working hours, as previously specified. Figure 7.4 also shows the heat flux injected to the "reception" which is necessary to maintain the air

It should be noticed that the heat source and the inlet positions cannot be spatially placed when using the standard approach.

temperature at 25°C.
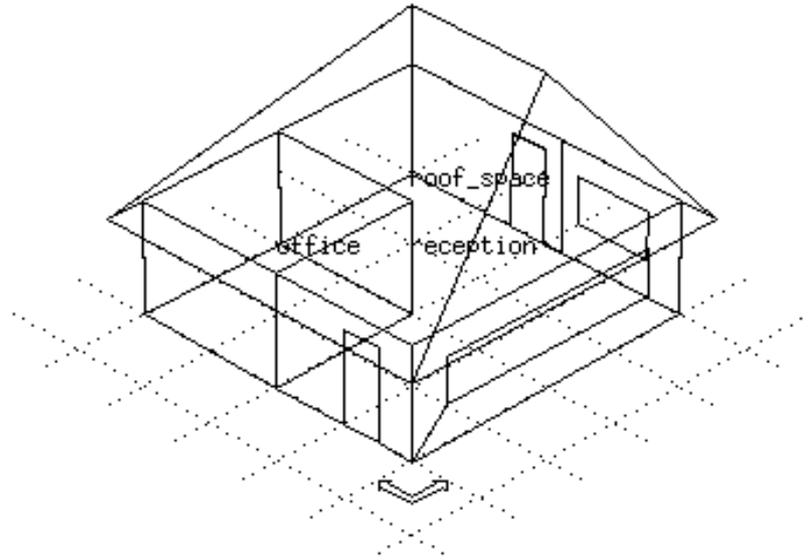
Figure 7.2 Small building with displacement ventilation.
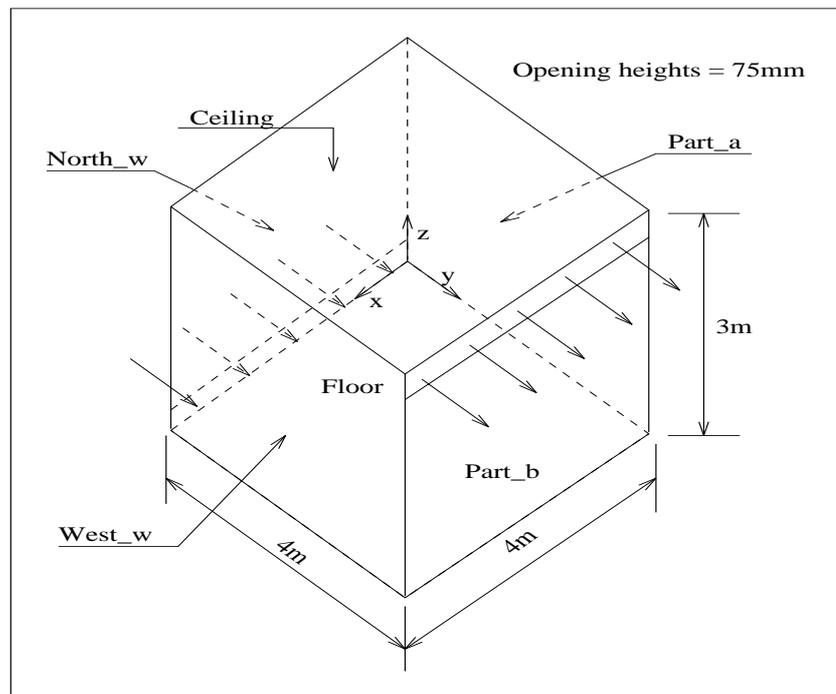
Figure 7.3 Geometry of the "office" of Figure 7.2.
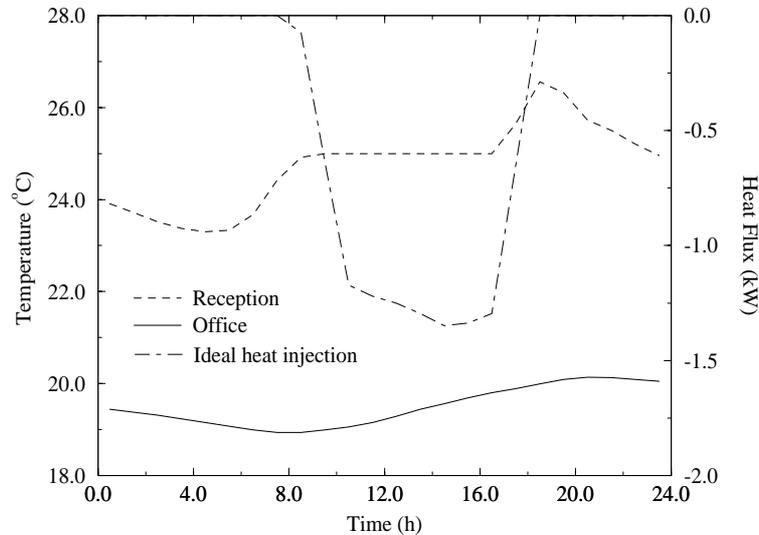
Figure 7.4 Air temperature within the "office" and "reception" and the ideal heat injected to the "reception" as evaluated by the *bps* standard approach.

The surface temperatures evaluated by the standard approach at a specific time (12:00) are now fed into *dfs* to model the "office" separately from the whole building. A steady simulation is then carried out and the temperature and velocity fields are produced (see Figure 7.5). As can be seen from Figure 7.5a, the air temperature within the "office" is not uniform as suggested by the results of Figure 7.4. However, at the occupied level (2.0m x 1.0m x 1.5m), the air temperature is in the order of 17.7^{o}C which differs 1.6^{o}C from the uniform temperature (19.3^{o}C) of the standard approach. Such a difference can significantly influence the room comfort level. Additionally, the *dfs* results produce the velocity distribution within the "office" which together with temperature distribution can define local comfort conditions.

Finally, the *simultaneous*, combined scheme (momentum coupling is not required in this case) is invoked to solve the flow problem within the "office" during four time-steps (at 10:00, 11:00, 12:00 and 13:00). In the remaining hours and over the three-day start-up period, the standard *bps* approach is used[*]. The standard approach is also employed in the other zones over the whole simulation. The air temperature and velocity distributions at 12:00 calculated by the combined approach are only slightly different from the steady state results computed by *dfs* alone, as can be seen from Figure 7.6. Additionally, the surface temperatures calculated at 12:00 are similar to their counterparts computed by *bps* standard approach, as can be observed in Table 7.1[#]. This indicates that the results of the simultaneous combined approach are comparable to the *dfs* results when the latter is assessed with the

---

[*] Note that *bps* allows the various approaches to be mixed and matched to the problem in hand.

[#] Surface temperatures are the only parameters which affects the convective flow computed by *dfs*.

boundary conditions supplied by the *bps* standard approach.

(a)

> 0.25 m/s

(b)
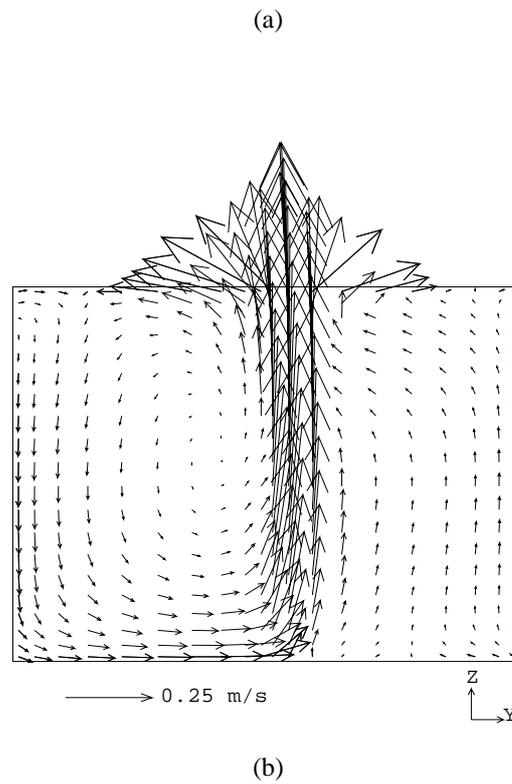
Figure 7.5 (a) Air temperature and (b) velocity fields within the "office" evaluated by *dfs* at 12:00 (x = 2m) based on *bps* supplied boundary conditions.

(a)

(b)
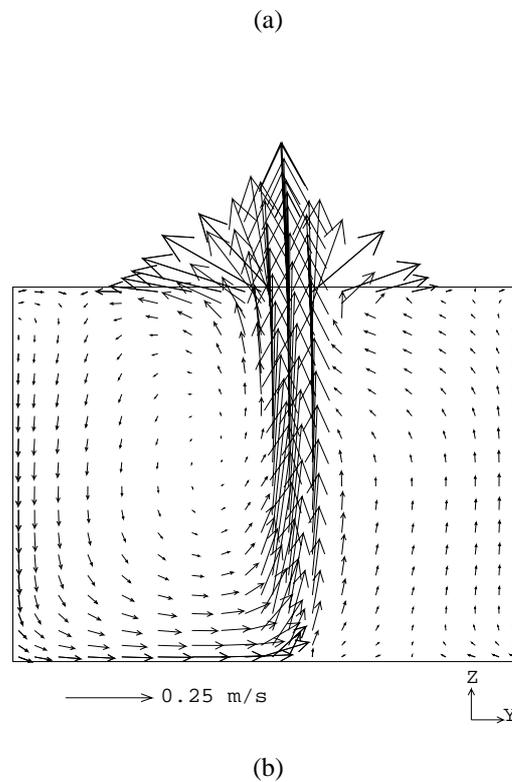
Figure 7.6 (a) Air temperature and (b) velocity fields within the "office" evaluated by the combined approach at 12:00 (x = 2m).

Figure 7.7 shows a comparison of the air temperature inside the "office" computed by the combined approach and the standard approach. The air temperature computed by the combined approach at 10:00, 11:00, 12:00 and 13:00, which obviously is not uniform, was evaluated on the basis of the weighted mass average:

$$\overline{T}_a = \frac{\sum\limits_{i=1}^{Nc} \rho_i \upsilon_i T_{a,i}}{\sum\limits_{i=1}^{Nc} \rho_i \upsilon_i} \tag{7.1}$$

where $\overline{T}_a$ is the average air temperature (^{o}C), Nc is the total number of cells within the "office", ρ is the air density at the cell i (kg/m^3) and υ_i is the volume of the cell i. As can be seen, during the time-steps when the combined approach is applied, the temperature tends towards lower values (apparently, two time-steps were necessary to remove the capacity effect of the standard approach). When the standard approach is assessed again, the air temperature tends to return to the original value, however, some oscillations take place (the oscillations are diminished as the time-step is reduced).

Table 7.1 Surface temperatures computed at 12:00.

Method	Surface temperatures					
	Part_a	Part_b	North_w	West_w	Ceiling	Floor
Standard approach	20.37	20.37	18.30	18.32	18.49	15.07
Combined method	19.97	19.92	17.99	18.03	18.22	15.10
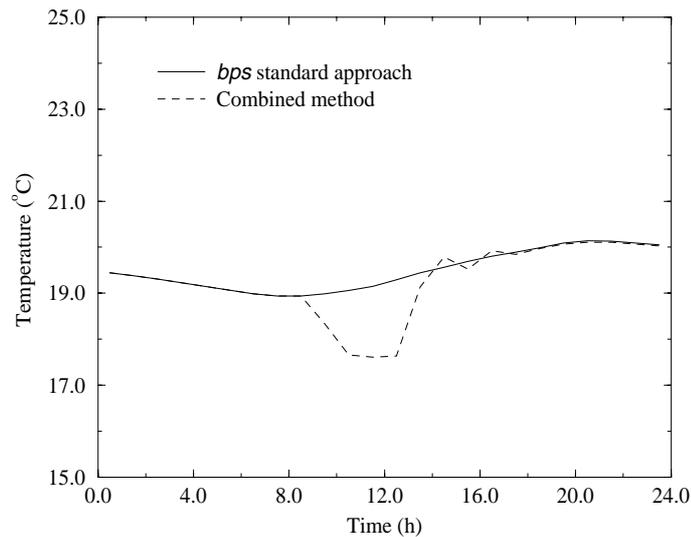
Figure 7.7 Comparison of the air temperature inside the "office" evaluated by the *bps* standard approach and the combined method.

Neither the air temperature within the other zone, nor the heat injected to the reception, are largely affected by the use of the combined approach in the "office". This conclusion could have been anticipated by the fact that the internal surface temperatures of the "office", computed by the combined method, are similar to their values as calculated by the *bps* standard approach.

This example shows that not only are the air temperature inside the office non-uniform but also that the temperature level computed by the combined approach is lower than that evaluated by the standard *bps* approach.

This implies that comfort level varies throughout the "office" and consequently the mixing air approach does not produce satisfactory results. However, considering the level of agreement of *dfs* and the combined approach results, the simple approach (the use of *bps* and *dfs* separately) seems to be adequate to analyse this problem since the property gradients in the "office" do not affect the air condition in the other zones.

7.3 RADIANT HEATING

This example illustrates the application of the combined approach with the system control capabilities. The case of a large temperature distribution within a room heated by a radiator is elucidated. The building shown in Figure 7.8 is the situation to be analysed. The problem is composed of five zones in which two are roof spaces ("roof_1" and "roof_2"). One of the zones has an L-shape geometry ("zone_L") and another, "zone_S", is square shaped. The larger zone, "room", is chosen to be investigated including CFD consideration and the remaining zones are modelled by the *bps* standard approach. The "room" zone is heated by a radiator as illustrated in Figure 7.9. In order to keep the air temperature within the heated room around 18^oC, a proportional-integral control is employed. Control schedules are not used in the other zones. The radiator is activated only between 8 o'clock in the morning and 5 o'clock in the evening. The controller proportional gain and integral action time constant are respectively $50\%/^oC$ and 200s. A one day simulation is performed in the winter (9th of January) after a start-up period of three days.

A grid of 10x20x20 cells is distributed within the heated room. The cells are located according to the power law equation (4.11) and the power law coefficients are respectively equal to 0.85, 1.5 and 1.3.

Initially, the system is simulated by the *bps* standard approach employing a one hour time-step. The air temperature and the radiator heat injection for such an approach are presented in Figure 7.10. Although the radiator is turned on and off at the specified time (between 8:00 and 17:00), the heat flux does not vary according to the air temperature (when the temperature rises above the set-point the radiator is not switched off).The reason is that the employed time-step (1 hour) is too large for the fast response of the system. Considering the order of magnitude of the time constant of the radiator, a small time-step must be employed in order to model properly the behaviour of the system. A

simulation was then performed with a six minutes time-step and the system performed well regarding the control schedule. Figure 7.11 shows the radiator heat injection and the "room" air temperature when the six minutes time-stepping scheme was used. As can be seen, the air temperature is reasonably controlled near the set-point (18^oC) and the heat injection is highly oscillating.
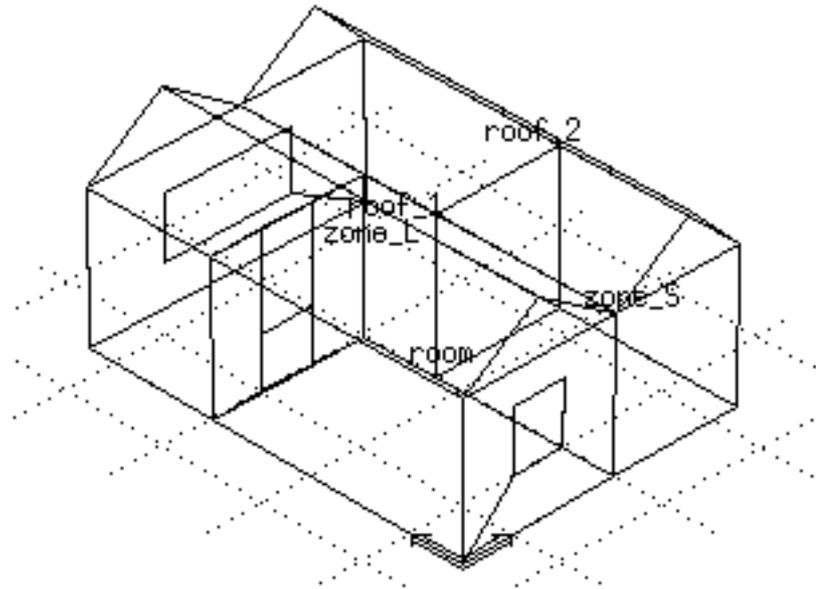

Figure 7.8 Geometry of the building.
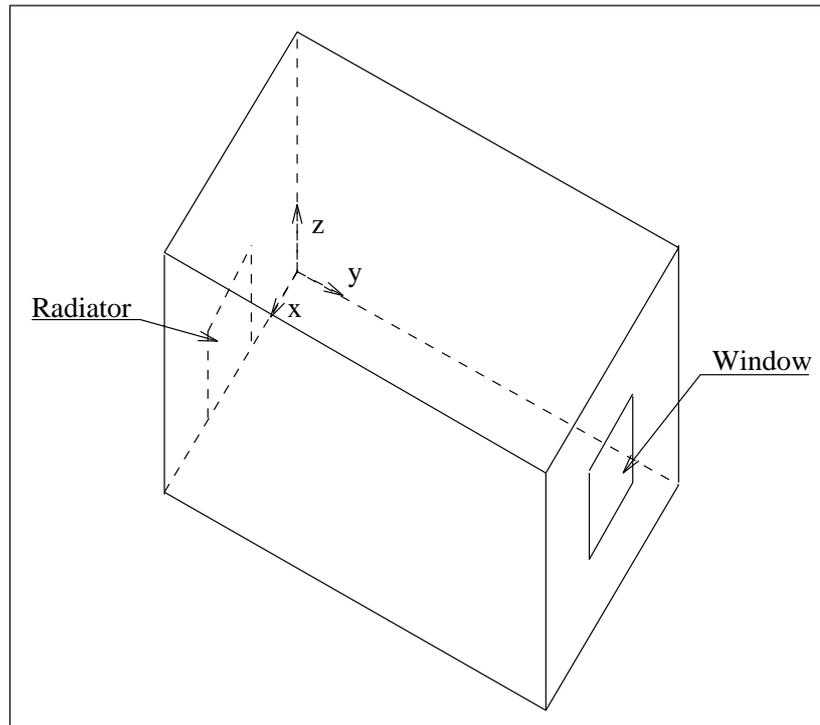
Figure 7.9 Room heated by radiator.

The surface temperatures obtained from the *bps* standard output at 16:00 using 6 minute time-step are now supplied to *dfs*. The *dfs* simulation is thus carried out to produce the temperature distribution as shown in Figure 7.12. As can be seen, a high temperature gradient exists but in most of the room the air temperature is below the uniform value presented in Figure 7.11.
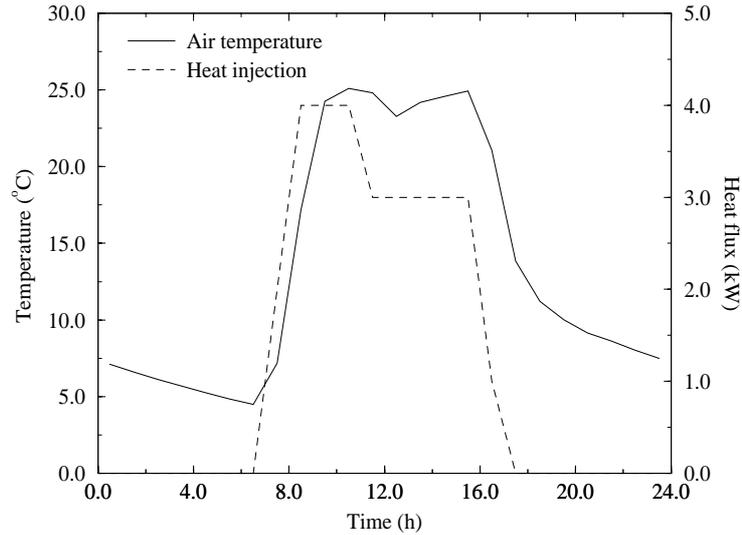
Figure 7.10 Air temperature within the "room" and radiator heat injection computed by the *bps* standard approach employing one hour time-step.
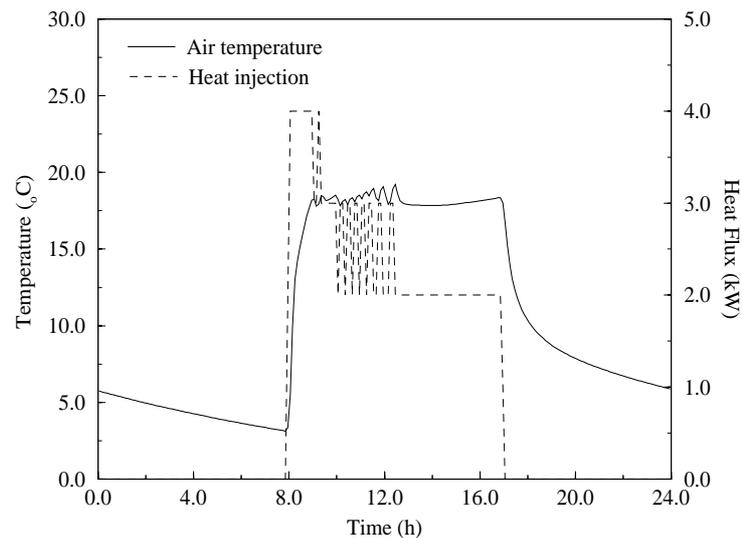
Figure 7.11 Air temperature within the "room" and radiator heat injection computed by the *bps* standard approach employing six minute time-step.

Figure 7.12 Temperature distribution within the "room" computed by *dfs* at 16:00 ($y - z$ plane, x=1500mm).

The temperature distribution on the first $x - z$ plane (y= 40mm) is shown in Figure 7.13. At the position close to the radiator, the higher temperature gradient occurs. The largest temperature is 18.7^oC which is in the order of the uniform value computed by the *bps* standard approach.

The simultaneous thermal coupling scheme is now activated only during the control period (between 8:00 and 17:00). Over this time interval, the control point is situated within the "room" at the position 191mm x 4242mm x 1310mm. A six minute time-step is employed over the whole simulation period. Figure 7.14 shows the air temperature at the control point and the heat supplied by the radiator. As can be seen, the temperature and the heat injection behave differently from the curves of Figure 7.11. In the case of the standard *bps* solution the response of the system is slower than in the case of the simultaneous scheme. As the control point is located away from the radiator when the simultaneous scheme is activated, it takes a longer period for the system to perceive the injected heat.

Figures 7.15 and 7.16 show the temperature distribution within "room" at two different planes as computed by the combined method. Although the temperature profiles show similar patterns to those presented in Figures 7.12 and 7.13, the temperature variation in this case is larger than that computed by *dfs* alone. Note that the minimum temperature value within "room" is in the order of the temperature of the control point.

Figure 7.13 Temperature distribution within the "room" computed by *dfs* at 16:00 ($x - z$ plane, y=40mm).
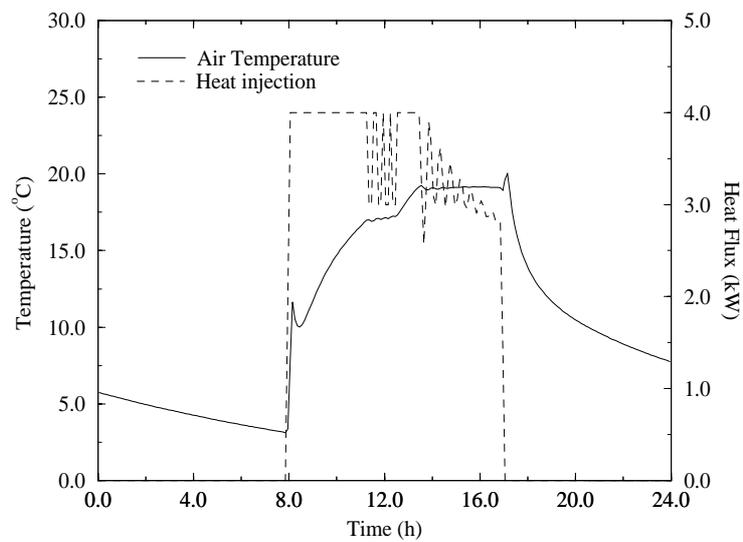

Figure 7.14 Air temperature of the control point within the "room" and radiator heat injection computed by the combined method.

Figure 7.15 Temperature distribution within the "room" computed by the combined approach at 16:00 ($y - z$ plane, x=1500mm).

Figure 7.16 Temperature distribution within the "room" computed by the combined approach at 16:00 ($x - z$ plane, y=40mm).

In addition, the air temperature within the other two occupied zones, "zone_L" and "zone_S", as computed by the two different approaches, are shown in Figures 7.17 and 7.18. As can be seen, the temperatures in the other zones are significantly affected by the method being applied. The temperature in "zone_S" is higher when the combined approach is used than when the *bps* standard approach is employed and the opposite takes place within "zone_L". As the heat injected in the "room" is higher when the combined approach is employed, it is expected that this would affect the other zones as well. This is true in the case of "zone_S" but not for "zone_L". As the convection model in "room" is dependent on the method being used, possibly the potential for the heat flux to enter "room" is greater than the potential with respect to "zone_L".

Thus, using the standard approach may compromise the results for "room", since temperature gradients are not taken into account. Also the results for the adjacent zones may be affected. Finally, the response of the control system is dependent on the sensor's position within the zone. The analysis of this case employing the combined approach seems to be crucial.
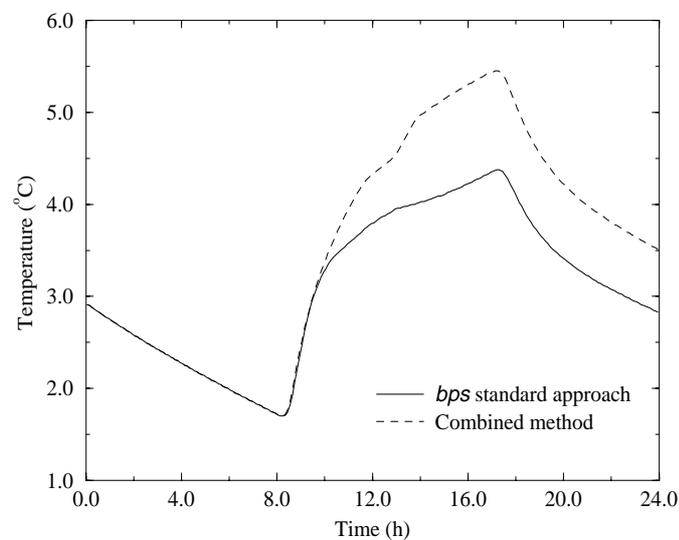

Figure 7.17 Air temperature within "zone_S" computed by the *bps* standard approach and by the combined method.
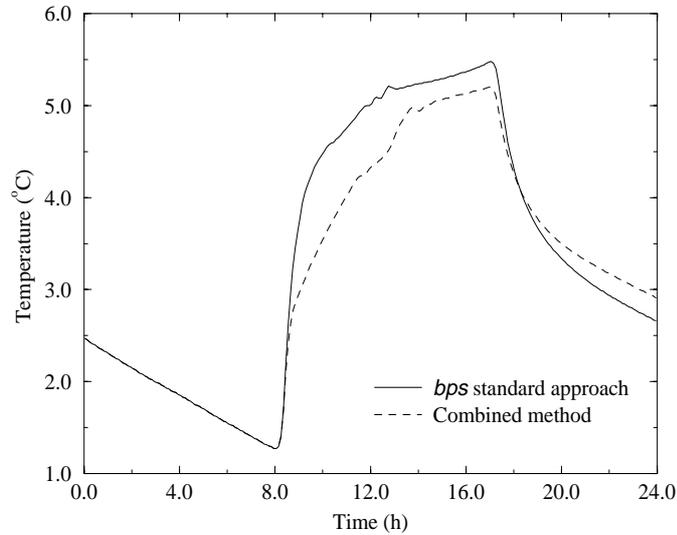
Figure 7.18 Air temperature within "zone_L" computed by the *bps* standard approach and by the combined method.

7.4 MIXING VENTILATION

In this situation the coupling between the air flow network and a CFD domain was analysed. The two-dimensional forced ventilation situation tested in Section 6.3.2 is the case studied here. The problem is simulated by employing the nodal flow network only, as shown in Figure 7.19a, and then by employing the combined method, as described by Figure 7.19b. The node "I" is located in the west facade of the building and node "O" is placed in the east facade. The two nodes are subjected to pressures induced by the wind. From climate information, pressures and temperatures at nodes "I" and "O" are known every hour. Unlike the situation in the previous chapter, the current case is non-isothermal and buoyancy is taken into account.

The relationship between pressure and mass flow, equation (6.17), is employed to represent the flow through the connections of Figure 7.19:

$$\dot{m} = e\sqrt{\Delta p} \qquad . \tag{7.2}$$

For the single connections of Figure 7.19a, the *e* resistance coefficients are equal to 0.1853185 for the inlet and 0.5294815 for the outlet. For the coupled domain, Figure 7.19b, the e_1 coefficients are equal to 9.265925×10^{-2} (1/2 of the previous value) for the inlet connections and 0.13237038 (1/4 of the previous value) for the outlet connections.

(a)

(b)
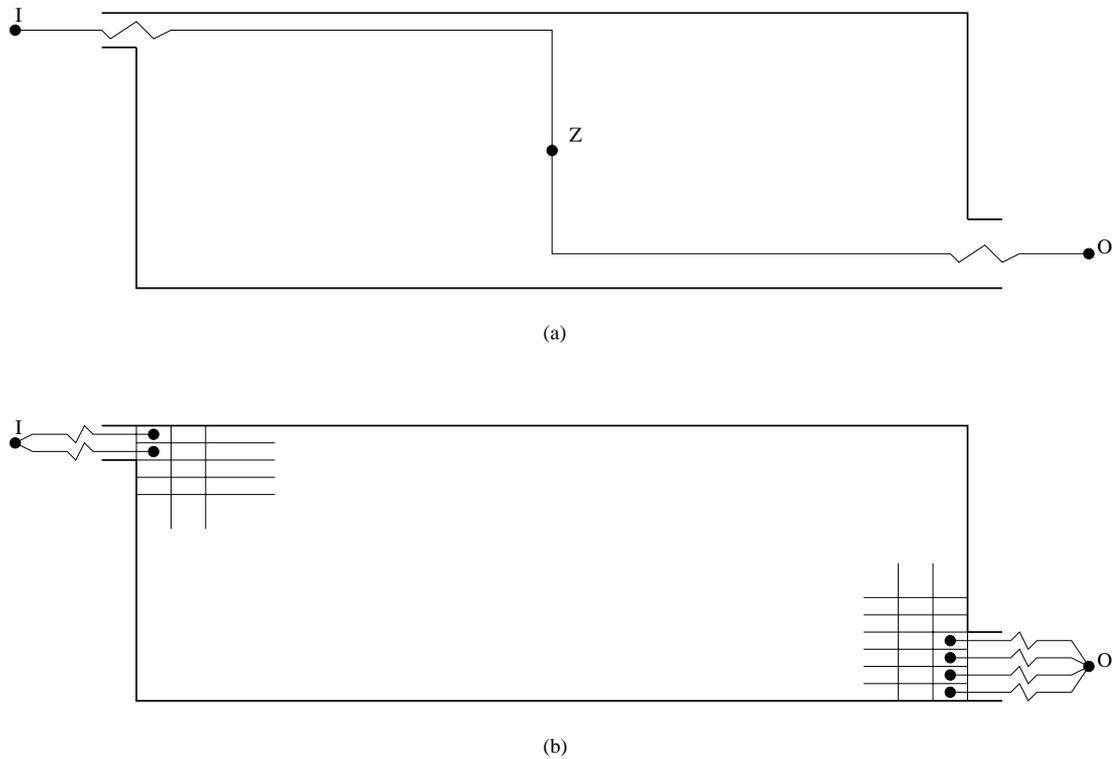
Figure 7.19 (a) Flow network and (b) combined approach diagrams of the flow domain of Figure 6.14.

The simulation was performed over one day (6th of June) with a one hour time-step. Such a high time-step was chosen because the flow is mostly induced by pressure, although buoyancy is included. Since ESP-r's database holds pressure coefficients (from which the boundary pressures are calculated) at one hour basis, the use of smaller time-step is ineffective. For that particular day, the wind direction and speed induced a pressure at node "I" higher than that at node "O" over the whole day. In the case of the combined domain, momentum is fixed at the inlet cells and pressure at the outlet cells. All surface temperatures are kept equal to 20°C during the whole simulation period. In the case of the network domain, the temperature of node "Z" is set equal to 20°C during the simulation period.

The results produced by the network approach and the combined method are presented in Figure 7.20. The inlet flow rate is the same as the outlet flow, since the flow is considered incompressible. The inlet/outlet flow rate to/from the zone computed by the combined method is the summation of the two/four flows through the connections at the openings. As can be seen, the results are similar, indicating that the modelling of such a case by the flow network approach gives a reasonable analysis of the problem. The small differences taking place at the hours near 12 o'clock can be attributed to the additional resistance imposed by the CFD domain. During such hours, the buoyancy is not expected to influence the flow since the flow rates are large and the surface

temperatures are close to the inlet temperature (20^oC). At the early hours of the day, the flow rates computed by both methods are even closer. This is because the flow rates are smaller and the temperature difference between the outside and internal surface temperatures are large. This causes the combined approach to calculate a higher flow rate than the isothermal flow rate, as the intensity of the recirculation is magnified by buoyancy and a higher flow is forced to enter the zone.

Despite the results of both approaches being close, the network approach is not able to produce information about the flow distribution within the zone as calculated by the combined method. Figure 7.21 presents the velocity and temperature distribution inside the zone as computed by the combined approach at 1 o'clock in the morning. Cold air entering the zone at 13.8^oC is heated by the walls. The hotter air accumulates at the left hand side, bottom corner as the air becomes slightly stagnant at that point (compare Figure 7.21a and 7.21b). The characteristics of the flow field at the other hours are similar, but with the intensity of velocities changed. The combined approach not only computes the flow rate entering the zone (the same information obtained from the flow network approach) but also allows the computation of localised comfort levels from temperature and velocity distributions.
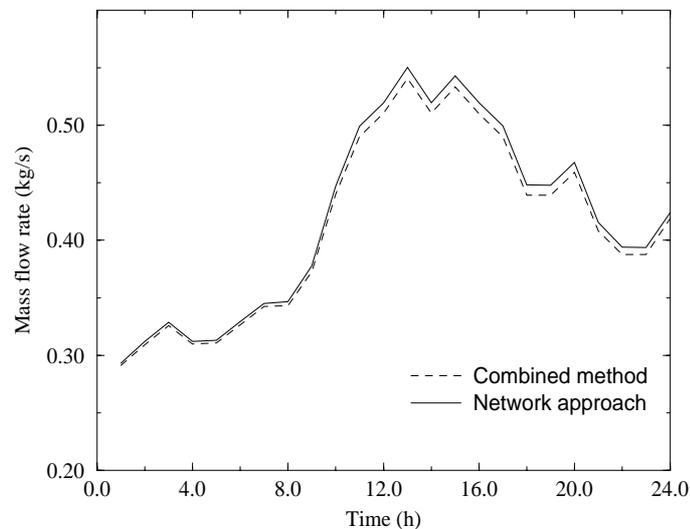

Figure 7.20 Mass flow through the ventilated room computed by the network approach and by the combined method.

Although the results are very similar, for a different situation, for example where openings are placed in positions other than the case above, the air flow network would have provided the same flow because momentum directions are not taken into account.

Clarke *et al* (1995) presents a case where the differences between the two approaches are more evident, mainly due to buoyancy. They analysed a situation similar to the one introduced above. The only difference is that the inlet and outlet resistances are different and consequently produce a different inlet/outlet flow. Firstly, they tested a case where buoyancy was not included and a case where buoyancy was included. The results are shown in Figure 7.22 and 7.23. In the first case the results of the combined and the network approaches are very similar. On the other hand, in the second case the difference between the combined method results and the network approach is more pronounced at the beginning and end of the day. At these times, the flow rate is smaller and the outside temperature is lower than the wall surface temperatures and therefore natural convection is more significant. During other times the ambient temperature approximates to the wall surface temperatures and also the flow rate is higher; consequently the buoyancy effect is not predominant.
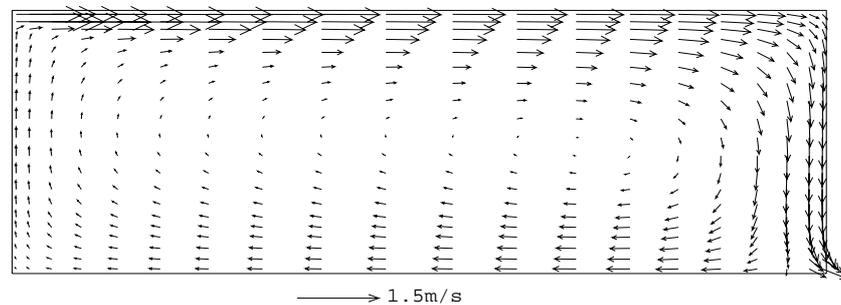
(a)

(b)

Figure 7.21 Velocity and temperature distribution calculated by the combined approach at 1 o'clock in the morning.

The combination of the network and CFD approaches is problematic in terms of convergence even for the simple case above. The solution of more complex networks was

attempted, however, its convergence was never achieved. It requires from the user a certain knowledge of how the coupling mechanism works. It is suggested for the future an improvement on the solution procedure.
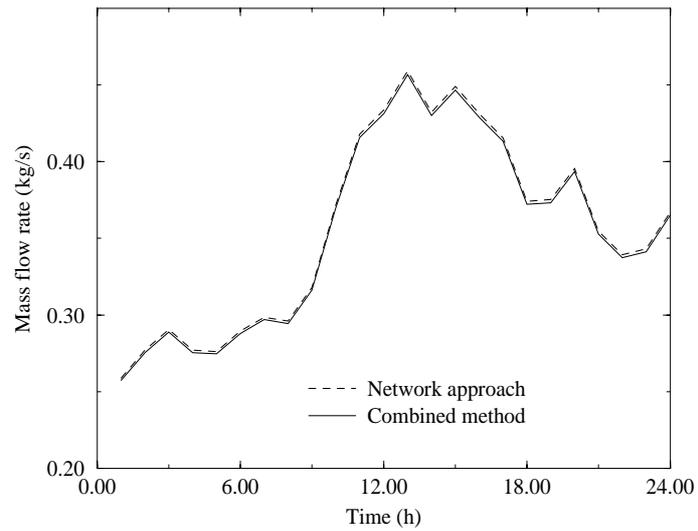

Figure 7.22 Mass flow rate in an isothermal case (Clarke *et al* 1995).
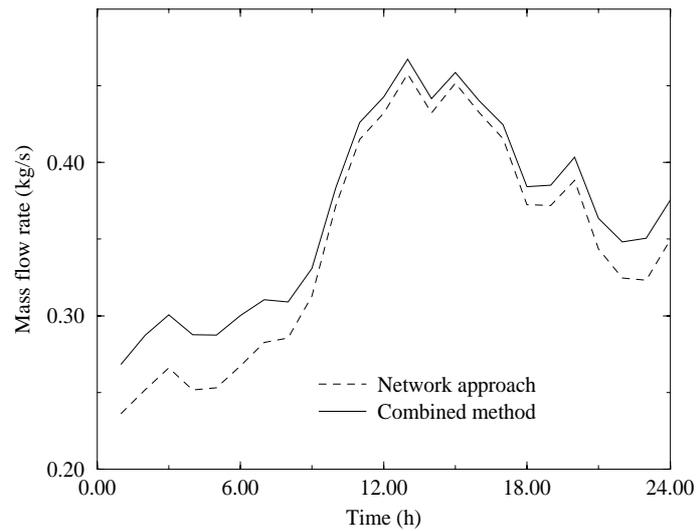
Figure 7.23 Mass flow rate in an non-isothermal case (Clarke *et al* 1995).

7.5 CONCLUSIONS

In the current chapter, the potential of analysis of the combined approach was shown by means of three different situations. In the first case, a small building in which one room is ventilated by displacement is analysed. The results indicate that a large temperature gradient occurs inside the room ventilated by displacement, and at the occupied level the temperature is lower than that calculated by the *bps* standard approach. In the second situation, a building in which its larger room is heated by a radiator was investigated. It was concluded that a large temperature gradient exists within the heated zone and that comfort levels can vary greatly throughout. Not only is the response of the control system substantially affected by the position of the control point and by its value, but also the air temperature of the zones adjacent to the heated zone are affected. Finally, a mixing ventilation system is analysed. Although it is suggested that in some cases the network approach can provide results similar to the combined method, additional information is obtained from the combined method, such as temperature and velocity distribution inside the zone.

REFERENCES

Chen, Q. and Van der Kooi, J., 1990, A Methodology for Indoor Airflow Computations and Energy Analysis for a Displacement Ventilation System, *Energy and Buildings*, Vol. 14, pp. 259-271.

Clarke, J. A., Dempster, W. M., Negrão, C. O. R., 1995, The Implementation of a Computational Fluid Dynamics Algorithm within ESP-r System, *Proceeding of Building Simulation '95*, Madison, Wisconsin.

Davidson, L., 1989, Ventilation by Displacement in a Three-Dimensional Room - A Numerical Study, *Building and Environment*, Vol. 24, No. 4, pp. 363-372.

Conclusions and Future Work

8.1 CONCLUSIONS

The present work is a contribution to building simulation developments and attempts to represent the reality and its complexities with a higher degree of integrity. Advanced fluid flow models with different degrees of detail were investigated and the shortfalls of contemporary simulation tools regarding air flow were identified. An approach, which has proven to be adequate to quantify the localised and overall building indoor air movement and the building energy requirements, was devised and developed.

A CFD technique which defines the fluid flow at the "micro" scale has been conflated with Building Thermal Simulation (BTS) by which fluid flow is described at a larger scale. The resulting combined approach strengthens the modelling potential of each methodology and overcomes their specific deficiencies. The BTS inability to predict air flow property gradients within a single space has been surmounted and the problematic CFD boundary conditions can now be supplied by BTS. The conflated methodology allows the analysis of part of the building via a detailed CFD technique where air property gradients are judged to be crucial, while in the rest of the building, where the air can be considered mixed, less resolved BTS approach is employed. The integration focuses on the CFD boundary conditions where the interactions of the systems take place. These are the inside zone surfaces and the zone openings.

The main conclusions of this study are summarised below and are discussed with respect to the three main areas of the investigation; conflation strategies, validation and applications.

The Approaches

Three conflation approaches were devised, with different degrees of complexity and sophistication. The first approach elaborates a simple method where the systems exchange information without a direct interaction. The advantage of such an approach lies in the fact that both systems run independently each from the other. This confers incorruptibility to the systems since convergence problems associated with CFD calculations can damage the whole simulation process. However, the simple approach does not account for the simultaneous dependence of one system on the other, which can reduce accuracy. Nevertheless, it can be used as a first approach to solve the problem before a full integration is employed.

The second approach involves three others schemes to handle the thermal coupling at the internal zone surfaces. At this interface convection heat transfers and inside surface temperatures are exchanged between the two systems. *Bps* provides *dfs* with surface temperatures and, in return, *dfs* supplies the convection heat transfer to *bps*. The first scheme, nominated *convection coefficient*, makes use of convection coefficients to combine the two methodology. Convection coefficients which link the air node and surface temperatures within *bps* are calculated by *dfs*. The main advantage of this approach is the fact that it can be easily implemented. The second scheme, called *sequential* approach, is a further improvement of the first scheme regarding accuracy, where the convection coefficients are dropped out and the convection heat transfer computed by *dfs* is directly inserted into the inside zone surface balance. However, a little more effort is required on its implementation. The third scheme, the *simultaneous*, treats the interactions of intra-construction energy balances (the BTS equations) and the zone air flow conservation processes (the CFD equations) in tandem within one time-step. The implementation of this scheme, when compared with the previous two, is more complex, however it tends to be more accurate.

The third approach involves the coupling of the flow network employed in *bps* and the continuity and momentum equations in *dfs*. Unlike the simple approach, the momentum coupling assumes that both domains are dependent each on the other. A simultaneous solution of the combined set of equations is proposed, in which case the original solvers of the two techniques interact with each other. The flow computed from the network approach can be imposed in two different ways within the CFD domain: a known pressure at the boundary cells or a known momentum at the interface of the opening cells. The program user can choose one or other depending on the case: large or small opening and inlet or outlet flow.

Validation

A methodology was employed to validate the standalone tools and the combined approach, which consists of analytical validation, inter-model comparison and empirical validation. Although the validation focuses on the evaluation of the combined technique, some attention was given to the standalone tools (*dfs* and *bps*) in order to check if program up-grading has not introduced code errors.

In the analytical verification, the laminar air flow through the three horizontal parallel-plate ducts connected in series was investigated. Two approximate analytical solutions were used to analyse the flow in its developing region. The velocity profile computed in this region by the combined approach is similar to the *dfs* solution and shows a good qualitative performance when compared to the analytical solutions. In the fully developed region, the combined velocity profile corresponds well to the one computed by *dfs* and is close to the *exact* analytical solution. The flow rate through the duct calculated by the combined approach is similar to the flow rate computed by the flow network method.

For the inter-model comparison, a natural and a forced ventilation situations were tested. The natural ventilation case consists of a steady-state and a transient, two and three-dimensional, laminar

and turbulent air flow in a sealed cavity. Most of the cases involved in the natural ventilation were used to check the *dfs* performance against PHOENICS. The *dfs* solution agrees well with the PHOENICS results. However, a combination of analytical and numerical techniques was employed to validate the combination of the *simultaneous* thermal coupling scheme. The heat flux through the construction, as computed by the combined approach, is coincident with its analytical counterpart. The forced ventilation case comprises a two-dimensional, turbulent isothermal flow. In this study, the combination involving the momentum coupling was compared against PHOENICS, *dfs* and the network approach. The air flow patterns computed by the combined approach and *dfs* are similar and both are comparable to PHOENICS. The flow rate computed by the combined approach is also similar to the value calculated by the flow network.

The empirical validation exercise conducted by the IEA to assess the performance of building simulation programs was the situation tested. The ability of the *simultaneous* thermal coupling scheme to predict air temperatures within a test cell was investigated. The combined approach agrees better with the measurements than the *bps* original approach. Although the convection heat transfer model seems to be improved, some discrepancies between the combined method and the measurements still exists. Such discrepancies can be attributed to possible measurement uncertainties or to other models within *bps*, such as the solar model. Nevertheless, overall, the combined approach has behaved qualitatively well.

Application

Three situations were discussed to demonstrate the combined method's applicability when compared with the air mixed approach. In the first situation, an office within a three zone building was ventilated by displacement. The existence of temperature gradients within the office indicates that a mixed air flow approach is not suitable for the evaluation of this case but that the simple approach provides a reasonable analysis for the problem. Secondly, a room within a small building was heated by a radiator. It was concluded that not only are these high temperature gradients within the room affected by the radiator control performance, but also that the air temperature within adjacent zones is influenced by such gradients. The last example was concerned with the application of the momentum coupling. In this situation, two cases were discussed. In the first one, the flow rate computed by the flow network was similar to the one calculated by the combined approach. In the second one, as the buoyancy is more predominant, the difference between the two approaches was pronounced. However, in none of the cases was the flow network able to evaluate temperature and velocity distribution within the zone, which are essential for the evaluation of comfort conditions. The convergence of the combined flow network and CFD domain is difficult to obtain, even for the simple case above, where only two nodes in the flow network were employed. The solution of more complex networks was attempted; however, convergence was never achieved.

Considering the high computational time and computer capacity required, and also the refined knowledge necessary to apply the combined approach, the application of such an approach in building design is a prospect for the future.

8.2 FUTURE WORK

Although the combined approach has demonstrated its analysis potential, much work needs is required before it can be fully employed. First of all, a more comprehensive validation process is needed in order to increase confidence in the developed technique. Inter-model comparisons should involve other models such as the IEA exercise for the validation of numerical models. An empirical validation, for example the heating situation of the IEA test cells, should be considered. The conflation of the mass flow network and *dfs* must also be explored by empirical validation. A sensitivity analysis should be carried out and comparison of the different conflation techniques are required to evaluate their applicability.

As CFD, and consequently the combined method, still requires a knowledgeable user and can be computationally very expensive for design purposes, alternative solutions for the analysis of indoor air flows should be developed for application in the short term. For example, the whole building can be modelled by the conventional BTS approach, with more nodes distributed within a zone in order to represent the non-uniform air condition. Developers could then employ the combined approach to identify the necessary inside zone flow correlations and local convection coefficients. This solution is more economical and does not request finer knowledge than the conventional BTS technique.

In this way, developers can make use of the CFD and BTS techniques separately and then conflate them as and where appropriate. This would help to analyse the influence of one system on the other, to evaluate to which extent they can be used separately, and therefore facilitate a better understanding of the problem in hand.

The combined approach can also be extended to incorporate other phenomena in building/plant systems. For example, the interaction of wind with a building's external boundaries can be modelled by the combined approach. In this case, a CFD domain can embody a building which is modelled by the BTS approach. However, small adjustments to the current model would be required. The problem would need to be considered from a different viewpoint: rather than internal convection, it is the external convection that must be modelled. The energy balance equation at the outside surfaces would need to be modified to include the convective heat transfer computed by the CFD technique. The interaction of the flow network with the CFD cells would not change in this case. Apart from the application of the whole integration, in an intermediate stage it could be employed to generate pressure coefficients to be used in building thermal simulations.

Plant components, such as boilers, cooling coils, etc., can also be modelled by the combined approach. For a boiler for example, the combustion process can be modelled by CFD technique,

while the other heat and fluid flow processes could be modelled by the BTS approach. Some adaptations to the CFD model would be required to account for the combustion process. Other areas could also benefit from the conflated technique, such as the refrigeration and chemical industries.

Although the combined approach still requires knowledge of the model from the user and a significant computing capacity, the evolution of computer technology, and the demonstrated potential of the present work to predict indoor air flows will encourage further developments in the area.

Turbulence Models

This appendix presents the different approaches commonly employed to simulate turbulent flow and also introduces the derivation of mean conservation equations discussed in Chapter 4.

A.1 TURBULENT FLOW APPROACHES

Three different approaches are currently used to predict turbulent flow: direct simulation, large-eddy simulation and turbulence transport models:

Direct simulation

In the direct simulation approach, turbulent motion is represented by solving the Navier-Stokes equations without assumptions. Since the length scale of turbulent flows is generally small (in room air flow, the scale is less than 0.1 mm (Murakami and Kato 1989)), the grid should be fine. According to Chen and Jiang (1992), the number of grid cells necessary to describe turbulent flow should be at least greater than $Re^{9/4}$. For such a case, and given computer capacity limitations, direct simulations are restricted to moderate Reynolds Number flows.

Large-eddy simulation

Considering that turbulent flow consists of an eddy motion with a wide spectrum of eddy sizes, this approach assumes that large eddies can be separated from the small ones and that such separation has no major consequence on the development of large eddies. The macroscopic scale of turbulence is responsible for all transport processes. Large-eddy motion is simulated transiently by a set of governing equations in a fine grid. The remaining scale of the motion smaller than the grid size is embodied in the large scale equations by means of turbulent transport approximations. Although the approach provides reasonable accuracy, the grid size must be sufficiently fine and the time-step considerably small in order to capture all influential eddies. Thus, the computational time necessary is still relatively large (Abbott and Basco 1989, Chen and Jiang 1992).

Turbulent transport models

Since engineers are usually not interested in the details of the high frequency fluctuating motion, a statistical approach can be taken whereby the governing equations are averaged over a time

scale much larger than that of turbulent motion. Such an averaging process creates averages of the product of fluctuating values (Reynolds stresses) which are unknown and must be approximated in order to have a closed set of fundamental equations. The turbulent transport models are thus reponsible for determining the Reynolds stress and are divided into two main categories: eddy diffusivity and Reynolds stress models. Eddy diffusivity suggests that the Reynolds stress is proportional to the gradient of the mean flow properties (Boussinesq suggestion (Rodi 1984)). Several models have been proposed to determine the constant of proportionality which is a turbulent diffusion coefficient (eddy viscosity). Rodi (1984) and Launder and Spalding (1972) present an extensive list of these models: the zero equation (constant eddy viscosity, Prandtl's mixing length models), the one transport equation (Bradshaw's model) and the two transport equation (k-kl, k-w, k-ε models) models. Among them the k-ε model has shown a certain superiority over the others and it is the most widely used. The Reynolds stress model represents a step closer to fundamental equations than the k-ε model since it employs six transport equations to describe explicitly the components of the Reynolds stress tensor. Nevertheless, the disadvantage of the method over the k-ε model is the considerably higher computational time (Jones and Whittle 1992). The turbulent transport models are computationally much less expensive than the direct and large-eddy simulation and it shows adequate accuracy for engineering purposes.

From the three different approaches, the turbulent transport models is the most computationaly economical. Particularly, the k-ε model is capable of describing the complexities of the indoor turbulent motion with acceptable accuracy. As reviewed by Chen and Jiang (1992) and Jones and Whittle (1992), the use of k-ε has achieved encouraging results when applied to the analysis of air velocity, temperature, relative humidity and contaminant concentration distribution within a room.

A.2 DERIVATION OF THE MEAN CONSERVATION EQUATIONS

The conservation equations of mass, momentum, energy, etc., known as field equations, represent the variation of problem variables in space and time. Conservation of mass, momentum and of any scalar property (temperature, concentration of contaminants, etc.) for a transient incompressible flow can be represented respectively by the following partial differential equations:

$$\frac{\partial \rho}{\partial t} + \frac{\partial}{\partial x_j}(\rho u_j) = 0 \tag{A.1}$$

$$\frac{\partial}{\partial t}(\rho u_i) + \frac{\partial}{\partial x_j}(\rho u_j u_i) = -\frac{\partial p}{\partial x_i} + \frac{\partial}{\partial x_j}\left[\mu\left(\frac{\partial u_i}{\partial x_j} + \frac{\partial u_j}{\partial x_i}\right)\right] + \rho g_i + s_{u_i} \tag{A.2}$$

$$\frac{\partial}{\partial t}(\rho\zeta) + \frac{\partial}{\partial x_j}(\rho u_j \zeta) = \frac{\partial}{\partial x_j}\left(\Gamma_\zeta \frac{\partial \zeta}{\partial x_j}\right) + s_\zeta \qquad (A.3)$$

where, u_i is the velocity components (u, v, w), p is the pressure, ζ is the scalar variable, s is the source term, μ is the molecular viscosity; Γ_ζ is the scalar diffusion coefficient, ρ is the density and s_ζ is the source term; x_i is the coordinate axis (x, y, z), t is the time and g_i is the gravitational acceleration. The last term on the right hand side of equation A.2 is the buoyancy effect caused either by temperature differences or concentration gradients. equation (A.1) to (A.3) are the complete set of conservation equations necessary to represent either laminar or turbulent flows. Nevertheless, as already mentioned, the random fluctuating characteristic of the turbulent flow is not easily obtained from the above equations. Since the objective of the analysis is not in the instantaneous fluctuation but in the mean values of flow properties, the equations of motion are time-averaged. In order to achieve the mean conservation equations for the turbulent flow, the instantaneous quantities are assumed to be the sum of their mean and fluctuating components:

$$\zeta = Z + \zeta' \;\; ; \;\; p = P + p' \;\; ; \;\; u_i = U_i + u_i' \;\; ; \;\; s_i = S_i + s_i' \qquad (A.4)$$

The capital symbols represent the time-averaged values and the lower case letters followed by an apostrophe are the fluctuations. Substituting the instantaneous values of equation (A.4) in equation (A.1) to (A.3) and observing the rules of time-averaging algebra, the set of mean conservation equation arises (See Rodi (1984) for details):

$$\frac{\partial \rho}{\partial t} + \frac{\partial}{\partial x_j}(\rho U_j) = 0 \qquad (A.5)$$

$$\frac{\partial}{\partial t}(\rho U_i) + \frac{\partial}{\partial x_j}(\rho U_j U_i) = -\frac{\partial P}{\partial x_i} + \frac{\partial}{\partial x_j}\left[\mu\left(\frac{\partial U_i}{\partial x_j} + \frac{\partial U_j}{\partial x_i}\right) - \overline{\rho u_j' u_i'}\right] + \rho g_i + S_{U_i} \qquad (A.6)$$

$$\frac{\partial}{\partial t}(\rho Z) + \frac{\partial}{\partial x_j}(\rho U_j Z) = \frac{\partial}{\partial x_j}\left(\Gamma_\zeta \frac{\partial Z}{\partial x_j} - \overline{\rho u_j' \zeta'}\right) + S_Z \qquad (A.7)$$

The average process gives rise to eddy shear stress or Reynolds stress $(-\overline{\rho u_j' u_i'})$ and eddy scalar fluxes $(-\overline{\rho u_j' \zeta'})$ increasing the number of unknowns. The determination of eddy fluxes in order to reduce the number of unknowns is defined as the *closure* problem. These new quantities are correlated

to the mean flow variables through turbulence models. According to the Boussinesq suggestion, the Reynolds stress and eddy scalar flux are related to the rate of the mean stream through an eddy diffusivity:

$$\tau_{ji} = -\overline{\rho u_j{}' u_i{}'} = \mu_t \left(\frac{\partial U_i}{\partial x_j} + \frac{\partial U_j}{\partial x_i} \right) - \frac{2}{3} \delta_{ji} \rho k \qquad (A.8)$$

$$-\overline{\rho u_j{}' \zeta'} = \Gamma_t \frac{\partial Z}{\partial x_i} \qquad (A.9)$$

where μ_t is the turbulent viscosity (or eddy viscosity), a characteristic of the flow rather than the fluid, Γ_t is the eddy scalar diffusivity (generally expressed as μ_t / σ_Z), δ_{ji} is Kronecker δ and k ($= \overline{u_i{}' u_i{}'/2}$) is the kinetic energy of turbulence. The last term on the right hand side of equation (A.8) is the normal stresses or pressures. Substituting equation (A.8) and equation (A.9) into equation (A.6) and (A.7) respectively and considering the term $-2/3 \delta_{ji} \rho k$ to be negligible compared to the hydrodynamic pressure, the set of mass, momentum and scalar conservation equations can be written in the following format:

$$\frac{\partial}{\partial t} (\rho \phi) = \frac{\partial}{\partial x_j} \left(\Gamma_\phi \frac{\partial \phi}{\partial x_j} - \rho U_j \phi \right) + S_\phi \qquad (A.10)$$

where ϕ ($= 1$ (continuity), U, V, W, T, C, etc.) represents any mean scalar variable or velocity component. The diffusion coefficient, Γ_ϕ, and the source terms, S_ϕ, can be seen in Table 4.1.

REFERENCES

Abbott, M. B., Basco, D. R., 1989, *Computational Fluid Dynamics An Introduction for Engineers*, Longman Scientific & Technical.

Chen, Q. and Jiang, Z., 1992, Significant Questions in Predicting Room Air Motion, *ASHRAE Transactions*, vol. 98, part 1, 929-939.

Jones, P. J. and Whittle, G. E., 1992, Computational Fluid Dynamics for Building Air Flow Prediction - Current Status and Capabilities, *Building and Environment*, vol. 27, n. 3, pp. 321-338.

Launder, B. E. and Spalding, D. B., 1972, *Lectures in Mathematical Models of Turbulence*, Academic Press, London and New York.

Murakami, S. and Kato, S., 1989, Numerical and Experimental Studey on Room Airflow - 3-D Predictions using the k-ε Turbulence Model, *Building and Environment*, vol. 24, n. 1, pp. 85-97.

Rodi, W., 1984, *Turbulence Models and Their Applications in Hydraulics - A State of the Art Review*, University of Karlsruhe, Karlsruhe, Federal Republic of Germany.